Characterising differences between the regenerative and non-regenerative immune response in the *Astyanax mexicanus*

Helen Grace Potts

New College, University of Oxford

Department of Physiology, Anatomy and Genetics

Primary Supervisor: Prof Mathilda Mommersteeg

Secondary Supervisor: Prof Robin Choudhury

A thesis presented for the degree of Doctor of Philosophy in Cardiovascular Science

2022

Abstract

The human heart cannot regenerate following myocardial infarction and instead forms a fibrotic scar that impairs cardiac function and can lead to heart failure. Cardiac regeneration aims to treat the injured heart by stimulating the heart to repair itself. The *Astyanax mexicanus* is a uniquely suited model of cardiac regeneration as it comprises two closely related populations: (1) the 'regenerative' surface (SF) population and (2) the 'non-regenerative' Pachón (PF) cave population. The immune response to injury is known to be a key regulator of successful regeneration. However, how this response differs between SF and PF populations is unknown.

To fully characterise the *A. mexicanus* immune response, single cell RNA-sequencing, differential gene expression analysis, histological staining and *in situ* hybridisation were used to determine the immune cell populations present in the heart at 1-, 3-, 7-, 14- and 30 days post-cryoinjury (dpci). Pharmacological perturbations of the *A. mexicanus* immune response were then used to explore whether identified differences in the regenerative and scarring immune responses to cardiac injury were exerting control on regenerative capacity.

Striking spatiotemporal differences were found in the dynamics of both myeloid and lymphoid populations in the PF and SF. Immediately after injury, the non-regenerative PF showed a stronger response to injury with a significantly greater influx of neutrophils into the wound (1dpci $p=0.0156$; 3dpci $p=0.0075$). By 7dpci, this inflammatory response was resolved, and differential gene expression analysis showed that PF neutrophils had returned to the uninjured state. In contrast, the regenerative SF showed a greater immune response at the late stages of cardiac healing (7-, 14- and 30dpci). Specifically, at 7- and 14dpci, a transcriptionally unique population of neutrophils was observed in the SF that remained activated and upregulated TNFα-NFκB signalling. Furthermore, a stark contrast in the B cell response was observed: SF displayed a significant influx of B cells at 14- and 30dpci that was absent in the PF ($p<0.005$). Inhibition of the SF immune response using 7-14dpci

Dexamethasone treatment did not impair the regenerative capacity of the SF but did significantly disrupt scar organisation, resulting in scars that closely resembled time-matched PF scars.

This research represents a significant leap forward in our understanding of how the immune response differs between successful regeneration (SF) and scarring (PF). However, further studies will be required to determine the role of late-stage SF neutrophils and B cells in successful regeneration before novel therapeutic targets can be identified for immunomodulation in heart attack patients.

Acknowledgments

This thesis would not have been possible without the support of my supervisors. Firstly, I want to thank Tilly Mommersteeg for giving me the opportunity to work on such a fascinating project, I never thought I would work on the immune system and now I can't imagine working on anything else! It has been so amazing to work with you over the years and you really have helped my confidence as a scientist to grow in leaps and bounds. I have learnt so much under your supervision that I hope to carry into the rest of my career, whether that is science or something else entirely. Additionally, I can't thank you enough for your continued support of life outside the lab, especially as I have faced some particularly chaotic times personally over the past 4 years and having the lab come to support me play rugby at Twickenham was a real highlight!

Secondly, I would like to thank my co-supervisor Robin Choudhury whose lab meetings I always thoroughly enjoyed and left feeling inspired about science. I really learnt how to always question the hypothesis of an experiment and tell the story of my work. I felt my project benefitted from so much from your critical thinking and fresh perspective and so it has been a real privilege to feel part of both the Choudhury and Mommersteeg groups.

I want to thank all the members of the Mommersteeg, Choudhury, Riley and Smart groups, both past and present for all their support, advice and input over the years and making the lab such a lovely place to work in. A special thanks go to Will, Irina and Andia for all your support and friendship.

I am incredibly grateful to have the best parents in the world and I cannot possibly do justice to how much your love, support and encouragement has helped me get to where I am today.

I couldn’t have ever made it through this DPhil without all my amazing friends that have made these past 5 years unforgettable! From all the great friends I made in Oxford and on the rugby team- you all truly made my time in Oxford so special – to the best housemates I could ever ask for in 3 Minster who were my lockdown family. And last, but not least to Caitlin, Ffion, Iisha, Jess, Nick, Pete, Rhys and Tom who I owe so much to. Some of the worst times of my life have been during this DPhil and I couldn’t have built myself back up without each and every one of you so thank you.

Finally, I would also like to thank Dr. Robert Peuß and Prof. Manuela Zaccolo for taking the time to examine this thesis.

Table of Contents

List of Figures

List of Tables

List of Abbreviations

10X	10X Genomics Chromium
AM	*Astyanax Mexicanus*
ATP	Adenosine triphosphate
BrdU	Bromodeoxyuridine
CHD	Coronary heart disease
DAMPs	Damage-associated molecular patterns
Dex	Dexamethasone
DNA	Deoxyribonucleic acid
dpci	Days post-cryoinjury
dpi	Days post-injury
dps	Days post-sham
DPA	Differential Proportion Analysis
ECM	Extracellular Matrix
FDR	False Discovery Rate
GEMs	Gel Bead-In Emulsions
GO	Gene Ontology
GSEA	Gene Set Enrichment Analysis
HMGB-1	High mobility group box-1
Ip	intraperitoneal

IκB	Inhibitor of NFκB
IKK	IκB kinases
IL-1β	Interleukin-1β
IL-6	Interleukin-6
IL-18	Interleukin-18
LA-1	Leukadherin-1
LAD	Left Anterior Descending
LR	Logistical Regression
MI	Myocardial infarction
MS-222	Tricaine methanesulfonate
NFκB	Nuclear factor kappa B
OSM	Oncostatin M
P1	Postnatal day 1
P7	Postnatal day 7
PAMPS	Pathogen-associated molecular patterns
PBS	Phosphate-buffered saline
PCA	Principal Component Analysis
PF	Pachón fish
PFA	Paraformaldehyde
PRRs	Pattern recognition receptors

ptprc	Protein Tyrosine Phosphatase Receptor Type C; also known as CD45
QTL	Quantitative Trait Locus
ROC	Receiver Operating Characteristic
scRNAseq	Single cell RNA sequencing
SF	Surface fish
TLRs	Toll-like receptors
TNFα	Tumour Necrosis Factor α
UMAP	Uniform manifold approximation projection

Chapter I
Introduction

1.1 Coronary Heart Disease, Myocardial Infarction and Heart Failure

1.1.1 Coronary Heart Disease and Myocardial Infarction

In 2022, the world faces a multitude of global health pandemics from Covid-19 to diabetes, obesity and coronary heart disease (CHD)[1–3]. Although no global health pandemic has impacted daily life like Covid-19, CHD is the biggest killer and has been the leading cause of death worldwide for the past 22 years[4,5]. CHD is characterised by the gradual accumulation of lipid deposits in the walls of coronary arteries, progressively narrowing their lumen and resulting in restricted blood flow to the heart[6]. Patients with CHD face a significantly increased risk of myocardial infarction (MI) in which ischaemic injury results in downstream necrosis, due to coronary artery occlusion, starving downstream cells of oxygen and nutrients[7].

Following MI, the adult human heart cannot replace any injured cardiomyocytes and, instead, faces severe depletion of contractile tissue as approximately 1 billion cardiomyocytes are lost[7]. To replace the lost tissue, a thick, collagenous scar is deposited that acts to preserve the integrity of the ventricular wall and prevent fatal cardiac rupture. However it is non-contractile and, depending on its size, can impair cardiac function, providing no compensation for the lost muscle[8]. To increase the contractile function of the diminished heart, a range of compensatory signalling pathways are activated that increase heart rate and arterial resistance, and stimulate cardiomyocyte hypertrophy[9,10]. Initially, these compensatory signalling pathways are beneficial and help to maintain cardiac output despite the massive loss of cardiac muscle. However, with time, these compensatory signals can become maladaptive in some patients, stimulating fibrosis; scar thinning; ventricular dilation; chronic inflammation; and a progressive decline in cardiac function until, eventually, they lead to heart failure[11].

1.1.2 Heart Failure

Heart failure occurs when the heart can no longer pump blood sufficiently to meet the needs of the body. Once a patient develops heart failure, they are faced with limited treatment options. A small number of the most severely affected cases may undergo heart transplant, which remains the only 'cure'[12]. This problem is exacerbated by the fact that current MI treatments are very effective and survival rates have increased to 70% in the UK since their discovery[13], resulting in more patients surviving MI and developing post-MI heart failure. Therefore, effective interventions that prevent the development of irreversible heart failure post-MI are desperately needed.

The only way to prevent post-MI heart failure is to restore the heart back to its full contractile capacity by replacing the cardiomyocytes that have been lost. In the last 2 decades, novel therapeutic strategies have emerged that aim to restore cardiac contractility after MI[14,15]:

1) **Cardiac reconstitution**-replacing lost MI tissue with exogenous cells such as *in vitro*-derived cardiomyocytes
2) **Direct *in vivo* reprogramming**-the *in situ* conversion of non-myocyte cardiac cells (eg fibroblasts/myofibroblasts) into cardiomyocytes
3) **Cardiac regeneration**-stimulating the heart to repair and renew itself by improving the adult human heart's endogenous repair capacity

Although both cardiac reconstitution and genetic reprogramming have been shown to improve cardiac function following injury in animal models[16–19], significant barriers remain before either of these approaches can be successfully translated into the clinic. To date, cardiac reconstitution strategies still require patients to be immunosuppressed and risk introducing potentially fatal arrhythmias as two beating tissues fail to synchronise[20]. Genetic reprogramming is limited by poor efficiency rates (at best <50%)[21] due to the introduction of transcription factors into residing cells, via viral vectors, to stimulate cardiomyocyte transdifferentiation. Additionally, both cardiac reconstruction and genetic reprogramming face the additional hurdle that they must overcome the

pro-inflammatory/pro-fibrotic environment of the post-MI human heart to produce therapeutic benefits. On the other hand, cardiac regeneration represents a promising therapeutic approach as it can overcome some of these barriers: it aims to repopulate a patient's heart with their own dividing cells; it does not require the use of poorly efficient viral vectors and it aims to change the micro-environment of the injured heart to a pro-reparative and anti-inflammatory setting.

1.1.3 Cardiac Regeneration

Cardiac regeneration aims to functionally restore the heart after injury by triggering the heart to repair itself. This field has exploded since two seminal papers discovered that, following cardiac injury, both the adult zebrafish (*Danio rerio*)[22] and the neonatal mouse (between P1-P7, *Mus musculus*)[23] can fully replenish damaged myocardium with healthy new cardiac tissue. In particular, the finding that mammals can perform innate regeneration, albeit in a time-restricted regenerative window, raises the tantalising possibility that a similar regenerative window may exist in humans. Indeed, a handful of case-studies have reported scar-free cardiac healing following surgery and full functional recovery following MI in newborn human infants[24–26].

Since these remarkable discoveries, full cardiac renewal has been observed in a range of fish, amphibian, and mammalian models (Fig. 1.1) in response to a variety of cardiac injuries (Table 1.1).

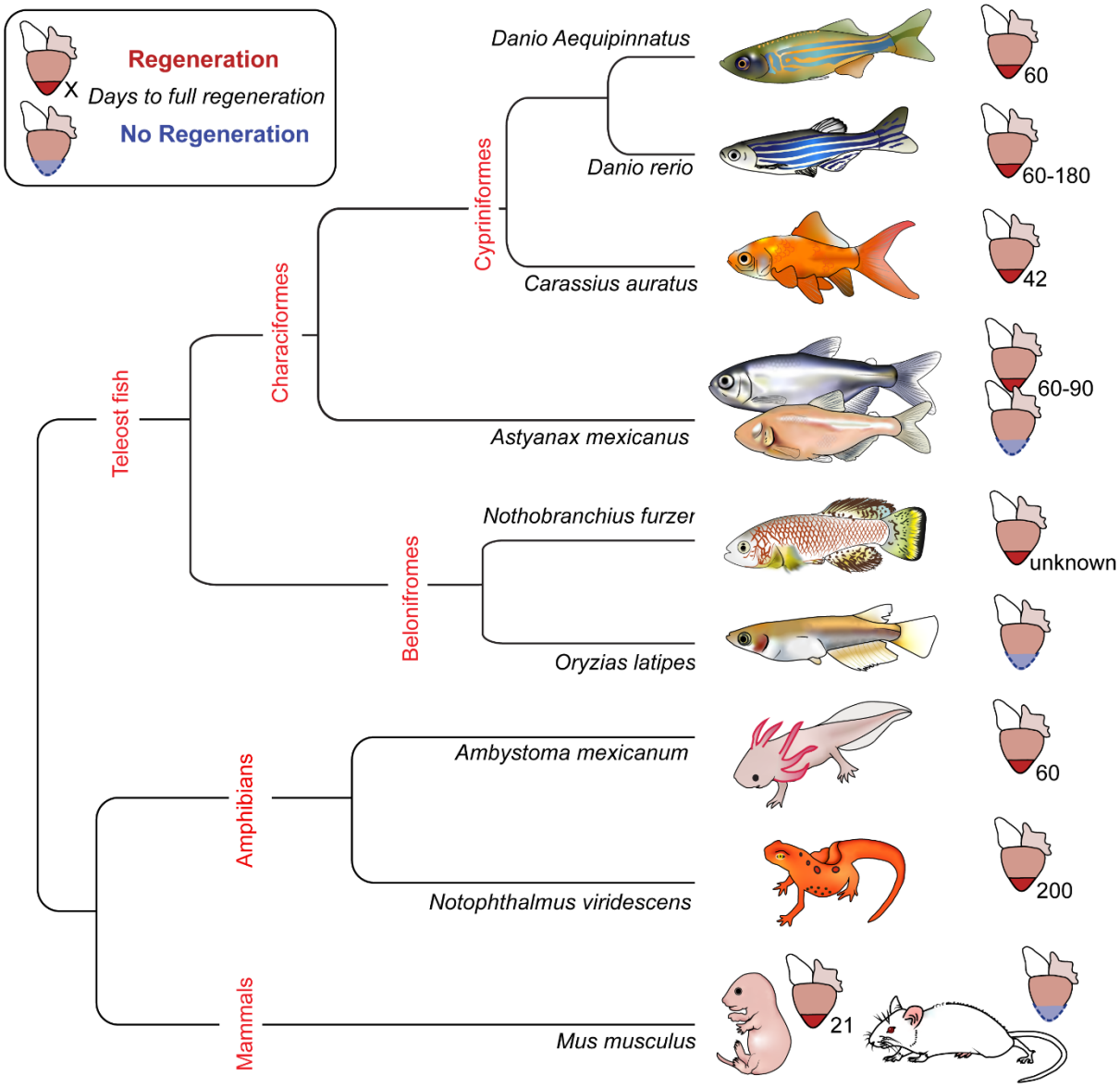

Figure 1. 1: Phylogenetic tree summarising the main models used to study cardiac regeneration and the time taken for full regeneration

In addition to the neonatal mouse and the zebrafish, full cardiac renewal has been observed in the giant zebrafish (D. Aequipinnatus)[27], the goldfish (C. auratus)[28], the Surface-morph of the A. mexicanus[29], the killifish (N. furzei)[30], the salamander/axolotl (A. mexicanum) and newts (N. viridescens[31–33]; Pleurodeles waltl[34]). In contrast, the medaka (O. latipes), the adult mouse (M. musculus) and the Pachón cave-dwelling morph of the A. mexicanus show a permanent scarring response to cardiac injury and are typically used in comparative studies that investigate regeneration success vs failure. A variety of cardiac insults have been tested in these models, with time taken for

full regeneration varying between injury model used. Figure made in collaboration with W. Stockdale and adapted from Potts et al (2021)[35].

	Genetic Ablation	***Cryoinjury***	***Cauterisation***	***Ventricular Resection***	***LAD ligation***
Type of damage	*Cardiomyocytes are specifically destroyed following cmlc2 or myl7-directed expression of diphtheria toxin A*	*Damages cardiac tissue by freezing/thawing using liquid nitrogen*	*Damages cardiac tissue by burning*	*Cardiac tissue is cut and removed by amputation using scissors*	*Left anterior descending (LAD) coronary artery is ligated to cause ischemic tissue death*
Extent of damage	*Up to 60% of cardiomyocytes throughout the ventricle*	*Causes localised tissue damage of 10-30% of the ventricle*	*Causes localised tissue damage of 10-30% of the ventricle*	*10-20% of the ventricle is amputated*	*Causes localised tissue damage below the ligature site*
Causes necrotic cell death?	*Yes*	*Yes*	*Yes*	*No*	*Yes*
Regenerative Models Tested	*Adult Zebrafish*[36] *Neonatal mouse*[37] *Larval Zebrafish*[38]	*Adult Zebrafish*[39,40] *Neonatal mouse*[41] *Newt*[34] *Axolotol*[42]	*Adult Zebrafish*[43] *Giant Zebrafish*[27] *Goldfish*[28]	*Adult zebrafish*[22] *Neonatal mouse*[23] *Newt*[33] *Axolotl*[44] *A. mexicanus*[29]	*Neonatal mouse*[45]

Table 1. 1: Summary of the main injury models used to study cardiac regeneration

1.2 Mechanisms of Cardiac Regeneration: what have we learnt from animal models with endogenous repair capacity?

Organ regeneration is a complex process that requires dead and damaged tissue to be cleared and replaced with a diverse range of new cell types to reconstitute the lost cardiomyocytes, blood vessels, interstitial cells, nerves, extracellular matrix (ECM) and resident immune cells. Therefore, regeneration must involve the tight coordination of cell proliferation, maturation and integration with the residing myocardium. To effectively trigger endogenous regeneration in the

human heart, it is hoped that understanding the molecular and cellular signals that govern innate regeneration in animal models will identify therapeutic targets to stimulate regeneration in MI patients. Studies in these animal models have so far elucidated several key mechanisms that are essential for successful endogenous regeneration.

1.2.1 Cardiomyocyte dedifferentiation and proliferation are the cornerstones of successful regeneration

To repopulate the lost cardiac muscle, a quintessential step of cardiac regeneration is the formation of *de novo* cardiomyocytes. As such, how cardiomyocytes are replaced in regeneration has been the focus of intensive investigation. Following some initial controversy as to the source of replacement cardiomyocytes, lineage tracing studies in both the adult zebrafish[46,47] and the neonatal mouse[48,49] have since shown that healthy, new cardiomyocytes arise from the dedifferentiation and proliferation of pre-existing mononucleated diploid cardiomyocytes. This may explain why the adult human heart has such a limited capacity for repair as human cardiomyocytes have a high degree of polyploidy and bi-/multi-nucleation which are both thought to be incompatible with proliferation[50]. Indeed, the adult human heart shows a very low rate of proliferation during homeostasis (annual turnover is <1%)[51] and there are no reports of a cardiomyocyte proliferative response in humans post-MI.

Extensive research has sought to delineate the complex intracellular and environmental mitogenic cues that regulate cardiomyocyte dedifferentiation and proliferation in the regenerating heart in the hope that these signals can eventually be replicated in the adult human heart post-injury to stimulate endogenous regeneration (Fig. 1.2). As such, numerous signal transduction pathways and molecules have so far been shown to regulate cardiomyocyte proliferation. However, it is beyond the scope of this thesis to discuss each proliferative signal in detail and so it is important to note that the pathways discussed here are not an exhaustive list.

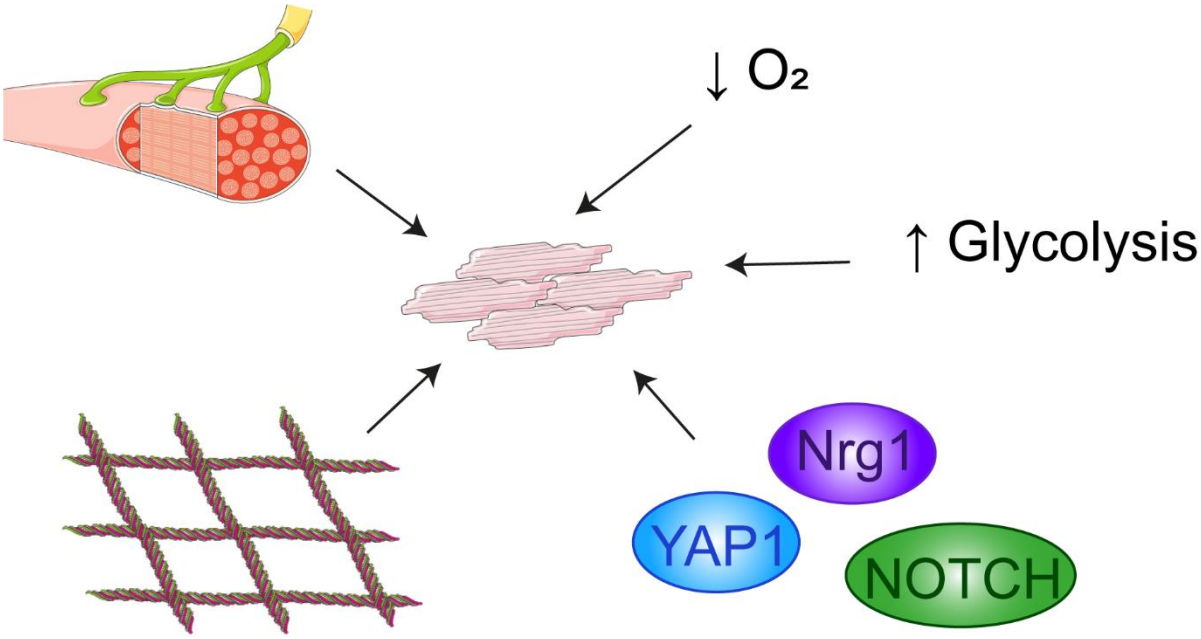

Figure 1. 2: Overview of the complex signalling pathways and environmental cutes that stimulate cardiomyocyte proliferation after injury

As discussed below, cardiomyocytes are stimulated to proliferate in response to signals from innervating nerves, the ECM, a decrease in available oxygen and a co-current metabolic shift away from oxidative phosphorylation and an upregulation of glycolysis, as well as be reactivation of developmental signalling pathways.

Signalling pathways important in cardiac development are re-activated after injury to regulate cardiomyocyte dedifferentiation and proliferation

Following injury, the endogenously regenerating heart re-employs many of the same ligands and signalling pathways that are active in heart development in order to facilitate cardiomyocyte dedifferentiation and proliferation. So far, four main developmental pathways have been found to be regulate regeneration: Wnt, Notch, Hippo, and Neuregulin 1 (Nrg1)-Erbb2 signalling.

Wnt Signalling

The dynamic activation and inhibition of Wnt signalling is crucial at different stages of cardiogenesis to ensure the correct patterning, differentiation and proliferation of cardiac cells

during heart formation[52]. Wnt signalling can occur via both canonical (i.e. β-catenin-dependent) and non-canonical pathways which exert differential effects on cardiomyocyte proliferation. Activation of canonical Wnt signalling directly inhibits cardiomyocyte proliferation and its inhibition enhances zebrafish regeneration by increasing both cardiomyocyte proliferation and dedifferentiation[53]. In contrast, activation of the noncanonical *jnk1/c-jun/creb1* Wnt signalling pathway induces cardiomyocyte proliferation and its inhibition leads to decreased cardiomyocyte proliferation and impaired regeneration in the zebrafish[54]. Strikingly, the canonical and non-canonical Wnt pathways seem to be directly antagonistic to each other: activation of the non-canonical Wnt pathway directly inhibits β-catenin signalling and *vice versa*[54]. This could explain why mammalian cardiomyocytes are unable to proliferate following MI as, in response to injury, they upregulate canonical Wnt signalling[55].

The Notch Pathway

During development, Notch signals from endocardial cells lining the inner lumen of the heart regulate the maturation (i.e. the trabeculation and compaction) of the underlying ventricular wall[56]. After injury, Notch signalling is re-activated and upregulated in zebrafish endocardial and epicardial cells proximal to the injury site[57]. This reactivation of Notch signalling is critical for cardiac regeneration as suppression of Notch, either genetically[57] or by pharmacological inhibition[58], impairs regeneration and results in decreased cardiomyocyte dedifferentiation[59], proliferation and scar formation. Although cardiomyocytes do not directly express receptors for ligands of the Notch signalling pathway, it has been recently shown that Notch indirectly promotes cardiomyocyte proliferation via antagonism of Wnt signalling; Notch signalling results in the increased secretion of *notum1b* and *wif1* from activated endocardial and epicardial cells, two Wnt pathway antagonists[60]. In contrast to the zebrafish, Notch signalling is not re-activated in the neonatal mouse following injury. However, studies of Notch signalling in the adult mouse do suggest that activating Notch is beneficial for mammalian cardiac repair as stimulation of Notch signalling following LAD ligation results in functional improvement, decreased scarring and increased cardiomyocyte survival[61,62].

Additionally, inhibition of Notch signalling in the adult mouse results in increased cardiomyocyte apoptosis following injury[63], suggesting that inducing mammalian cardiomyocytes to re-enter the cell cycle will be enhanced by Notch stimulation.

The Hippo-Yap Pathway

The Hippo pathway controls the size of the heart during heart formation by regulating the proliferation of the endoderm, mesoderm and ectoderm as well as restricting cardiomyocyte proliferation[64]. Activation of the Hippo pathway triggers a downstream kinase signalling cascade that culminates in the phosphorylation and destruction of the transcriptional coactivators YAP/TAZ. When unphosphorylated, YAP/TAZ translocate to the nucleus and associate with transcription factors to promote the expression of genes involved in proliferation.

The Hippo pathway has been shown to actively suppress the regenerative capacity of the adult mammalian heart as genetic knock-out of Hippo signalling improves the regenerative potential of the adult mouse heart, leading to increased proliferation and reduced scarring[65]. In contrast, in the neonatal mouse, the Hippo pathway is endogenously silenced following injury, enabling neonatal cardiomyocytes to re-enter the cell cycle and proliferate. This inhibition of Hippo signalling in the neonate has been shown to be critically important to regeneration as cardiomyocyte-specific deletion of *Yap1* prevents cardiomyocyte proliferation in the neonatal mouse, whilst Yap1 activation results in the upregulation of an embryonic and proliferative gene program in neonatal cardiomyocytes[66]. Although *Yap1* deletion does not impair myocardial proliferation in the zebrafish[67], Yap1 knock-out does lead to increased scar formation and fibroblast activation[68], suggesting that modulating the Hippo pathway will be a key part of stimulating endogenous regeneration in the mammalian heart by both promoting cardiomyocyte proliferation and inhibiting scar formation.

Nrg1-Erbb2 Signalling

During development, Nrg1 signalling critically regulates the thickening of cardiac fibres via Erbb2 receptors present on cardiomyocytes. After injury, Nrg1 is reactivated in the zebrafish and is upregulated in perivascular cells where it signals to surviving cardiomyocytes to proliferate[69]. Cardiomyocyte proliferation in the mouse has also been shown to be regulated by Nrg1/Erbb2 signalling as cardiomyocyte-specific knock-out of Erbb2 results in decreased levels of cardiomyocyte proliferation, resulting in hearts with thinner walls and fewer cardiomyocytes[70]. Recently, a zebrafish single cell RNA sequencing (scRNAseq) study has revealed the mechanism by which Nrg1/Erbb2 signalling facilitates cardiomyocyte proliferation: Nrg1 metabolically reprograms $Erbb2^{+}$ cardiomyocytes from oxidative phosphorylation towards glycolysis[71]. They showed that inhibition of glycolysis could impair regeneration in the zebrafish whilst overexpression of Erbb2 in mouse cardiomyocytes resulted in increased cardiomyocyte proliferation due to an upregulation of glycolysis, suggesting that stimulation of glycolysis via Erbb2 receptors promotes mammalian cardiac repair.

Mitogenic cues from epicardial cells and nerves

In addition to the activation of developmental signalling pathways within proliferating cardiomyocytes, other non-myocyte cells are specifically activated following injury and release paracrine mitogenic signals that stimulate cardiomyocyte proliferation.

Epicardium

The epicardium (i.e. the outer layer of the heart) is typically quiescent in the adult heart. However, in response to cardiac injury, the epicardium shows global activation and re-initiates its embryonic gene program. The activation of the epicardium is essential to revascularizing the wound as activated epicardial cells proliferate and form new fibroblasts, endothelial cells and smooth muscle cells[72]. In addition, activated epicardial cells secrete a plethora of paracrine factors that have been shown to stimulate cardiomyocytes to proliferate such as retinoic acid[73], insulin growth factor

signals[74] and TGFβ ligands[75], as well as secreting Notch ligands[57,59] and Nrg1[69]. Indeed, genetic ablation of epicardial cells reduces the efficiency of zebrafish heart regeneration and results in decreased rates of cardiomyocyte proliferation[76].

Nerves

The rate, force of contraction, and velocity of conduction of the heart are all regulated by adrenergic and muscarinic signals from innervating nerves. Following MI, the sympathetic nervous system is activated to maintain cardiac output, despite the loss of cardiac tissue, by increasing heart rate and blood pressure[77–81]. Cardiomyocyte proliferation has been shown to be crucially reliant on this sympathetic drive as disruption of cholinergic nerve-derived signals can abolish regeneration in both the zebrafish and the neonatal mouse by decreasing cardiomyocyte proliferation[82].

Pro-regenerative ECM induces cardiomyocytes to re-enter the cell cycle

Cardiomyocytes are embedded within the ECM, a 3D-network of proteins that provide structural support and intercellular signalling information to the surrounding cells[8384]. Changes in ECM tensile strength have been observed to coincide with changes in cardiomyocyte proliferation. From P7, the ECM of the neonatal mouse remodels and matures, becoming stiffer and forming a honeycomb-like structure that encases each cardiomyocyte individually[84]. This maturation coincides with neonatal cardiomyocytes exiting the cell-cycle and the end of the regenerative window. Alterations to the mechanical properties of the ECM have been shown to directly regulate cardiomyocyte proliferation and cytokinesis *in vitro*, with reduced matrix rigidity enhancing the proliferation of neonatal cardiomyocytes[85]. Therefore, the cell cycle arrest of mammalian cardiomyocytes seems to be strongly linked to the developmental stiffening of the ECM, whilst the pro-regenerative ECM is less rigid.

Comparisons between the regenerative and non-regenerative setting have also revealed significant compositional differences in ECM proteins, with the zebrafish ECM containing more elastins than the collagenous adult mouse ECM[86]. As components of the ECM such as Agrin[87],

Periostin[88] and Fibronectin[89], have been shown to directly induce cardiomyocyte proliferation *in vitro,* it is clear that cardiomyocytes require cues from a pro-regenerative ECM to proliferate following injury. This has been further supported by the findings that Periostin knock-out inhibits regeneration in neonatal mice[90] whilst injection of decellularized pro-regenerative ECM from the zebrafish[86] and the neonatal mouse[91] can induce cardiomyocytes to re-enter the cell cycle *in vivo* in the non-regenerative adult mouse.

Hypoxia induces a metabolic shift in cardiomyocytes to induce proliferation

The loss of the regenerative window in neonates also coincides with an increase in environmental oxygen (hypoxia to normoxia) and a corresponding metabolic shift away from anaerobic glycolysis to the oxidative phosphorylation of free fatty acids (FFAs)[92]. This post-natal metabolic shift results in increased energy production which is essential for the demands of the post-natal heart. However, it also leads to the increased production of reactive oxygen species (ROS) which causes deoxyribonucleic acid (DNA) damage and global cardiomyocyte cell cycle arrest[93]. Both hypoxia and glycolysis have been shown to be important regulators of the cardiomyocyte cell cycle that are essential in regeneration. Indeed, hypoxia has been shown to induce the dedifferentiation and proliferation of cardiomyocytes during regeneration in the zebrafish[94], whilst exposure to hypoxic conditions can induce non-regenerative adult mouse cardiomyocytes to divide after injury[95]. Similarly, dedifferentiating and proliferating cardiomyocytes have been shown to re-upregulate glycolysis whilst mutations of key glycolytic genes abolish regeneration in the zebrafish by preventing cardiomyocyte dedifferentiation and proliferation[96].

1.2.2 Cardiomyocyte proliferation is insufficient for cardiac regeneration and requires a pro-regenerative immune response

Despite the fundamental need for *de novo* cardiomyocytes during regenerative repair, the presence of proliferating cardiomyocytes post cardiac injury is insufficient for the successful completion of regeneration. Full tissue replenishment requires a coordinated effort across a range of

cardiac cells to replace the lost blood vessels, interstitial cells and ECM within the regenerating myocardium. Additionally, the deposited collagen scar must be resorbed and removed at the same rate that healthy new myocardium is produced for regeneration to succeed. As such, studies have shown that, even when myocardial proliferation is unaffected, regeneration can fail when:

- Revascularisation of the wound is inhibited[97–99]
- Cardiomyocytes do not migrate into the wounded tissue[100]
- Scar formation is disrupted[75,101,102]

Furthermore, two independent studies in separate models of regeneration have shown that macrophage depletion post-injury results in regenerative failure, whilst cardiomyocyte proliferation remains unaffected. Aurora et al found in the neonatal mouse that macrophage depletion led to impaired angiogenesis and fibrotic scar formation, resulting in decreased cardiac function[103]. Similarly in the axolotl, Godwin et al showed that macrophage depletion resulted in alternative fibroblast activation and the formation of a permanent and highly cross-linked fibrotic scar that could not be reabsorbed[104]. Therefore, although cardiomyocyte proliferation is still a pre-requisite for cardiac replenishment, regenerative success also relies on the immune system and its ability to regulate revascularisation, fibrosis, and the formation and degradation of a transient scar.

Since these studies initially highlighted macrophages as playing key roles in regeneration, much evidence has now accumulated that reveals that the entire immune response regulates regenerative success. Disruption of the immune response, either by broad-spectrum anti-inflammatory treatment[105,106] or by genetic-perturbations that result in excessive inflammation[107], completely abolishes regeneration in the zebrafish and the neonatal mouse. On the other hand, stimulation of the immune response enhances regeneration in the zebrafish via preconditioning[108], and can even improve regenerative repair in the non-regenerative medaka[109]. Therefore, if we are to ever develop effective regenerative therapies, it is imperative that we understand the role of the immune system in cardiac regeneration.

1.3 The Immune System is a master regulator of regeneration and scarring following injury

1.3.1 The Immune System: a universal tool kit that is essential for survival and homeostasis

The need to defend against pathogens and toxins; respond to damage; and distinguish between 'self' and 'non-self' is fundamental to the homeostasis and survival of all living organisms. Life is simply not viable without a functioning immune system and conditions with defective immune systems, such as severe combined immunodeficiency (SCID), are fatal[110]. The immune system is a broad term that refers to the complex and interconnected network of effector cells, inflammatory signals, chemicals, proteins, tissues and organs that make up an organism's defence mechanisms. In higher vertebrates, the immune system is made up of two branches (Fig 1.3):

1) The Innate Immune System
2) The Adaptive Immune System

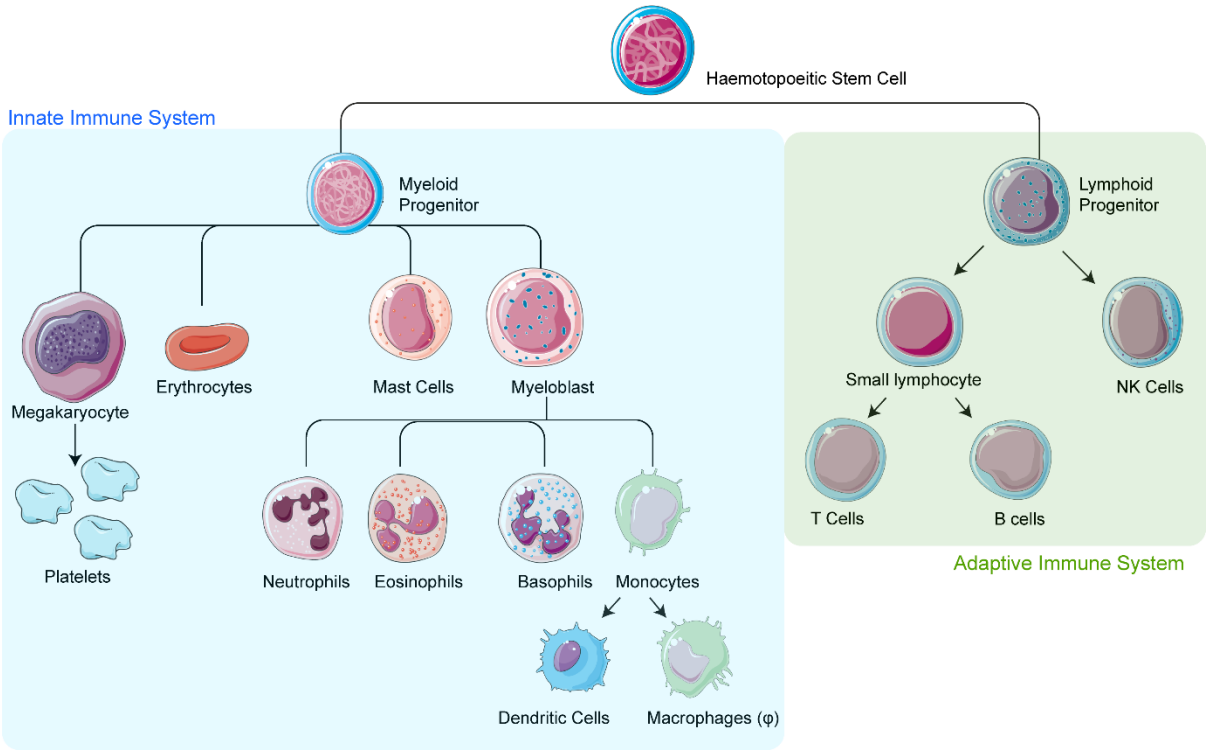

Figure 1. 3: Overview of innate and adaptive immune systems

Cells of the innate immune system are collectively referred to as myeloid cells as they originate from a common myeloid progenitor whilst cells of the adaptive immune response originate from a common lymphoid precursor and thus are collectively referred to as lymphoid cells. NK-Natural Killer Cells

Although the presence of an immune system is universal across the animal kingdom, it varies in its complexity and sophistication. The main drivers of complexity in the immune system are the ability to produce antigen-specific receptors and to form immunological memory following pathogen exposure. In higher vertebrates, the adaptive immune system evolved approximately 150-100 million years[111,112] after the innate immune system and, as such, is responsible for specific antigen-recognition and immunological memory. In higher vertebrates, cells of the innate immune system (i.e. myeloid cells) express germline-encoded pattern-recognition receptors (PRRs) which recognise non-specific patterns present on distinct classes of pathogen. In contrast, cells of the adaptive immune system (i.e. lymphoid cells) can produce a diverse repertoire of receptors that recognise specific antigens through the somatic diversification of antigen-recognition receptor genes[113]. These receptors are expressed on adaptive immune cells so that each cell expresses one unique receptor. This ability to recognise specific antigens confers the adaptive immune system with immunological memory – it can remember antigens it has previously encountered and, in response to re-exposure, will launch a rapid and more intense immune response that efficiently eliminates the pathogen[114].

1.3.2 The Adaptive Immune system: a barrier to regeneration?

Whilst a mature and complex adaptive immune system provides the huge benefit of lifelong immunity to higher vertebrates and mammals, its complexity seems to be counter-productive for regeneration. Comparisons across the phylogenetic tree have revealed an inverse correlation between immune system complexity and regenerative capacity (Fig. 1.4). Indeed, a common theme amongst adult regenerative models, such as the zebrafish and the axolotl, is the presence of an immature and unsophisticated immune system that is characterised by limited pro-inflammatory responses and a lack of adaptive immune cell diversity. This association is further supported by

models, like the neonatal mouse and the frog, in which the end of the regenerative window coincides with the maturation of the adaptive immune system[115] (P1-P6 neonatal mice have an immature and undeveloped adaptive immune system[116]). From these associations, a widely-respected theory has emerged that a component of the adult mammalian adaptive immune system acts as a barrier to regeneration which is absent in primitive regenerative models with unsophisticated adaptive immune systems[117–119].

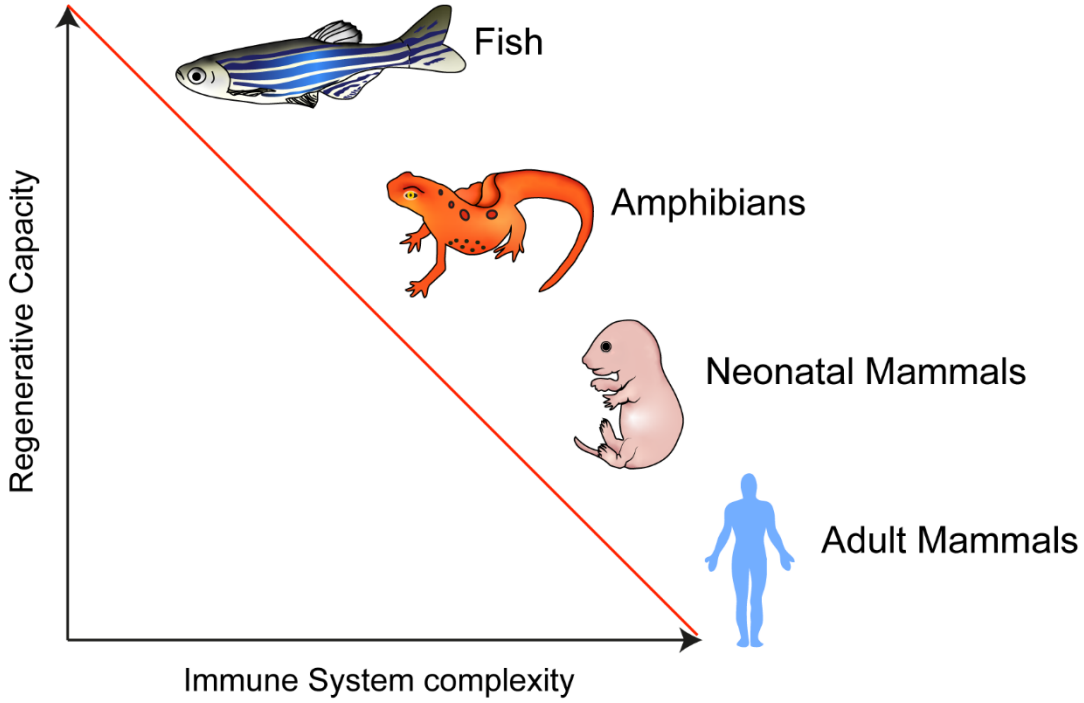

Figure 1. 4: Regenerative capacity and immune system complexity show an inverse relationship

The zebrafish and other lower vertebrates (i.e. fish, salamanders and amphibians) have the ability to regenerate many of their organs and tissues such as their spinal cord, retinas, fins and limbs. However, as vertebrates have evolved into higher vertebrates (i.e. birds and mammals), their immune systems have increased in complexity with a corresponding decrease in regenerative capacity. In mammals, regenerative capacity decreases with developmental stage (from foetal to neonate to adult) as their immune systems mature. Figure adapted from Julier et al (2017)[119]

1.3.3 What is the immune response to cardiac injury?

The immune response to cardiac injury is a dynamic response in which, following the release of activating inflammatory signals, innate and adaptive leukocytes are sequentially recruited to the wound to remove tissue debris, resolve inflammation, and coordinate revascularisation and scar formation. It can be temporally divided into 1) a **pro-inflammatory** phase (1-7 days post-injury (dpi)) during which leukocytes are recruited to the wound to clear necrotic debris; and 2) a **reparative** phase (7-14dpi) during which inflammation is resolved and leukocytes orchestrate cardiac repair. The processes of inflammation initiation, propagation and resolution, and leukocyte recruitment are common between the regenerative and scarring response[8,120]. However, significant differences in the extent of inflammation; the response of cardiac resident cells and recruited leukocytes to inflammatory signals; and the spatiotemporal dynamics of leukocytes have been shown to critically regulate permanent scarring vs complete tissue replenishment.

The inflammatory phase

Following MI, a plethora of proteins, enzymes and chemicals burst into the extracellular space as damaged cells release their internal contents. The aberrant presence of these intracellular components raises the alarm and signals to the surrounding cells, via their PRRs, that tissue damage has occurred. In response, a downstream cascade of inflammatory signalling is induced in the surrounding endothelium, fibroblasts, surviving cardiomyocytes and tissue-resident leukocytes, which results in the production and secretion of a diverse range of pro-inflammatory cytokines such as interleukin-6 (IL-6), interleukin-18 (IL-18), interleukin-1β (IL-1β) and tumour necrosis factor α (TNFα)[121]. These pro-inflammatory signals act as chemotactic gradients that recruit cells of the immune system to the site of injury in order to coordinate cardiac repair.

Inflammasome activation

The proteins released by injured cells upon necrotic cell death are collectively referred to as damaged-associated molecular patterns (DAMPs) and include nucleic acids, ATP, fragmented ECM

and heat-shock proteins[122,123]. Necrotic cells also release reactive oxygen species (ROS) from their necrotic mitochondria. Both DAMPs and ROS act as activating ligands for PRRs, such as Toll-like receptors (TLRs) and NOD-like receptors (NLRs), which in turn activate the inflammasome[124]. The inflammasome is a multiprotein oligomeric complex found in tissue-resident leukocytes, fibroblasts, endothelial cells and cardiomyocytes that results in the proteolysis and secretion of IL-1β and IL-18. IL-1β is a major inflammatory signal that propagates inflammation by stimulating the release of additional pro-inflammatory cytokines such as IL-6, TNFα and IL-1α[121].

Complement System Activation

DAMPs can additionally activate the complement system. The complement system is a critical part of the innate immune system and facilitates the phagocytosis of dead/dying cells by leukocytes. It is made up of circulating inactive proteins and enzymes that, when activated, perform a succession of proteolytic reactions that culminate in the cleavage and release of biologically active peptides. These peptides, such as C3a and C5a, act as chemoattractants to recruit leukocytes[125]. Additionally, they facilitate leukocyte recruitment and extravasation by activating the endothelium, increasing vascular permeability and the expression of endothelial leukocyte-adhesion proteins[126].

Leukocyte Recruitment

Leukocytes are serially recruited to the injured myocardium in response to the extensive pro-inflammatory cytokines, chemokines and chemoattractant signals where they act to remove dead/dying cells by phagocytosis and clear the tissue of any remaining debris[127]. Neutrophils are the first myeloid cells to be rapidly recruited to the wound where they engulf tissue debris; release degradative enzymes that break down the ECM; and release chemoattractants that recruit monocytes[128]. Recruited monocytes differentiate into phagocytic inflammatory macrophages and dendritic cells when they enter the wound that further clear the injury site of debris by phagocytosis and protease secretion[129]. Additionally, monocytes/macrophages are antigen-presenting cells and activate lymphoid cells of the adaptive immune system to directly lyse dying cells, further secrete

inflammatory signals and perform an immunomodulatory role[130]. Inflammatory immune cells are continually recruited during the inflammatory phase until the wound is cleared of all tissue debris. At this point, inflammation is actively repressed and the reparative phase takes over.

The reparative phase of the immune response orchestrates revascularisation, fibroblast proliferation and scar deposition

In the reparative phase of the immune response, recruited leukocytes polarise towards an anti-inflammatory phenotype. These recruited innate and adaptive immune cells act as extensive sources of pro-reparative signals such as cytokines, chemokines, proteases and growth factors that are necessary to: stimulate the restoration of the coronary vasculature; remodel the wounded ECM; promote the proliferation of (myo)fibroblasts; and stimulate scar deposition.

Revascularisation and angiogenesis

In order to supply the healing infarcted tissue with oxygen and nutrients from the blood, the coordinated proliferation and migration of endothelium, pericytes and smooth muscle is required to form new blood vessels. Anti-inflammatory neutrophils, macrophages and dendritic cells, have been shown to coordinate and stimulate this complex process through the release of mitogenic paracrine signals, such as vascular endothelial growth factor (VEGF) and platelet-derived growth factor (PDGF), as well as through cell-cell interactions that help prune and organise the new network of blood vessels[131].

ECM remodelling

After MI, the ECM is broken down by matrix metalloproteinases (MMPs) released by recruited leukocytes and resident cardiac cells during the inflammatory phase. In its place, a provisional matrix of fibrin proteins is formed by plasma cells during blood coagulation and clot formation after injury[132]. Although this fibrin clot seems to play several key signalling roles, it does not provide any structural support and needs to be degraded to make way for the collagen scar. This

is largely mediated by macrophages which directly secrete MMPs[133] and activate the secretion of MMPs and additional matrix-remodelling enzymes from fibroblasts.

Fibroblast activation, myofibroblasts and scar deposition

The formation of the collagen scar is the ultimate goal of cardiac repair in the adult mammalian heart. Scar deposition is critically coordinated via the immune response through a multitude of mechanisms. Firstly, macrophages secrete transforming growth factor β (TGFβ)[134] which is essential for the production of ECM-producing myofibroblasts. Myofibroblasts are absent from the uninjured heart but show a significant increase in their population following injury as TGFβ-activated fibroblasts undergo a phenotypic switch, upregulate α-smooth muscle actin, and transdifferentiate into scar-producing cells. Secondly, macrophages actively recruit myofibroblasts to the site of injury by secreting attractive chemokines such as CCL7 and CCL8[135], ensuring the correct spatial organisation of the deposited scar. Recently, macrophages have been shown to not only coordinate scar deposition but to also secrete collagen proteins to the scar, revealing that leukocytes also contribute to scar formation directly[136]. Once the collagen scar is initially deposited, it undergoes a period of maturation, during which fibrillar type I and type II collagens are deposited and cross-linked to form a strong and stable scar.

1.3.4 How is the immune response different between regeneration and scarring?

Once the scar has been formed post-MI, the regenerative and scarring responses significantly diverge. In non-regenerative models like the human, the collagen scar is permanent and, for reasons still unknown, it will either remain stable or will re-trigger inflammation and fibrosis, leading to cardiac decline and HF. In contrast, in regenerative models, the collagen scar is gradually resorbed, and the wounded tissue is replenished with healthy new myocardium. Although the exact signals governing scar resorption are yet to be elucidated, it seems that the immune response plays a master regulatory role throughout post-MI repair, finetuning the balance between inflammation, cardiomyocyte proliferation and scar deposition[137]. Although much research still

needs to be done, comparative studies between the regenerative and scarring responses, as well as between regenerative models, have highlighted key components of the immune response that are essential for regenerative capacity.

The immune response directly induces cardiomyocyte proliferation in regenerative models

The initiation of sterile inflammation is shared between the regenerative and scarring responses; however, it results in vastly different outcomes in the two settings. In non-regenerative models, inflammation can exacerbate tissue injury and lead to increased infarct sizes whereas in regenerative models, inflammatory signals directly induce cardiomyocytes to proliferate. Indeed, inhibition of inflammatory signal transduction in cardiomyocytes through cardiomyocyte-specific deletion of signal transducer and activator of transcription 3 (STAT3, acts downstream of IL-6), will inhibit cardiomyocyte proliferation in the neonatal mouse[106]. Furthermore, inflammation has been shown to induce neonatal cardiomyocyte proliferation *in vitro* and in the absence of injury *in vivo*[106], revealing that inflammation is a sufficient signal to induce proliferation and suggesting that inflammation plays a prominent role in regulating cardiomyocyte renewal. This is further supported as the regulation of cardiomyocyte proliferation by inflammation has been evolutionarily conserved across the animal kingdom: in the axolotl, zebrafish and neonatal mouse, inhibition of inflammatory signalling via C5aR1 inhibits cardiomyocyte proliferation after injury[138].

In addition to inflammation, the regenerative immune response triggers cardiomyocyte proliferation through paracrine mitogenic signals released by recruited leukocytes. So far, these paracrine factors seem to be uniquely expressed in regenerative leukocytes and are absent in their scarring leukocyte counterparts. Zebrafish regulatory T cells (Tregs) have been shown to secrete Neuregulin-1[139] whilst neonatal mouse Tregs secrete Ccl24, Gas6 and Areg[140] to trigger cardiomyocyte proliferation. Macrophages have also been observed to secrete many mitogenic factors in the neonatal mouse in response to injury such as Ccl24, Areg[141] and Clcf1[141]. Additionally,

macrophages also secrete oncostatin M (OSM) which promotes sarcomere disassembly and cardiomyocyte dedifferentiation[142].

Leukocytes show key transcriptomic differences in the regenerative and scarring setting

Transcriptomic comparisons between regenerative and non-regenerative models have highlighted key differences in leukocyte gene expression. Bulk RNAseq data from neonatal and adult mouse macrophages has shown that, in response to injury, P1 macrophages specifically upregulate genes involved in angiogenesis and oxidative stress whereas P14 macrophages upregulate cell motility genes[103]. Furthermore, comparison between P1 and P8 neonatal hearts has shown that P1 immune cells uniquely upregulate T cell activation and humoral immunity which was not seen in P8 hearts[143]. Additionally, the medaka and zebrafish show significant transcriptomic differences, with the non-regenerating medaka strongly upregulating neutrophil/monocyte chemotaxis and neutrophil differentiation whereas the zebrafish upregulates phagocytosis and the adaptive immune system[109].

Regeneration and scarring show significantly different spatiotemporal leukocyte dynamics

Comparisons between the regenerative and scarring responses have revealed that significant differences in leukocyte spatiotemporal dynamics can drive differential regenerative capacity. Reciprocal analysis between the regenerative zebrafish and the closely-related medaka has found that the spatiotemporal dynamics of both neutrophils and macrophages were significantly different between regeneration and scarring[109]. The medaka showed delayed neutrophil clearance as well as a delayed and reduced macrophage response. Strikingly, however, when TLR signalling in the medaka was stimulated to accelerate neutrophil clearance and increase the macrophage response, the regenerative capacity of the medaka was improved; there was increased cardiomyocyte proliferation, scar resorption and revascularisation. Furthermore, comparisons between the neonatal and adult mouse identified significantly different monocyte and macrophage responses between regeneration and scaring in terms of the magnitude and kinetics[103]. Therefore, it

seems that the number of recruited leukocytes, as well as the timing of influx and efflux, is critical for regenerative success. This is further exemplified by ablation studies which disrupt the timing of macrophage and Treg[139] entry and exit from the wound. These ablation studies have led to the total inhibition of regeneration in the axolotl[104], zebrafish[109] and neonatal mouse[103] due to increased fibrosis, impaired angiogenesis and cardiomyocyte proliferation.

As leukocytes seemingly play critical roles in the coordination of key regenerative processes such as angiogenesis, cardiomyocyte proliferation, debris removal, inflammation resolution and scar deposition, it seems very likely that any disruption to their tightly coordinated and regulated influx and efflux from the injured heart would have a wide range of knock-on effects that disrupt regenerative repair.

Distinct leukocyte subpopulations mediate different aspects of regenerative repair

So far, we have discussed innate and adaptive immune cells broadly as uniform populations. However, immune cells are much more complex than that and neutrophils, monocytes, macrophages, T cells etc, can be further classified into distinct, heterogeneous sub-populations that play differential roles within regenerative repair. For instance, *tnfa*$^{+}$ and *tnfa*$^{-}$ macrophages have recently been characterised in the zebrafish which play distinct roles within cardiac repair: *tnfa*$^{+}$ macrophages promote scar deposition whilst *tnfa*$^{-}$ macrophages facilitate scar removal during regenerative healing[144]. Distinct macrophage and monocyte populations have also been observed in the mouse: Ly6C^{high} monocytes give rise to pro-inflammatory macrophages that facilitate debris removal from the wound whereas Ly6C^{low} monocytes differentiate into anti-inflammatory macrophages that stimulate angiogenesis and scar deposition[145–147].

Comparisons between the regenerative and non-regenerative setting have shown that differences in leukocyte subpopulations can drive differential regenerative capacity. Indeed, comparisons between the neonatal and adult mouse have shown significant differences in their macrophage subpopulations. Prior to injury, the neonatal mouse is populated by embryonically-

derived MHC-II^{low}CCR2^{-} macrophages. In response to injury, this macrophage population selectively expands where it stimulates regeneration via promoting angiogenesis and cardiomyocyte proliferation. In contrast, adult mice are unable to proliferate their MHC-II^{low}CCR2^{-} tissue-resident macrophages after injury. Instead, these cells die and are replaced by recruited CCR2^{+} monocyte-derived macrophages which are pro-inflammatory and promote adverse ventricular remodelling[37]. Furthermore, transplantation of neonatal macrophage subpopulations into adult hearts leads to improved regenerative capacity, with decreased scarring and increased cardiomyocyte proliferation, suggesting the distinct leukocytes can mediate their regenerative roles, regardless of the cellular environment.

Timely resolution of inflammation is crucial to regenerative success

The key theme that emerges from regenerative models is that a "goldilocks" level of inflammation is required for regenerative success. "Too much" and excessive inflammation will abolish regeneration and lead to fibrotic scarring, whilst "not enough" inflammation that is insufficient/inhibited/or terminated too early will also result in regeneration inhibition. However, when this inflammatory signalling is "just right" it can initiate regeneration by promoting cardiomyocyte proliferation, scar deposition and degradation, and even induce non-proliferative cardiomyocytes in the medaka and adult mouse to re-enter the cell cycle and proliferate. As many regenerative models have a limited and dampened inflammatory response to tissue damage, it is thought that excessive inflammation in mammals is critically contributing to their regenerative failure. Indeed, prolonged inflammation has been shown to enhance fibrosis and worsen functional recovery in adult rodents[148] whilst completely inhibiting regeneration in the zebrafish[144]. Furthermore, in the clinic, chronic inflammation leads to increased infarct sizes and adverse ventricular remodelling in post-MI patients and is associated with increased incidences of HF[149–152]. As such, the contemporary consensus is that the timely resolution of inflammation is critical to regenerative success.

Although the exact signals that resolve inflammation are far from being elucidated, accumulating evidence suggests that leukocytes play a major role in actively suppressing inflammation post cardiac injury. The removal of apoptotic neutrophils by macrophage engulfment has been shown to initiate the process of inflammation resolution[153] and stimulates the production of anti-inflammatory cytokines VEGF, TGFβ1[154] and IL-10[155]. Macrophages also secrete oncostatin M which actively supresses fibroblast activation to prevent fibrosis[156]. Furthermore, recruited Tregs have been shown to secrete TGFβ1 and IL-10 to resolve inflammation, as well as attenuating the inflammatory response by promoting the polarisation of Ly6C^{high} monocytes towards anti-inflammatory macrophages[157].

In conclusion, it is apparent that a pro-regenerative immune response requires:

1) The onset of inflammation to induce CM proliferation and recruit leukocytes
2) Tightly controlled influx of distinct leukocyte subpopulations that perform specific reparative and regenerative roles of wound debris clearance; inflammation resolution; secretion of paracrine factors which stimulate CM proliferation, angiogenesis and myofibroblast activation; and regulation of scar deposition and degradation

1.4 The *Astyanax Mexicanus*: a uniquely suited model for studying cardiac regeneration

1.4.1 The key to unlocking the secrets of the regenerating heart is comparing fibrotic scarring with regenerative success

Despite the numerous mechanisms and models of cardiac regeneration that have been discovered, we are not much closer to stimulating regeneration in the human heart. This is largely because many studies have relied on candidate approaches and reverse genetics. In these approaches, genes, molecules or signalling pathways that are already predicted to be important in regeneration are investigated. Although the candidate approach has enabled highly relevant genes

and signalling pathways to be prioritised and tested, it is limited by a significant drawback: it is inherently biased and cannot be used to identify previously unknown pathways that may be key to regeneration. In contrast, the comparative approach (i.e. the comparison of at least two different models of regeneration) offers an unbiased way to screen for key genes, signalling pathways and regenerative cells. As it is not limited by previous knowledge, it can be used to identify novel pathways that have not previously been linked to regeneration and holds great promise for unlocking the secrets of the regenerating heart[*].

To date, applying the comparative approach to the mysteries of the regenerative heart has led to significant breakthroughs in our understanding of the key cellular and molecular signals that govern regenerative success and failure. For example, Wang et al were able to identify regenerative-responsive enhancers as master regulators of regeneration by comparing the regenerative zebrafish and killifish[30]. Critically, they showed that these enhancers triggered a pro-regulatory gene program in response to injury, whilst their counterparts in non-regenerative models like the human were mutated. Additionally, the comparative approach has been used to identify novel cell behaviours that have not previously been linked to regeneration as it does not rely on previous, and potentially biased, knowledge. Indeed, Simões et al. used the comparative approach to identify that macrophages directly contribute collagen proteins to the forming scar[136], a cellular behaviour which was unknown for macrophages. Finally, comparisons between successful regeneration and scarring have already identified that both the temporal dynamics of myeloid cells post-injury[109] and the structural composition of the ECM[86], are key checkpoints that regulate regenerative success vs fibrotic scarring. Therefore, the comparative approach holds great promise for enhancing our understanding of the key signals that regulate regeneration and will ultimately be essential to the development of an effective therapy for stimulating the adult human heart to repair itself.

[*] Denotes paragraph I have previously published in "Unlocking the Secrets of the Regenerating Fish Heart: Comparing Regenerative Models to Shed Light on Successful Regeneration" Potts et al (2021)

Unfortunately, however, despite the great potential of the comparative and forward genetics approach, its application to cardiac regeneration has so far been limited due to some uniquely challenging barriers. One of the major limiting factors of the comparative approach is that comparisons can be confounded by both developmental (such as neonate vs adult mouse) and interspecies differences (such as zebrafish vs medaka). Different physiologies, morphologies and epigenetic changes that arise from different evolutionary selection pressures and developmental stages can make it difficult to identify which differences are driving regenerative capacity, rather than just being artefacts of evolutionary distance and development. In addition, traditional forward mutagenic screens for cardiac regeneration are simply not feasible in animal models. This is because assessing regenerative capacity requires culling the unique mutant so that its heart can be dissected and stained. This means that, to prevent any mutations of interest from being lost, all mutants would need to be bred prior to screening which would require the use of too many animals.[†]

Therefore, to truly capitalise on the power of the comparative approach, a new model of cardiac regeneration is required which can overcome the barriers of developmental and interspecies differences, and is amenable to forwards genetics. Ideally, such a model would consist of 2 populations from the same species that showed distinct regenerative and scarring responses to injury at the same developmental stage. Furthermore, in an ideal model, the regenerative and scarring populations would be able to interbreed so that the genetic heritability of regenerative success could be probed. It is only through directly comparing regenerative models to non-regenerative models that we can fully understand how regeneration can fail and what key signals need to be replicated to induce cardiac healing in the adult human heart.

[†] I have previously published text within the paragraph in “Unlocking the Secrets of the Regenerating Fish Heart: Comparing Regenerative Models to Shed Light on Successful Regeneration” Potts et al (2021)

1.4.2 *Astyanax mexicanus (AM):* a comparative model uniquely suited for studying cardiac regeneration

The *A. mexicanus* is a teleost fish that has recently been introduced by the Mommersteeg lab as a novel comparative model of human-like scarring and complete cardiac regeneration[29]. The AM is made up of closely related surface-dwelling and cave-dwelling populations that have a differential regenerative capacity. These separate fish populations arose 10,000-1 million years ago when changes in river levels isolated a series of caves in North-Eastern Mexico from the surrounding rivers[158–161]. From this point, the surface- and cave-dwelling populations began to diverge in their evolution as they adapted to their local environment. During this process of divergence and adaptation, cave-dwelling populations lost redundant features, such as their eyes and pigment, and instead gained features that are beneficial to cave life like their altered metabolism which enables them to cope with a scarcity of food and long periods of fasting[162–164] (Fig. 1.5a & b).

Despite showing the same capacity for fin regeneration, cave-dwelling populations have lost the capacity to fully repair their hearts following injury. Indeed, following ventricular resection, adult surface-dwelling fish (SF) and adult fish from the Pachón cave (PF) will both initially form a collagen scar (Fig. 1.5c & d). However, the SF can gradually resorb this scar and replace it with healthy new myocardium (Fig. 1.5e), reaching full regeneration by 90dpi. In contrast, the PF scarring response is permanent, much like the adult human heart, with PF hearts still showing scar tissue at 100dpi and one-year after injury (Fig. 1.5f & g). Therefore, the SF and PF populations of the AM enable powerful comparisons to be made between successful cardiac regeneration and scarring that are not limited by either interspecies or developmental differences.

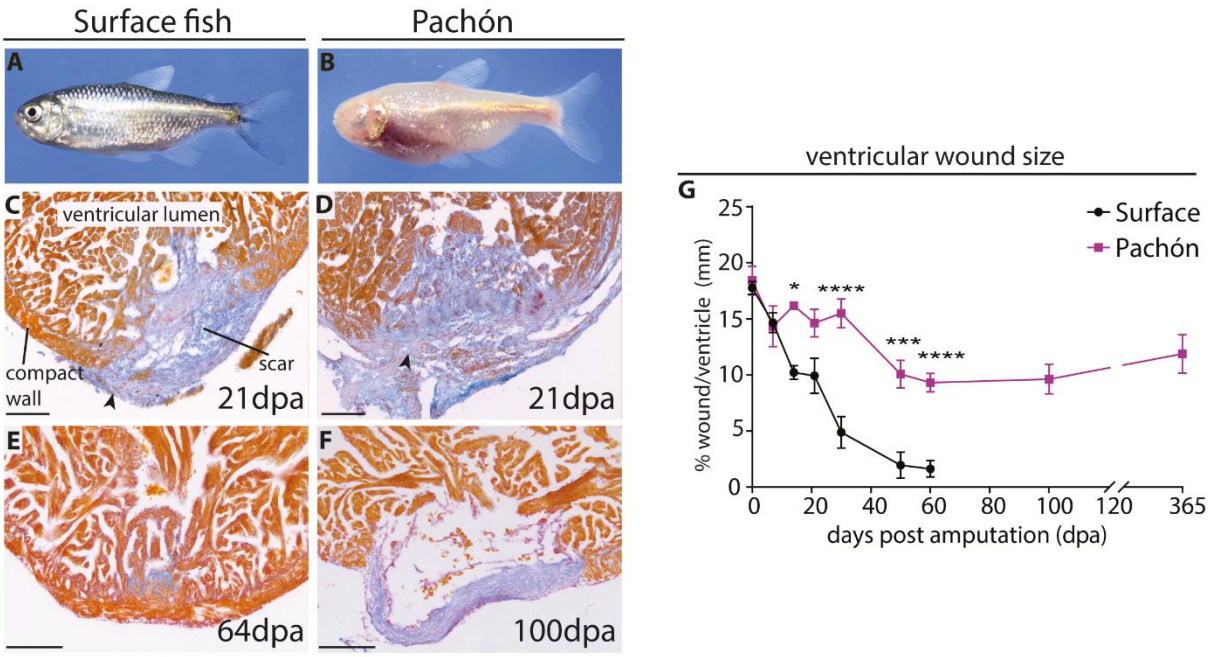

Figure 1. 5: The AM is the best comparative model of successful regeneration and scarring

(A*) Adult SF. (B) Adult PF. (C-F) AFOG staining is a histological stain that is used to assess regenerative capacity as it stains healthy myocardium orange, collagen scar blue and fibrin in red. After amputation of the ventricle apex, both the SF (C) and PF (D) initially form a collagen scar at 21dpi. However, by 64dpi, the SF has resorbed much of the collagen scar and replaced it with healthy new myocardium (E). In contrast, a permanent collagen scar can still be visualised in the PF at 100dpi (F). (G) Quantification of the percentage of heart that was wounded was performed for SF and PF for up to 1 year after injury, showing that the persistence of the scar in PF is permanent. Figure adapted from Stockdale et al (2018)*[29]

Additionally, as the SF and PF are still members of the same species (and thus can interbreed to produce fertile offspring), the AM model is uniquely amenable to a forwards genetics approach and can be used to identify novel genes that are necessary for regenerative repair. Indeed, in Stockdale et al[29], such an approach was taken. The authors interbred a PF and a SF (the founding F_0 generation) to produce the F_1 generation, in which each fish had chromosomal pairs made up of 1 PF chromosome and 1 SF chromosome. Two F_1 siblings were then incrossed to produce the F_2

generation. Due to the process of homologous recombination that occurs during meiosis and the formation of gametes, the chromosomes of the F_2 generation were made up of a mixture of PF and SF genomic DNA (Fig. 1.6a). Remarkably, rather than having a binary range of regenerative capacity, this F_2 generation showed a continuous range of regenerative ability at 90dpi, from full cardiomyocyte replacement to no regeneration (Fig. 1.6b & c). Following characterisation of the regenerative capacity of the F2 generation, their genomes were sequenced, and a Quantitative Trait Locus (QTL) analysis was performed. QTL analysis is a statistical method that enables the genetic basis of complex phenotypic traits to be explored by linking genotypic data with distinct phenotypic traits[165]. Here, Stockdale et al categorised the F2 generation into different groups according to their regenerative capacity (i.e. the phenotypic trait, Fig. 1.6b & c) and, using their sequencing data, were able to identify 3 loci in the AM genome that were significantly linked to the degree of regeneration (Fig. 1.6d). These loci contain many novel genes that have never previously been linked to regeneration, such as *lrrc10,* and represent a list of potential candidate genes that could be driving the AM differential regenerative capacity.

Therefore, the AM represents a unique model that holds great promise for unlocking the secrets of the regenerating heart. It is hoped that by fully understanding the PF and SF responses to cardiac injury, the key checkpoints at which regeneration either succeeds or fails can be pinpointed. If these checkpoints can be manipulated in the PF to reverse regenerative failure, this would be a significant breakthrough in the development of effective therapeutics that stimulate cardiac regeneration in the adult human heart.

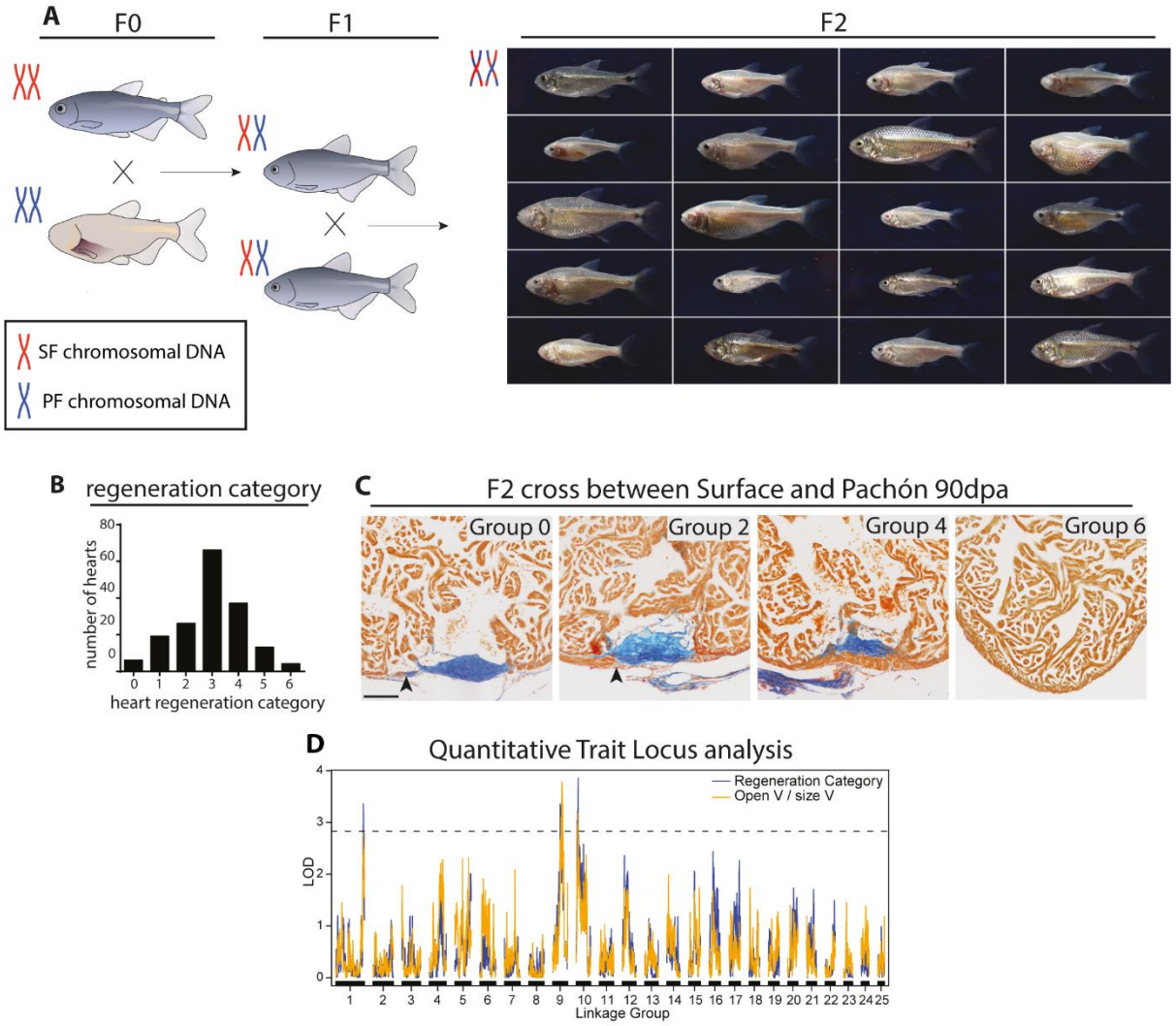

Figure 1. 6: Forwards genetic approach has unbiasedly identified three loci of the AM genome that are significantly linked to cardiac regeneration

(A) Schematic for the generation of the F_2 offspring. During the crossing of the F_1 generation, PF and SF chromosomes undergo homologous recombination, resulting in the production of F_2 chromosomes that are a random mix of both PF and SF genomic DNA. For the QTL analysis, 188 F2 generation fish were injured by resection and stained with AFOG. The resultant AFOG images were sorted into degree of regeneration (0=no regeneration 6=full regeneration). (B) Bar chart of the number of hearts that fell into each regeneration category. (C) Representative AFOG images of each regeneration category. Group 0 showed no sign of regeneration; Group 2 shows some thickening of the compact wall but no overgrowth of over the scar; Group 4 has a completely regenerated compact

wall; Group 6 display full regeneration. (D) As a result of the QTL analysis, three regions of the AM genome were significantly associated with regeneration by de novo linkage analysis (as visualised by the dotted line). The QTL analysis was performed using two measurements of regenerative capacity for each heart: 1) categorisation into 1 of 7 discrete regeneration categories 2) calculation of the percentage of open wound in each heart (proportion of open wound: total ventricle). Figure adapted from (Stockdale et al, 2018)[29]

1.5 DPhil Project

1.5.1 Rationale

To identify the complex cellular and molecular mechanisms that are regulating differential regenerative capacity in the AM, the Mommersteeg lab has already characterised the proliferative response of PF/SF cardiomyocytes to injury and performed a powerful comparison of bulk RNAseq data (Table 1.2).

	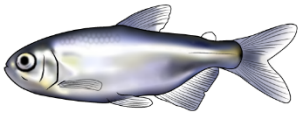	
Cell Proliferation	CM peaks at 7dpi Able to complete CM cytokinesis and form new cells	CM peaks at 7dpi Unknown if unable to complete CM cytokinesis or proliferating CM die by apoptosis ↑ Endocardial proliferation at 14/30dpi ↑ Epicardial proliferation
Metabolism	↑ Amino acid activation ↑ Ribosome biogenesis ↑ Ion channel complex	↓ mitochondrial pathways ↓ glycolytic pathways
Immune Response	↓ Innate immune response ↓ Adaptive immune response	↑ Innate immune response ↑ Adaptive immune response
Scarring Response	↓ Collagen turnover ↓ ECM	↑ Collagen turnover ↑ ECM

Table 1. 2: Summary of what is currently known about the SF and PF responses to cardiac injury

Findings from Stockdale et al (2018)[29]

Remarkably, the PF and SF show the same ability to initiate cardiomyocyte proliferation following injury. Using Pcna and Mef2 to visualise proliferating cardiomyocyte nuclei, Stockdale et al found that PF and SF show similar numbers of proliferating cardiomyocytes at 3-, 7-, 14- and 30dpi (Fig. 1.7a-c) whilst bromodeoxyuridine (BrdU) incorporation revealed similar levels of DNA synthesis at 7dpi. However, using a BrdU pulse-chase experiment, Stockdale et al also found that PF and SF do show a significant difference in their ability to complete cardiomyocyte proliferation. Cell counts of $BrdU^+$ cardiomyocytes at 7- and 14dpi revealed that at 14dpi, only the numbers of SF $BrdU^+$ cardiomyocytes had increased whereas PF levels were unchanged from 7dpi (Fig. 1.7d-f). This striking difference suggests that both PF and SF cardiomyocytes can enter the S phase of the cell cycle. However, whilst SF cardiomyocytes can successfully proliferate, PF cardiomyocytes seem to get stuck in the G2/M phase of the cell cycle and cannot complete cytokinesis. Therefore, to determine what network of signals might be regulating the cell cycle roadblock in PF, Stockdale et al performed a powerful bulk RNAseq comparison at 3-, 7-, and 14dpi (Fig. 1.7g). This transcriptomic comparison has pointed towards significant differences in metabolism, scarring and the immune response to injury between PF and SF that could be driving their differential regenerative capacity.

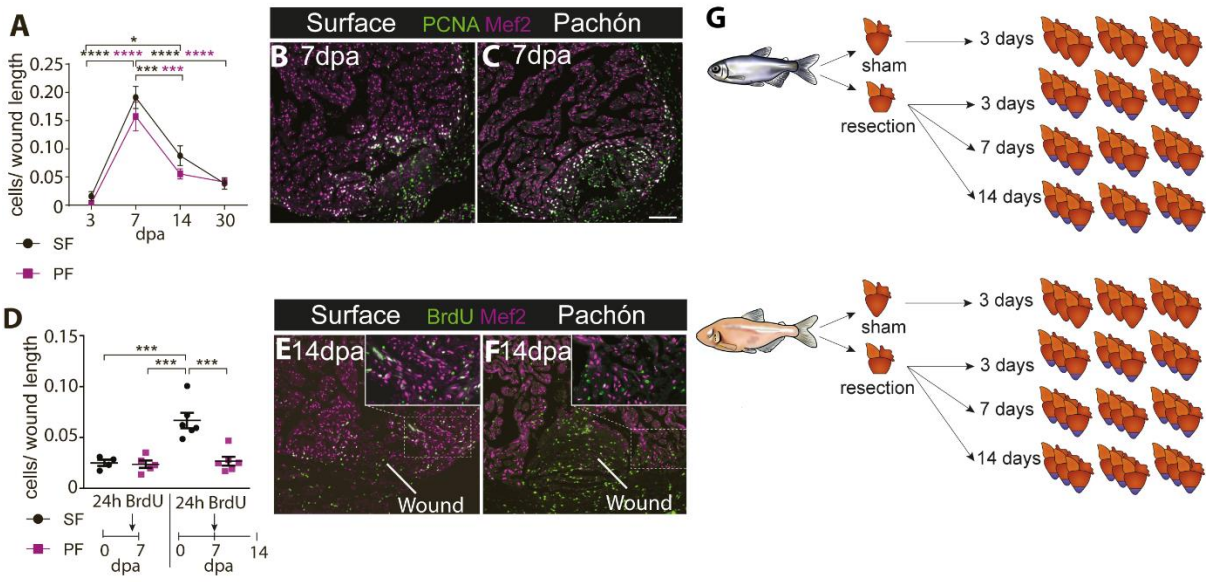

Figure 1. 7: Although cardiomyocyte proliferation peaks at 7dpi in both the Pachón and Surface fish, the Pachón show impaired cardiomyocyte cytokinesis

(A) Pcna (proliferative marker) and Mef2 (cardiomyocyte nuclei marker) were used to stain proliferating cardiomyocytes in PF and SF hearts at 3, 7, 14 and 30dpi. The number of Pcna+ Mef2 nuclei were counted and normalised to the size of the wound, showing that proliferation rates peaked at 7dpi and that the PF and SF show no significant differences in proliferation rates at any time point after injury. (B) Representative images of Pcna staining in PF (B) and SF (C) at 7dpci. (D) 24-hour BrdU incorporation was used to assess proliferation rates at 7- and 14dpi. At 7dpi, PF and SF show no difference in the number of BrdU+ cells. However, at 14dpi, SF show significantly elevated numbers of BrdU+ cells suggesting an increased production of daughter cells following BrdU exposure at 6-7dpi. (B) Representative images of BrdU staining in PF (E) and SF (F) at 14dpci. (G) Schematic of experimental design for the comparative PF/SF bulk RNSAseq dataset. 3 hearts were pooled for PF and SF at each time point.

Although differences in metabolism, scarring and the immune response all demand further exploration, three key pieces of evidence suggest that the AM immune responses are significantly different and could be driving the SF to regenerate whilst resulting in regenerative failure in the PF.

Firstly, the bulk RNAseq identified that the PF show increased upregulation of both the innate and adaptive immune response in comparison to the SF (Fig. 1.8). This is critical as both an excessive innate response and an over-active adaptive immune response have been linked to regenerative failure. As discussed, an overaccumulation of leukocytes and excessive inflammation after cardiac injury are associated with increased infract sizes and fibrosis, suggesting that an unnecessary innate immune response in the PF could be driving permanent scarring. Additionally, the adaptive immune response has been linked to decreased regenerative capacity across the animal kingdom and is associated with autoimmunity, chronic inflammation, and HF in the clinic. As the PF show consistent upregulation of the adaptive immune response whereas the SF specifically

downregulate the adaptive immune response at 7- and 14dpi, this suggests that a late-stage adaptative immune response in the PF could be key in driving its regenerative failure. Therefore, it seems likely that the AM immune responses will differ in their strength, with the PF heart potentially facing a greater burden of innate and adaptive leukocyte infiltration following injury.

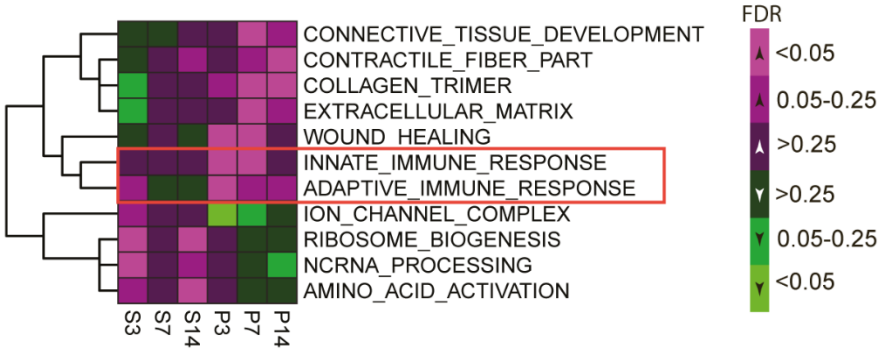

Figure 1. 8: The Pachón immune response is significantly upregulated following injury in comparison to the Surface fish

Data from the bulk RNAseq dataset unbiasedly highlighted significant differences in the PF and SF innate and adaptive immune responses, with the PF showing consistently higher upregulation of the immune response at 3-, 7- and 14dpi in comparison to the SF.

Secondly, many of the genes identified in the QTL analysis are involved in the immune response (Fig. 1.9). This further suggests that differences in the immune response are significantly linked to regenerative capacity in the AM. Critically, the top candidate gene from the QTL analysis was *itgam*, a leukocyte adhesion protein. *Itgam* had the highest number of mutations in its protein-coding regions of all QTL-identified genes. This therefore suggests that the *itgam* protein may be functionally different in the PF/SF, resulting in leukocytes with different binding properties. As *itgam* is expressed on almost all cells of the immune system and regulates leukocyte binding to the endothelium and extravasation into the wound, PF/SF leukocytes may well show significantly different leukocyte kinetics. As regenerative success has already been shown to be critically

dependent on leukocyte spatiotemporal dynamics, especially on the dynamics of neutrophils and macrophages, it again seems likely that significant differences in the PF and SF immune response could be driving their differential regenerative capacity.

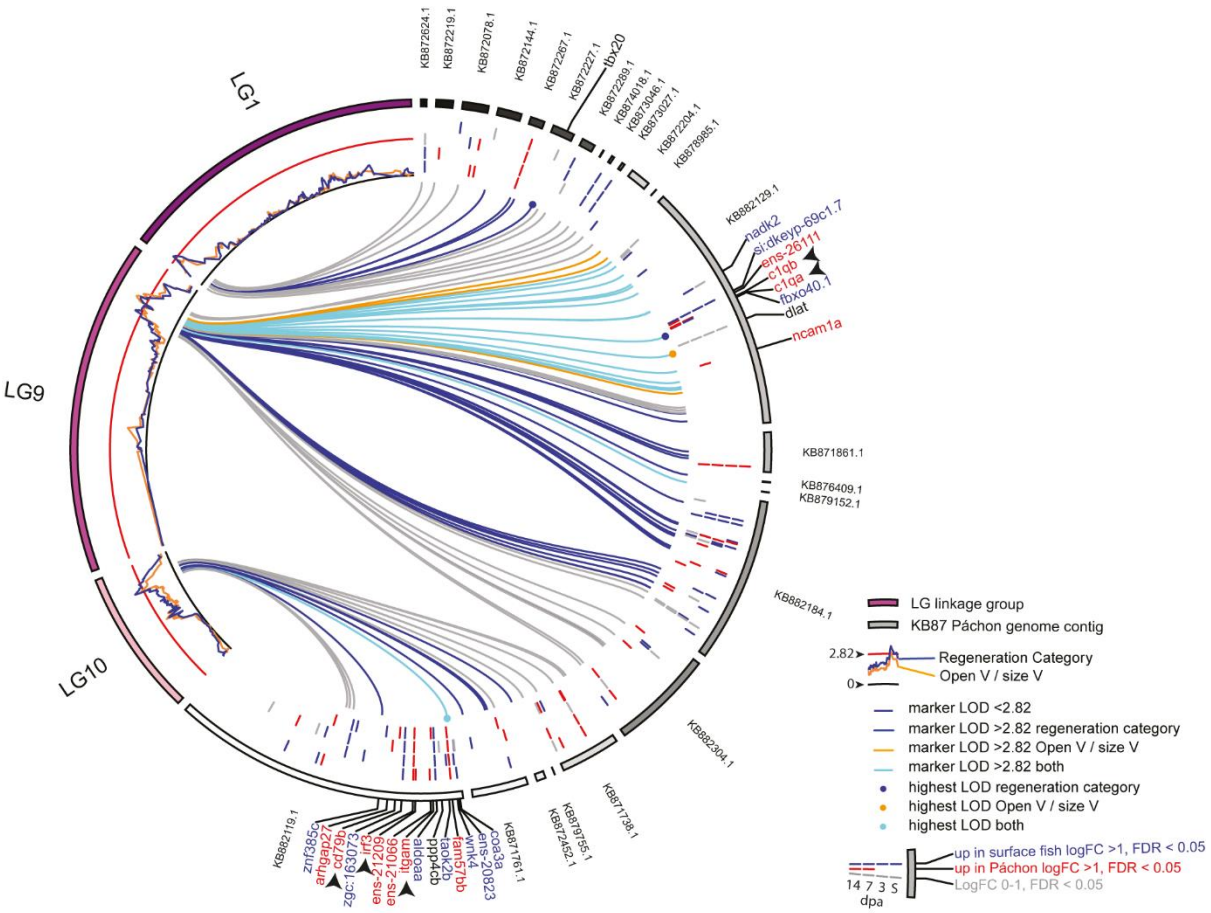

Figure 1. 9: QTL analysis of the PF and SF populations identified numerous genes involved in the immune system that are significantly linked to regeneration

Black arrows indicate immune response genes highlighted by the QTL that are all upregulated in the Pachón.

Thirdly, previous work from Peuß et al has revealed that PF/SF leukocytes are functionally different[166]. The authors found that, *in vitro*, PF leukocytes show decreased phagocytosis; increased sensitivity to stimulation; and a greater pro-inflammatory response, characterised by prolonged and elevated inflammatory cytokine production. These findings have a plethora of implications for the PF

immune response to cardiac tissue damage. A decreased phagocytic ability will mean that tissue debris takes longer to remove in the PF than in the SF, resulting in a prolonged inflammatory phase which could lead to increased fibrosis and scarring. This will seemingly be exacerbated by PF leukocytes that show increased sensitivity to stimulation and secrete greater levels of inflammatory cytokines for prolonged periods of time, further exacerbating the prolonged PF inflammatory phase. Furthermore, Peuß et al also found that, *in vivo,* PF/SF show overall differences in the composition of their immune response to lipopolysaccharides (LPS) injection in the head kidney, with PF showing a reduction in innate immune cells and an overrepresentation of T cells[166]. Taken together, Peuß's *in vitro* and *in vivo* findings suggest that following cardiac injury, the PF and SF could also display significant differences in both the type of leukocytes that influx to the heart and in PF/SF leukocyte functionality.

Finally, there is a wealth of evidence that the immune system is essential to regenerative success, not only in the injured heart, but in many different tissues such as the skin[167], retina[168] and limb[169]. Perturbations of the immune response within the regenerating heart have already been shown to both enhance and inhibit regeneration, suggesting that the immune system exerts fine control over the decision to regenerate after tissue damage or heal by scarring.

Therefore, it seems very likely that the PF/SF will show significantly different immune responses to cardiac injury and, specifically, that the AM immune responses may differ in terms of their inflammatory response, leukocyte functions, leukocyte composition and spatiotemporal leukocyte dynamics. Currently, however, the AM immune response is completely unknown.

1.5.2 Hypothesis

The observed differential regenerative capacity of the Pachón and Surface fish is caused, at least in part, by differences in the immune response to cardiac injury.

1.5.3 Aims

The overarching aim of this thesis was therefore to characterise the AM immune response to cardiac injury. To identify differences in the PF and SF immune response, the following sub-aims were established as experimental objectives:

1) Characterise the number of leukocytes present in the heart after injury
2) Characterise the spatiotemporal dynamics of recruited SF and PF leukocytes
3) Determine whether SF and PF leukocytes are functionally similar
4) Identify any unique SF and/or PF leukocyte populations
5) Pharmacologically manipulate the AM immune response to establish whether differences in SF and PF leukocytes are driving differential regenerative capacity

1.5.4 Methodology

Previously, the AM heart has been injured using ventricular resection. Although this injury model results in the effective removal of up to 20% of the ventricle, it is not very representative of MI where coronary artery occlusion and cardiac cell death results in ischaemia and masses of apoptotic, necrotic and inflammatory signals. Since the field of cardiac regeneration was discovered, alternative models to resection have been developed that better model the post-MI setting. For example, in the neonatal mouse, MI is accurately modelled by obstructing a coronary artery using LAD ligation. However, alternative cardiac injury models have been developed in fish where LAD ligation is not possible due to prohibitively small coronary arteries, such as cryoinjury, cauterisation and mechanical destruction. Within the Mommersteeg lab, unpublished data has already shown that the PF and SF show the same regenerative and scarring responses to both resection and cryoinjury. Therefore, cryoinjury was chosen as the model injury of choice for this thesis so that the AM immune response would be studied within a setting of necrotic cell death and inflammation, to better reflect the necrosis and inflammation observed in the post-MI human heart.

To characterise the AM immune response following necrotic cell death, single cell RNA sequencing of SF and PF ventricles was performed at uninjured, sham, 1-, 3-, 7- and 14- days post-cryoinjury (dpci). Findings from the scRNAseq dataset were validated in heart sections using *in situ* hybridisation and immunofluorescent staining. Finally, *in vivo* pharmacological studies were utilised to test whether inhibiting key signalling pathways in the SF immune response could prevent regeneration.

Chapter II

Materials and Methods

Table 2. 1: Summary of Reagents

Reagent	Supplier & Catalog Number
***In vivo* Drugs**	
Tricaine methanesulfonate (MS-222)	Sigma, # A5040
DMSO	ThermoFisher, # 022914.M1
Saline	CD Medical, # FS533
DHMEQ	Med-Chem Express, # HY-14645
CAY10500	Santa Cruz, # 869998-49-2
Ac-YVAD-cmk	Med-Chem Express, # HY-16990
Leukadherin-1	Med-Chem Express, # 344897-95-6
Dexamethasone	Sigma, # D2915-100MG
Heart Digestion	
2,3-butanedione monoxime	Sigma, # B0753
HEPES	Sigma, # H3393
$CaCl_2$	Sigma, # C4901
Sheep serum	Sigma, # S3772
Glucose	Sigma, # G7528
Taurine	Sigma, # T8691
Collagenase II	Gibco, # 17101-015
Collagenase IV	Gibco, # 17104-019
DNAse I	Sigma, #10104159001
DMEM	Life Technologies, # 22320-022
Fetal Bovine Serum	ThermoFisher, # A3840001
Liberase	Sigma, # 5401119001
HBSS	ThermoFisher, # 14175095
pluriStrainer® 100 µm	Pluriselect, # 43-50100-51
Chemicals	

Phosphate Buffered Saline (PBS)	Sigma, # P4417
Xylene	Sigma, # 214736
4% paraformaldehyde (PFA) in PBS	Santa Cruz, # sc-281692
TNB block	Perkin Elmer # NEL702001KT
Butanol	Sigma, # 281549-1L
Ethanol	Sigma, # 51976
Paraffin wax	Sigma, # 327212
Histoclear	National diagnostics, # AGR1353
Bouin's solution	Sigma, # HT10132
Nuclease-free water	ThermoFisher, # AM9935
Histology	
Methyl blue	Sigma, # 95290
Orange g	Sigma, # O7252
Acid fuchsin	Sigma, # F8129
Phosphomolybdic acid	Alfa Aesar, # 56166
Mowiol 4-88	Sigma, # 81381
DPX mountant	Sigma, # 06522-500ML
Prolong^{tm} gold antifade mountant	ThermoFisher, # P36930
SuperFrost adhesion slides	VWR, # 631-0108
Antigen Unmasking Solution (H-3300)	Vector Laboratories Inc, # H-3301-250
Commercial kits	
10x Chromium Chip B	10x Genomics, # 1000073
10x Chromium Next GEM Single Cell 3' v3.1	10x Genomics, # 1000092
Illumina Nextseq® 500/550 High Output Kit V2	Illumina, # FC-404-2005
RNAscope Multiplex Fluorescent V2 Assay	ACD Biosciences, # 323100
TSA plus Cy3	Perkin Elmer, # NEL744001KT
TSA plus Cy5	Perkin Elmer, # NEL745001KT
TSA plus FITC	Perkin Elmer, # NEL756001KT
Quick-RNA Microprep Kit	Zymo Research, # R1050
Qubit RNA High Sensitivity Assay Kit	Invitrogen, # Q32852
Pico-Sirius Red Stain Kit	Abcam, # ab245887

2.1 Animal husbandry

2.1.1 *Astyanax mexicanus*

All experimental procedures were performed in accordance with the UK Animals (Scientific Procedures) Act 1986 and institutional guidelines. All animal procedures conformed to the guidelines from Directive 2010/63/EU of the European Parliament on the protection of animals used for scientific purposes. Adult male and female *A. mexicanus* fish were maintained in the laboratory on a 14/10-hour photo-period at 22-25°C whilst adult zebrafish were maintained on a 12/12-hour light/dark cycle at 28°C[3].

2.1.2 Cardiac surgery - Cryoinjury

Prior to cryoinjury, fish were anaesthetized in MS-222. Cryoinjury was performed aseptically in a similar manner to that previously described for the zebrafish[40]. First, a small incision was made in the thorax using forceps and spring scissors. Then the chest cavity was held open using forceps to expose the heart. Hearts were dried using sterile tissue paper before a copper cryoprobe was cooled in liquid nitrogen and placed on the ventricle surface until thawing was observed. For sham surgery, the thorax and pericardial sac were opened, and a room temperature cryoprobe was placed on the ventricle. Sham surgery hearts were isolated 3 days after sham surgery and cryoinjured hearts were isolated at 1-, 3-, 7-, 14-, 30- and 60- days post-cryoinjury.

2.1.3 Intraperitoneal *in vivo* inhibitor injections

To keep final concentrations of DMSO to a minimum, all inhibitors were dissolved in DMSO and diluted using sterile saline to reach a maximum final concentration of ≤3% DMSO. Following cryoinjury, fish were randomly assigned to one of five groups: DMSO control, DHMEQ, CAY10500, Ac-YVAD-cmk or Leukadherin-1 (Table 2.2). For intraperitoneal (ip) injections, fish were

[3] Denotes paragraph I have previously published in "Discordant Genome Assemblies Drastically Alter the Interpretation of Single-Cell RNA Sequencing Data Which Can Be Mitigated by a Novel Integration Method" Potts et al (2022)

anaesthetised in MS-222 and injected every 24hrs with 20µL of inhibitor into the ip cavity. Hearts were isolated at the specified time points and processed for RNAseq or paraffin embedding. Inhibitor doses were chosen based on concentrations previously used in zebrafish and in mice[170–173].

Table 2. 2 Summary of inhibitor concentrations used

Drug	Concentration used
DMSO	3%
DHMEQ	4µg/g fish
CAY10500	15µg/g fish
Ac-YVAD-cmk	100µM
Leukadherin-1	100µM

2.1.4 Dexamethasone Exposure

SF morphs were cryoinjured and randomly assigned to one of 4 groups: 30dpci control, 30dpci Dexamethasone, 60dpci control, 60dpci Dexamethasone. At 7-14dpci, fish were exposed to either water-soluble Dexamethasone at 10mg/L or system water for 7 consecutive days. The system/Dexamethasone water was replenished every 24 hours until 15dpci, at which time the fish were washed 3 times for 5 minutes each in fresh system water before returning to system water until their stated end point.

2.2 Single Cell RNA sequencing

2.2.1 *Astyanax mexicanus* heart digestion

Ventricles were isolated and digested using the protocol described previously in Potts et al (2022)[174]. Three ventricles were pooled per sample, collected into ice-cold PBS and minced using spring scissors before transferral into Eppendorf tubes containing 500µL fresh Digestion Buffer. Digestion Buffer was optimised from the recipe described in Sander et al (2013)[175] and consisted of: 1X PBS, 30mM Taurine, 5.5mM Glucose, 10mM 2,3-Butanedione Monoxime, 10mM HEPES, 12.5µM $CaCl_2$, 5mg/mL Collagenase II, 5mg/mL Collagenase IV and 30µg/mL DNAse I. [$CaCl_2$] was kept at

12.5µM to ensure adequate cell survival of both cardiomyocyte and non-myocyte cardiac cells. Samples were incubated at 32°C on an Eppendorf thermomixer at 800rpm. Every 15 minutes, supernatants were collected on ice and neutralised using 1% sheep serum. Samples were replenished with fresh Digestion Buffer and supernatants continued to be collected until all tissue had been digested (approx. 1-2 hours). Dissociated cells were filtered through 100µm filters and spun at 300g for 5 minutes at 4°C to form a cell pellet. Cell pellets were resuspended and counted before being spun down again and resuspended at 2000 cells/µL in DMEM plus 10% fetal bovine serum ready for 10X chip loading.

2.2.2 10X Chromium Single Cell RNA-sequencing

AM samples at 2000 cells/µL were processed individually by the Oxford Single Cell Facility at the MRC Weatherall Institute of Molecular Medicine using the 10X Chromium Next GEM Single Cell 3' v3.1 kit. Samples were processed according to manufacturer's instructions and sequenced in 6 rounds using the Illumina NextSeq® 500/550 High Output Kit v2 with the Illumina NextSeq500 sequencer to reach an average depth of 50,000 reads/cell. An average depth of 50,000 reads/cell was chosen to achieve sufficient sequencing saturation for cell clustering into distinct populations, based on 10X recommendations for 3' v2 libraries. The raw BAM files were then collected for scRNAseq pre-processing.

The CellRanger pipeline was used to pre-process the Chromium single cell RNAseq data and was performed by Dr. Madeleine E. Lemieux. Firstly, cellranger mkfastq (v3.0.2) was used to demultiplex the raw reads and generate fastq files. Then cellranger count was used to map the fastq files to the AM v1.0.2 and v2.0 genome assemblies and perform filtering, barcode counting and UMI counting to produce filtered feature matrices for each sample. Custom extended 3'UTR gtf files were used during genome alignment (see below)

2.2.3 Custom 3’ UTR extension of *A. mexicanus* genome assemblies

Custom 3’UTR extended gtf files were created by Dr. Madeleine E. Lemieux to mitigate the problems caused by poor 3’UTR annotation of the v1.0.2 and v2.0 AM genome assemblies.

To extend the 3’UTR annotation and enable the maximum capture of transcripts during data exploration, a terminal exon extension algorithm was applied. The extension algorithm used a full-length poly(A) RNA-seq sample as a reference and applied the following heuristic:

1. Identify transcripts without 3'UTR annotation in the Ensembl GTF file

2. Compare fragment coverage over 100bp flanking the terminal exon

3. If median 3' coverage > median 5' coverage, extend last exon 100bp in the 3' direction and repeat steps 2 & 3 until no further extension occurs.

The extension algorithm was used to create two custom extended GTF files that were used for read counting with the corresponding v1.0.2 and v2.0 genome assemblies (available in Supplementary Materials of Potts et al (2022)[174]). In all, 5,077/25,489 gene-level annotations on 2,530 contigs were extended for v1.0.2 and 8,721/27,420 on 25 chromosomes and 1,363 contigs were extended for v2.0[4].

2.2.3 Sample Integration and Cluster Annotation

The filtered feature matrices were analysed in R studio using the Seurat package (version 4.0.6). To create the Seurat object, initial filtering removed all cells with <50 captured genes and all genes present in <2 cells. Poor quality cells and doublets were further removed from each sample based on the average nFeature and nCount values in each sample. Cells with relatively low nFeature counts were filtered out to remove cells which had likely burst during GEM capture and lost many of

[4] I have previously published this methodology in “Discordant Genome Assemblies Drastically Alter the Interpretation of Single-Cell RNA Sequencing Data Which Can Be Mitigated by a Novel Integration Method” Potts et al (2022)

their cytoplasmic RNAs. Cells with very high nFeatures or nCounts most likely represented captured doublets and thus were also removed during quality control.

After cell quality control, the v1.0.2 and v2.0 versions of each scRNAseq sample were processed using Seurat. SCTransform[176] was used to normalise each sample to account for variability in sequencing depth between cells. 2000 highly variable features were found using SCTransform which were then used to centre and scale the data. The v1.0.2 and v2.0 datasets for each scRNAseq sample were integrated together using 3000 integration features in the SCTIntegration pipeline. The dimensions of each integrated sample were reduced using Principal Component analysis (PCA) and uniform manifold approximation projection (UMAP). Cells were assigned to clusters using the FindNeighbours and FindClusters functions and the appropriate resolution was chosen using the Clustree package (version 0.4.3)[177]. Marker genes for each cluster were found using FindAllMarkers. Cell type annotations were based on the results of FindAllMarkers and the expression of canonical markers of cardiac cell types. Once cell identity had been determined for each integrated sample, the annotated cell identities were embedded into the metadata for the v2.0 scRNAseq datasets.

2.2.4 Harmony Integration

To create the overall scRNAseq dataset and integrate all 12 scRNAseq samples together, the v2.0 filtered feature matrices with cell identity embeddings were used. Following quality control, SCTransform without scaling was used to normalise each sample individually prior to merging into one matrix. After merging, 5000 variable features across all 12 samples were found and used to centre and scale the data. The dimensionality of the merged dataset was reduced using 50 components in PCA. Batch effects between scRNAseq samples were corrected for using Harmony (version 1.0)[178], an iterative integration methodology. After integration, UMAP was used to project the data into 2D space whilst similar cells were clustered together using the Seurat functions FindNeighbours and FindClusters. Cell identity embeddings were used to annotate the overall scRNAseq dataset. To further facilitate the annotation of cell types, identity embeddings were cross-

referenced to the results of FindAllMarkers and the expression of canonical cell type markers. Neutrophil, monocyte/macrophage and B cell scRNAseq datasets were subset from the overall dataset and re-scaled prior to downstream analysis.

2.2.4 Differential Gene Expression (DGE) Analysis

Differential gene expression analysis was performed using the MAST[179] test and the LR test in the FindMarkers function and visualized using EnhancedVolcano (version 1.8.0), violin plots, heatmaps and Euler plots (eulerr, version 6.1.1). DGE results were analysed for their associated GO terms/signalling pathways by converting AM genes to their correspondent mouse homologs via BiomaRt (v2.46.3). Any genes which did not have a mouse homolog or mapped to multiple mouse genes were removed and the final mouse gene lists were tested using fGSEA (v1.16.0)[180], topGO (v2.42.0) and PROGENy (v1.12.0)[181]. The weight01 algorithm in topGO was used to pull the top 20 associated Biological Process GO terms and significance was set at $p<0.05$ for the Fisher's test. The results of the DGE analysis were tested for enrichment in the MSigDB Hallmarks Gene Sets using the fGSEA package. False Discovery Rate (FDR) was set at <0.25 to determine significant enrichment.

2.2.5 Differential Proportion Analysis

Differential Proportion Analysis (DPA) was performed on the overall Seurat object using the code provided in Farbehi et al (2019)[182]. All identified doublet clusters were excluded from the analysis. An error rate of 0.01 was set and significance threshold was set to $p<0.01$ for stringency.

2.2.6 Ligand-Receptor Analysis

Ligand-Receptor Analysis was performed on the overall Seurat object using the code provided in Farbehi et al (2019)[182]. All AM genes were mapped to their human homologs using biomaRt and ligand-receptor interactions were weighted and calculated based on the published database of known protein-protein interactions in humans, and the STRING database[183,184].

2.3 Molecular Biology

2.3.1 RNA isolation

Zebrafish hearts were isolated on ice 6 hours after the final ip injection (n=3/treatment group) and snap-frozen using liquid nitrogen before RNA isolation. RNA isolation was performed using the Quick-RNA Microprep kit according to manufacturer's instructions. Each RNA sample consisted of a single ventricle. Isolated RNA concentrations were measured using the Qubit RNA High Sensitivity Assay kit according to manufacturer's instructions. 260/280 ratios were calculated using a NanoDrop™ spectrophotometer.

2.3.2 RNA sequencing

Following RNA isolation, samples were prepared according to the instructions set by the Oxford Genomics Centre, where all RNA sequencing was performed. RNA sequencing was performed using the Illumina NextSeq500 sequencer with the Illumina NextSeq® 500/550 High Output Kit v2.

Principal component analysis of the RNAseq data was performed by Dr. Madeleine E. Lemieux.

2.4 Imaging

2.4.1 Sample processing

Hearts were isolated at baseline, sham and at the indicated time points after cryoinjury and fixed overnight in 4% PFA with gentle agitation. After fixation, samples were washed (3 X 5 mins) in 1X PBS before dehydration in increasing EtOH concentrations (70%, 80%, 90%, 96%, 100%, 100%). Hearts were incubated for 1 hour in each [EtOH] before incubation in Butanol overnight at 4°C with gentle agitation. For paraffin embedding, samples were washed three times in melted paraffin (1 hr/wash), to ensure adequate penetration of paraffin into the tissue, before embedding using plastic cassettes. Samples were sectioned at 7-10µm, mounted onto SuperFrost slides and dried overnight at 37°C before staining.

2.4.2 Immunofluorescent staining

For fluorescent immunohistochemistry, mounted sections were deparaffinised in Xylene (2 X 7 mins) and rehydrated in decreasing concentrations of EtOH (1 min/[EtOH]: 100%, 100%, 96%, 90%, 80%, 70%). Following immersion in distilled water, sections were pressure cooked for 4 minutes in 1x Antigen Unmasking solution, before blocking of non-specific binding by incubating sections for 30 minutes at room temperature in TNB. Primary antibodies (Table 2.3) were left to bind overnight in TNB before washing in 3 X 5 mins PBS-Tween 80 and incubating with secondary antibodies for 2 hours (Table 2.4). Sections were then counter-stained with DAPI, washed again with 3 X 5 mins PBS-Tween 80 and mounted in Mowiol 4-88 ready for imaging.

Table 2. 3: Primary Antibodies

Primary Antibodies	Clonality	Concentration Used	Catalog number
Myosin Heavy Chain (MF20)	Monoclonal Mouse	1 in 200	Developmental Studies Hybridoma Bank, # AB_2147781
Lysozyme (Lyz)	Polyclonal Rabbit	1 in 200	GeneTex, # GTX132379
Proliferating Cell Nuclear Antigen (Pcna)	Monoclonal Mouse	1 in 200	Dako, # M0879
L-plastin 1 (Lcp1)	Polyclonal Rabbit	1 in 200	GeneTex, # GTX124420

Table 2. 4: Secondary Antibodies

Secondary Antibodies	Clonality	Concentration Used	Catalog number
Alexa 488	Goat anti-mouse	1 in 200	Invitrogen, # A55058
Alexa 546	Donkey anti-rabbit	1 in 200	Invitrogen, # A10040

2.4.3 RNAscope

RNAscope® (Advanced Cell Diagnostics Biosciences) is a commercial *in situ* hybridisation technique. The RNAscope Multiplex Fluorescent Reagent Kit V2 Assay was performed according to manufacturer's instructions. Briefly, mounted sections were deparaffinised before sections were washed twice in 100% EtOH. After air drying, sections were incubated for 10 minutes at room temperature in 3% hydrogen peroxide and washed in distilled water. To retrieve mRNA targets for visualisation, sections were boiled (98-102°C) with RNAscope target retrieval for 15 minutes and then incubated in 100% EtOH for 3 minutes. After drying, sections were digested using Protease III digestion at 40°C for 12 minutes. Following protease treatment, sections were incubated with RNAscope probes for 2 hours at 40°C before the signal was amplified according to manufacturer's instructions. TSA plus Cyanine 3 (1:1500); Cyanine 5 (1:1500) and Fluorescein (1:500) were used to detect the hybridisation signal. ACD Biosciences designed all probes as summarised in Table 2.5. All sections were counterstained with DAPI and mounted using ProLong™ Gold Antifade Mountant. For sections that were counterstained with antibodies, the immunofluorescent protocol described above was applied from the 30 minutes TNB blocking step.

When a C1 channel was not used, probes were diluted using RNAscope probe diluent (#300041). All RNAscope staining procedures included a section stained with ACD Negative Control probe mix to assess background levels of staining.

Table 2. 5: RNAscope probes

Probe	Channel	Catalog Number
itgam	C3	532001-C3
tnfa	C1	535021
nfkb2	C3	1052861-C3
mpeg1	C2	814911-C2
ptprc	C2	874211-C2
lcp1	C2	551161-C2
cd37	C1	1052831-C1

mmp9	C1	532021- C1

2.4.4 Histology

Mounted sections were deparaffinised with two X 5 mins washes in Xylene or Histoclear. Sections were then rehydrated in decreasing concentrations of EtOH with approximately 1 minute of incubation in each [EtOH] (100%, 100%, 96%, 90%, 80%, 70%). After the final incubation in 70% EtOH, sections were washed in distilled water and stained with Acid Fuchsin Orange-G (AFOG) or Pico-Sirius Red, prior to mounting in DPX.

AFOG

For AFOG staining, AFOG solution was made up as follows: 1L of distilled water was boiled with 5g of Methyl Blue. Once cooled, 10g of Orange G and 15g of Acid Fuchsin were added and pH was adjusted to 1.09 using HCL. Rehydrated mounted sections were incubated in Bouin's Solution for 3 hours at 60°C and washed in distilled water until clear. Sections were then submerged in 1% phosphomolybdic acid for 5 mins before submersion in AFOG solution for 10 mins, followed by rapid washing using distilled water and dehydration through increasing concentration of EtOH (70%, 80%, 90%, 95%, 100%, 100%). Sections were then rapidly dipped in Xylene prior to mounting with DPX.

Pico-Sirius Red

For Pico-Sirius Red Staining, rehydrated sections were incubated for 1 hour in Pico-Sirius Red Solution at room temperature. After incubation, sections were quickly washed twice in 0.5% Acetic Acid Solution (provided in the Pico-Sirius staining kit), followed by two rapid washes in 100% EtOH and Xylene before mounting.

2.4.5 Acquisition

RNAscope images were acquired using an Olympus FV3000 confocal and Pico-Sirius Red images were acquired using am Olympus BX53 Polarised Light microscope. All other images were

acquired using a Nikon Digital Sight stereo microscope. Images were processed using FIJI/ImageJ. All measurements and cell counts were performed blinded.

2.4.6 Leukocyte Cell Counts

Cell counts were performed by counting the number of positive cells showing DAPI and probe/antibody overlap in ImageJ. Counts were normalised to either total ventricle area or fractional wound area (area of wound/area of total ventricle). Fractional wound area was devised to account for differences in the morphological size of the PF and SF hearts as well as for variable wound sizes. At least 3 sections/heart were used to calculate an average cell count value for each sample.

For the *lcp1* RNAscope probe, staining at 3dpci in PF was so dense that individual cells could not be easily distinguished. Therefore, to avoid random clicking during cell counts, the area of wounded tissue positive for *lcp1* staining was used as a substitute for cell counts. To calculate the percentage of wound that showed positive *lcp1* staining above background levels, images were thresholded in ImageJ to remove background staining and the 'Area Fraction' (i.e. the percentage area of wound positive for *lcp1* staining) was measured. This methodology was also used to calculate the degree of MF20 degradation in 3dpci sections when comparing the rate of myocardial wound death in PF/SF hearts.

2.4.7 Neutrophil Density Measurements

To assess neutrophil density within AM wounds, the number of *mmp9*$^{+}$ cells was counted and normalised to the measured area of the wound.

2.4.8 Regenerative Capacity Measurements

To assess the ability of the SF to regenerate following *in vivo* inhibitor exposure, serial paraffin sections of the entire ventricle were mounted (i.e. 1 in 10 sections were mounted throughout the heart). The results of AFOG staining were used to assess regenerative capacity. Two measurements were calculated to independently assess SF regenerative capacity: scar size and the ratio of open wound: ventricle perimeter

Scar size

Scar size was calculated as follows: using ImageJ, the area of the scar and the ventricle were measured in each section. Total scar area and total ventricle area were then summed across all sections. Total scar area was divided by total ventricle area and then multiplied by 100 to derive the percentage of the SF heart that was scarred.

Open Wound: Ventricle perimeter

The ratio of open wound: ventricle perimeter was calculated as follows: 3 sections with the largest wounds from each heart were used. In sections with wound, the length between openings of the compact myocardial wall was measured (i.e. the length of scar tissue not overgrown by the myocardial wall was measured). To measure ventricular perimeter, the section that captured the largest part of the ventricle was used. The ratio of open wound: ventricle perimeter was then calculated and averaged across all 3 sections.

2.4.9 Scar Composition

Scar composition analysis was performed in ImageJ using the Colour Threshold feature. Sections were thresholded according to blue, red and orange/brown channels to measure the area of the wound that was made up of collagen, fibrin and blood clot/tissue debris respectively. The area of the wound was measured and the percentage of collagen/fibrin/tissue debris was calculated. At least three of the largest wound sections were used to calculate an average percentage value for each heart.

2.4.10 Collagen Fibre Alignment

To assess collagen fibres for differences in straightness, length and orientation, sections were stained with Pico-Sirius Red. Images were captured using both brightfield and linear polarisers. Captured images were first converted into greyscale and thresholded using ImageJ before analysing using CT-FIRE software (v2, loci.wisc.edu/software/ctfire)[185].

All collagen fibre alignment analysis was performed by Esra Şengül.

2.5 Statistics

The number of samples (n) and statistical test used are detailed in each figure legend. Only time points that had at least n=3 were tested for statistical significance using parametric tests. Parametric tests were applied based on previous data that found PF and SF populations to display normally distributed responses to cardiac injury[29] that passed normality and equal variance tests. All statistical tests were performed using GraphPad Prism 7.

Chapter III

Characterisation of the *A. mexicanus* heart following cryoinjury using single cell transcriptomics

3.1 Background

The aim of this project was to characterise the AM immune response to cardiac injury and identify differences in the PF/SF immune response that could be driving their differential regenerative capacity. However, as the AM immune response to cryoinjury had never previously been explored, no data was available on PF/SF cardiac-resident leukocytes, the number of leukocytes recruited in response to injury, the transcriptional profile of recruited AM leukocytes, nor on the kinetics of leukocyte recruitment. Therefore, to achieve this aim, an experimental approach was required that would enable AM leukocytes to be comprehensively characterised at multiple time points after necrotic cardiac cell death.

3.1.1 Single Cell RNA Sequencing

Since it was first developed in 2009[186], single cell RNA sequencing (scRNAseq) technology has proven to be a powerful tool that provides transcriptomic information about individual cells[187]. scRNAseq enables researchers to answer a wide variety of biological questions about topics such as cell-cell heterogeneity, tissue composition and cell-specific gene expression responses to disease and/or injury[188]. As commercialised kits have helped to lower costs, scRNAseq is becoming a routine investigatory approach and has been used extensively for characterising heterogeneous tissues in novel non-model organisms[189–191].

The rising popularity of scRNAseq has led to the development of many different scRNAseq technologies such as Smart-seq2[192], In-Drop[193], C1[194] and Drop-seq[195]. The major difference between the main scRNAseq options is the platform in which cells are captured. Most scRNAseq technologies

are either plate-based (cells are sorted into one cell/well plates for scRNAseq) or are droplet-based (each cell is captured within a droplet). Plate-based technologies, such as Smart-seq2, are typically limited in the number of cells that can be captured within an experiment. However, low cell capture rates offer the select advantage that captured cells can be sequenced to very high depths, producing scRNAseq data that is more representative of the cellular transcriptome. On the other hand, droplet-based approaches, such as In-drop, offer lower sequencing depths but much higher cell capture rates, enabling many cells from a tissue to be captured (plates: 100-1000 cells Vs droplets: 1000-10,000 cells)[188]. Droplet-based approaches can achieve higher capture rates with reasonable sequencing depth as they use cellular barcoding during cell capture. This enables sequenced reads to be pooled for high-throughput sequencing, keeping costs affordable (Fig. 3.1)[188,196].

Studies which aim to characterise complex, heterogeneous tissues for the first time are best-suited to a droplet-based approach so that the diverse range of cells present within a tissue can be comprehensively profiled. 10X Genomics Chromium[197] is one of the most established droplet-based scRNAseq technologies due to its low cost and high-throughput[198] and thus it is well suited to large-scale characterisation studies.

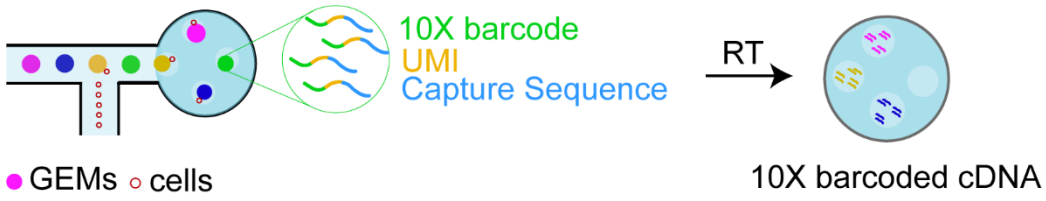

Figure 3. 1: Overview of the 10X Genomics Chromium (10X) droplet-based approach

10X captures cells for sequencing in gel bead-in emulsions (GEMs) droplets. Each GEM contains all the necessary enzymes, nucleotides and oligos to lyse the captured cell, and reverse transcribe its component mRNA molecules into cDNA. 10X uses specially designed oligos that adhere to mRNA molecules and result in the incorporation of cellular barcodes in the final cDNA molecules. Cellular barcoding labels each captured read with specific and unique sequences that enable the final sequencing data to be demultiplexed into a cell x genes matrix. Each GEM has a unique 10X barcode

sequence that labels all reads from the same cell with a cellular identifier, enabling reads from individual cells to be grouped together. The unique molecular identifier (UMI) sequences are attached to all reads within a cell. UMIs ensure accurate read counting as there are millions of different UMIs within a GEM, allowing individual reads to be counted separately. The capture sequence is typically a poly-thymine tail and adheres to the complimentary poly-adenosine tail of mRNA molecules.

3.1.2 Why scRNAseq of the entire *A. mexicanus* heart

Despite the unique suitability of the AM as a model for cardiac regeneration, very little is known about its heart. A morphological study has shown that the PF have smaller, rounder ventricles that beat faster that the SF[199]; and the Mommersteeg lab has shown that, after injury, the PF and SF hearts show differences in cardiomyocyte cytokinesis, scarring, metabolism and the immune response[29]. Otherwise, this diverse and complex tissue has not yet been fully explored. Cardiac cell type-specific markers have not been established and the proportion of the major cardiac cell types such as fibroblasts, cardiomyocytes and endothelial cells are unknown at baseline and post-injury. Therefore, scRNAseq of the entire AM heart will provide answers to many of the basic questions that still remain about the AM heart.

Additionally, to date, no comparative studies have been performed in the AM following cryoinjury. Previous work in the Mommersteeg lab has used ventricular resection as a cardiac injury model. Cryoinjury and resection are significantly different injury models: cryoinjury results in substantial necrosis, inflammation[200], tissue damage and scar deposition whereas resection induces minimal levels of apoptosis, tissue damage and collagen deposition[201,202]. As necrotic cell death is the initial trigger of the immune response, whilst collagen deposition will impact the scarring responses, it is very likely that the PF and SF will respond in substantially different ways to cryoinjury than to resection. Therefore, it is essential that cellular transcriptomes are collected from the entire AM heart. This will enable unbiased comparisons to be made, confirming whether scarring, metabolism

and the immune response (i.e. findings from previous bulk RNAseq data) remain the major differences between the PF/SF following cryoinjury-induced necrosis. Furthermore, unbiased comparisons of scRNAseq data from the entire AM heart have the potential to identify novel and unknown differences that could also be regulating regenerative capacity in the PF/SF.

Finally, scRNAseq of the entire heart is essential in order to fully characterise the AM regenerative and scarring immune responses to injury. Leukocytes have been shown to communicate with a wide range of cells across the heart to stimulate repair: they induce fibroblasts to secrete scar proteins; they stimulate angiogenesis via endothelial cells; they secrete mitogens to cardiomyocytes and directly contribute to scar formation[136]. Therefore, to fully understand how the PF and SF might differently coordinate scar deposition, cardiomyocyte proliferation and revascularisation, it is critical that the entire AM heart is captured so that leukocyte interactions with non-immune cardiac cells can be interrogated.

Therefore, scRNAseq of the whole AM heart will answer a wealth of questions about the AM heart, as well as enable the regenerative and scarring immune responses to cardiac injury to be fully characterised. Understanding the molecular and cellular signals governing regeneration and scarring in AM single cells will represent a significant leap forward in our ability to unpick the key differences between regenerative success and failure.

3.1.3 The potential pitfalls of applying 10X scRNAseq to *A. mexicanus* cardiac cells

The successful application of scRNAseq to the AM heart will require optimisation. The application of 10X scRNAseq is dependent on 2 key factors:

1) Cell size and viability following sample preparation
2) The quality and availability of an organism's reference genome and associated gene annotations

<u>Cell size and viability following sample preparation</u>

10X technology requires samples to be processed into single cell suspensions that are free from doublets, dead/dying cells and erythrocytes (Fig. 3.2). However, this recommended workflow presents major problems for cardiac researchers as cardiomyocytes are very vulnerable to both single cell dissociation and fluorescence activated cell sorting (FACS) and show poor survival rates after such rigorous treatment[203]. Furthermore, cardiomyocytes are notoriously hard to capture using 10X technology. This is because a major technical limitation of 10X scRNAseq is cell size exclusion as the gel bead-in emulsions (GEMs) used for cell capture can only capture cells ≤30µm in diameter (Fig. 3.2). Cardiomyocytes are very large cells (adult mammalian cardiomyocyte diameter is ~100µm[204]) and, as a result, have not been successfully captured in previous, large-scale 10X characterisation studies of the heart[141,182,205–207]. Although teleost cardiomyocytes are much smaller than their mammalian counterparts, they are also largely missing from zebrafish 10X datasets[208,209].

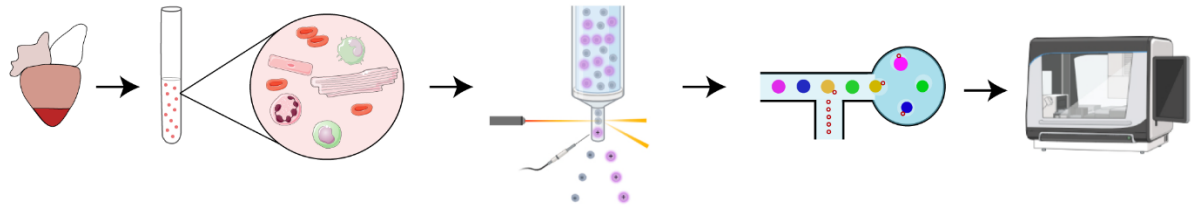

Figure 3. 2: Schematic of the recommended workflow for sample preparation for 10X Genomics Chromium.

1) Tissues should first be either enzymatically and/or mechanically dissociated to form a single cell suspension 2) Sample suspensions should then be processed by FACS to remove dead/dying cells, tissue debris, erythrocytes and doublets 3) Samples should be suspended at the optimal concentration for chip loading and cell capture in GEMs and RNA sequencing.

Therefore, as scRNAseq has never previously been applied to the AM heart, the diameter of AM cardiomyocytes is unknown and the viability of all PF and SF cardiac cells following dissociation and FACS remains to be determined. Equally, it has not been explored whether the omission of FACS

treatment will lead to unacceptably poor data quality due to increased capture rates of erythrocytes, dead/dying cells and doublets.

The quality and availability of an organism's reference genome and associated gene annotations

10X technology requires sequenced reads to be aligned to an organism's reference genome during analysis to determine the transcriptome of captured single cells. Therefore, the data quality produced by scRNAseq is directly reliant on the quality and gene annotation of an organism's reference genome. Organisms that are best suited to 10X scRNAseq have a high-quality reference genome that is well annotated in the untranslated regions (UTR) as 10X captures mRNA molecules for sequencing via their 3' polyadenylated tails.

Unfortunately, as the AM is a relatively understudied non-model organism, its genome is far from complete and new assemblies continue to be published every few years. There are currently two AM genome assemblies available on Ensembl: v1.0.2 (listed as Pachón cavefish) a scaffold-level short-read assembly created using a single fish taken from the Pachón cave[210], and v2.0 (listed as "Mexican tetra"), a chromosome-level long-read assembly of a single SF that was a cross from two Surface populations in the Rio Sabinas and Rio Valles[211]. Additionally, a new Pachón build has been recently published that is only available on NCBI[212], whilst a fourth assembly is set to be published later this year. This co-occurrence of multiple AM reference genomes creates significant problems for scRNAseq data analysis which requires sequenced reads to be mapped and aligned to a single reference genome[188]. Currently, there is no consensus within the AM field on which genome assembly should be used for sequencing experiments. Recent publications have used v1.0.2[29,213]; v2.0[214]; an archived version of the v1.0.2 Pachón build (astmex1, Ensembl 87 gene model)[166]; and the most recent NCBI Pachón build[212]. As new versions of the AM genome continue to be published, this inconsistent use of AM genome assemblies will only worsen as AM researchers become faced with an ever-expanding repertoire of genome assemblies to choose from, with no knowledge of which genome will offer the best quality of data. Furthermore, as each AM genome assembly differs in the

quality of its annotations and sequence, AM researchers can face the frustrating task of repeatedly re-analysing their datasets with each new assembly publication, with no certainty that the resultant dataset will improve each time.

To date, the optimal AM genome assembly to use in scRNAseq has not been explored nor has whether AM genome assembly choice impacts the results of scRNAseq analysis. Additionally, a unifying solution that enables multiple assemblies to be used simultaneously during data analysis has yet to be identified.

3.1.4 Aims

In this chapter, I aimed to:

1) Optimise the application of scRNAseq to the *A. mexicanus* heart
2) Characterise the dynamics of the overall *A. mexicanus* immune response at baseline and at 1, 3, 7 and 14 days after injury
3) Identify the leukocyte subpopulations present in the *A. mexicanus* heart at baseline and at 1, 3, 7 and 14 days after injury

3.2 Results

3.2.1 Optimisation of scRNAseq of the *A. mexicanus* heart

1) Optimisation of AM heart dissociation into a single cell suspension

To achieve a single cell suspension of the entire AM heart, different protocols were trialled for digesting PF/SF hearts into viable single cells. Firstly, a digestion mixture of Liberase and Hank's balanced salt solution was tested in which supernatants were collected and neutralised every 5 minutes using sheep serum. Although this protocol had previously been used in scRNAseq of the zebrafish ventricle[208,215], only small and rounded cells were successfully dissociated from the PF/SF hearts, whilst cardiomyocytes were completely absent from the final digestion mixture. To achieve successful liberation of PF/SF cardiomyocytes, a collagenase-based digestion mixture was next

trialled. This protocol had previously been developed to isolate zebrafish cardiomyocytes for primary culture[175] and resulted in the isolation of individual, beating cardiomyocytes. However, fewer small and rounded non-myocyte cells were liberated using collagenase treatment than the Liberase digestion mixture.

Therefore, to achieve a balance between the digestion of healthy cardiomyocytes and the release of smaller, non-myocyte cells, an optimised protocol was developed that combined the use of collagenase II and IV with regular sheep serum neutralisation to liberate both beating cardiomyocytes and non-myocyte cells. This digestion mixture was then used for all PF/SF heart digestions (see methods for detailed protocol).

2) FACS is damaging to a plethora of AM cardiac cell types

Following the optimisation of AM heart digestion, the next questions were:

1) Can AM cardiomyocytes be captured within 10X GEMs?
2) Are AM cardiomyocytes vulnerable to FACS treatment?
3) Does FACS omission result in poor quality data?

To answer these questions, an initial 10X trial was performed in which 1dpci PF ventricles were dissociated and were either sorted by FACS prior to Chromium Chip B loading or were directly loaded onto a Chromium Chip B with no FACS. The resultant filtered feature matrices were analysed using the standard Seurat pipeline and similar cells were clustered together. During cell-type annotation, cardiomyocytes were identified in both samples, regardless of FACS treatment, revealing that AM cardiomyocytes can be captured within 10X GEMs (Fig. 3.3a&c).

However, FACs treatment resulted in substantially different cell capture rates, although cell numbers were kept consistent for chip loading: the FACS+ sample captured 1,267 cells, whereas the FACS- sample captured 8,418 cells (Fig. 3.3b&d). Cluster identification revealed that a wide range of expected cell types such as fibroblasts and epicardial cells were missing from the FACS+ sample (Fig.

3.3a) but were present in the FACS- sample (Fig. 3.3c). Additionally, FACS treatment resulted in a very low-yield of cardiomyocytes, with the cardiomyocyte cluster representing <7% of the overall sample (Fig. 3.3b) whereas 41.4% of the FACS- sample consisted of cardiomyocytes (Fig. 3.3d). Previous studies of teleost hearts have found cardiomyocytes to account for approximately 40% of the total heart[216], suggesting that FACS treatment resulted in a scRNAseq dataset that was not representative of the cellular composition of the AM heart. Furthermore, a comparison of data quality between the FACS+ and FACS- samples showed that FACS omission did not result in poor quality data as both samples showed very similar correlations between the average number of mRNA molecules and genes detected per cell (Fig. 3.3e).

Therefore, from the results of this trial, it was possible to conclude:

- AM cardiomyocytes could be captured by 10X GEMs
- Optimal cell capture required FACs omission prior to Chip B loading
- FACS omission did not produce poor quality data

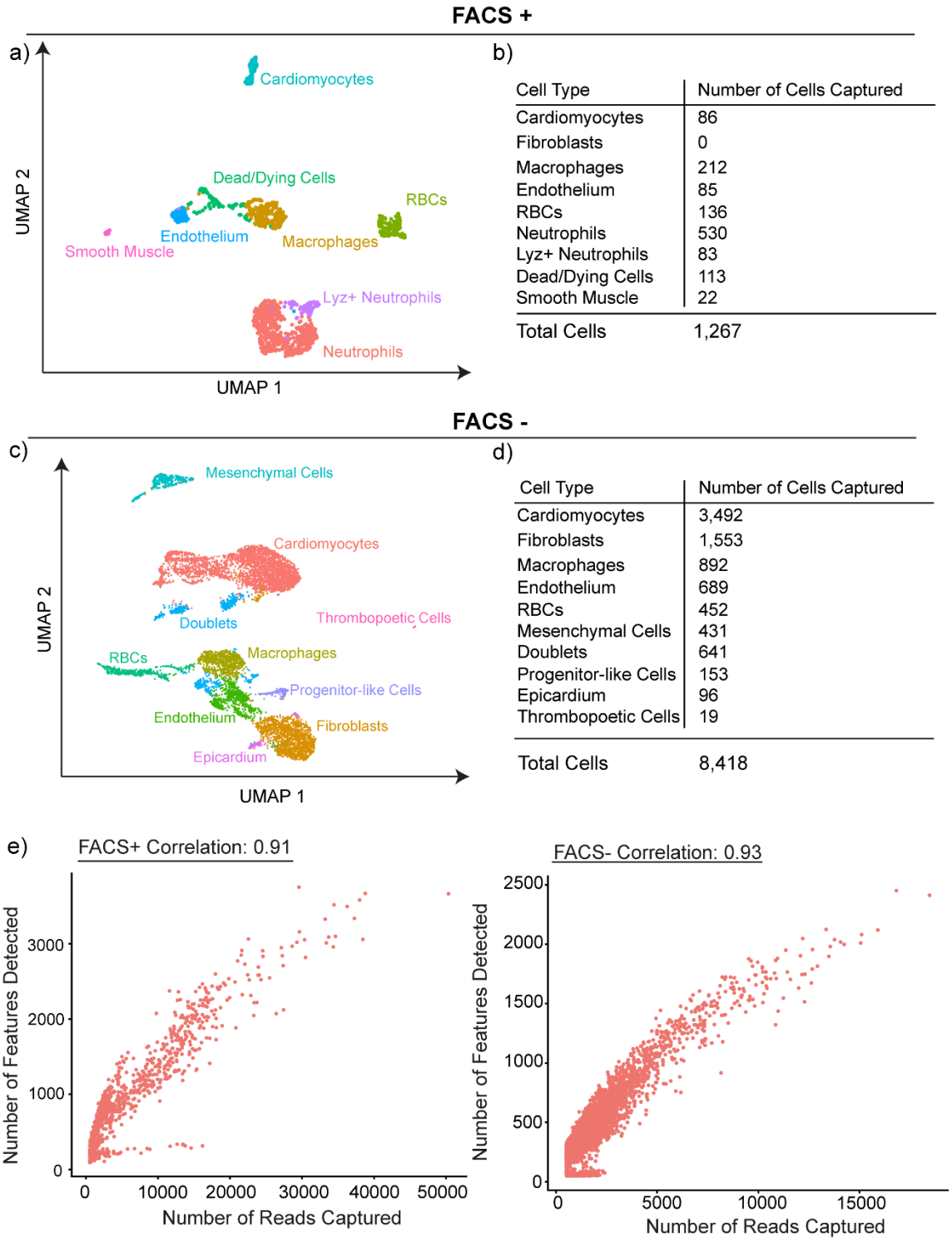

Figure 3. 3: FACS is damaging to a plethora of AM cardiac cell types

Annotated UMAPs of PF ventricle single cell suspensions that underwent: (A) FACs treatment; and (C) FACS omission during sample preparation. Comparison of UMAPS (A) and (C) show that many expected cell types were lost during FACS treatment such as cardiomyocytes and mesenchymal cells.

Tables (B) and (D) display the number of each cardiac cell type captured following FACS treatment (B) and FACS omission (D), showing that FACS treatment resulted in a significant decrease in cell capture rates. (E) Scatter plots of the number of reads captured per cell vs the number of genes detected showed that data quality is very similar for both the FACS+ and FACS- samples.

3) 10X scRNAseq sample collection

To characterise the regenerative and scarring immune response in the first 14 days after cardiac tissue necrosis, PF and SF were subject to cryoinjury, in which necrotic cell death was induced by rapid freeze-thawing of the ventricular tissue. PF and SF ventricles were then collected at uninjured, 3 days-post sham (dps), 1-, 3-, 7- and 14-days post-cryoinjury (dpci) and dissociated into single cell suspensions. Single cell suspensions were washed 3 times to remove as much tissue debris, erythrocytes, and ambient RNA as possible without FACs treatment (Fig. 3.4). Sample multiplexing with barcoded antibodies (known as cell hashing) was not available for the AM and so each PF/SF sample was sequenced separately and underwent 6-rounds of sequencing to reach the appropriate depth of ~50,000 reads/cell.

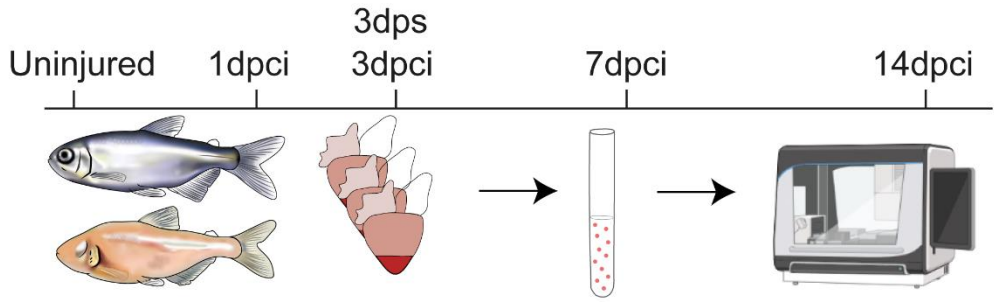

Figure 3. 4: Schematic of sample collection for 10X scRNAseq experiment

2 PF/SF ventricles were pooled for each sample.

4) AM genome assembly choice impacts the number of cells and genes present in scRNAseq data

Once the scRNAseq data had been collected, the next question was to determine which AM genome assembly was best suited to scRNAseq analysis. At the time of scRNAseq analysis, the only available AM assemblies were the Pachón cavefish (Ensembl v1.0.2) and the Mexican Tetra (Ensembl v2.0). Prior to this work, an archived version of the v1.0.2 assembly had been successfully used in a 10X study of the AM head kidney[166]. However, in theory, the v2.0 assembly should produce better results as it is more complete, contiguous, and continuous than the v1.0.2 assembly. Therefore, to test the suitability of both the v1.0.2 and v2.0 genome assemblies for scRNAseq, the sequenced reads from one scRNAseq sample (SF uninjured) were mapped and aligned to both available AM assemblies using Cell Ranger. This produced two filtered feature matrices: a v1.0.2 and a v2.0 dataset.

To determine whether AM genome assembly choice had an impact on cell and gene capture rates, Cell Ranger outputs were first compared. Strikingly, the v1.0.2 and v2.0 datasets had different matrix dimensions (i.e. cells x genes, Table 3.1), despite originating from the same sequenced reads, suggesting different cell and gene capture rates between the two datasets. The v2.0 dataset had increased gene capture rates as a greater percentage of sequenced reads mapped to the transcriptome (52.4% vs 41.7%), resulting in a higher average number of reads and genes detected per cell. The difference in genes present in the matrix had an unexpected impact on cell capture rates: the v2.0 assembly captured an additional 148 cells compared to the v1.0.2. Further comparison between the captured cells showed that both datasets had assembly-specific cells (16 in v1.0.2 and 225 in v2.0). These fundamental differences in cell and gene capture rates required quality control thresholds to be set according to genome-assembly (Fig. 3.5), resulting in a difference of 209 cells available for downstream analysis post-filtering. Therefore, from the Cell Ranger output it was apparent that genome assembly choice would impact on the fundamental structure of the

resultant scRNAseq data and would alter the number of cells and genes available for downstream analysis[5].

		
	v1.0.2 Assembly	**v2.0 Assembly**
Matrix Dimensions	25,489 genes, 8,870 cells	27,420 genes, 9,018 cells
Reads Mapped to Genome	72.6%	74.1%
Reads Mapped to Transcriptome	41.7%	52.4%
Median Reads/Cell	30,901	30,394
Median Genes/Cell	794	1,201
Assembly-specific cells	16	225
Assembly-specific genes	4,311	5,638
nCount vs nFeature Correlation	0.84	0.88
Quality Control Thresholds	nFeatures: 200-2,500 nCounts: <20,000	nFeatures:200-3,500 nCounts <28,000
% Cells Passed Filtering	98.2%	98.9%
Cell Numbers Post-Filtering	8,717 cells	8,926 cells
% Genes Passed Filtering	64.3%	63.9%
Gene Numbers Post-Filtering	16,408 genes	17,528 genes
PCA Dimensions	30	30
Clustering Resolution	1.25	1.25
Number of Clusters Found	26	27

Table 3. 1: Table of differences in the 2 datasets generated using v1.0.2 and v2.0 genome assemblies

nCount refers to the number of mRNA molecules detected per cell whilst nFeature refers to the number of genes detected per cell[6]

[5] I have previously published text from this paragraph in Potts et al (2022): 'Discordant Genome Assemblies Drastically Alter the Interpretation of Single-Cell RNA Sequencing Data Which Can Be Mitigated by a Novel Integration Method'[174]

[6] I have previously published Table 3.1, Table 3.2, Figure 3.5, Figure 3.6, Figure 3.7, Figure 3.9 and Figure 3.10 their corresponding figure legends in Potts et al (2022): 'Discordant Genome Assemblies Drastically Alter the Interpretation of Single-Cell RNA Sequencing Data Which Can Be Mitigated by a Novel Integration Method'

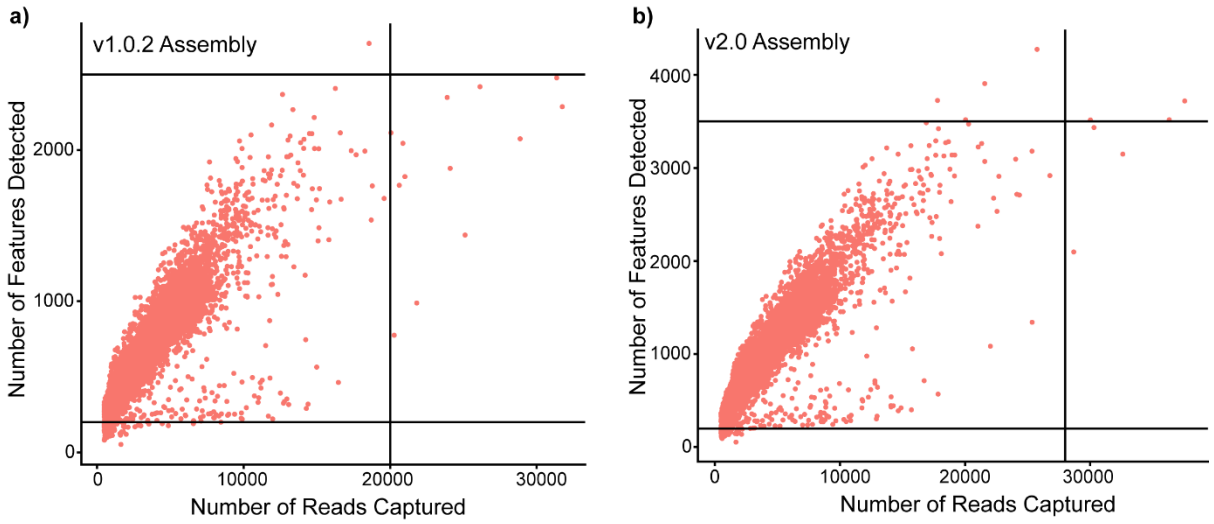

Figure 3. 5: Genome assembly can alter the nFeatures and nCounts of a scRNAseq dataset, impacting the number of cells and genes available for downstream analysis.

Scatter plots of the number of counts (reads) vs number of features (genes) in each captured cell when aligned to: (A) the v1.0.2 genome assembly and; (B) to the v2.0 assembly. The lines on each scatter plot represent the quality control thresholds that were set for each genome assembly, highlighting the increase in the number of features and reads captured in the v2.0 dataset vs v1.0.2 dataset[1]

5) The v1.0.2 and v2.0 datasets produce significantly different cell-type markers for AM cardiac cells

To determine whether the observed differences in matrix dimensions would impact downstream scRNAseq analysis, the v1.0.2 and the v2.0 datasets were processed using Seurat. The underlying differences in cell/gene capture rates did not alter AM cardiac cell type detection, nor prevent similar cells clustering together as the v1.0.2 and v2.0 UMAPs were very similar in their structure and number of clusters identified (Fig. 3.6).

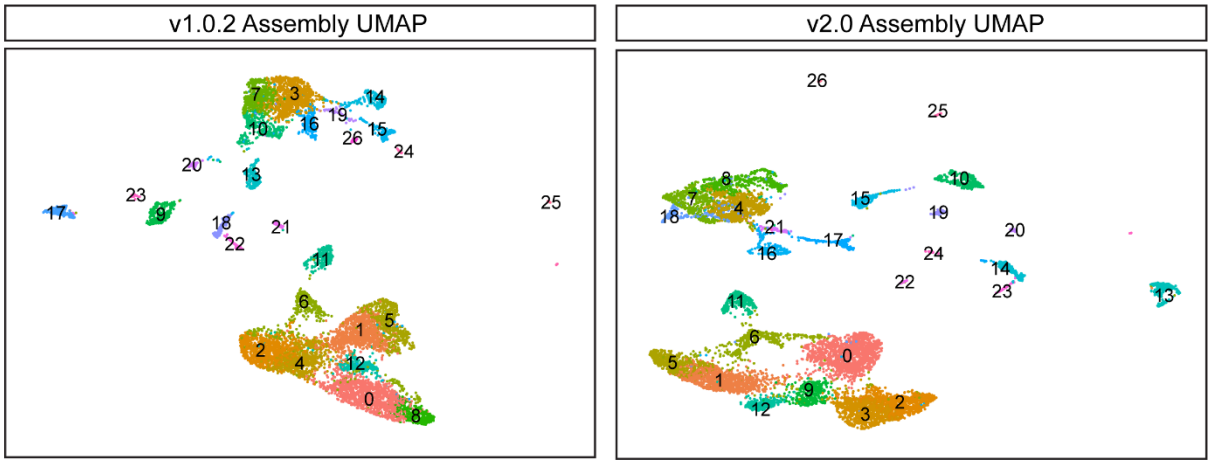

0 - Cardiomyocytes	13- Smooth Muscle
1 - Cardiomyocytes	14- Macrophages
2 - Cardiomyocytes	15- T Cells
3 - Endothelium	16- Endo/CM
4 - Cardiomyocytes	17- Pacemaker CMs
5 - Cardiomyocytes	18- Erythrocytes
6 - Cardiomyocytes	19- Granulocytes
7- Endothelium	20- HSCs
8 - Cardiomyocytes	21- Smooth Muscle
9 - Fibroblasts	22- Erythrocytes/CM
10- Endothelium	23- Epicardium
11- Cardiomyocytes	24- Thrombopoeitic Cells
12- Cardiomyocytes	25- Neutrophils
	26- B Cells

0 - Cardiomyocytes	13- Pacemaker CMs
1 - Cardiomyocytes	14- Erythrocytes
2 - Cardiomyocytes	15- Smooth Muscle
3 - Cardiomyocytes	16- Macrophages
4 - Endothelium	17- T Cells
5 - Cardiomyocytes	18- Endothelium
6 - Cardiomyocytes	19- HSCs
7- Endothelium	20- B Cells
8 - Endothelium	21- Granulocytes
9 - Cardiomyocytes	22- Epicardium
10- Fibroblasts	23- Erythrocytes
11- Cardiomyocytes	24- Thrombopoeitic Cells
12- Cardiomyocytes	25- Neutrophils
	26- Platelets/Megakaryocytes

Figure 3. 6**: **Genome assembly does not impact dimension reduction and cell clustering

UMAPs generated from the v1.0.2 and v2.0 datasets are very similar. The v1.0.2 B cell cluster was manually annotated. HSCs- Hematopoietic Stem Cells

During cluster annotation, however, it became startingly apparent that the v1.0.2 and v2.0 assemblies were very discordant in their annotated genes. To annotate the v1.0.2 and v2.0 cell clusters without bias, differential gene expression (DGE) analysis was performed using the Receiver Operator Characteristic (ROC) test to identify top gene markers for each cell cluster. As the v1.0.2 and v2.0 datasets are generated using the same reads, the ROC test results were expected to be very similar for both datasets. However, the ROC test produced two divergent lists of genes for each dataset, with few genes being identified as top cell-type markers in both datasets (Table 3.2). As cell-specific markers of the AM heart have not yet been established, these divergent results posed a problem as there was no way to know whether the results from the v1.0.2 or the v2.0 dataset were

the most reliable set of AM cardiac cell-type markers that could be used in future studies of AM cardiac cells. Additionally, the divergent results of the ROC test suggested that the results of any DGE analysis used to compare the SF and PF AM immune responses within the scRNAseq data would be completely different depending on the choice of genome assembly.

Cell Type	v1.0.2 Assembly	v2.0 Assembly
Cardiomyocytes	*ENSAMXG00005008576**	*myh7l**
	actc1a	*ENSAMXG00000004797**
	tnnc1a	*nme2b.1**
	*cox6a2**	*TNNC1*
	aldoaa	*aldoab*
	zgc:193541	*idh2*
	*ENSAMXG00005013223**	*cox7b*
	IDH2	*slc25a5*
	atp5mc3a	*cox7c*
	*atp5if1a**	*tnnt2b*
Endothelium	*ENSAMXG00005007750**	*lyve1a*
	*ENSAMXG00005016906**	*ENSAMXG00000041928**
	*ENSAMXG00005003412**	*krt18a.1*
	*ENSAMXG00005021204**	*rgs5b*
	plpp2a	*ENSAMXG00000036379**
	*ENSAMXG00005022026**	*il13ra2*
	krt5	*sat1a.2*
	*ucmaa**	*serpinh1b*
	*ENSAMXG00005012084**	*her6*
	*ENSAMXG00005004741**	*ENSAMXG00000035697**
Fibroblasts	*thbs1a*	*ccl25b*
	tcf21	*rbp4*
	lxn	*apoeb*
	kcne4	*pmp22a*
	mustn1a	*tagln*
	*ENSAMXG00005006660**	*TCF21*
	pltp	*dcn*
	clec19a	*col1a2*

	*BAMBI**	*anxa1a (ENSAMXG00000035597)*
	hmx4	*sostdc1a*
Neutrophils	*ENSAMXG00005022612**	*ENSAMXG00000006427**
	c6ast1	*mmp9 (ENSAMXG00000007722)*
	*ENSAMXG00005012967**	*ENSAMXG00000035474**
	*ENSAMXG00005007030**	*LECT2*
	*ENSAMXG00005022013**	*c6ast1*
	adam8a	*ENSAMXG00000037167**
	ltb4r	*cebp1*
	*ENSAMXG00005015365**	*ENSAMXG00000001798**
	mmp9	*Scinlb*
	*ENSAMXG00005024801**	*ENSAMXG00000034260**
T cells	*pfn1*	*ENSAMXG00000036068**
	laptm5	*pfn1*
	cxcr4b	*laptm5*
	*ENSAMXG00005014236**	*ctsl.1 (ENSAMXG00000029871)*
	coro1a	*cxcr4b*
	*ENSAMXG00005012967**	*rac2**
	rgs13	*dusp2*
	PTPRC	*rgs13*
	runx3	*cotl1*
	*ENSAMXG00005022013**	*ENSAMXG00000001798**
B cells	*ENSAMXG00005001652**	*ENSAMXG00000033936**
	*ENSAMXG00005007434**	*zgc:194275*
	cd37	*ENSAMXG00000029163**
	*ENSAMXG00005014280**	*ENSAMXG00000038512**
	si:dkey-24p1.1	*ENSAMXG00000006777**
	*ENSAMXG00005006484**	*cd37*
	*ENSAMXG00005014291**	*ENSAMXG00000036191**
	*ENSAMXG00005012813**	*ENSAMXG00000034153**
	*ENSAMXG00005000610**	*ENSAMXG00000043949**
	*ENSAMXG00005002435**	*ENSAMXG00000043088**
Erythrocytes	*hbaa2*	*ENSAMXG00000029151**
	*ENSAMXG00005017042**	*hbaa2 (ENSAMXG00000029181)*
	wu:fj16a03	*ENSAMXG00000037273**
	cahz	*hbba2*
	nt5c2l1	*HBE1 (ENSAMXG00000037475)**
	*ENSAMXG00005020328**	*si:ch211-250g4.3**

	*ENSAMXG00005017060**	*si:ch211-103n10.5*
	mt2.2	*cahz*
	*zgc:163057**	*slc4a1a*
	*ENSAMXG00005017061**	*wu:fj16a03*
Epicardium	*ENSAMXG00005022849**	*ENSAMXG00000036050**
	tcf21	*TCF21*
	*ENSAMXG00005007716**	*cfd*
	*ENSAMXG00005012482**	*c3a.1**
	zgc:158846	*ENSAMXG00000036137**
	*ENSAMXG00005022791**	*igfbp5a*
	*ENSAMXG00005009039**	*stmn1a*
	*ENSAMXG00005008245**	*wt1b*
	*ENSAMXG00005022313**	*glis2a*
	wt1b	*slc29a1a*
Smooth Muscle	*si:dkey-57k2.6*	*CASP6*
	*ENSAMXG00005003735**	*tagln*
	thbs1b	*angptl7*
	*ENSAMXG00005011018**	*ENSAMXG00000031755**
	TPM1	*acta2**
	anxa1a	*si:dkey-57k2.6*
	ITIH3	*rbp4*
	*ENSAMXG00005005681**	*sox9b*
	*ENSAMXG00005018089**	*anxa1a (ENSAMXG00000035597)*
	thbs4a	*thbs1b*
Dendritic Cells/Macrophages	*ENSAMXG00005011614**	*ENSAMXG00000036068**
	*ENSAMXG00005002001**	*ccl35.1**
	*ENSAMXG00005021693**	*ENSAMXG00000037572**
	*ccl34a.3**	*cd74a*
	cxcr4b	*ENSAMXG00000004394**
	*ENSAMXG00005014236**	*cxcl8a*
	cd74a	*cxcr4b*
	*ENSAMXG00005001734**	*ENSAMXG00000042210**
	*ENSAMXG00005009773**	*si:dkey-5n18.1*
	c1qb	*il1b (ENSAMXG00000035729)**

Table 3. 2: Table of the top 10 marker genes identified using FindMarkers for the major cardiac cell types

Gene symbols have been provided where possible; for genes where gene symbol annotation is not available or multiple Ensembl IDs have the same gene symbol, Ensembl IDs have been provided. Genes identified in both genome assemblies are highlighted in red. denotes genes that are assembly-specific.*

6) Due to poor reference genome quality, both v1.0.2 and v2.0 assemblies partially capture the available single cell AM transcriptomic information

To facilitate cell identity annotation, the expression patterns of well-established cardiac cell type markers were explored. However, this exploration presented two major problems.

Firstly, many cardiac canonical cell-type markers were found to be only annotated in one genome assembly, rendering their presence in the final dataset dependent on assembly alignment. For instance, α-smooth muscle actin (*acta2*: a marker of pericytes, smooth muscle and myofibroblasts[217–219]) is only annotated in the v2.0 assembly whilst troponin C1 (*tnnc1a*: a cardiomyocyte contractile protein[220]) is only annotated in the v1.0.2 assembly. This is problematic as, due to the incomplete but divergent gene annotation of each assembly, both the v1.0.2 and v2.0 datasets only partially captured the full transcriptomic information available in the sequencing data and, frustratingly, captured different parts of the transcriptome.

Secondly, different patterns of gene expression were found for genes annotated in both genome assemblies. *arhgap27,* a gene previously linked to cardiac regeneration by the Mommersteeg lab[29] was found to have different patterns of expression. In the v1.0.2 dataset, *arhgap27* was expressed in very few leukocyte cells. On the other hand, *arhgap27* had higher expression levels in the v2.0 dataset and was also found in endothelial cells and smooth muscle cells (Figure 3.7). When the gene-level annotation of *arhgap27* was assessed in IGV browser, a greater number of *arhgap27* reads were found to align to the v2.0 annotation than the v1.0.2 annotation, likely explaining the observed differential patterns of expression. However, this finding is particularly

troubling as without further validation of *arhgap27* expression levels in leukocytes, endothelial cells and smooth muscle cells, no evidence is available to determine whether the v1.0.2 or the v2.0 annotation of *arhgap27* most accurately reflects 'true' *arhgap27* expression in the AM.

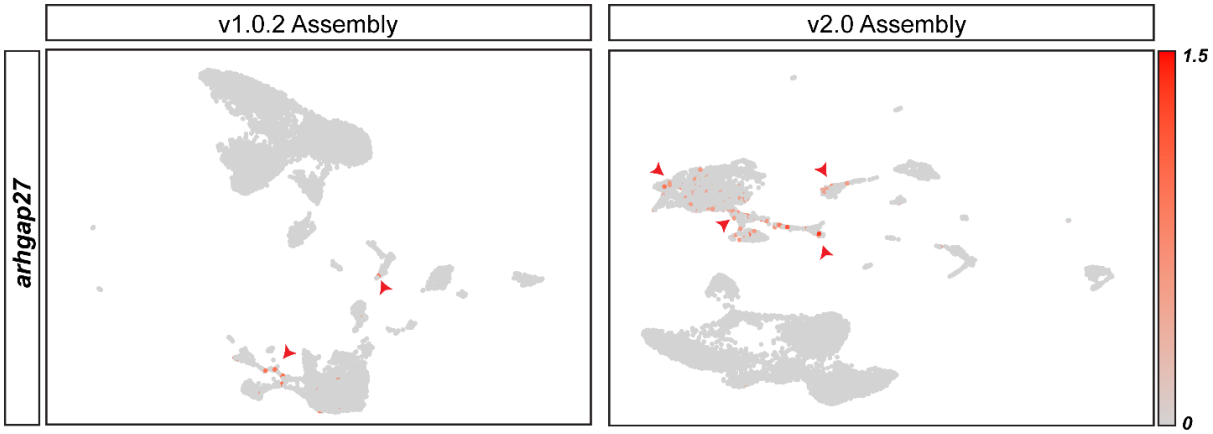

Figure 3. 7: arhgap27 is discordantly annotated in the Pachón Cavefish and Mexican Tetra genome assemblies

FeaturePlot show the distribution of arhgap27⁺ cells on the v1.0.2 and v2.0 datasets as highlighted in red.

Therefore, the discordant gene annotations of the v1.0.2 and v2.0 assemblies produced two distinct scRNAseq datasets that differed in terms of: the number of cells and genes captured, the top cardiac cell type markers, the annotation of key canonical cardiac genes, and the expression pattern of shared genes of interest. However, it was unknown whether the observed differences in individual genes would impact the results of downstream functional pathway analysis.

7) A. mexicanus genome assembly alignment can distort the interpretation of scRNAseq data due to the problems created by underlying genome assembly differences

To test whether functional pathway analysis of the v1.0.2 and v2.0 datasets would produce the same results, v1.0.2 and v2.0 cells were tested for significant differences in the expression of the MSigDB Hallmark signalling pathways using Gene Set Enrichment Analysis (GSEA).

To select which cell-type to use for GSEA, the number of unique genes detected in each cell type was compared. This revealed that endothelial cells showed the greatest difference in the number of features detected between v1.0.2 and v2.0 cells, with v2.0 cells expressing a greater number of genes per cell than their v1.0.2 counterparts (Fig. 3.8a&b). DGE analysis between v1.0.2 and v2.0 endothelial cells was performed using the logistic regression test which identified 2,512 genes that were upregulated in an assembly-specific manner (Fig. 3.8c). Remarkably, GSEA of the 2,512 differentially expressed genes showed that only v2.0 endothelial cells were enriched for genes downregulated in response to UV radiation, showing that the v1.0.2 and v2.0 datasets can generate different functional results, despite originating from the same sequenced reads (Fig. 3.8d). Therefore, the results of the GSEA confirmed that genome assembly choice has a significant impact on the interpretation of the AM scRNAseq data.

In conclusion, AM genome assembly alignment can produce scRNAseq datasets that differ in:

- Cell capture rates
- Gene capture rates
- Top cell type markers
- Gene expression patterns
- Functional pathway enrichment

The incomplete annotation of the v1.0.2 and v2.0 genome assemblies also resulted in scRNAseq datasets that only partially captured the transcriptomic picture of the AM heart. Therefore, optimal analysis of the AM scRNAseq dataset requires novel solutions to overcome the problems caused by discordant and incomplete underlying reference AM genomes.

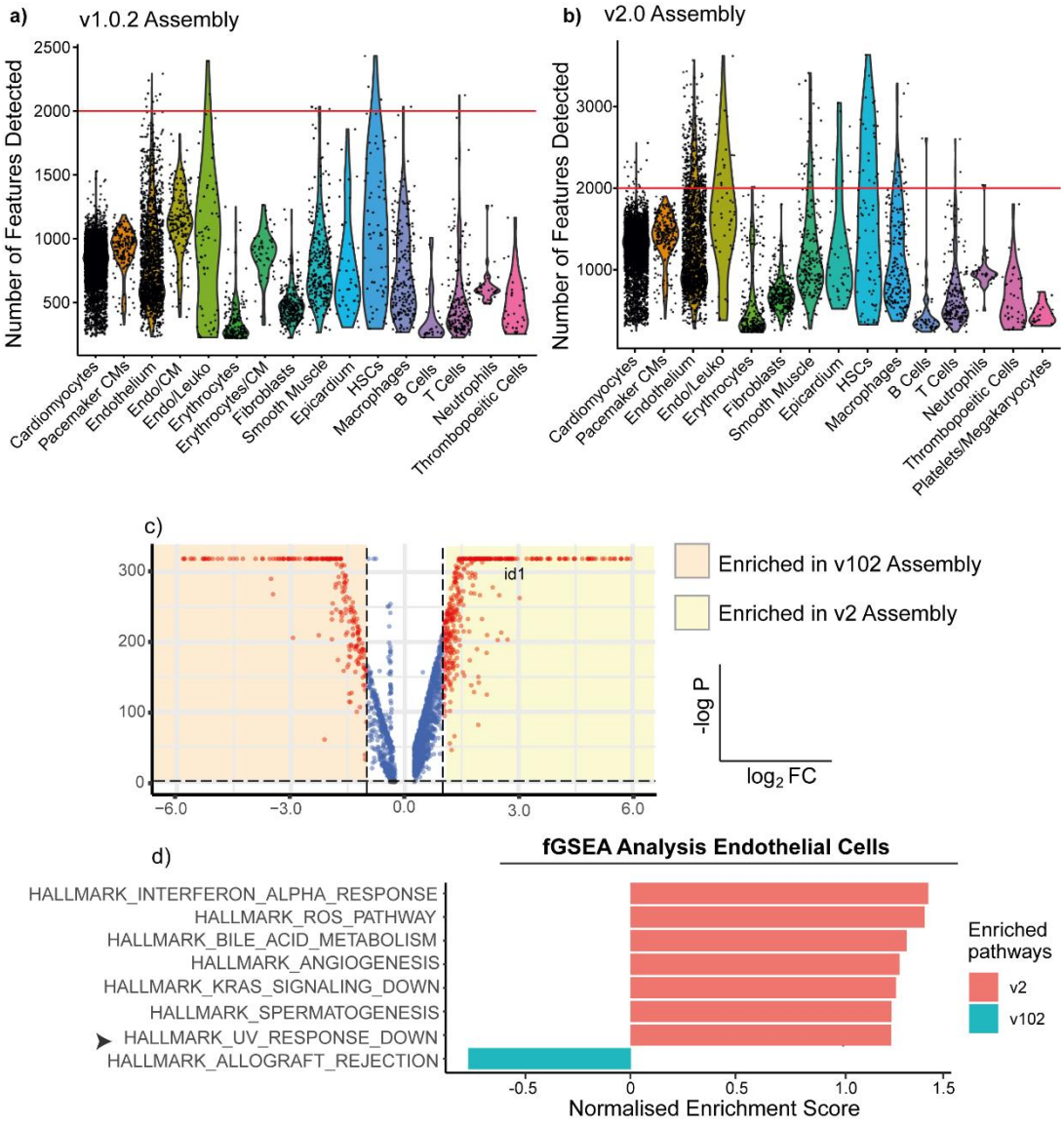

Figure 3. 8: Genome alignment choice produces assembly-specific results due to discordant genome annotations

Violin plots showing the distribution of the number of genes detected/cell in each major cardiac cell type in the v1.0.2 assembly (A) and the v2.0 assembly (B). The red line is drawn at 2000 features/cell to show how many v2.0 endothelial cells express a greater number of unique genes. (C) Volcano Plot showing the results of DGE analysis of v.1.0.2 vs v2.0 endothelial cells. id1 is upregulated in the v2.0 endothelial cells and is annotated in the Hallmark pathway of genes downregulated in response to UV radiation. (D) GSEA analysis showing the top hallmark terms per dataset, with the pathway that reached the 0.25 false discovery rate (FDR) threshold highlighted by the black arrow, showing that

genes annotated in the hallmark pathway as downregulated in response to UV radiation are significantly enriched in v2.0 endothelial cells[7].

8) *A novel integration methodology and 3' UTR extension algorithm can mitigate the problems created by discordant genome assembly annotations*

To overcome the major hurdles posed by the incomplete and discordant AM reference genome assemblies, I devised two novel solutions that would improve the quality of the scRNAseq dataset.

Firstly, the 3'UTR annotation of both v1.0.2 and v2.0 assemblies was improved to minimise the problems caused by incomplete genome annotation. Lack of adequate 3'UTR annotation leads to the loss of transcriptomic information during scRNAseq analysis as scRNAseq reads which don't align to 3' UTR annotations are filtered out and removed from the final dataset by Cell Ranger. However, both v1.0.2 and v2.0 genome assemblies are poorly annotated in their 3'UTRs, resulting in the unnecessary filtration of meaningful transcripts. Therefore, to increase the annotation of the 3'UTR, a terminal extension algorithm was applied to both assemblies. This created custom GTF annotation files in which the 3' UTRs were extended in regions where there was good sequencing evidence that the annotation had been prematurely terminated (Fig. 3.9). As a result, thousands of gene-level annotations were extended in both assemblies, resulting in a significant increase in the capacity to detect the expression of thousands of genes within the scRNAseq data (5,077/25,489 for the v1.0.2

[7] Figure adapted from Potts et al (2022): 'Discordant Genome Assemblies Drastically Alter the Interpretation of Single-Cell RNA Sequencing Data Which Can Be Mitigated by a Novel Integration Method'

assembly; 8,721/27,420 for the v2.0 assembly).

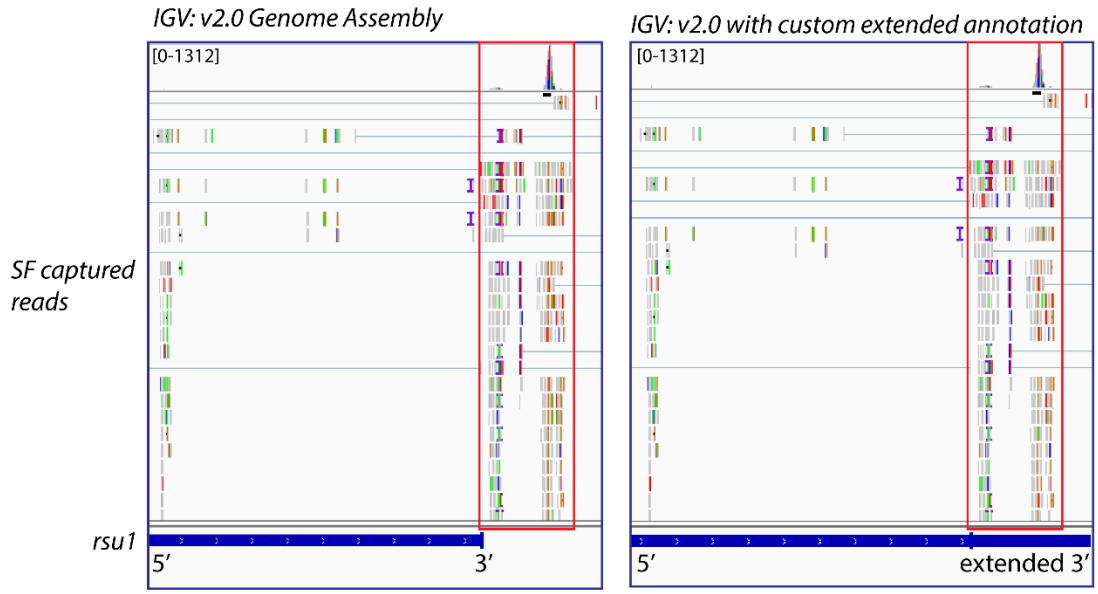

Figure 3. 9: Custom 3' UTR extension maximises transcript capture for genes with incomplete 3'UTR annotation

IGV browser was used to compare aligned reads using the v2.0 gtf file available from Ensembl (v103) with our the custom extended gtf file. This revealed that many reads captured by scRNAseq are removed during genome assembly alignment due to poor 3'UTR annotation whilst the custom extension algorithm helps to mitigate this problem of unnecessary read exclusion (as highlighted by the red box).

Secondly, both datasets were integrated using the SCTIntegration pipeline to produce an overall integrated dataset (Fig. 3.10a). Cells that originated from either the v1.0.2 or the v2.0 dataset were present and treated as unique within the integrated dataset, preventing the loss of assembly-specific cells from analysis. Furthermore, the integrated dataset enabled the inclusion of 4,311 assembly-specific genes for v1.0.2, and 5,638 for v2.0 within the same dataset, ensuring that all possible transcriptomic information was available for simultaneous interrogation. SCTIntegration clustered similar cells together regardless of genome alignment and did not introduce any assembly-

specific cell clusters (Fig. 3.10b), enabling all 241 genome-specific cells to be included (Fig. 3.10c). The inclusion of assembly-specific cells increased the size of a wide range of cell type clusters such as erythrocytes, endothelial cells, cardiomyocytes, leukocytes, smooth muscle and fibroblasts, increasing the likelihood that rare cell types are not lost during Cell Ranger filtration.

Critically, the integrated dataset improved the quality of the scRNAseq data by enabling accurate cell type identification as assembly-specific canonical markers, like *acta2*, could be used simultaneously with cluster marker genes to annotate cell identities (Fig. 3.10d). Additionally, 525 v1.0.2 cells and 765 v2.0 cells changed their cell identity annotation in the integrated dataset. Specifically, the integrated dataset allowed more accurate annotation of doublets (see Appendix 3.1 for transcriptional profile of doublets) as many of the cells that changed annotation during integration were found in doublet clusters in the integrated dataset (25.5% for v1.0.2 cells and 68.5% for v2.0 cells, Fig. 3.10e).[8]

Thus, these novel solutions (i.e. 3' UTR extension and assembly integration) maximised the amount of scRNAseq data available for exploration by ensuring that all possible cells, genes and transcripts were included in the final dataset.

[8] I have previously published text from this paragraph in Potts et al (2022): 'Discordant Genome Assemblies Drastically Alter the Interpretation of Single-Cell RNA Sequencing Data Which Can Be Mitigated by a Novel Integration Method'[174]

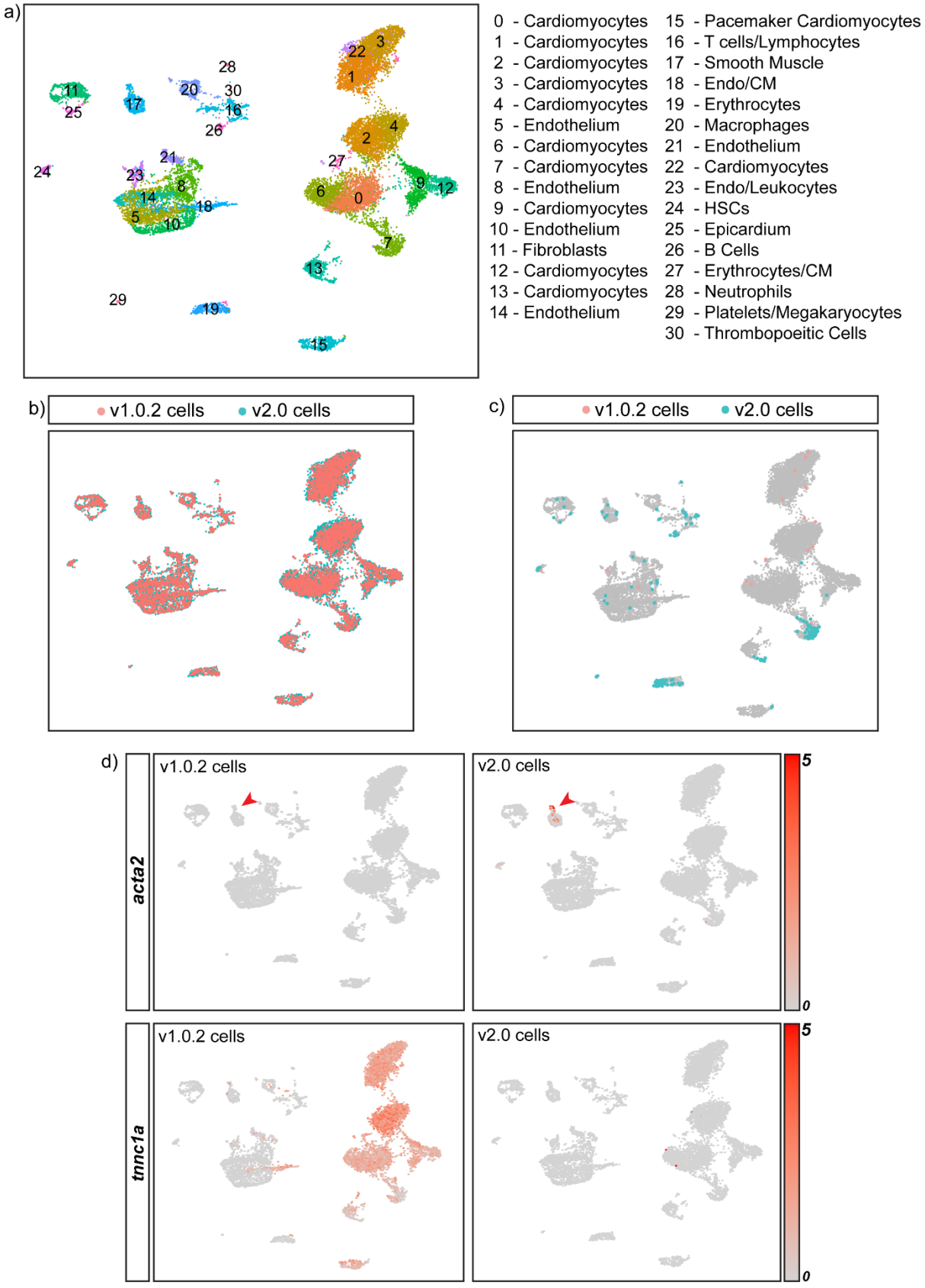
a)
0 - Cardiomyocytes
1 - Cardiomyocytes
2 - Cardiomyocytes
3 - Cardiomyocytes
4 - Cardiomyocytes
5 - Endothelium
6 - Cardiomyocytes
7 - Cardiomyocytes
8 - Endothelium
9 - Cardiomyocytes
10 - Endothelium
11 - Fibroblasts
12 - Cardiomyocytes
13 - Cardiomyocytes
14 - Endothelium
15 - Pacemaker Cardiomyocytes
16 - T cells/Lymphocytes
17 - Smooth Muscle
18 - Endo/CM
19 - Erythrocytes
20 - Macrophages
21 - Endothelium
22 - Cardiomyocytes
23 - Endo/Leukocytes
24 - HSCs
25 - Epicardium
26 - B Cells
27 - Erythrocytes/CM
28 - Neutrophils
29 - Platelets/Megakaryocytes
30 - Thrombopoeitic Cells
b)
v1.0.2 cells
v2.0 cells
c)
v1.0.2 cells
v2.0 cells
d)
acta2
v1.0.2 cells
v2.0 cells
5
0
tnnc1a
v1.0.2 cells
v2.0 cells
5
0

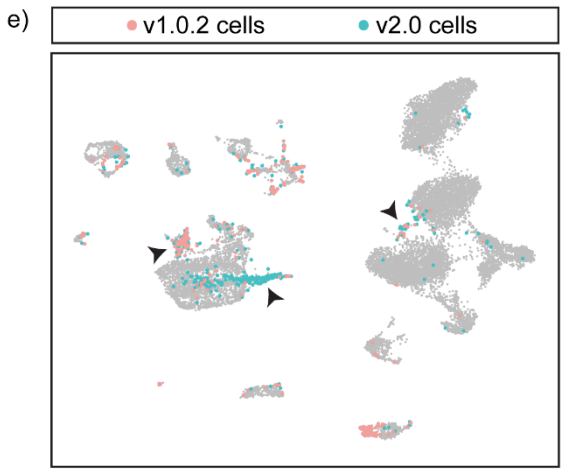

Figure 3. 10: Integrating the v1.0.2 and v2.0 datasets improves cell type identification and maximises the number of cells included in the final dataset

(A) Annotated UMAP of the integrated dataset showing all the expected cell types of the heart. (B) Cells coloured according to genome assembly on the UMAP shows that SCTIntegration produces a UMAP in which cells from both assemblies cluster together. (C) 241 cells present in the integrated dataset are genome assembly-specific. These cells fall within a range of cell type clusters such as erythrocytes, endothelial cells, cardiomyocytes and fibroblasts and would be excluded if either the v1.0.2 or the v2.0 assembly was used in isolation. (D) FeaturePlot split by genome assembly was used to plot 2 separate UMAPs in which each UMAP contains cells from either the v2.0 dataset or the v1.0.2 dataset, revealing the cluster expression of assembly-specific marker genes like acta2 and tnnc1a in the integrated dataset. (E) 525 cells from the v1.0.2 dataset and 765 cells from the v2.0 dataset were annotated differently in the integrated dataset. Many of these cells were found to cluster in doublet clusters and were re-annotated as doublets, as indicated by the black arrows.

9) Conclusions of optimisation of the application of scRNAseq to the A. mexicanus heart

Although integrating the v1.0.2 and v2.0 datasets increased the accuracy of AM cardiac cell type annotation, it is not suitable for many types of downstream scRNAseq analysis. The results of DGE analysis and functional pathway analysis would be completely distorted by the presence of assembly-specific genes in the scRNAseq matrix, as well as by the double representation of genes

present in both assemblies. Therefore, although assembly integration is essential during cell-type identification, I concluded that further downstream analysis should be limited to one genome assembly. Based on the finding that a greater percentage of reads mapped to the v2.0 transcriptome, the v2.0 assembly was chosen as the focus for this thesis. Therefore, for the overall, large-scale scRNAseq dataset, the following schematic was applied to every sample (Fig. 3.11).

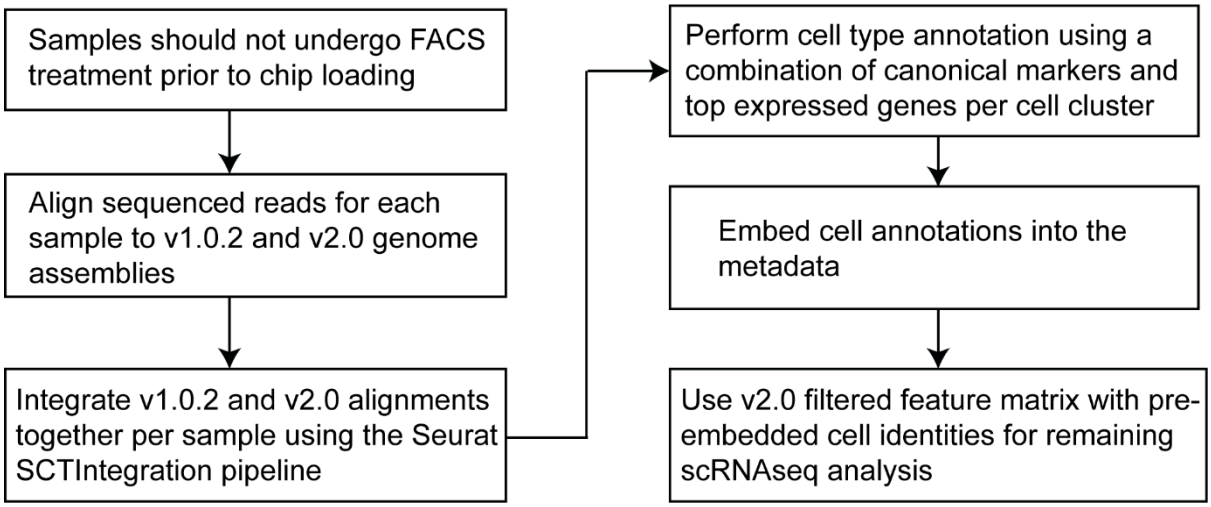

Figure 3. 11: Schematic of the optimal AM scRNAseq analysis pipeline

3.2.2 scRNAseq of the AM response to cryoinjury

Following cell identity embedding within each scRNAseq sample using the above method, Harmony was used to integrate all 12 samples together, creating a final, overall dataset of 85,516 cells (Fig. 3.12a, see Appendix 3.2 for integration optimisation). Overall dataset clusters were annotated using a combination of cell-identity embedding, cluster markers and the expression of canonical cell type-specific genes (Fig, 3.12b) to identify the range of expected cardiac cell types such as myocardial, endocardial, epicardial cells, fibroblasts and blood circulating cells (see Appendix 3.3 for additional characterisation).

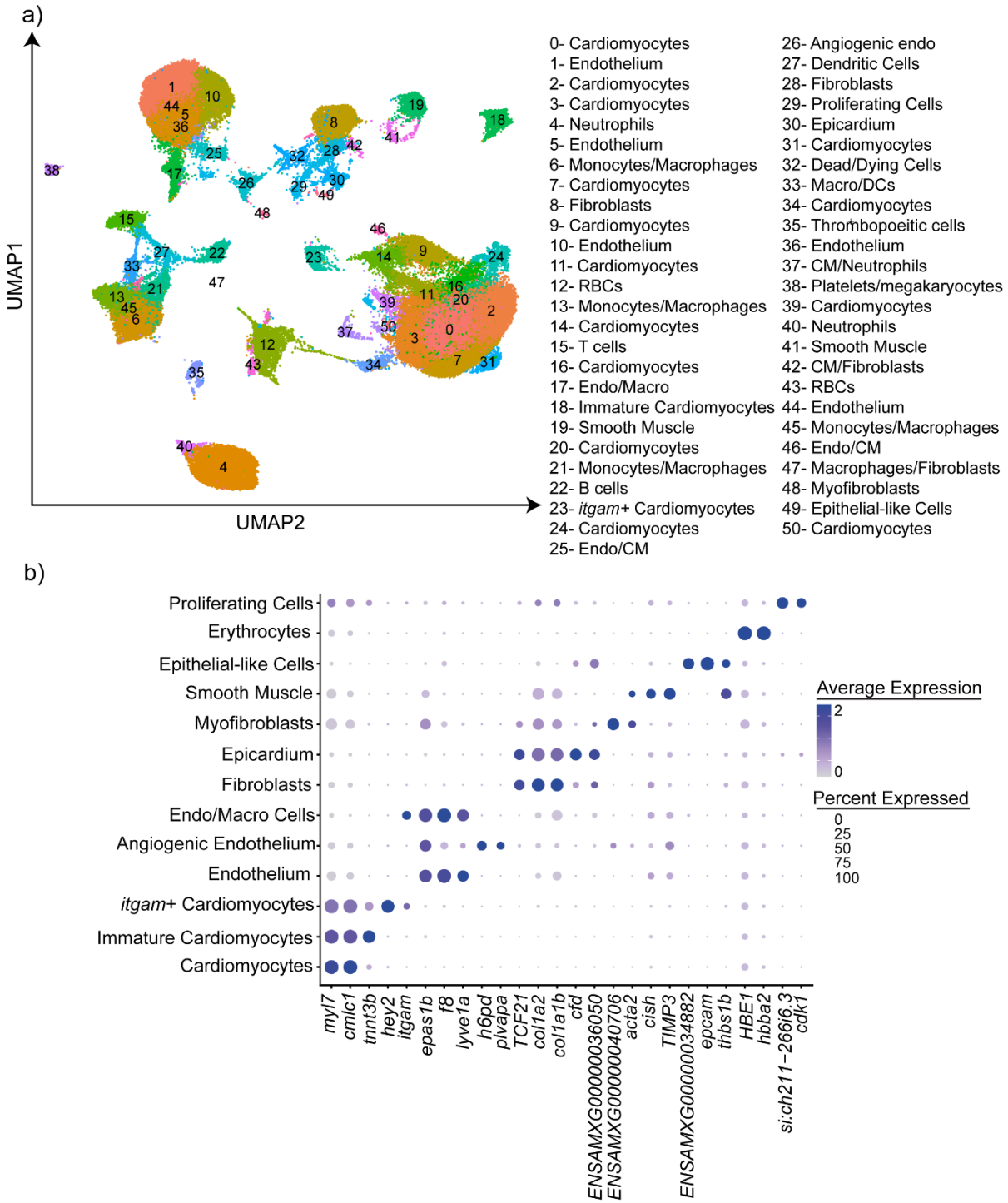

Figure 3. 12: Overview of the scRNAseq A. mexicanus dataset

(A) UMAP of the integrated scRNAseq dataset, containing all SF and PF cells from each time point. (B) DotPlot showing examples of the top marker genes used during cluster annotations of non-leukocyte cells.

3.2.3 Characterisation of overall *A. mexicanus* leukocyte dynamics following injury

To specifically investigate the AM immune response, PF/SF leukocytes were identified in the scRNAseq data using well-established pan-leukocyte markers such as *ptprc*[221], *lcp1* and *cxcr4b.* 14 leukocyte clusters were found in the overall scRNAseq dataset (Fig 3.13a) and the proportion of leukocytes that made up the PF and SF hearts at every time point was visualised (Fig.13.13b&c). To identify whether the PF/SF immune responses showed significant differences in their leukocyte proportions, differential proportion analysis (DPA)[182] was used to test for statistically significant differences. Firstly, PF/SF leukocyte proportions were compared to their respective baseline levels using DPA. This showed that PF leukocytes were significantly elevated immediately after injury at 1- and 3dpci, but by 7- and 14dpci leukocyte proportions were no longer elevated (Fig. 3.13d, $p<0.01$). In contrast, the SF showed significant elevation of leukocyte proportions following injury at all time points (Fig. 3.13e, $p<0.01$), revealing that the PF and SF overall immune responses differed significantly in their temporal kinetics. Leukocyte proportions were then compared at every time point between PF and SF hearts to identify any differences in the PF/SF leukocyte responses. This analysis found that PF and SF leukocyte proportions were significantly different at 7dpci, when the PF immune response seemed to return to the uninjured state whereas SF leukocyte proportions remained elevated (Fig. 3.13f, $*p<0.01$). At 14dpci, a similar pattern to 7dpci was observed, with the SF showing elevated leukocyte proportions compared to the PF. However, this difference did not reach the DPA significance threshold. Therefore, from the results of the DPA analysis it is possible to conclude that the PF and SF immune responses to cardiac injury are significantly different, with the SF immune response dominating at the later stages of cardiac healing.

To confirm that the immune response to necrotic cell death was greater than to sham surgery, DPA was also used to compare injured immune cell proportions to the sham samples. This found that for both SF and PF, sham surgery resulted in a significant increase of leukocyte proportions compared to uninjured hearts (Fig. 3.13g & h). However, leukocyte proportions at 3dpci in PF, and at 1- and 3dpci in SF, were significantly greater than the 3-day sham samples (Fig. 3.13g &

h). Therefore, this analysis confirmed that necrotic cell death stimulates a substantial immune response in both PF and SF that is greater than the immune response to sham surgery.

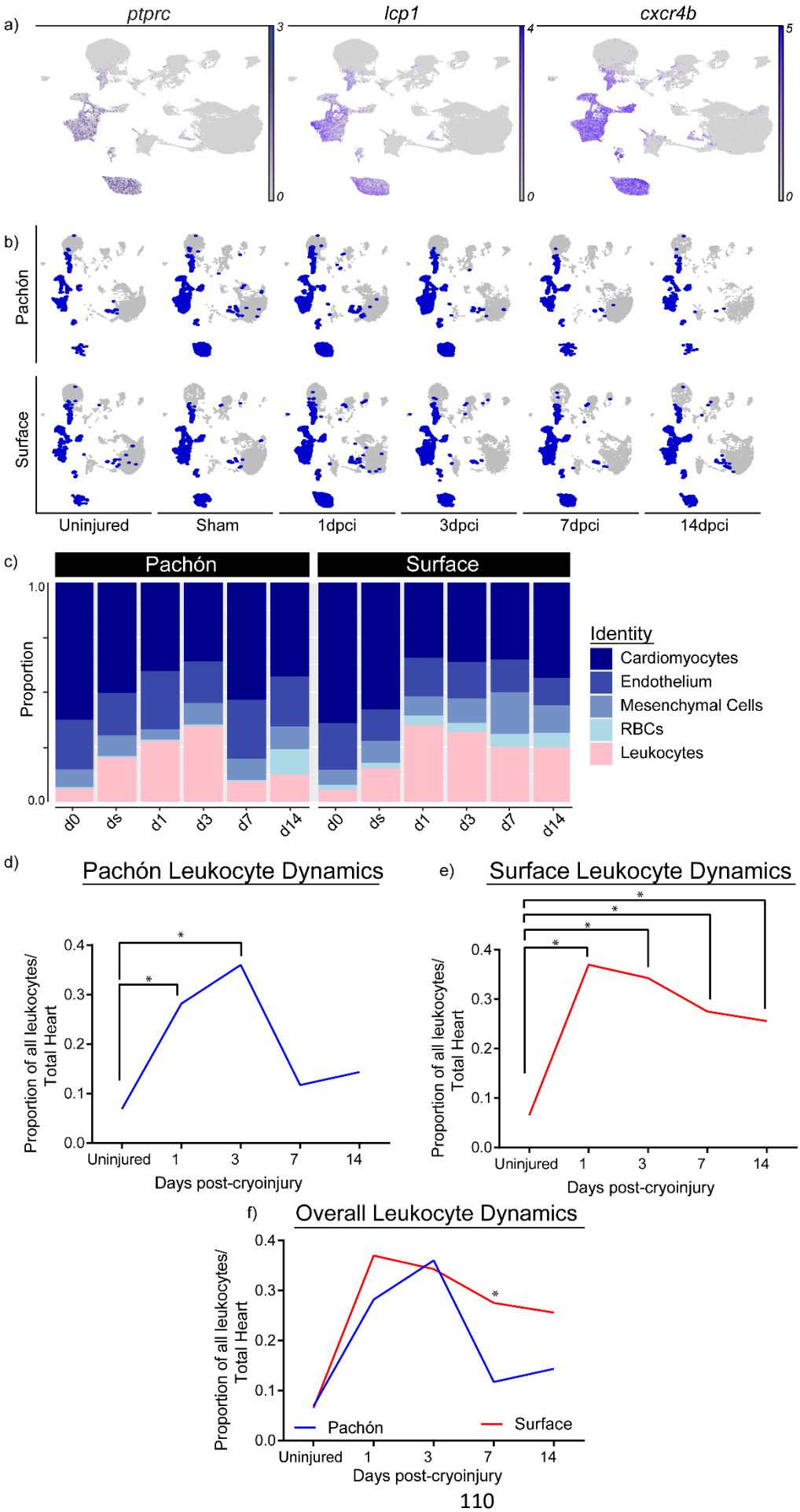
a)
ptprc
lcp1
cxcr4b
b)
Pachón
Surface
Uninjured
Sham
1dpci
3dpci
7dpci
14dpci
c)
Pachón
Surface
Proportion
Identity
Cardiomyocytes
Endothelium
Mesenchymal Cells
RBCs
Leukocytes
d0
ds
d1
d3
d7
d14
d)
Pachón Leukocyte Dynamics
e)
Surface Leukocyte Dynamics
Proportion of all leukocytes/ Total Heart
Days post-cryoinjury
f)
Overall Leukocyte Dynamics
Pachón
Surface

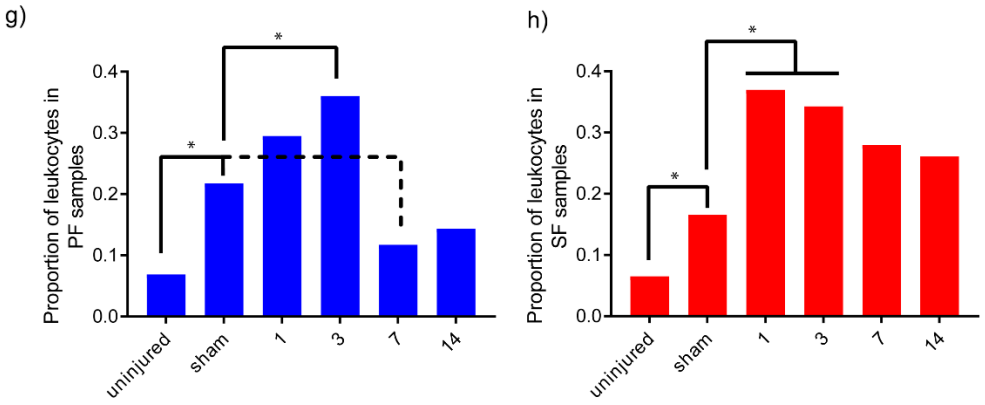

Figure 3. 13: PF and SF show statistically different overall leukocyte dynamics following injury

*(A) FeaturePlots of ptprc, lcp1 and cxcr4b expression, identifying clusters 4, 6, 13, 15, 17, 21, 22, 27, 33, 35, 37, 40, 45 and 47 as leukocytes. (B) UMAP highlighting the number of leukocyte cells captured at each time point from the PF and SF hearts. Cells in leukocyte clusters are highlighted in blue. (C) Stacked histograms of major cardiac cell population proportions for PF and SF hearts at each time point. (D) DPA analysis shows that PF leukocytes are significantly elevated compared to baseline proportions at 1- and 3dpci. (E) DPA analysis shows that SF leukocyte proportions are significantly elevated compared to uninjured levels at all time points following cryoinjury. (F) DPA analysis comparing PF and SF leukocyte proportions at each time point shows that SF leukocytes are significantly elevated at 7dpci. (G) DPA analysis comparing leukocyte proportions to sham shows that sham leukocytes are significantly elevated compared to uninjured and 7dpci. However, PF leukocytes recruited at 3dpci are significantly elevated compared to sham. (H) DPA analysis comparing SF leukocyte proportions to sham shows that sham leukocytes are significantly elevated compared to uninjured. However, SF leukocytes at 1dpci and 3dpci are significantly elevated compared to sham (DPA *, $p<0.01$).*

To confirm the observed leukocyte dynamics from the scRNAseq, cell counts were initially performed using the L-plastin 1 (Lcp1) antibody to stain for all leukocytes in uninjured, 1- and 3dpci hearts (Fig. 3.14a), and normalised to total ventricular area. Lcp1 counts found that, at baseline and

at 3dpci, PF and SF show no difference in the numbers of leukocytes (Fig. 3.14b), confirming the scRNAseq data. However, at 1dpci, the PF showed a significantly greater influx of leukocytes than the SF (Fig. 3.14b). Although this result was not observed in the scRNAseq data, as the scRNAseq dataset represents n=1, this finding revealed the importance of cell count validations for all PF/SF leukocyte dynamics.

As the number of leukocytes influxing into the heart is likely to depend on the size of injury, with bigger injuries resulting in a greater influx of immune cells, counts of Lcp1+ cells present just in the wound were also performed. Wound area is typically defined as lack of myocardial staining. However, at 1dpci the MF20 signal (which stains myosin heavy chain in the myocardium) was not detectably degraded and could not be used to define wound area. Therefore, DAPI staining was used as a substitute to define wound area specifically at 1dpci as the blood clot which forms in response to injury could be visualised using DAPI (in fish, blood clot-forming thrombocytes are nucleated). Counts of Lcp1+ cells in the wound were normalised to fractional wound area (wound area/ventricular area) to account for the larger size of the SF hearts and heart size variability within PF/SF groups. Consistent with the previous total Lcp1 counts, wound Lcp1 counts also showed that a significantly greater number of leukocytes influx into PF wounds than into SF wounds at 1dpci (Fig. 3.14c).

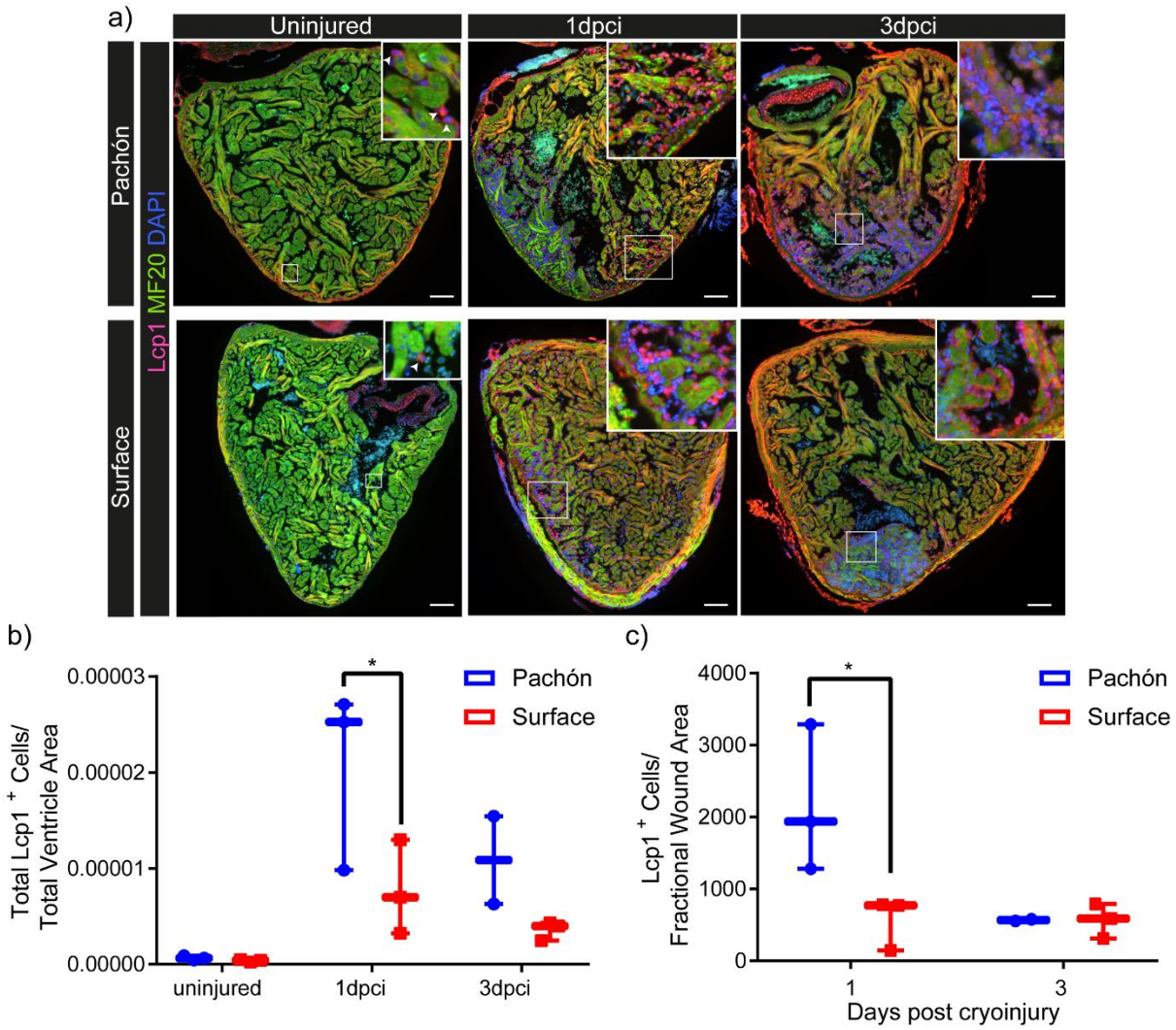

Figure 3. 14: The scarring PF have a greater influx of leukocytes into the wound immediately following injury at 1dpci

*(A) Leukocytes were visualised using Lcp1 antibody at baseline, 1- and 3dpci in PF and SF. Sections were counterstained with MF20 and DAPI. Scale bars represent 100µM. (B) Total Lcp1+ cells present in the heart were counted and normalised to ventricular area, showing that PF leukocyte levels are significantly higher than at SF at 1dpci (2-way ANOVA with Sidak's multiple comparisons test, *p<0.05, n=3). (C) Lcp1+ cells localised to the wound were counted and normalised to fractional wound area (wound area/total ventricular area), showing that at 1dpci, PF leukocyte levels are significantly elevated compared to SF (2-way ANOVA with Sidak's multiple comparisons test, *p<0.05, n=3).*

Unfortunately, antibodies that work well in fish are notoriously hard to find. Although Lcp1 has been used extensively in the zebrafish[222–225], a large increase in the level of background staining in the Lcp1 channel was observed at 3dpci, making cell counts less reliable (Fig. 3.14a). Therefore, an alternate methodology was sought to characterise AM leukocyte dynamics. RNAscope is a novel *in situ* hybridisation technology that enables species-specific fluorescent mRNA probes to be designed to target a gene of interest. To re-do overall leukocyte counts, PF and SF hearts were thus stained with a RNAscope *lcp1* probe (Fig. 3.15a) and the ventricular area positive for *lcp1* staining was measured. This showed that, at 1dpci, *lcp1* staining significantly increased from baseline in the PF whereas the SF showed no difference in *lcp1* staining throughout the heart at any time point (Fig. 3.15b). When positive *lcp1* staining was normalised to the wound area, the PF showed significantly greater areas of *lcp1* staining than SF at both 1- and 3dpci (Fig. 3.15c), suggesting that PF immune response is much stronger than the SF immune response immediately after injury.

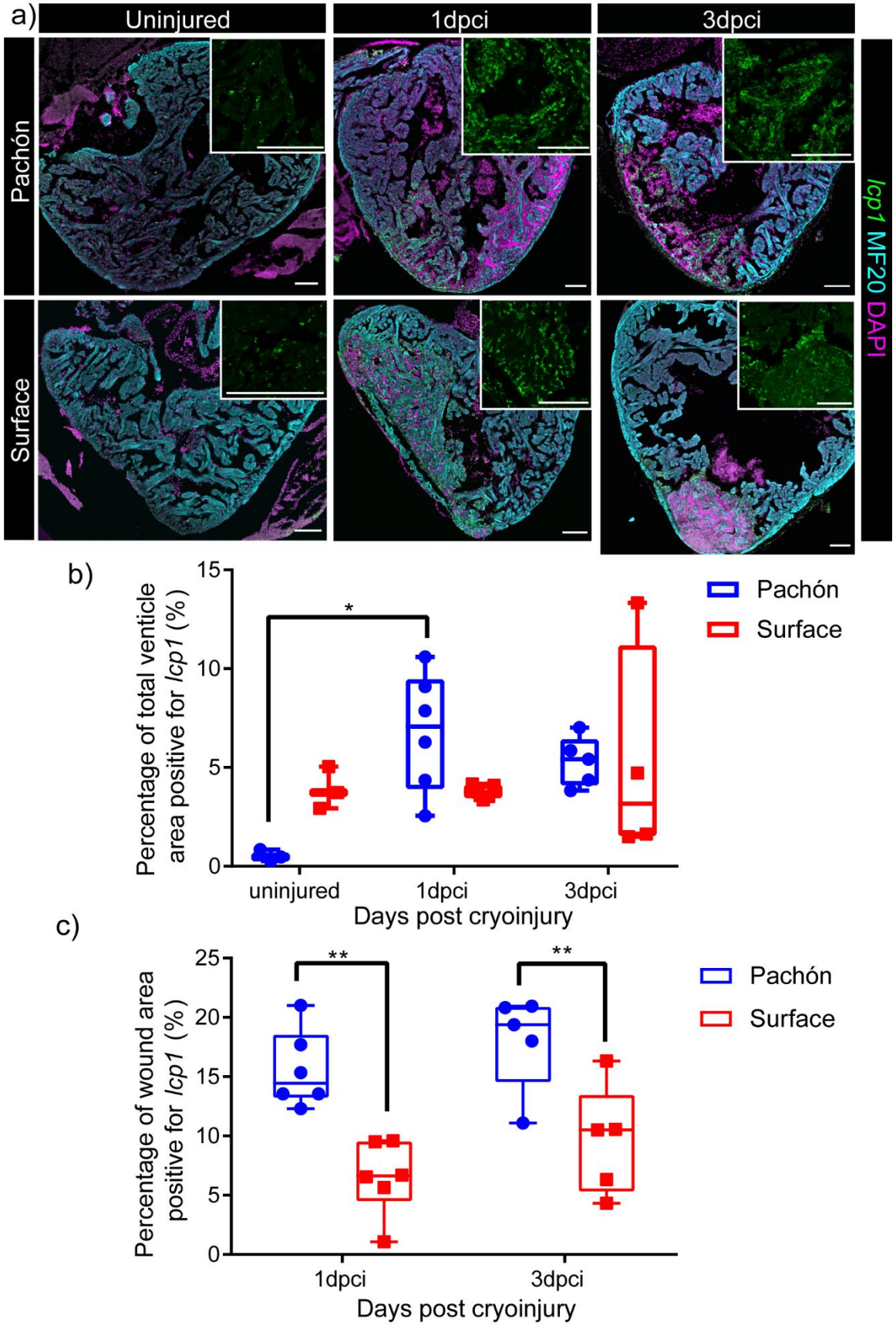
a)
Uninjured
1dpci
3dpci
Pachón
Surface
Icp1 MF20 DAPI
b)
Percentage of total venticle area positive for Icp1 (%)
15
10
5
0
*
uninjured
1dpci
3dpci
Days post cryoinjury
Pachón
Surface
c)
Percentage of wound area positive for Icp1 (%)
25
20
15
10
5
0
**
**
1dpci
3dpci
Days post cryoinjury
Pachón
Surface

Figure 3. 15: The scarring PF have a seemingly greater immune response at 1- and 3dpci than the regenerative SF

*(A) Leukocytes were visualised using lcp1 RNAscope probe and sections were counterstained with MF20 and DAPI. Scale bars represent 100µM. (B) To assess lcp1 staining, images were thresholded using ImageJ and the area of the heart positive for lcp1 staining was measured and normalised to ventricular size, showing that lcp1 staining increases in the PF at 1dpci from baseline levels (2-way ANOVA with Sidak's multiple comparisons test, *p<0.05, n=5-6). (C) Positive lcp1 staining in the wound was measured and normalised to wound area, revealing that at both 1- and 3dpci, PF showed a greater degree of lcp1 staining than SF (2-way ANOVA with Sidak's multiple comparisons test, **p<0.01, n=5-6).*

Following the finding that PF/SF leukocytes showed significantly different temporal kinetics, the spatial localisation of PF/SF leukocytes was next compared. At 1dpci, both PF and SF leukocytes show strong localisation to the wound as leukocytes flood to the wound to surround the newly formed blood clot (Fig. 3.16a). However, when the spatial distribution of PF/SF leukocytes within the wound was explored further, a significantly different pattern in PF/SF leukocytes was observed: PF leukocytes tightly surrounded the injured myocardium and were present on almost every surface of damaged cardiac muscle whereas, in contrast, SF leukocytes spread diffusely throughout the wound and did not show this tight coupling to damaged tissue (Fig. 3.16b). This disparity in wound distribution was even more apparent at 3dpci when PF leukocytes were observed to completely cover the wounded myocardium whereas SF leukocytes were restricted to the wound border (Fig. 3.16c). Interestingly, this striking difference in *lcp1*+ cell distribution at 3dpci coincided with a significant difference in MF20 staining: at 3dpci the PF MF20 signal was almost absent within the wound whereas, in SF, MF20 staining was still visible. This suggested that PF leukocytes could be driving an accelerated rate of apoptosis and necrosis in injured PF cardiomyocytes whereas, as SF leukocytes localised to the wound border, SF injured cardiomyocytes were spared from any

damaging signals from their leukocytes. To test whether injured PF/SF myocardium showed significantly different rates of cell death at 3dpci, the percentage of the wound area that was positive for MF20 staining at 3dpci was quantified. This showed that SF wounds displayed a significantly greater percentage area that was positive for MF20 staining in comparison to PF wounds, suggesting that injured PF myocardium has a substantially accelerated rate of cell death at 3dpci (Fig. 3.16d).

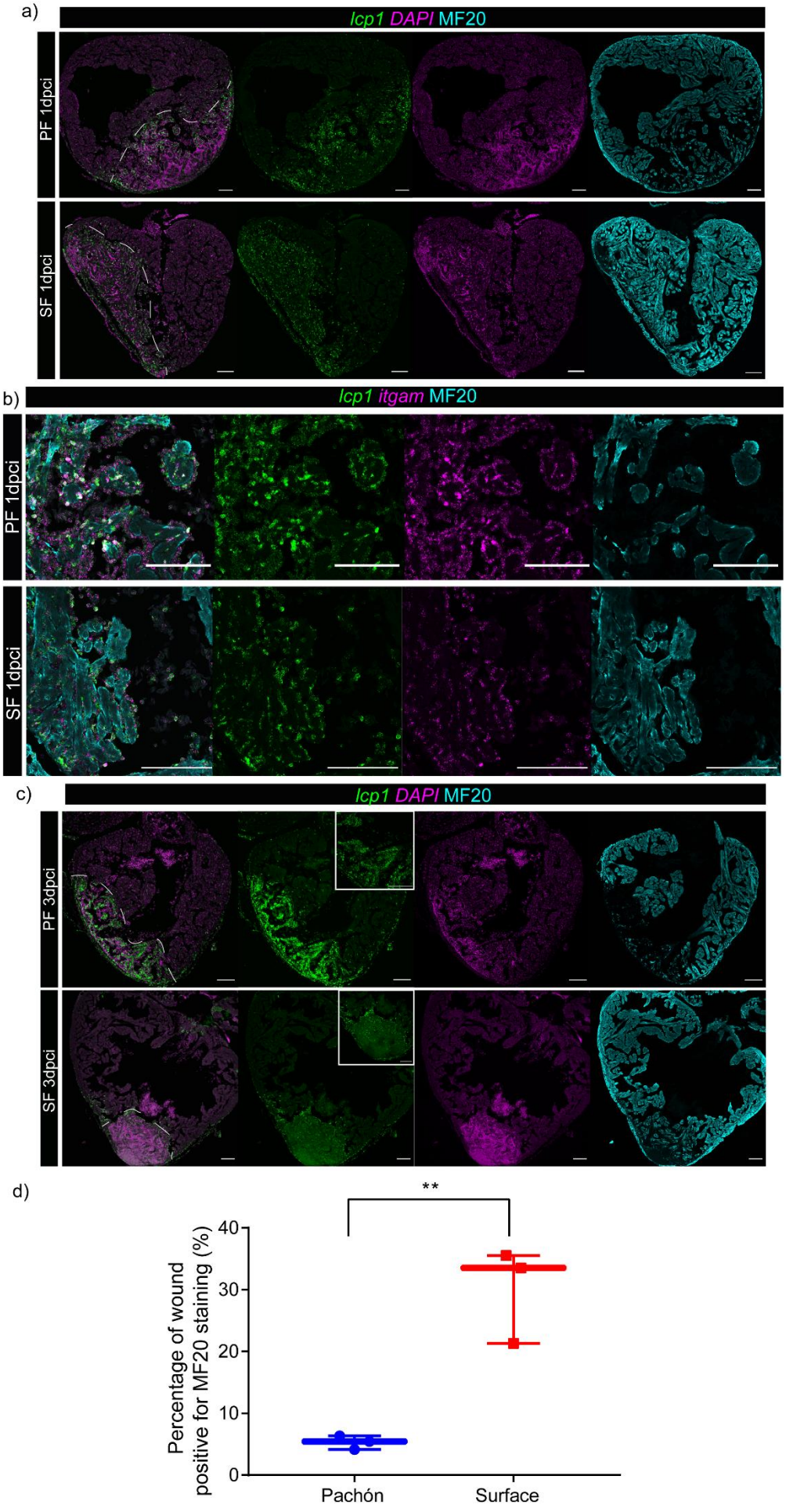
a)
lcp1 DAPI MF20
PF 1dpci
SF 1dpci
b)
lcp1 itgam MF20
PF 1dpci
SF 1dpci
c)
lcp1 DAPI MF20
PF 3dpci
SF 3dpci
d)
**
Percentage of wound positive for MF20 staining (%)
40
30
20
10
0
Pachón
Surface

Figure 3. 16: PF and SF leukocytes show distinctly different spatial distribution throughout the wounded ventricle at both 1- and 3dpci

*Leukocytes were visualised using the lcp1 probe and sections were counterstained with MF20 and DAPI at 1dpci (A), with itgam at 1dpci (B) and with MF20 and DAPI at 3dpci (C). Scale bars represent 100μM. Plot (D) shows quantification of the percentage of PF/SF wounds positive for MF20 staining. (Student's t-test, **p<0.001, n=3).*

Despite RNAscope offering excellent signal-to-noise, *lcp1* staining in 3dpci PF hearts no longer resembled the circular leukocytes that had been observed at 1dpci and instead displayed an almost homogenous area of positive *lcp1* staining that overlapped with the dead/dying regions of the PF myocardium (Fig. 3.16c). Due to the high density of *lcp1* staining in the PF wound, it was difficult to distinguish whether the dead/dying cardiomyocytes were upregulating *lcp1* or whether the *lcp1*+ signal was due to a high density of PF leukocytes covering the dying tissue. Therefore, PF/SF hearts were stained at 3dpci with MF20 to mark the dead/dying myocardium and a RNAscope probe for *itgam* to act as an alternative leukocyte marker, to distinguish more clearly whether dead/dying PF cardiomyocytes were expressing *lcp1*. Remarkably, *itgam* showed the same pattern of expression as *lcp1* in 3dpci PF (Fig. 3.6a), whilst this staining pattern was absent in SF and in sections stained with negative control probe mix, suggesting that the observed upregulation of immune cell markers within wounded PF myocardium is not due to autofluorescence from dead/dying cells (Fig. 3.17b). Sections were then co-stained with both the *lcp1* probe and antibody to further confirm this unique pattern, revealing almost identical co-staining that perfectly mapped the dead/dying PF myocardium. This finding suggested that in fact injured PF myocardial cells do upregulate *lcp1* at both the mRNA and protein level at 3dpci (Fig. 3.17c). Furthermore, the scRNAseq data revealed that PF dead/dying cardiomyocytes contain detectable levels of *lcp1* transcripts at 3dpci which were completely absent in SF dead/dying cardiomyocytes (Fig. 3.17d). Although the upregulation of immune cell markers in dying myocardium certainly warrants further investigation,

as this was outside the scope of this thesis, it was not followed up further. Instead, it was concluded that *lcp1* was not a suitable marker for characterisation of the AM immune response to injury.

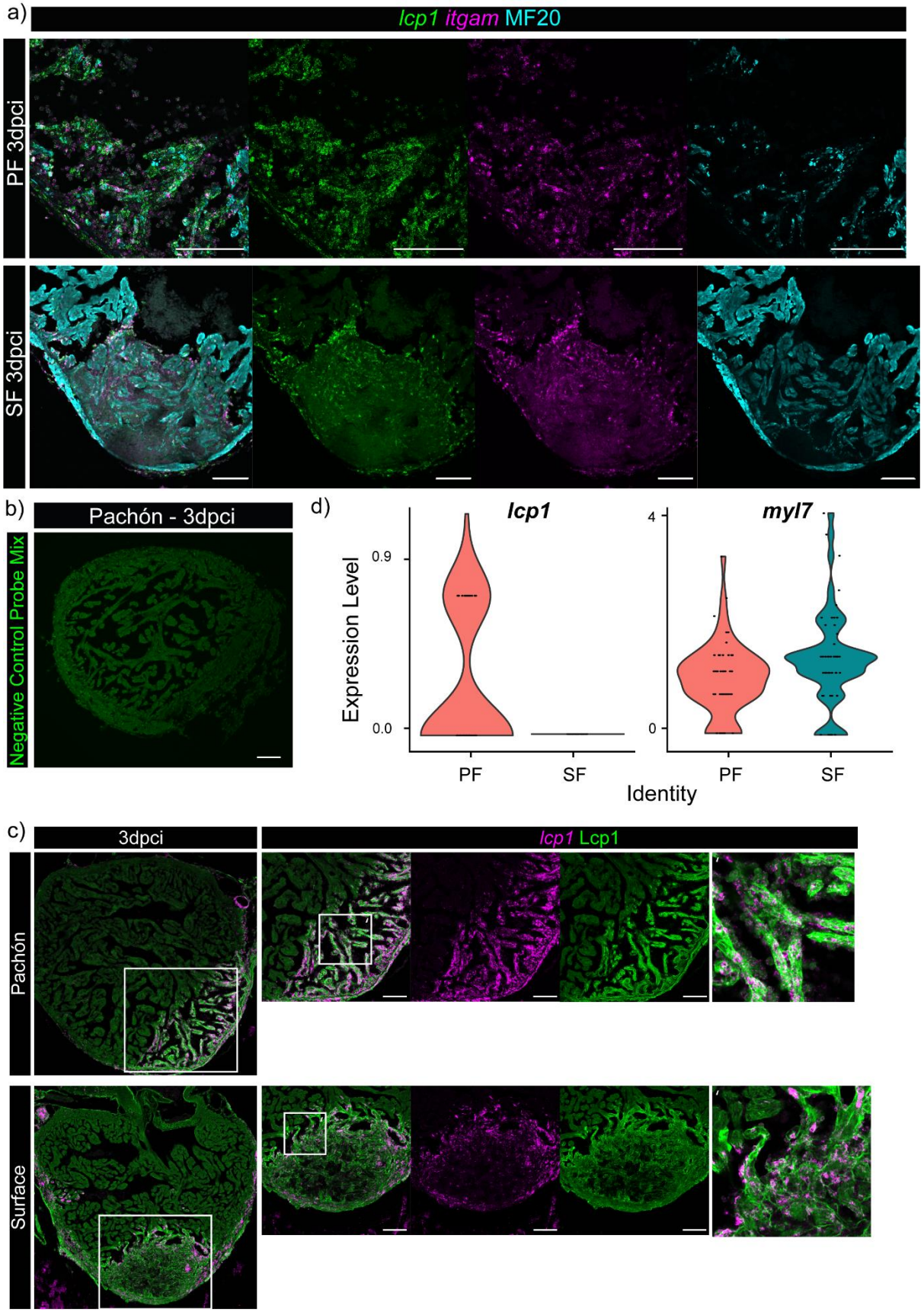

Figure 3. 17: Dead/dying PF cardiomyocytes show expression of leukocyte markers at 3dpci

(A) 3dpci hearts were stained with MF20, lcp1 and itgam, revealing that PF dead/dying myocardium upregulates lcp1 and itgam. (B) RNAscope probe staining with negative control probe mix reveals no positive staining in the dead/dying PF myocardium. (C) 3dpci hearts were co-stained with lcp1 RNAscope probe and lcp1 antibody, revealing that both lcp1 mRNA and protein are found overlapping with dead/dying PF myocardium at 3dpci. Scale bars represent 100μM. (D) scRNAseq data shows that some dead/dying PF cardiomyocytes express lcp1 at 3dpci, albeit at very low levels.

To conclusively characterise the AM leukocyte response, *ptprc* (also known as CD45) was chosen as a new pan-leukocyte marker as it is not expressed in dead/dying PF myocardium (Appendix 3.4). Injured hearts were stained using a RNAscope *ptprc* probe and immune cells present in the wound were counted and normalised to fractional wound area (Fig. 3.18a). *ptprc* staining showed that in the immediate and early stages after injury, PF leukocytes influx into the heart in significantly greater numbers than in the SF at 3dpci (Fig. 3.18b). However, at the late stages of wound healing, the regenerative SF immune response dominates and the SF showed significantly elevated leukocyte levels compared to PF at 14dpci (Fig. 3.18b). These *ptprc*+ cell counts confirmed the previous and independent *lcp1* findings that the SF and PF immune responses show strikingly different temporal dynamics and that, specifically, the initial PF immune response is stronger than the SF.

Following the finding that the SF immune response is significantly elevated at 14dpci, the next logical step was to extend the characterisation of AM leukocyte dynamics to 30dpci to determine whether the SF leukocyte response remains dominant throughout the late stages of wound healing (Fig. 3.18c). Unfortunately, I was unable to assess whether SF leukocyte levels remain significantly elevated at 30dpci due to a low sample number (n=2). However, these preliminary counts suggest that the SF immune response may be active throughout wound healing whereas, in comparison, PF levels remain significantly decreased from 3dpci onwards (Fig. 3.18b).

Overall, leukocyte temporal dynamics using *ptprc* cell counts and scRNAseq DPA results showed a high degree of similarity, especially for the PF. Both methodologies have independently shown that the PF show a strong initial immune response immediately after injury, but that this response subsides from 3dpci and returns towards baseline levels. In contrast, the SF immune response seems to be significantly elevated during the late stages of wound healing, especially at 14dpci (Fig. 3.18d).

From this data, it is therefore possible to conclude that the kinetics of leukocyte recruitment significantly differ in the regenerative and scarring responses to cardiac cell death. However, as *ptprc* is a pan-leukocyte marker, these results do not show whether the PF/SF also show differences in the composition of recruited leukocytes. Thus, the next question was to determine which leukocyte subpopulations are responsible for the initial PF immune response and the late-stage SF immune response.

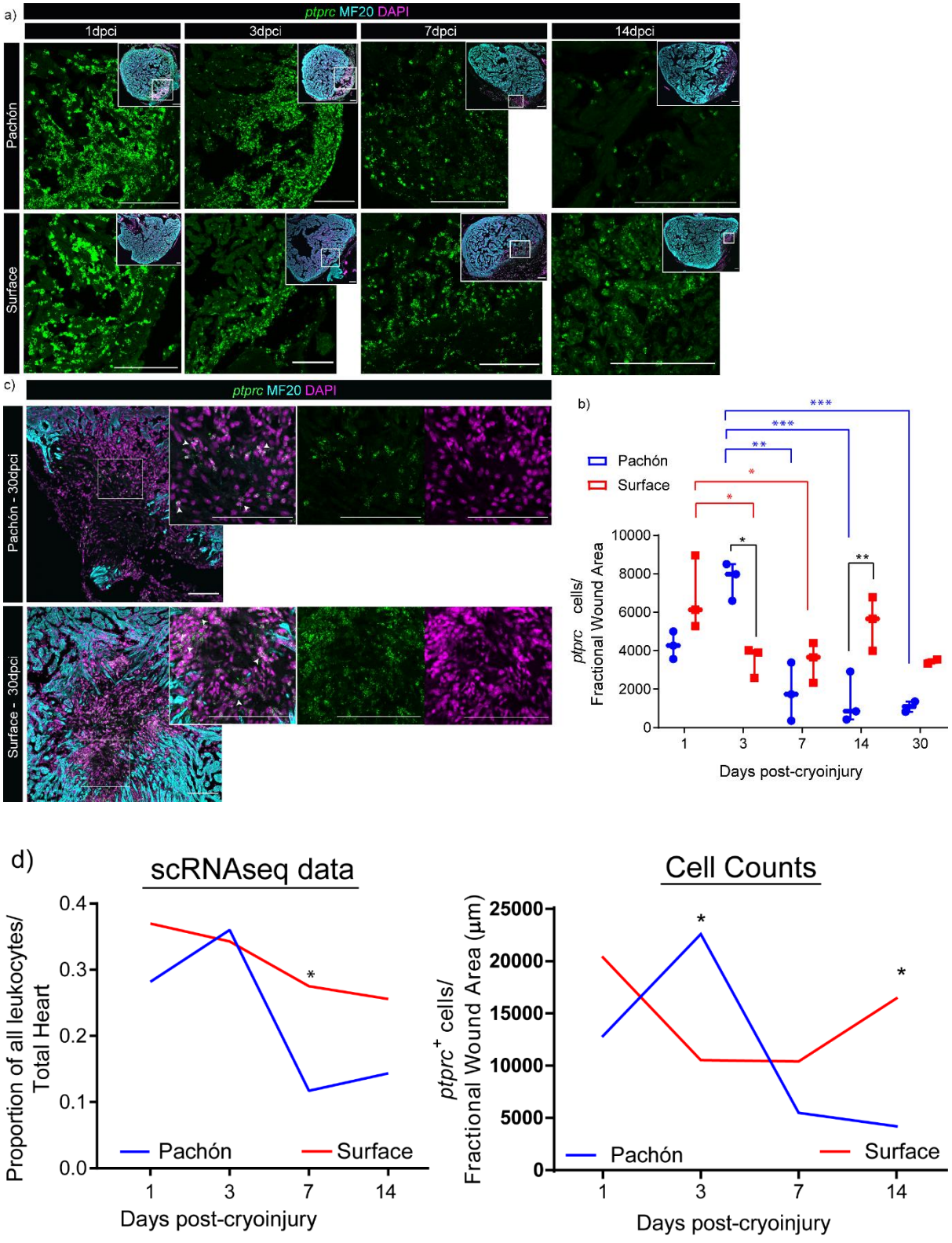

Figure 3. 18: Ptprc counts show that the AM immune response significantly differs at 3dpci and 14dpci with the PF response dominating in the early-stages of wound healing, whilst the SF response takes over at the late stages of wound-healing

*(A) Sections were stained with the ptprc RNAscope probe and counter-stained with MF20 and DAPI at 1-, 3-, 7-, 14- and (C) 30dpci. Scale bars represent 100µM. (B) ptprc+ cell counts were normalised to fractional wound area (2-way ANOVAs with Sidak's multiple comparisons tests were used to compare PF and SF ptprc+ cells at each time point, and to compare all SF leukocyte levels and all PF leukocyte levels to baseline, *p<0.05, **p<0.01, ***p<0,0001, n=3 for all time points except for 30dpci where n=2). (D) Line graphs of leukocyte proportions in the scRNAseq data (left panel) and mean values of ptprc+ cell counts (right panel) show that the results from the scRNAseq and cell counts are very similar.*

3.2.4 Identification of the *A. mexicanus* leukocytes present in the heart at baseline and following injury

To identify the leukocyte subpopulations that constituted the respective PF and SF immune responses, leukocyte clusters were subset from the overall scRNAseq dataset and re-analysed (Fig. 3.19a). The ROC test was used to find cell-type specific markers for each cluster (see Appendix 3.5) and, in combination with AM leukocyte markers previously identified[166], the major leukocyte subpopulations present in the heart were annotated (Fig. 3.19b, see Appendix 3.6 for remaining leukocyte sub-cluster markers). Once all leukocyte subpopulations had been identified, AM immune cells were then systematically compared to screen for differences in AM immune cells without bias.

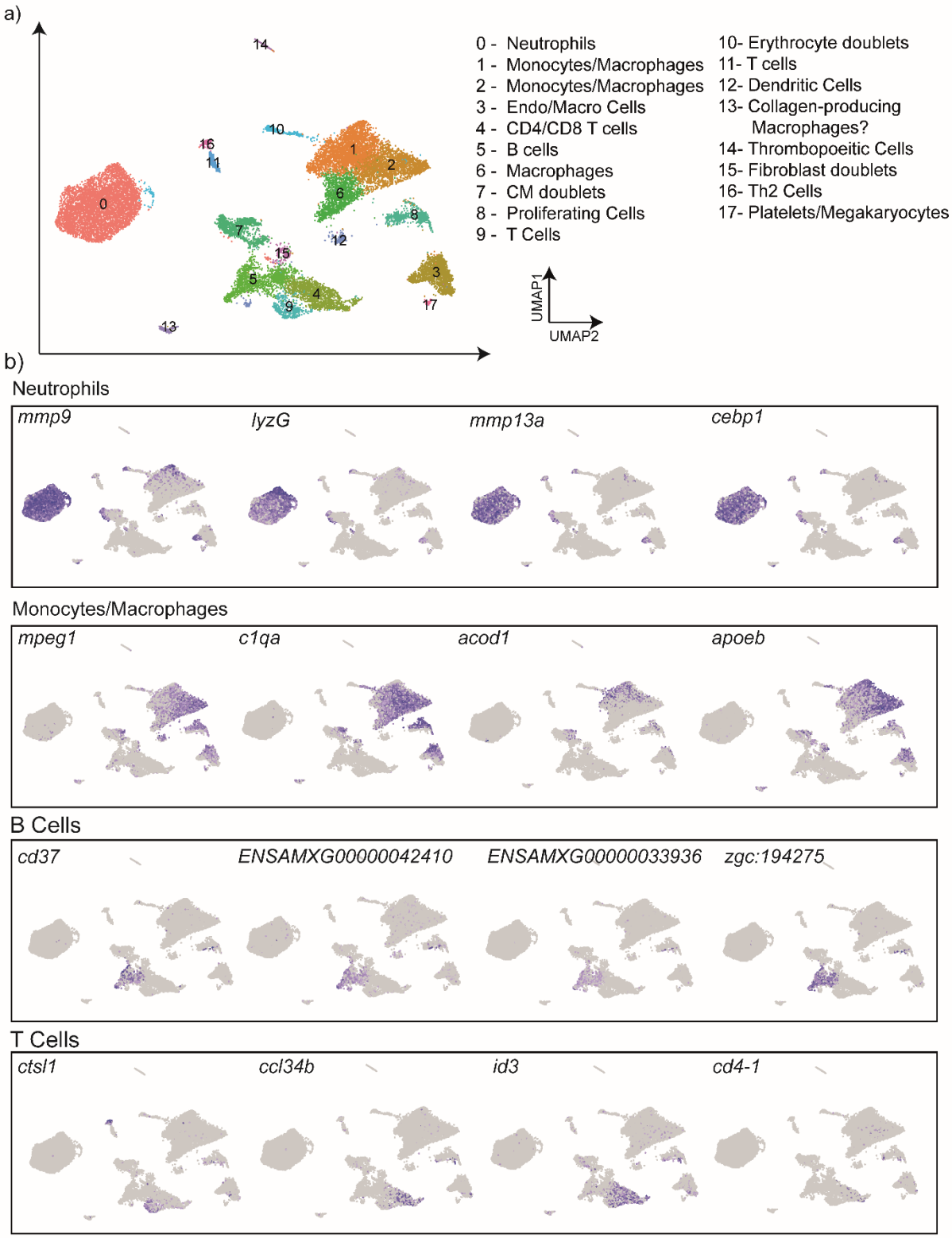

Figure 3. 19: Characterisation of A. mexicanus leukocyte subpopulations

(A) Labelled UMAP of leukocyte scRNAseq dataset showing that the AM immune response consists of a range of leukocytes. (B) FeaturePlots of top cell markers for neutrophils, monocytes/macrophages, B cells and T cells.

Firstly, the leukocyte scRNAseq data was split into PF and SF cells to assess whether there were any PF/SF-specific leukocyte clusters. This showed that all identified leukocyte-subpopulations were present in both morphotypes (Fig. 3.20a). Next, the scRNAseq data was split across time, to assess whether any leukocyte clusters were present in the PF/SF at different timepoints after injury. This revealed that *vwa11*+ thrombopoietic cells showed different dynamics between the SF and PF: thrombopoietic cells were consistently present in the SF, both at baseline and following injury whereas they only appeared in PF ventricles following injury (at 1-, 3- and 7dpci, Fig. 3.20b). From this finding, the temporal dynamics of all PF/SF leukocyte populations were then explored to determine whether any PF/SF leukocyte subpopulation showed significant differences in their kinetics.

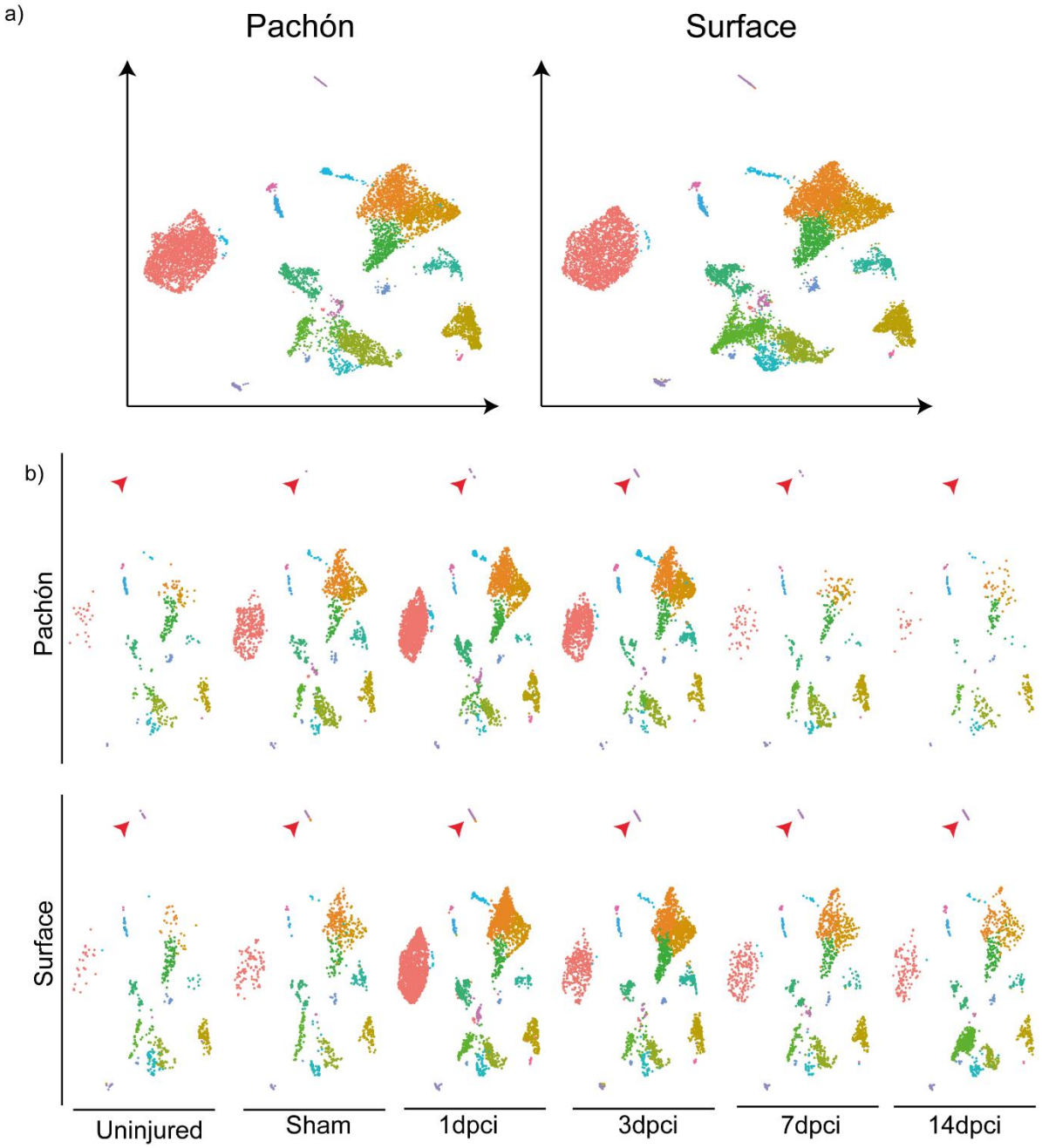

Figure 3. 20: An unbiased screening of the leukocyte scRNAseq data for PF/SF differences identified different temporal dynamics for thrombopoietic cells

(A) Leukocyte scRNAseq data UMAP split into PF/SF cells shows that there are no population-specific leukocyte populations. (B) Leukocyte scRNAseq data UMAP split across time and PF/SF population shows that thrombopoietic cells display different dynamics in the PF/SF (cells highlighted by the red arrows).

DPA was used to assess PF/SF leukocytes for significantly different temporal dynamics (Figure 3.21, see Appendix 3.6 for non-immune cell DPA analysis). The DPA results showed that, despite the observation that thrombopoietic cells represent a SF-only leukocyte population at baseline and at 14dpci, only neutrophils, B cells and monocytes/macrophages were significantly different in their PF/SF proportions following cryoinjury. For neutrophils, it was observed that at 3dpci, PF had a significantly elevated neutrophil proportion, whereas SF neutrophils had returned towards baseline proportions ($p<0.01$). For B cells, similar, low proportions were observed for both PF and SF at all time points until 14dpci when, strikingly, SF B cell proportions showed a large increase (up to almost 10% of the entire heart, $p<0.001$). Finally, PF and SF showed similar monocyte/macrophage proportions at all time points but SF macrophage proportions were consistently greater than the PF, with this difference reaching significance at 7dpci ($p<0.01$).

Therefore, the DPA identified that neutrophils, monocytes/macrophages and B cells show significant differences in their temporal dynamics and should be the focus of further investigations in the next chapter. It seems that neutrophils might be responsible for the dominant PF immune response that occurs during the early phases of cardiac healing, whilst monocytes/macrophages and B cells may be responsible for the dominant late-stage SF immune response.

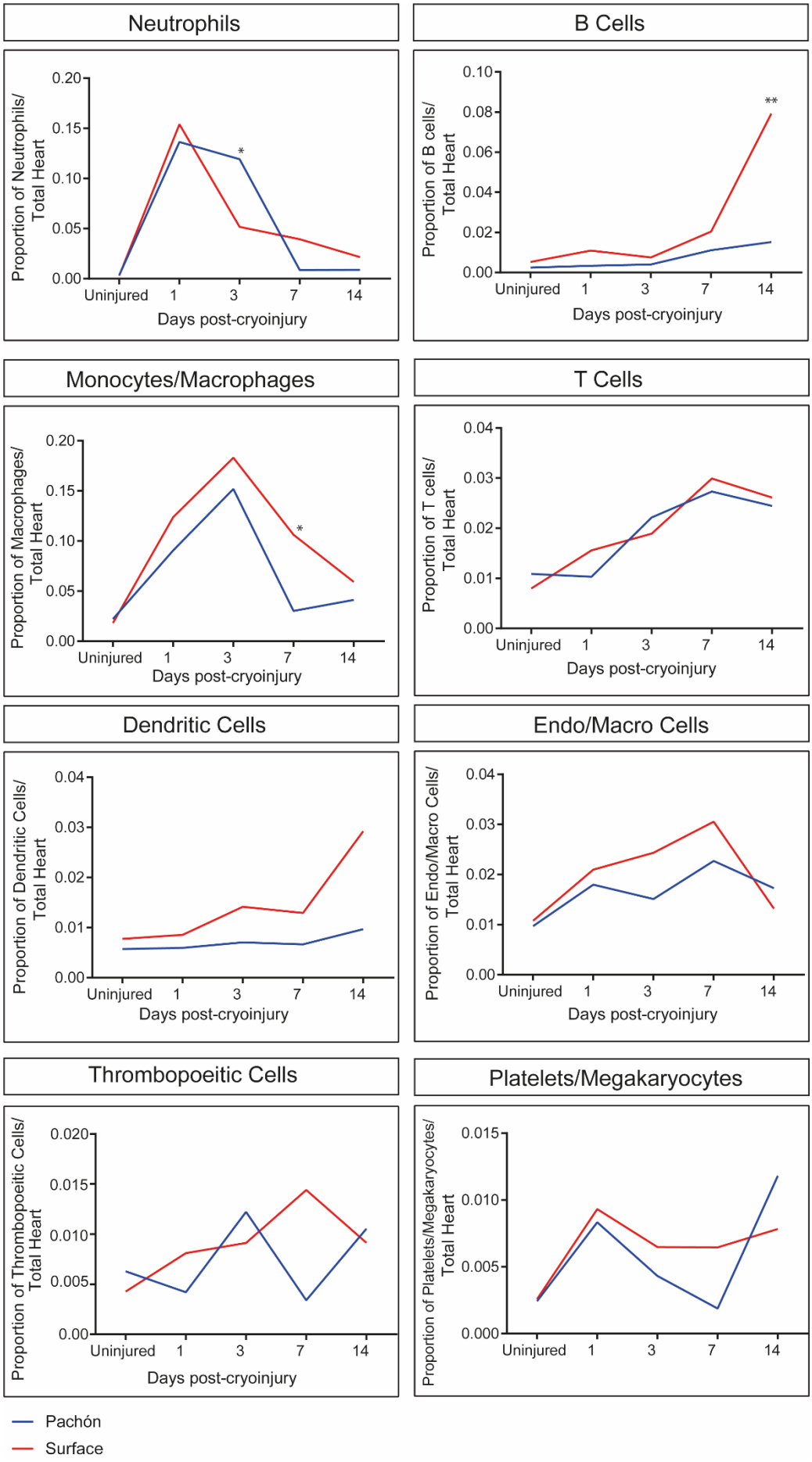
Neutrophils
Proportion of Neutrophils/ Total Heart
0.20
0.15
0.10
0.05
0.00
*
Uninjured 1 3 7 14
Days post-cryoinjury
B Cells
Proportion of B cells/ Total Heart
0.10
0.08
0.06
0.04
0.02
0.00
**
Uninjured 1 3 7 14
Days post-cryoinjury
Monocytes/Macrophages
Proportion of Macrophages/ Total Heart
0.20
0.15
0.10
0.05
0.00
*
Uninjured 1 3 7 14
Days post-cryoinjury
T Cells
Proportion of T cells/ Total Heart
0.04
0.03
0.02
0.01
0.00
Uninjured 1 3 7 14
Days post-cryoinjury
Dendritic Cells
Proportion of Dendritic Cells/ Total Heart
0.04
0.03
0.02
0.01
0.00
Uninjured 1 3 7 14
Days post-cryoinjury
Endo/Macro Cells
Proportion of Endo/Macro Cells/ Total Heart
0.04
0.03
0.02
0.01
0.00
Uninjured 1 3 7 14
Days post-cryoinjury
Thrombopoeitic Cells
Proportion of Thrombopoeitic Cells/ Total Heart
0.020
0.015
0.010
0.005
0.00
Uninjured 1 3 7 14
Days post-cryoinjury
Platelets/Megakaryocytes
Proportion of Platelets/Megakaryocytes/ Total Heart
0.015
0.010
0.005
0.000
Uninjured 1 3 7 14
Pachón
Surface

***Figure 3. 21: DPA analysis* of scRNAseq immune populations**

DPA analysis shows that PF and SF have significantly different neutrophil, macrophage and B cell responses to cryoinjury (p<0.01; ** p<0.001).*

3.3 Discussion

3.3.1 scRNAseq of the entire AM heart

Despite the prevalence of scRNAseq technologies, almost no comparative single cell studies have been attempted between cardiac regenerative and non-regenerative models, whilst the only study to take this approach completely fails to characterise the response of cardiomyocytes[141]. This study has generated a comprehensive transcriptomic database that characterises, for the first time, the regenerative and scarring responses of the entire AM heart within the first 14 days after cryoinjury-induced necrosis. Although not directly relevant to the aims of this thesis, the production of the AM scRNAseq dataset generated findings that warrant discussion.

1) Teleost cardiomyocytes can be successfully captured within 10X GEMs

So far, the capture of cardiomyocytes within large-scale scRNAseq characterisation studies has been limited as cardiomyocytes are too large for droplet-based scRNAseq approaches. Instead, researchers wishing to study the cardiomyocyte transcriptome have had to opt for alternative scRNAseq methodologies which are either: 1) limited in the number of cells that they can capture, such as SORT-seq which sorts cells via FACS into 384-well plates[71,226], or 2) limited in their ability to capture cytoplasmic transcripts, such as single nucleus RNAseq (snRNAseq)[204] which only captures transcripts present in the nucleus (nuclear transcripts are representative of ~20-50% of a cell's transcriptome[227]). Here, trials using 10X Chromium have shown that viable teleost cardiomyocytes can be captured by GEMs, generating a scRNAseq dataset that captures the cytoplasmic transcriptome of thousands of cardiomyocytes. Although zebrafish cardiomyocytes have recently been captured in a 10X dataset deposited on biorxiv[228], the scRNAseq dataset presented here

uniquely contains both proliferative and non-proliferative cardiomyocytes from the SF and PF. Currently, no other scRNAseq datasets enable regenerative and non-regenerative cardiomyocytes to be compared at the single cell level. Therefore, this dataset will enable, for the first time, the complex intracellular signalling pathways that govern cardiomyocyte proliferation within the regenerative and scarring setting to be explored. Furthermore, this AM scRNAseq dataset has captured the range of AM cardiac cells, enabling cardiomyocyte-non-myocyte cell-cell interactions to be explored which may be governing cardiomyocyte proliferative potential (eg cardiomyocytes-epicardial cells). Therefore, this dataset will act as a useful tool for future studies aiming to unpick the complex network of signals regulating cardiomyocyte proliferation.

2) A novel integration strategy can mitigate the problems posed by multiple, incomplete reference genomes

As the AM is a novel non-model organism, its reference genome is far from complete and new genome assemblies are being published every year with no consensus within the AM field as to which genome assembly is best suited to sequencing experiments. To address this, I have explored whether the v1.0.2 or the v2.0 assembly was better suited to scRNAseq analysis. Strikingly, this work has found, for the first time, that different results can be produced from the same set of sequenced reads depending on genome assembly alignment. Specifically, it was found that genome assembly alignment can produce differences in cell and gene capture rates, gene expression patterns, cell identities and functional pathway analysis. Although, well established model organisms like the zebrafish and neonatal mouse are unlikely to face the problem of multiple, discordant genome assemblies, the reference genome of alternative regenerative models like the axolotl[229] is far from complete whilst scRNAseq is being increasingly applied to non-model organisms, resulting in the publication of scRNAseq datasets with no awareness of the impact that genome assembly alignment can have on functional results and scRNAseq interpretation. Therefore, these findings are relevant not only to the field of cardiac regeneration but to the wider scRNAseq community. Additionally, a novel integration and 3’ UTR extension methodology was developed in this chapter that will be a

useful tool for other non-model organism researchers faced with the vexing problem of multiple, discordant genome assemblies. Indeed, this novel methodology has recently been published and will enable researchers to maximise the transcriptomic information available in non-model organism scRNAseq datasets whilst they await the publication of high-quality genome builds for their non-model organism of choice[174].

3) Limitations of the AM scRNAseq dataset

Although the AM scRNAseq dataset is the first of its kind, the necessary omission of FACS has resulted in a final dataset with atypical capture rates of dead/dying cells, erythrocytes and doublets (5,130 cells/85,516 cells, see Appendix 3.3). Dead/dying cells and erythrocytes are easy to identify and thus present little challenge during scRNAseq analysis as, once identified, they can be filtered out and removed from the final dataset. Doublets, on the other hand, present a specific challenge as they have the potential to mask rare cells undergoing transdifferentiation that similarly express gene expression profiles of two or more cells. Indeed, transdifferentiating cells have already been shown to play key roles in cardiac regeneration as cells which undergo epithelial-to-mesenchymal transition (EMT) contribute to revascularisation of the injured heart[230]. To avoid overlooking potentially important cells, therefore the high levels of doublets cannot be removed from the scRNAseq dataset and any transdifferentiating cells identified in this scRNAseq data must be treated with caution. Additionally, the custom 3' UTR extension methodology employed here may have led to the inclusion of transcripts in the scRNAseq data that should have been removed, potentially resulting in false positive results as genes may show incorrect expression levels and patterns of expression in our scRNAseq dataset. To prevent the follow up of any potentially false leads, the reads of all genes of interest highlighted in this thesis have therefore been checked for custom extension in IGV. As none of the genes of interest in this thesis have been custom extended, no validation experiments were pursued. However, future studies which focus on genes that have been custom extended in the 3' end, will require additional validation of gene expression by qPCR or

in situ hybridisation. This will remain the case for all future studies using this AM scRNAseq dataset until a complete and well annotated AM genome build is available.

3.3.2 The AM Immune Response

Using scRNAseq, *in situ* hybridisation and immunofluorescent staining, this chapter has identified significant differences in both the extent and the spatiotemporal dynamics of PF/SF leukocytes, revealing that the PF immune response dominates immediately after injury (1- and 3dpci), whereas the SF immune response takes over during the late stages of wound healing (7- and 14dpci).

1) The initial immune response to injury is significantly stronger in the scarring setting than in the regenerative setting

PF leukocytes have been found to be significantly elevated at 1- and 3dpci in response to cardiac necrotic cell death using Lcp1 and *ptprc*+ cell count data. The finding that PF leukocytes are significantly elevated above SF leukocytes suggests that the injured PF heart faces a burden of excessive leukocyte accumulation. This accumulation of leukocytes immediately after injury could be actively prohibiting successful regeneration in the PF. Indeed, excessive leukocyte accumulation has already been shown to drive regenerative failure in the zebrafish following cardiac injury[107] whilst increased leukocyte recruitment post-MI exacerbates ischaemia-reperfusion injury in the adult mouse and leads to increased infarct sizes. Furthermore, the timing of elevated PF leukocyte levels at 3dpci coincided with an accelerated rate of myocardial death in the PF, suggesting that the PF immune response could be stimulating apoptosis and necrosis of surviving cardiac tissue. Leukocyte levels have already been shown to positively correlate with infarct size in post-MI patients[231,232] whilst evidence from the zebrafish has shown that increased leukocyte levels exert direct control on apoptosis within wounded myocardium[107]. Therefore, it seems likely that elevated leukocytes are responsible for the observed accelerated rate of cell death in the PF heart. Although the leukocyte subpopulations responsible for elevated PF leukocytes at 3dpci have not been confirmed in this

chapter, the scRNAseq data suggests that PF neutrophils are elevated at 3dpci. Elevated neutrophils could result in an increased secretion of ROS, inflammatory cytokines and proteases which are all damaging to cardiomyocytes and induce myocardial apoptosis. Therefore, future characterisation and proteomic studies should determine whether PF wounds show elevated levels of pro-apoptotic factors which could be driving myocardial death.

2) PF and SF leukocyte dynamics significantly diverge at the late stages of cardiac healing

In contrast to the early immune response, which was dominated by the PF, the late-stages of leukocyte recruitment were dominated by the SF response, with SF *ptprc+* cells reaching significant levels of elevation at 14dpci. This finding was particularly unexpected as previous characterisations of the immune response in the regenerative zebrafish and neonatal mouse have reported that by 14dpci, the immune response is resolved[103,144,233]. Furthermore, continual leukocyte recruitment during the late stages of cardiac healing is typically associated with regenerative failure (i.e. the adult mouse)[234] whilst, clinically, elevated leukocyte levels post-MI are associated with increased fibrosis, adverse ventricular remodelling, and pathological HF development[235–238]. Therefore, evidence from the literature suggests that a prolonged immune response after injury in the SF would be detrimental to cardiac healing and would prevent regeneration. Thus, the data presented here is the first evidence to suggest that a late-stage immune response is not necessarily damaging to the heart. In future studies, it will be essential to confirm that the SF immune response dominates during the late stages of cardiac healing and further explore whether SF leukocytes remain elevated at 30dpci in comparison to the PF (as suggested by the preliminary *ptprc* counts reported here).

3) The PF immune response is resolved by 7dpci

In contrast to the SF, both the single cell and the *ptprc* data show that at 7- and 14dpci, PF leukocyte recruitment significantly decreases. This finding is remarkable because, as discussed, fibrosis and scarring are typically associated with chronic inflammation and the continual recruitment of leukocytes which are seemingly absent in the PF. However, an absence of leukocytes

in the PF during the late stages of cardiac healing could, in fact, be contributing to the regenerative failure of the PF. Specifically, the lack of leukocyte recruitment at 7dpci could mean that the PF ventricle is deficient in key pro-regenerative and anti-inflammatory leukocytes that are mainly recruited in the late stages of cardiac repair. Anti-inflammatory macrophages and Tregs are both essential to regeneration and their absence causes regeneration to fail in the zebrafish and the neonatal mouse. However, these cells do not reach peak levels of recruitment to the injured heart until 7dpi. Furthermore, macrophages and Tregs have both been shown to stimulate cardiomyocytes proliferation by secreting cardiac mitogens[139–143]. As the absence of PF leukocytes at 7- and 14dpci critically coincides with when PF cardiomyocytes fail to divide[29], this raises the tantalising possibility that lack of PF leukocyte recruitment could directly result in impaired PF cardiomyocyte proliferation due to the absence of key paracrine mitogenic signals released from anti-inflammatory macrophages and Tregs. Therefore, it will be imperative to test in the following chapters what leukocytes are present in the PF and SF at the late stages of wound healing and thus determine whether PF show a dampened recruitment of anti-inflammatory leukocytes at 7- and 14dpci.

4) Baseline AM leukocytes are very similar

Finally, from the scRNAseq data and Lcp1 antibody counts, it is possible to conclude that the PF and SF have very similar tissue-resident leukocytes prior to injury, both in terms of their leukocyte composition and in the number of cells present. This finding is contrary to the significant differences that have been observed in other regenerative and scarring models: the uninjured neonatal mouse heart is mainly populated by tissue-resident CCR2+ macrophages that are critical for regenerative success whilst these cells are absent from the uninjured adult mouse heart[37]. Although it is currently unknown whether the zebrafish and medaka show significant differences in their baseline leukocytes, tissue-resident macrophages have also been identified as essential for regenerative success in the zebrafish[108]. Therefore, this finding from the AM challenges the view that regenerative success relies on unique and pro-regenerative tissue-resident leukocytes. Indeed, the finding that there were almost no differences in uninjured AM leukocytes suggests that any significant

differences in the AM immune system driving PF/SF differential regenerative capacity occur solely within injury-responsive and recruited leukocytes. Therefore, future studies should focus on the early PF immune response and the late-stage SF immune response rather than analysing differences in PF/SF leukocytes at baseline.

5) *Future Work*

So far, only the spatiotemporal dynamics of all PF/SF leukocytes have been investigated. However, to truly characterise the PF/SF immune responses to cardiac damage, it is imperative that the dynamics of different leukocyte subpopulations are explored. Critically, the results of the DPA have highlighted significant differences in the proportions of neutrophils, monocytes/macrophages and B cells, suggesting that these cell types represent the most likely targets to be driving significant differences in the AM immune response. Therefore, these three cell types will be the focus of the next chapter.

Chapter IV

Pachón and Surface fish show significant spatiotemporal differences in their neutrophil and B cell dynamics

4.1 Background

4.1.1 The neutrophil response to MI

Neutrophils are the first line-responders of the innate immune system and are rapidly recruited to the heart after MI (within minutes to hours). Upon arrival in the infarcted heart, neutrophils act to clear the wound of tissue debris: they release the contents of their proteolytic granules, secrete ROS and inflammatory cytokines, and phagocytose dead/dying cells. Once the wound has been cleared of DAMPs and tissue debris, neutrophils are no longer recruited to the injured heart and neutrophil levels return to baseline by 7dpi.

4.1.2 Neutrophils are both detrimental and beneficial to mammalian cardiac repair

Neutrophils are highly inflammatory cells and, clinically, high levels of neutrophils are associated with increased infarct sizes, HF development and death in post-MI patients[239–241]. Neutrophils release ROS, degradative enzymes and inflammatory cytokines that can exacerbate myocardial injury post-MI[242]. Indeed, ROS directly induce cell death in surrounding cardiomyocytes[243], leading to increased infarct sizes, whilst secreted enzymes like myeloperoxidases increase acute inflammation and enhance local vascular and tissue injury[128].

However, neutrophil depletion in animal models has led to conflicting results and, clinically, neutrophil depletion has not resulted in therapeutic benefit[244–246]. In the past decade, it has been discovered that neutrophils are not exclusively detrimental to cardiac repair and can also play beneficial, anti-inflammatory roles. During the phagocytosis of tissue debris, neutrophils attenuate inflammation by scavenging inflammatory cytokines, chemokines and DAMPs. Additionally,

neutrophils can secrete pro-resolving factors such as neutrophil gelatinase-associated lipocalin (NGAL), which result in the increased expression of anti-inflammatory cytokines in recruited macrophages[246]. Furthermore, neutrophils polarise macrophages towards an anti-inflammatory phenotype by forming apoptotic bodies and stimulating their own engulfment in efferocytosis[247], resulting in the increased secretion of anti-inflammatory cytokines from macrophages such as VEGF[248], TGFβ1[154] and IL-10[155].

The pro- and anti-inflammatory roles of neutrophils post-MI have so far been attributed to neutrophil heterogeneity, with distinct neutrophil subsets performing distinct roles post-MI. Although, the study of neutrophil heterogeneity post-MI is still in its infancy, so far neutrophils have been shown to display distinct inflammatory[246], proteomic[249] and transcriptomic[250,251] profiles that change over the course of cardiac repair. Immediately after injury (1-3dpi), neutrophils are inflammatory as they clear the wound of tissue debris, and they break down the ECM. However, during the later stages after injury, (3-7dpi), anti-inflammatory neutrophils begin to emerge which facilitate scar formation, ECM remodelling and the resolution of inflammation.

4.1.3 The role of neutrophils in cardiac regeneration

Currently, it is unclear whether a neutrophil response is essential to successful regeneration as the zebrafish and neonatal mouse show very different neutrophil dynamics (Fig. 4.1). In the zebrafish, neutrophils are briefly recruited to the injured heart during the first 48 hours after injury, before the neutrophil response is resolved. In the neonatal mouse, on the other hand, neutrophils do not seem to be recruited in substantial numbers following LAD ligation[37,103], suggesting that neutrophils are not required for successful mammalian heart regeneration. However, as the neutrophil response has not yet been comprehensively characterised in the neonatal mouse, I shall instead focus on what has been learnt from the zebrafish neutrophil response.

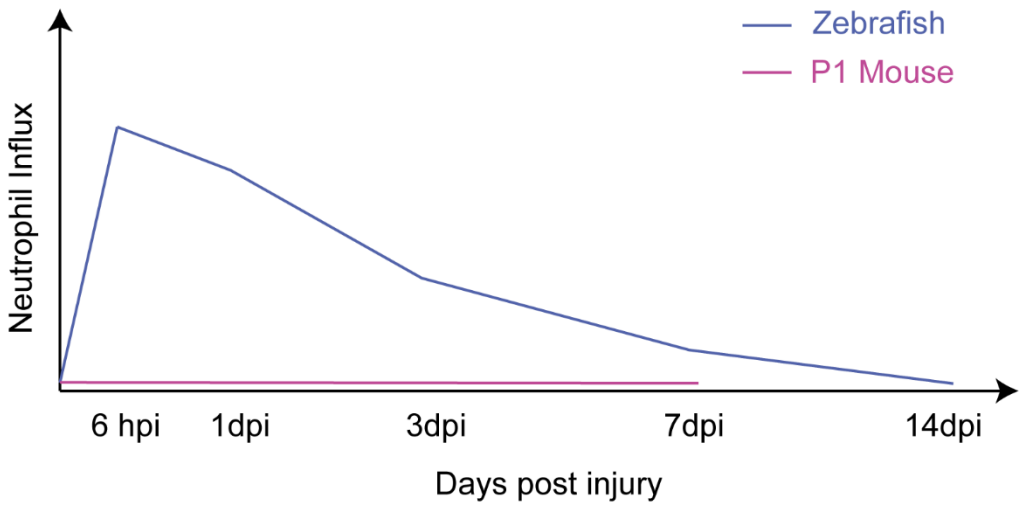

Figure 4. 1: Schematic of temporal neutrophil dynamics in the regenerating zebrafish and neonatal mouse heart post-injury

Zebrafish dynamics based on data from Lai et al (2017) and Bevan et al (2020). P1 data based on Lavine et al (2014) and Aurora et al (2014).

Zebrafish neutrophil dynamics suggest that the timely resolution of the neutrophil response is essential to regenerative success. Indeed, in comparison to the zebrafish, the scarring medaka show a neutrophil response that is slow to resolve whilst accelerating the resolution of the medaka neutrophil response significantly improves their cardiac regenerative capacity[109]. On the other hand, pharmacologically prolonging neutrophil retention in the zebrafish heart results in regenerative failure, regardless of the mechanism used[109,252]. Therefore, it seems that a prolonged neutrophil response is prohibitive to regeneration whilst successful regeneration requires the quick resolution of neutrophils.

4.1.4 The monocyte/macrophage response to MI

Similarly to neutrophils, monocytes/macrophages can be both beneficial and detrimental to cardiac repair due to the presence of distinct pro- and anti-inflammatory monocyte/macrophage subsets which populate the heart at different time points after injury. Immediately after injury, pro-inflammatory monocytes are recruited to the wound where, upon tissue extravasation, they

differentiate into pro-inflammatory macrophages, reaching peak levels at 3dpi. These cells are then followed by a wave of anti-inflammatory monocytes/macrophages from 5dpi that reach peak levels at 7dpi (Fig. 4.2). Anti-inflammatory macrophages arise via two mechanisms: from the recruitment and differentiation of anti-inflammatory monocytes; and from the repolarisation of pro-inflammatory macrophages into an anti-inflammatory phenotype[147]. Crucially, these two distinct phases of the monocyte/macrophage response coordinate different aspects of cardiac repair.

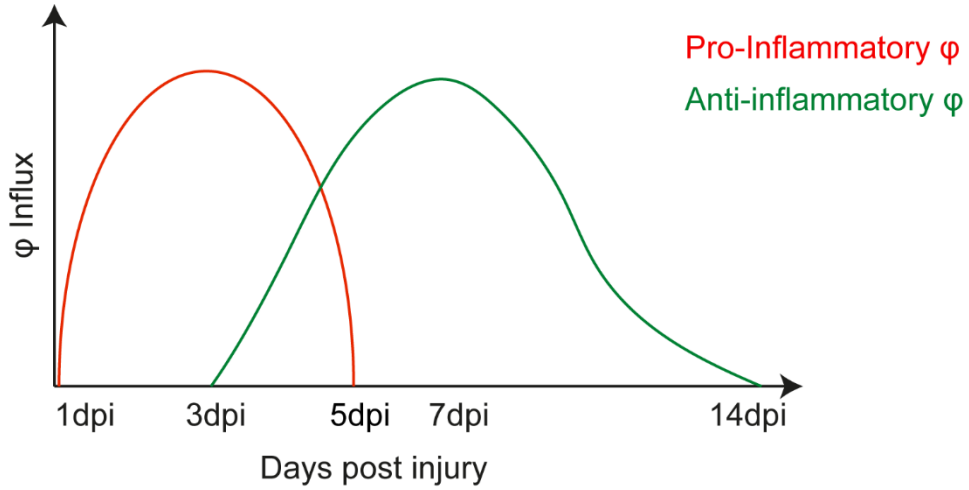

Figure 4. 2: Schematic of the temporal dynamics of the monocyte/macrophage response to cardiac injury

Although this diagram is useful to talk about the distinct pro-inflammatory and anti-inflammatory phases of the monocyte/macrophage response, it is also important to note that is a very simplistic overview and monocyte/macrophage dynamics following cardiac injury are likely much more complex.

Pro-inflammatory macrophages

Pro-inflammatory macrophages (or "M1") are professional phagocytes that coordinate clearance of the wounded tissue. They secrete proteolytic enzymes to degrade the ECM, inflammatory cytokines to recruit additional leukocytes, and phagocytose tissue debris and

dead/dying cells. Due to their inflammatory nature, pro-inflammatory macrophages can be detrimental to cardiac repair and excessive levels of inflammatory monocytes lead to adverse ventricular remodelling[253]. However, when pro-inflammatory macrophages are ablated, cardiac repair is impaired due to the incomplete clearance of necrotic cells and tissue debris[254].

Anti-inflammatory macrophages

Anti-inflammatory macrophages (or "M2") are pro-reparative and are responsible for repopulating the wounded tissue after injury. They secrete a variety of anti-inflammatory cytokines and growth factors that stimulate endothelial cells, smooth muscle cells and fibroblasts to proliferate and form new blood vessels and deposit collagen. Recently, it has been shown that 7dpi macrophages can also directly contribute to scar formation by secreting collagen proteins[136].

Historically, it was thought that two distinct waves of pro-inflammatory and anti-inflammatory macrophages arose due to the serial recruitment of two distinct monocyte subsets ($Ly6C^{high}$ and $Ly6C^{low}$ monocytes)[254]. However, in recent years it has become apparent that following injury, the heart is populated by a diverse range of macrophage populations that differ in their inflammatory state and transcriptional profile[255]. As these divergent macrophage subsets continue to be discovered, it is now clear that the pro-inflammatory and anti-inflammatory phases of the macrophage response are in fact made up of a range of heterogeneous macrophages which are responsible for distinct aspects of cardiac repair.

4.1.5 Monocytes/macrophages in cardiac regeneration

Macrophage ablation studies in the zebrafish[109], neonatal mouse[103] and axolotl[104] have well-established that macrophages are essential for successful regeneration. Indeed, the importance of macrophages for regenerative success can also been seen in other regenerative organs like the limb[169] and caudal fin[256] which fail to regenerate in the absence of macrophages. The loss of macrophages from the regenerating heart results in regenerative failure due to the disruption of many key regenerative processes. Indeed, macrophage ablation has been reported to lead to:

impaired angiogenesis, decreased cardiomyocyte proliferation, impaired scar resolution, incomplete debris removal, adverse ECM remodelling, and delayed neutrophil clearance[103,104,109].

Although the divergent macrophage populations which might mediate these different aspects of cardiac regeneration are only beginning to emerge, studies in the zebrafish and neonatal mouse have so far identified that a population of tissue-resident macrophages are essential for regenerative success. In the neonatal mouse, tissue resident macrophages selectively expand following LAD ligation and drive regeneration by stimulating cardiomyocyte proliferation and angiogenesis[37]. Similarly, depletion of macrophages from the zebrafish heart prior to injury results in impaired cardiomyocyte proliferation, scar resolution and angiogenesis[109].

Furthermore, successful regeneration is also associated with significantly elevated levels of macrophages in the heart after injury. Both the zebrafish and the P1 mouse show greater macrophage levels at 7dpi in comparison to the medaka and the adult mouse respectively[103,109], suggesting that successful regeneration requires a substantial macrophage response during the late stages of cardiac healing.

4.1.6 The role of B cells in cardiac regeneration

To date, the role of B cells in regulating successful regeneration vs fibrotic scarring has been largely unexplored. B cells are an important part of the adaptive immune response and are responsible for humoral immunity; they act to produce antibodies, present antigens and secrete regulatory cytokines. Traditionally, humoral immunity has been associated with cardiac fibrosis as B cells have been shown to drive the progression of atherosclerosis[257] and heart failure[258] by producing autoreactive cardiac antibodies that promote hypertrophy, chronic inflammation and maladaptive tissue remodelling.

However, recent research has reported conflicting results following MI which suggest that B cells can both ameliorate and exacerbate myocardial injury. Depletion studies have shown that, in the absence of B cells, cardiac function improves post-MI with decreased fibrosis, collagen content

and impaired monocyte mobilisation to the heart, accelerating inflammation resolution[259,260]. In contrast, B cell injection studies have reported that B cells improve cardiac function post-MI and decrease scar size and fibrosis[261,262] whilst B cell-specific IL-10 knock-out exacerbates myocardial injury[263].

Thus, it is unclear as to what role B cells might play in cardiac regeneration. B cells have not yet been reported to play a role in successful regeneration in either the zebrafish or the neonatal mouse. Indeed, the presence of B cells within the P1 regenerating heart has been completely unreported whilst the zebrafish immune response to injury does contain a B cell-like population[264] which reaches peak levels at 7dpi[255].

4.1.7 Neutrophils, Monocytes/Macrophages and B cells in the AM

To date, the only available knowledge about AM leukocytes comes from one study which characterised the AM head kidney (the main organ of the immune system in teleosts)[166]. Using flow cytometry, Peuß et al determined the numbers of leukocyte populations present in the SF/PF head kidney at baseline. They reported that the SF contained significantly higher numbers of neutrophils and monocytes at baseline than the PF, whilst the PF had significantly elevated numbers of lymphoid/progenitor cells. Additionally, the authors found that PF/SF leukocytes showed significant functional differences: PF leukocytes were more sensitive to LPS stimulation and produced significantly greater amounts of inflammatory cytokines than SF leukocytes. Furthermore, PF leukocytes isolated from the head kidney showed a substantially decreased ability to phagocytose bacteria than their SF counterparts.

However, apart from this study, very little is known about PF/SF leukocytes. There is no data exploring leukocyte recruitment from the head kidney or investigating whether leukocyte transcriptional profiles might change during the different temporal phases of wound healing.

4.1.8 Aims

In the previous chapter, DPA identified significant differences in the kinetics of PF/SF neutrophils, macrophages and B cells. However, due to the stochastic nature of scRNAseq cell capture, the identified differences in PF/SF leukocyte populations could be the result of random chance. Furthermore, although each scRNAseq sample was derived from 3 pooled hearts, the scRNAseq dataset only represents n=1. Therefore, the results of the DPA require validation with additional cell counts before it can be concluded whether the PF/SF show any significant differences in their neutrophil, B cell and monocyte/macrophage responses to cardiac injury.

From the DPA results, I hypothesised that:

1) PF neutrophils will be significantly elevated at 3dpci
2) SF macrophage levels will be significantly elevated at 7dpci
3) SF B cells will significantly influx into the heart at 14dpci

Additionally, following the work of Peuß et al that found that PF/SF leukocytes show significantly different rates of phagocytosis[166], I hypothesised that PF/SF leukocytes will also show key functional differences post-MI that drive their differential regenerative capacity.

Therefore, this chapter had two major aims:

1) Characterise the number and spatiotemporal dynamics of neutrophils, macrophages and B cells to determine the strength and length of each respective leukocyte response
2) Characterise the transcriptional profile of PF/SF neutrophils, macrophages and B cells at each time point following injury to determine whether the cells present at each time point are playing functional roles in regeneration and/or fibrotic scarring

4.2 Results

4.2.1 The PF and SF show major differences in their neutrophil responses

Uninjured PF and SF neutrophils show no differences

To explore whether PF/SF hearts show any differences in their numbers of inflammatory cells prior to injury, the number of neutrophils present in the PF/SF hearts at baseline was first characterised. From the scRNAseq data, *mmp9* was identified as a neutrophil-specific marker (Fig. 4.3a) and RNAscope was performed to visualise and count uninjured *mmp9*+ cells (Fig. 4.3b). *mmp9*+ cell counts showed no difference in neutrophil numbers at baseline (Fig. 4.3c) nor spatial location as neutrophils were found throughout the heart in both PF and SF.

The transcriptional profile of uninjured PF/SF neutrophils was next compared to determine whether PF/SF neutrophils showed any differences in their inflammatory status at baseline. The ROC test was used to identify cell-specific markers for PF and SF neutrophils and the number of marker genes shared in both populations was calculated. This found that uninjured PF/SF neutrophils shared 762 marker genes but that both morphotypes also expressed many population-specific marker genes (Fig. 4.3d). However, when PF and SF uninjured neutrophils were tested for differential gene expression, only 5 genes reached the cut-off for significance (Fig. 4.3e), suggesting that PF/SF neutrophils show no meaningful differences in their neutrophil transcriptional profiles prior to injury. From these results, I concluded that, prior to injury, PF/SF neutrophils present in the heart are very similar both in number and transcriptionally.

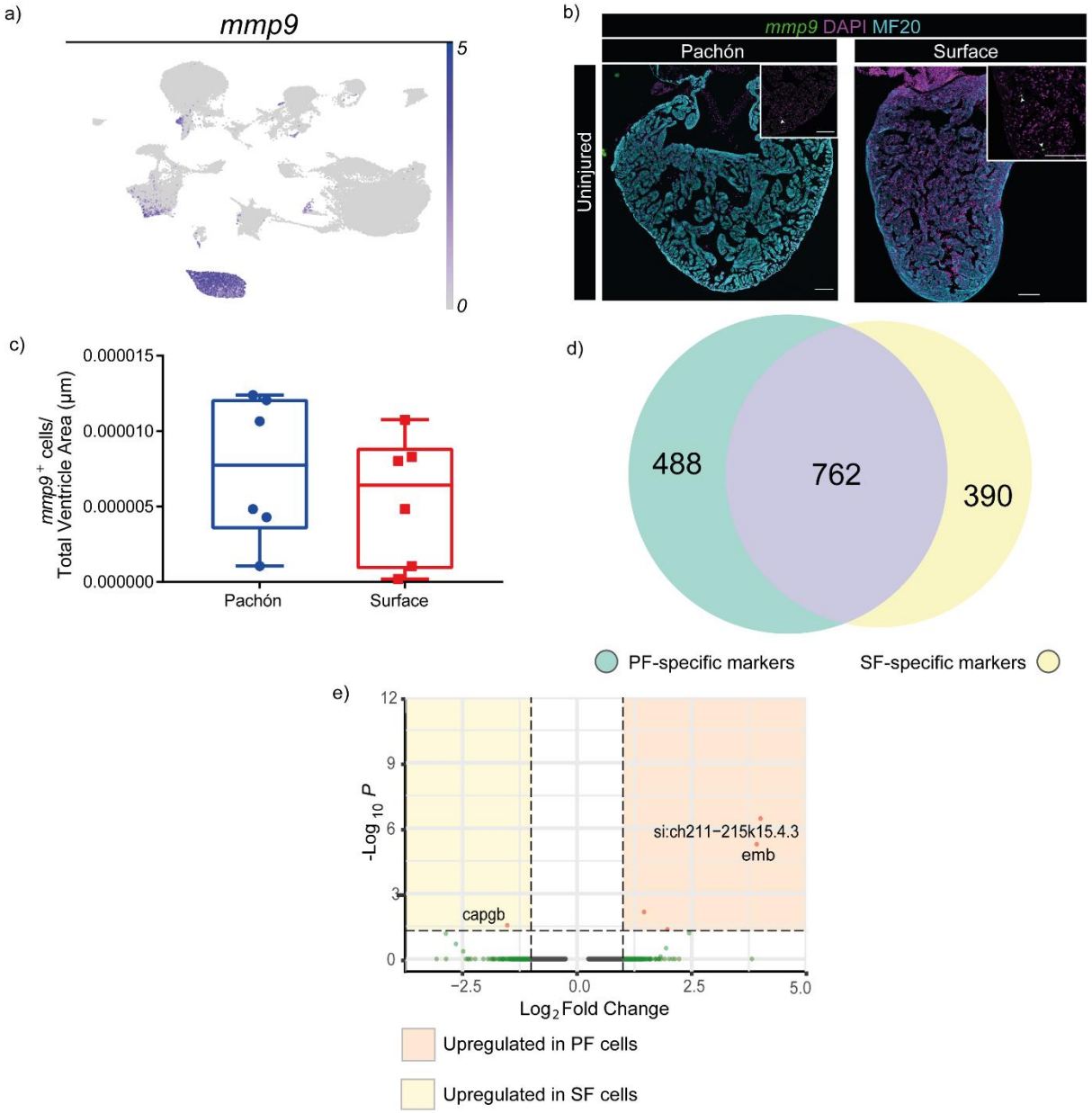

Figure 4. 3: Uninjured PF and SF neutrophils show no differences in their number, spatial location or transcriptional profile

(A) FeaturePlot of mmp9 expression in overall scRNAseq dataset confirms that mmp9 is a specific, pan-neutrophil marker. (B) Representative mmp9 RNAscope staining of PF and SF uninjured hearts. Sections were counterstained with MF20 and DAPI. (C) Normalised mmp9+ cell counts show that PF and SF neutrophil levels are the same prior to injury (Student's t test, p=0.44, n=6). (D) Euler Plot showing the overlap of shared cell-specific markers for uninjured PF and SF neutrophils. (E) Volcano

plot of DGE results. Only 5 genes were differentially expressed between PF and SF uninjured neutrophils.

The PF neutrophil response is stronger and takes longer to resolve than the SF neutrophil response

Next, to confirm the previous DPA results, the temporal dynamics of PF/SF neutrophils were characterised in response to injury. Using the *mmp9* RNAscope probe, cell counts were performed at 1-, 3-, 7-, 14- and 30dpci (Fig. 4.4a) and neutrophil numbers present in the entire ventricle were normalised to the total ventricle area.

Firstly, PF/SF neutrophil counts were compared to uninjured levels. This revealed that SF neutrophil levels were only elevated at 1dpci whereas PF neutrophils were significantly elevated at both 1- and 3dpci (Fig. 4.4b), showing that the PF neutrophil is prolonged in comparison to the SF.

Secondly, neutrophil levels were compared between the SF and PF at each time point. This found that PF neutrophil levels were significantly elevated at both 1- and 3dpci in comparison to the SF (Fig. 4.3b), showing that the PF neutrophil response is much stronger than the SF as a greater number of neutrophils influx into the PF heart immediately after injury. When *mmp9*+ cells present in the wound were normalised to the fractional wound area, a similar trend was observed as PF neutrophil levels were increased in comparison to the SF (Fig. 4.4c).

Therefore, it is possible to conclude from this data that the temporal dynamics of the PF and SF neutrophil response are very different; the SF neutrophil response is very short and lasts between 24-48 hours before resolution by 3dpci whereas the PF show a prolonged neutrophil response that is still active at 3dpci and is characterised by an excessive influx of neutrophils.

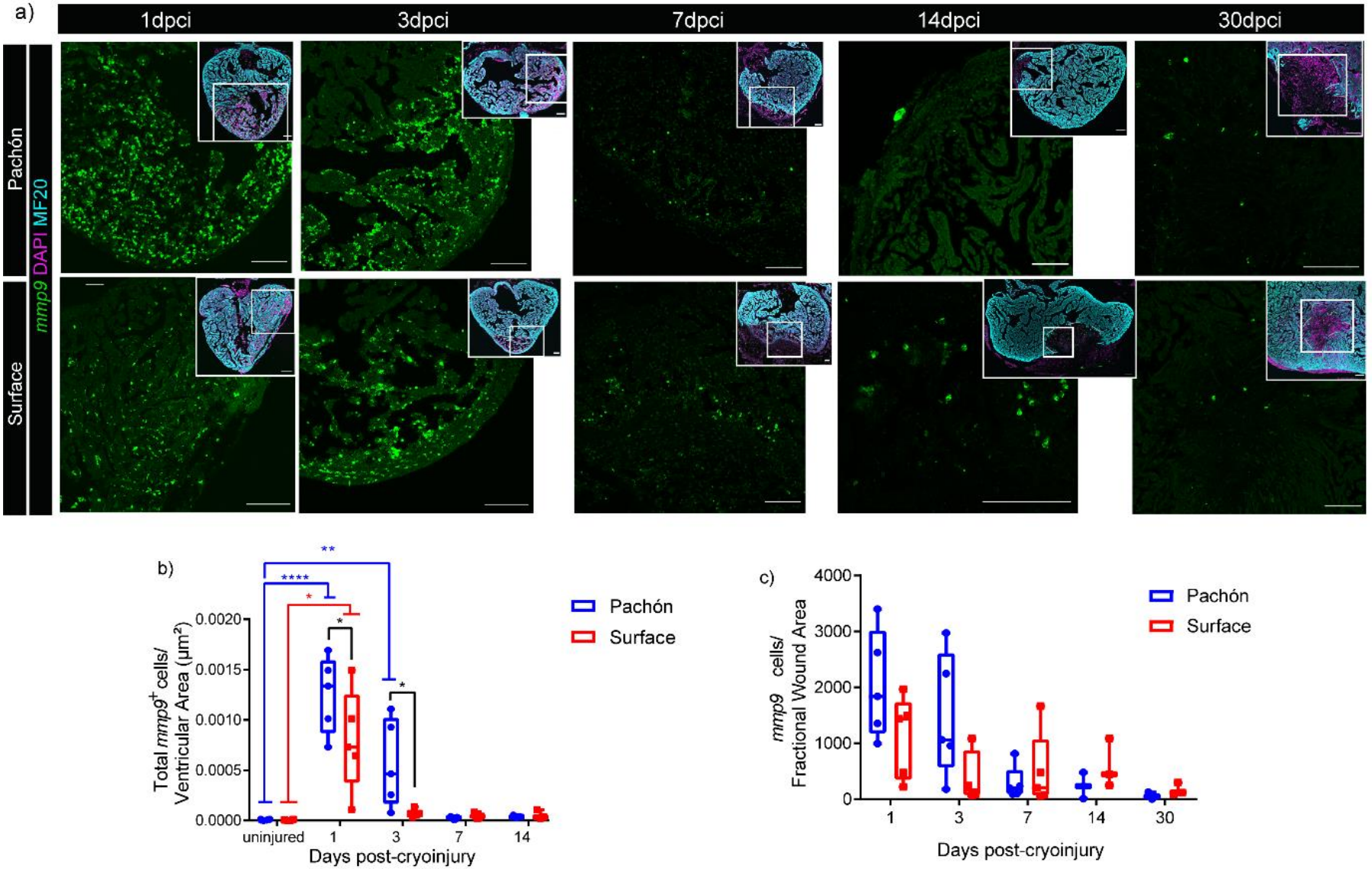
a)
1dpci
3dpci
7dpci
14dpci
30dpci
Pachón
Surface
mmp9 DAPI MF20
b)
Total mmp9+ cells/ Ventricular Area (µm2)
0.0020
0.0015
0.0010
0.0005
0.0000
uninjured
1
3
7
14
Days post-cryoinjury
Pachón
Surface
c)
mmp9 cells/ Fractional Wound Area
4000
3000
2000
1000
0
1
3
7
14
30
Days post-cryoinjury
Pachón
Surface

Figure 4. 4: The PF and SF neutrophil response to injury is significantly different with the PF showing a stronger initial neutrophil response that is prolonged and does not resolve rapidly

*(A) RNAscope staining for mmp9 was used to count neutrophil numbers in uninjured, 1-, 3-, 7- and 14dpci hearts. (B) Total mmp9+ cell counts were normalised to total ventricular area. At 1- and 3dpci, PF neutrophils are significantly elevated from uninjured levels whereas SF neutrophils are only significantly elevated at 1dpci (2-way ANOVA with Sidak's multiple comparisons test, **** p<0.0001, ** p<0.01, n=3-5). Compared to each other, a significantly greater number of PF neutrophils influx into the heart at 1- and 3dpci than in SF (2- way ANOVA with Sidak's multiple comparisons test, * p<0.05, n=3-5). (C) Total mmp9+ cells present in the wound were normalised to fractional wound area (2-way ANOVA with Sidak's multiple comparisons test, n=3-5).*

The PF/SF neutrophil responses show significant differences in their localisation following injury

Differences in the spatial localisation of PF/SF neutrophils in response to injury were next explored as I hypothesised that SF/PF neutrophils could be mediating different effects during cardiac repair if they localised differentially to the wound vs remote wound regions. Using the *mmp9*$^{+}$ cell count data, the percentages of neutrophils that localised to the wound (Fig. 4.5a) and to remote wound regions (Fig. 4.5b) were calculated. Comparison of wound localisation percentages found that, during the active phase of the PF/SF respective neutrophil responses, similar proportions of both PF and SF neutrophils localise to the wound (>80% of PF neutrophils at 1- and 3dpci; <70% for 1dpci SF neutrophils). However, at 3dpci (i.e. when the PF neutrophil response is still active but the SF neutrophil response has been resolved), the PF showed a significantly greater proportion of neutrophils localising the wound than the SF (Fig. 4.5a).

Therefore, from this data it is possible to conclude that when the neutrophil response is active, both PF/SF neutrophils show a strong wound localisation response, with the majority of active neutrophils localising to the site of injury. This conclusion is further supported by the finding that at 7dpci, PF neutrophils displayed a significant increase in the proportion of neutrophils found

remote from the wound (Fig. 4.5b), indicating that the PF neutrophil response resolves between 3- and 7dpci. These significant differences in neutrophil wound localisation additionally support the finding that the PF neutrophil response is prolonged and is slow to resolve in comparison to the SF.

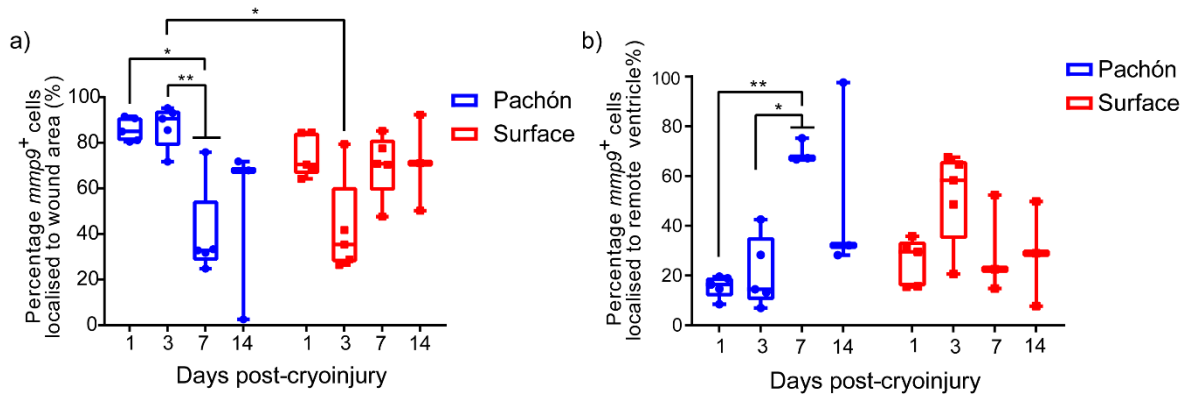

Figure 4. 5: PF and SF neutrophil responses are characterised by strong localisation to the wound

*(A) The percentage of mmp9+ cells present in the wound was calculated from the number of total mmp9+ cells present in the ventricle. Comparison of PF/SF wound localisation revealed that a significantly greater proportion of PF neutrophils localise to the wound at 3dpci than SF neutrophils at 3dpci and PF neutrophils at 7dpci. (2-way ANOVA with Sidak's multiple comparisons test, *p<0.05, **P<0.01, n=3-5). (B) Neutrophils remote from the wound were classified as all neutrophils present in the ventricle that did not localise to the wound. Comparison of PF/SF remote neutrophils revealed that at 7dpci, PF neutrophils show a significant increase in localisation to remote regions of the ventricle from 1dpci and 3dpci whilst SF neutrophils show a similar trend with SF neutrophils showing increased localisation to remote regions of the ventricle at 3dpci (2-way ANOVA with Sidak's multiple comparisons test, *p<0.05, **P<0.01, n=3-5).*

PF wounds show a greater density of neutrophils than SF

Following the finding that a significantly greater number of neutrophils influx into PF hearts at 1- and 3dpci, and that most of these neutrophils localise to the wound, I postulated that PF

neutrophils may populate the wound at a significantly higher density than in SF. To explore PF/SF neutrophil density in the wound, the pattern of PF/SF neutrophils at 1- and 3dpci was visualised. At 1dpci, PF neutrophils were observed on almost all surfaces of the injured PF myocardium, suggesting a high density of neutrophils (Fig. 4.6a). In contrast, SF neutrophils were spread diffusely throughout the wound, suggesting that the density of SF neutrophils in the wound was much less than the PF. Similarly, at 3dpci, PF neutrophils were once again observed at high densities within the wound whereas, in the SF, many neutrophils had been cleared from the wound and the remaining neutrophils were present at low densities (Fig. 4.6b). To confirm these observations, neutrophil density within PF/SF wounds was quantified by calculating the number of *mmp9*+ cells present/wound area. This found that PF wounds showed significantly greater densities of neutrophils than SF at both 1- and 3dpci (Fig. 4.6c).

From the *mmp9* cell count data, it can be concluded that, in comparison to SF, the PF face a significantly greater neutrophil burden at 1- and 3dpci in terms of the number of neutrophils that influx the heart, the duration of neutrophil recruitment and the density at which neutrophils enter the injury site. These differences suggest that the PF neutrophil response could be exacerbating myocardial damage and driving regenerative failure if PF neutrophils show a pro-inflammatory transcriptional profile and secrete damaging levels of ROS, inflammatory cytokines and proteolytic enzymes. Therefore, the transcriptional profile of PF/SF neutrophils at each time point after injury was next explored to determine whether PF/SF neutrophils show any key differences in neutrophil cellular behaviour.

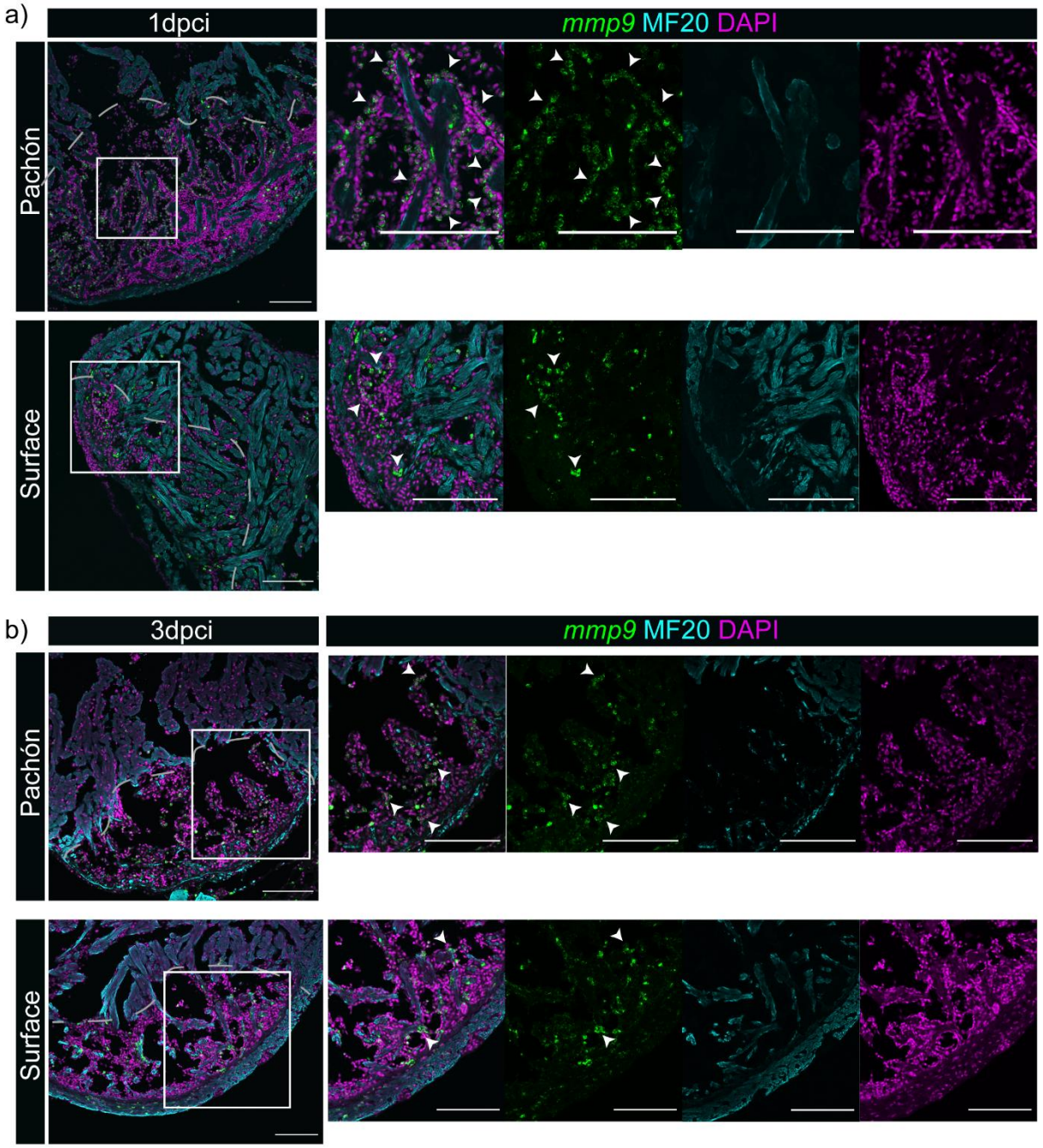
a)
1dpci
mmp9 MF20 DAPI
Pachón
Surface
b)
3dpci
mmp9 MF20 DAPI
Pachón
Surface

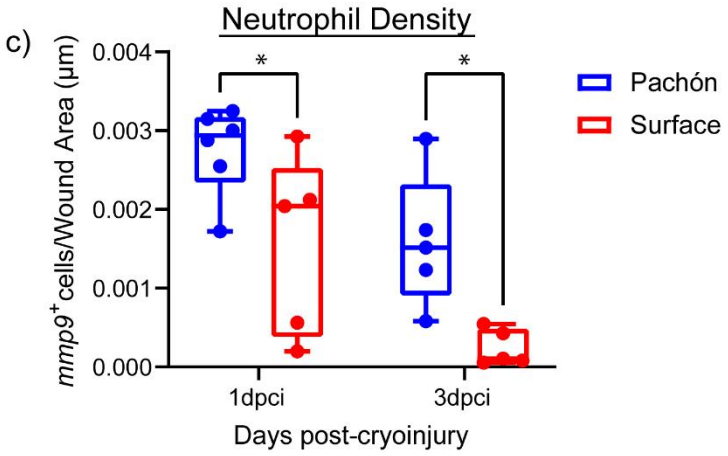
c)
Neutrophil Density
mmp9+ cells/Wound Area (µm)
0.004
0.003
0.002
0.001
0.000
*
*
1dpci
3dpci
Days post-cryoinjury
Pachón
Surface

Figure 4. 6: PF wounds have a greater density of neutrophils than SF wounds at 1dpci and 3dpci

*Representative images of PF/SF mmp9+ cells at (A) 1dpci and (B) 3dpci, showing that PF neutrophils tightly surround the injured myocardium. Wounds demarcated by grey dashed line and scale bars represent 100µm. (C) mmp9+ cells present in the wound were normalised to wound area to measure neutrophil density, revealing that PF wounds show a significantly greater density of neutrophils at 1- and 3dpci than SF (2-way ANOVA with Sidak's multiple comparisons test, * 0<0.05, n=5-6).*

PF and SF neutrophils are functionally different at each time point after cardiac injury

To investigate the transcriptional profile of PF/SF neutrophils at each time point after injury, neutrophil clusters were subset from the overall scRNAseq dataset and re-analysed. Based on the expression of canonical neutrophil markers (*mmp9, cebp1, mmp13a, lect2*, see Appendix 4.1), two neutrophil clusters were identified in the overall scRNAseq dataset and subset for re-analysis. Clustering analysis of the neutrophil scRNAseq subset data identified 4 doublet clusters, which were excluded from the downstream analysis, and 9 unique neutrophil clusters (Fig. 4.7a, see Appendix 4.2 for neutrophil cluster markers).

To systematically compare PF/SF neutrophil transcriptional profiles without bias, the neutrophil scRNAseq data was first screened for any unique PF/SF neutrophil clusters that could be specifically promoting scarring/regeneration. However, there were no unique PF/SF neutrophil subclusters overall (Fig. 4.7b) or at any time point after injury (Fig. 4.7c).

Therefore, the transcriptional profile of PF/SF neutrophils at each time point after injury was next characterised to determine whether PF/SF neutrophils showed distinct functional behaviours over the time course of cardiac scarring/regeneration.

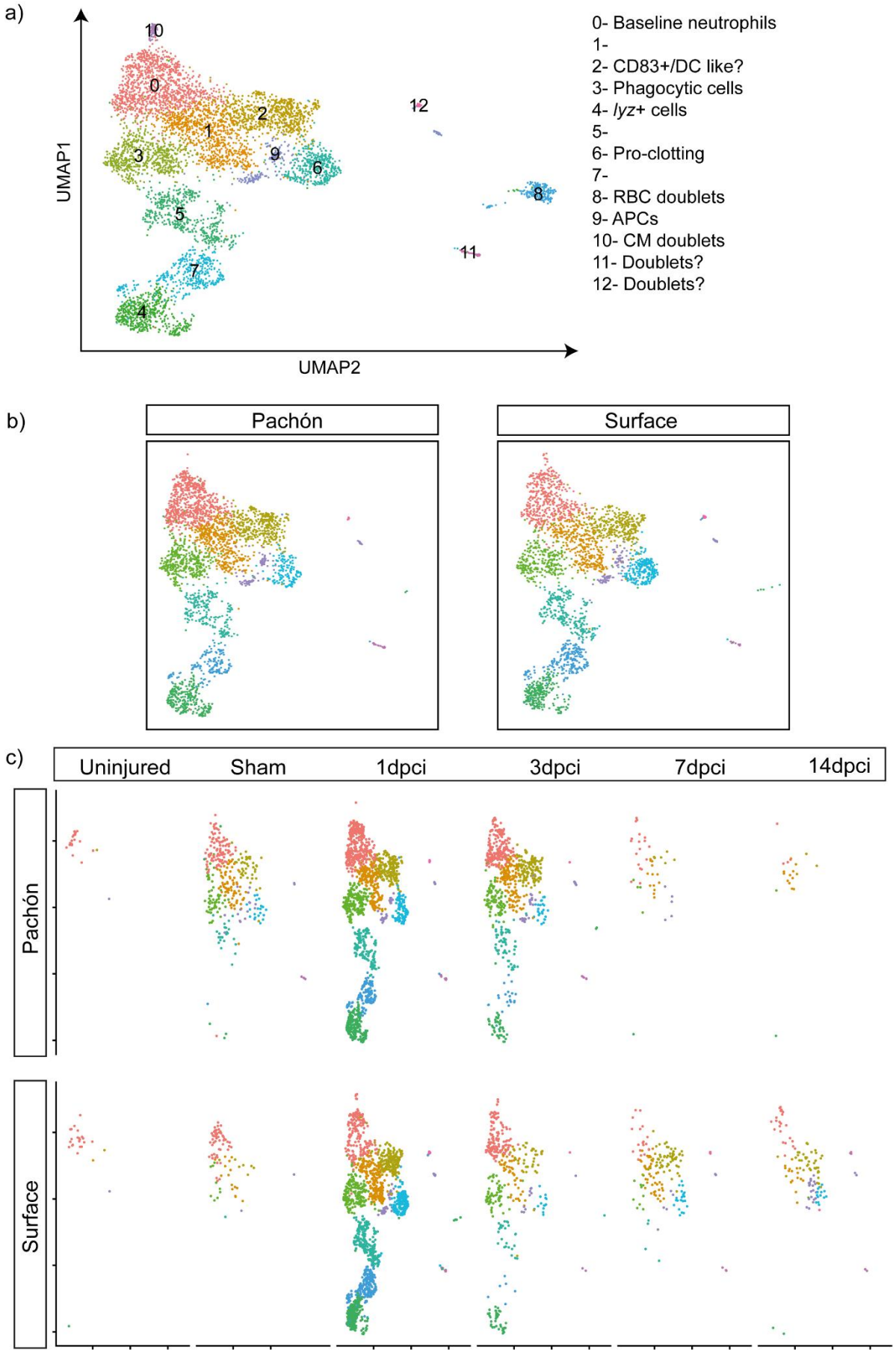

Figure 4. 7: Overview of the PF and SF neutrophil scRNAseq dataset

(A) UMAP displaying the neutrophil sub-clusters identified. 9 unique neutrophil clusters and 4 doublet clusters were identified. (B) UMAP, splitting by PF/SF-origin, shows that there are no PF/SF-specific neutrophil subclusters. (C) UMAP, splitting by time and PF/SF-origin shows that there are no population-specific neutrophil sub-clusters at any time-point.

To compare PF/SF neutrophil transcriptional profiles at each time point and identify any significant differences in gene expression, DGE analysis was performed using ROC and MAST testing. Firstly, the top cell-markers of PF/SF neutrophils were identified at each time point and the number of marker genes shared between PF and SF neutrophils was compared (Fig. 4.8a). This revealed that, at each time point, many genes were shared, whilst 3dpci neutrophils showed the greatest similarity between PF and SF (60.1% shared genes) and 14dpci neutrophils showed the least similarity (47.3% shared genes). To further probe PF/SF functional differences, MAST testing was used to compare neutrophil gene expression between PF/SF cells at each time point to ascertain if there were any meaningful transcriptional differences. Unlike uninjured PF/SF neutrophils, many genes were found to be differentially expressed at 1-, 3-, 7- and 14dpci, with 1dpci showing the highest number of differentially expressed genes (Fig. 4.8b).

To explore whether differential gene expression between PF/SF neutrophils resulted in functional neutrophil differences that could be driving regeneration or scarring, DGE lists were analysed for enrichment in Hallmark pathways using Gene Set Enrichment Analysis (GSEA). The threshold for significant enrichment (false discovery rate<0.25) was only met at 14dpci for PF/SF neutrophils (see Appendix 4.3 for results from 1-, 3-, and 7dpci). At 14dpci, PF and SF neutrophils showed opposing enrichment for KRAS signalling, with SF showing enrichment for genes involved in upregulation of KRAS signalling whilst PF showed enrichment for genes involved in downregulation (Fig. 4.8c). KRAS is a GTPase that, when activated, typically stimulates cell growth, differentiation and survival, suggesting that 14dpci PF/SF neutrophils could show differences in their differentiated

or anti-apoptotic state. Furthermore, PF 14dpci neutrophils showed enrichment for genes down-regulated in response to UV radiation, and for genes involved in myogenesis whilst SF showed enrichment for genes involved in allograft rejection, and TNFα/NFκB signalling, a transcription factor pathway typically associated with the early stages of wound healing and the inflammatory response.

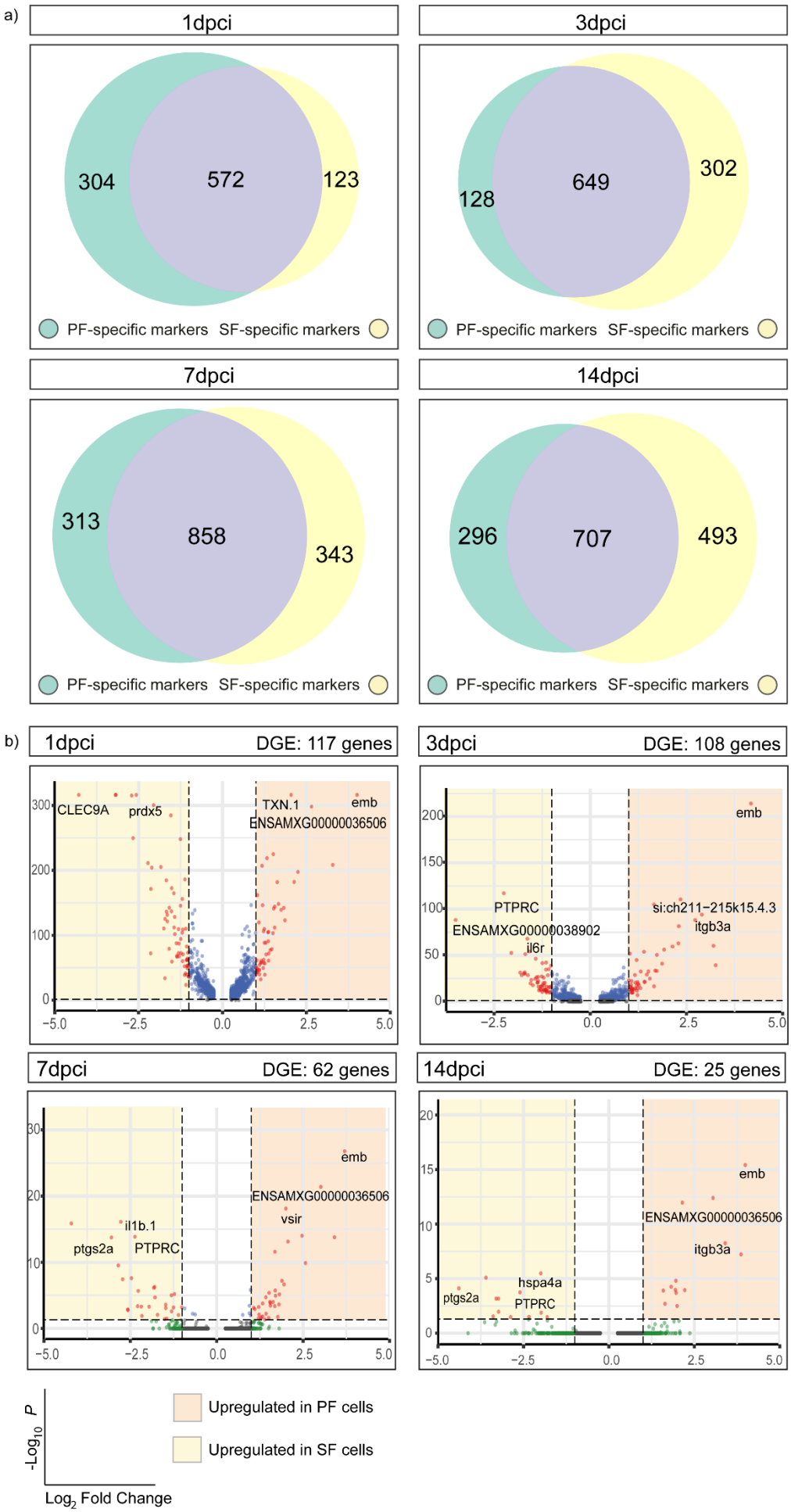
a)
1dpci
304
572
123
PF-specific markers
SF-specific markers
3dpci
128
649
302
PF-specific markers
SF-specific markers
7dpci
313
858
343
PF-specific markers
SF-specific markers
14dpci
296
707
493
PF-specific markers
SF-specific markers
b)
1dpci
DGE: 117 genes
CLEC9A
prdx5
TXN.1
emb
ENSAMXG00000036506
3dpci
DGE: 108 genes
emb
PTPRC
ENSAMXG00000038902
il6r
si:ch211−215k15.4.3
itgb3a
7dpci
DGE: 62 genes
emb
ENSAMXG00000036506
vsir
il1b.1
ptgs2a
PTPRC
14dpci
DGE: 25 genes
emb
ENSAMXG00000036506
itgb3a
hspa4a
ptgs2a
PTPRC
Upregulated in PF cells
Upregulated in SF cells
-Log10 P
Log2 Fold Change

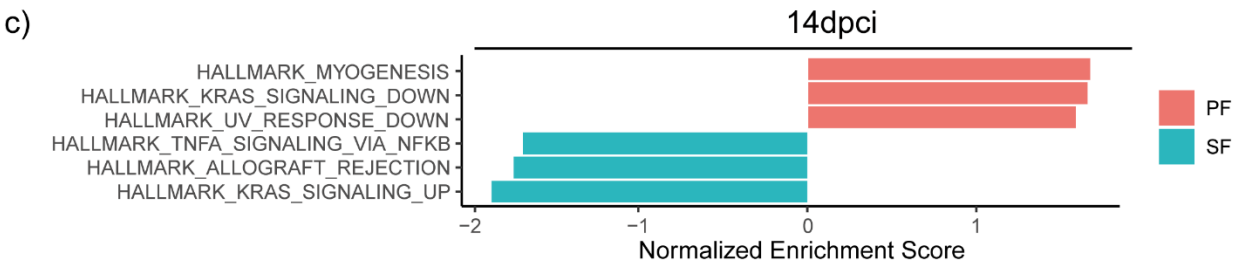

Figure 4. 8: PF and SF neutrophils are transcriptionally diverse following cryoinjury

(A) Euler plots comparing the proportion of shared PF- and SF- top cell marker genes. At 1dpci, 57.2% of genes are shared; at 3dpci 60.1% of genes are shared; at 7dpci 56.6% of genes are shared; at 14dpci, 47.3% of genes are shared. (B) Volcano plots showing the results of DGE analysis between PF and SF at each time point. (C) Plot showing the top GSEA results for 14dpci.

As the Hallmark pathways are very broad, it was possible that some functional differences between PF and SF neutrophils may not have been captured by GSEA. Therefore, the DGE lists were also tested for the top-associated GO terms at each time point. At every time point, the top associated GO terms for PF and SF neutrophils were very different and few GO terms were shared between PF and SF neutrophils (Fig. 4.9). At 1dpci, GO term analysis suggested that PF neutrophils were actively producing proteins and upregulating glycolysis; whereas SF neutrophils seemed to be taking up extracellular debris by phagocytosis and trafficking proteins to the ER (Fig. 4.9a). At 3dpci, PF neutrophils seemed to be dying by apoptosis and releasing detrimental superoxide anions. In contrast, SF neutrophils were responding to external signals such as IL-7, hypoxia and insulin (Fig. 4.9b).

During the later stages after cardiac injury (7- and 14dpci), when both the PF and SF neutrophil responses have been seemingly resolved, an interesting divergence in the GO term results was observed. As expected, at 7dpci, the few remaining PF neutrophils were transcriptionally inactive and dying by apoptosis (Fig. 4.9c) whilst at 14dpci, PF neutrophils were no longer actively

transcribing sufficient genes for meaningful GO term analysis (Fig. 4.9d). In contrast, however, cell differentiation was one of the top GO terms for 7- and 14dpci SF neutrophils (Fig. 4.9c & 4.9d), suggesting that these cells were still transcriptionally active and potentially entering a new differentiated state. Indeed, at 7dpci, GO term analysis suggested that SF neutrophils were responding to cytokines whilst at 14dpci, SF neutrophils were seemingly responding to inflammation.

The results of the GO term analysis suggested that late-stage SF neutrophils were transcriptionally active and might be differentiating, suggesting that the SF neutrophil response had not been resolved. Therefore, to confirm whether late-stage PF/SF neutrophils were still transcriptionally active, the next logical step was to compare late-stage PF/SF neutrophils to uninjured neutrophils.

a)

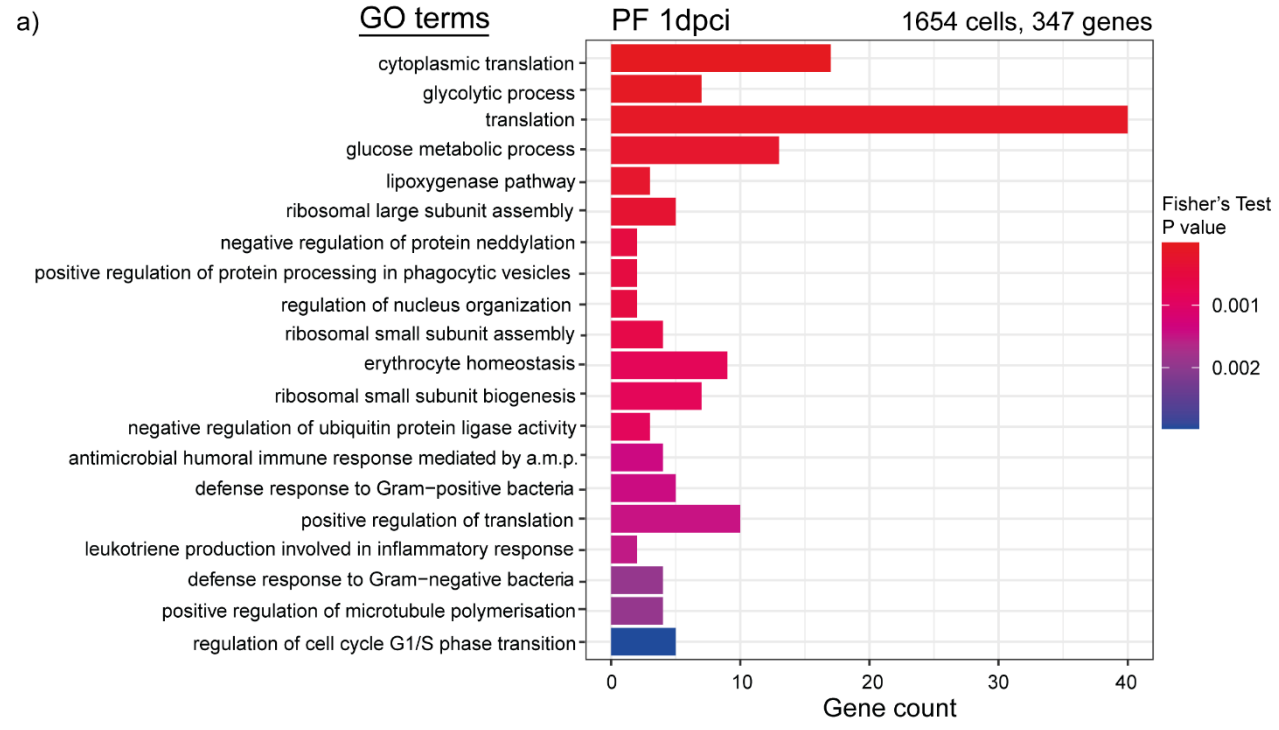
GO terms
PF 1dpci
1654 cells, 347 genes
cytoplasmic translation
glycolytic process
translation
glucose metabolic process
lipoxygenase pathway
ribosomal large subunit assembly
negative regulation of protein neddylation
positive regulation of protein processing in phagocytic vesicles
regulation of nucleus organization
ribosomal small subunit assembly
erythrocyte homeostasis
ribosomal small subunit biogenesis
negative regulation of ubiquitin protein ligase activity
antimicrobial humoral immune response mediated by a.m.p.
defense response to Gram−positive bacteria
positive regulation of translation
leukotriene production involved in inflammatory response
defense response to Gram−negative bacteria
positive regulation of microtubule polymerisation
regulation of cell cycle G1/S phase transition
0
10
20
30
40
Gene count
Fisher's Test
P value
0.001
0.002

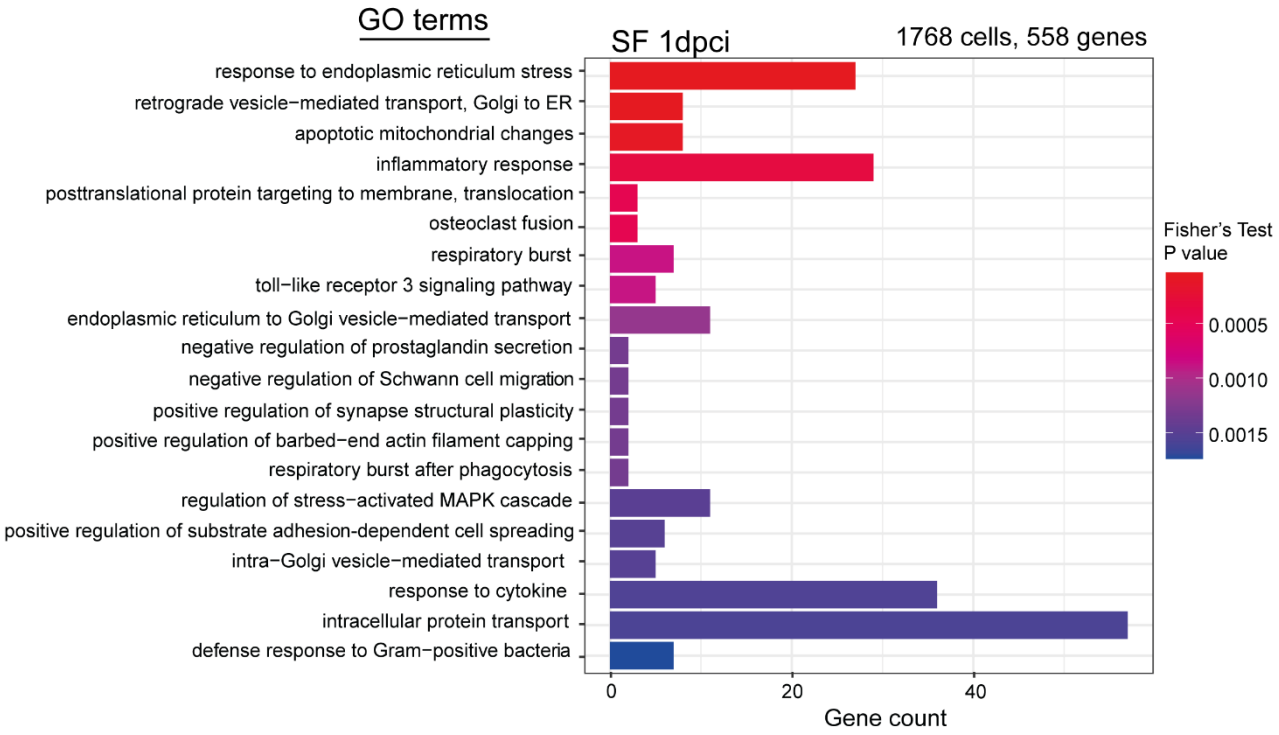
GO terms
SF 1dpci
1768 cells, 558 genes
response to endoplasmic reticulum stress
retrograde vesicle−mediated transport, Golgi to ER
apoptotic mitochondrial changes
inflammatory response
posttranslational protein targeting to membrane, translocation
osteoclast fusion
respiratory burst
toll−like receptor 3 signaling pathway
endoplasmic reticulum to Golgi vesicle−mediated transport
negative regulation of prostaglandin secretion
negative regulation of Schwann cell migration
positive regulation of synapse structural plasticity
positive regulation of barbed−end actin filament capping
respiratory burst after phagocytosis
regulation of stress−activated MAPK cascade
positive regulation of substrate adhesion-dependent cell spreading
intra−Golgi vesicle−mediated transport
response to cytokine
intracellular protein transport
defense response to Gram−positive bacteria
0
20
40
Gene count
Fisher's Test
P value
0.0005
0.0010
0.0015

b)

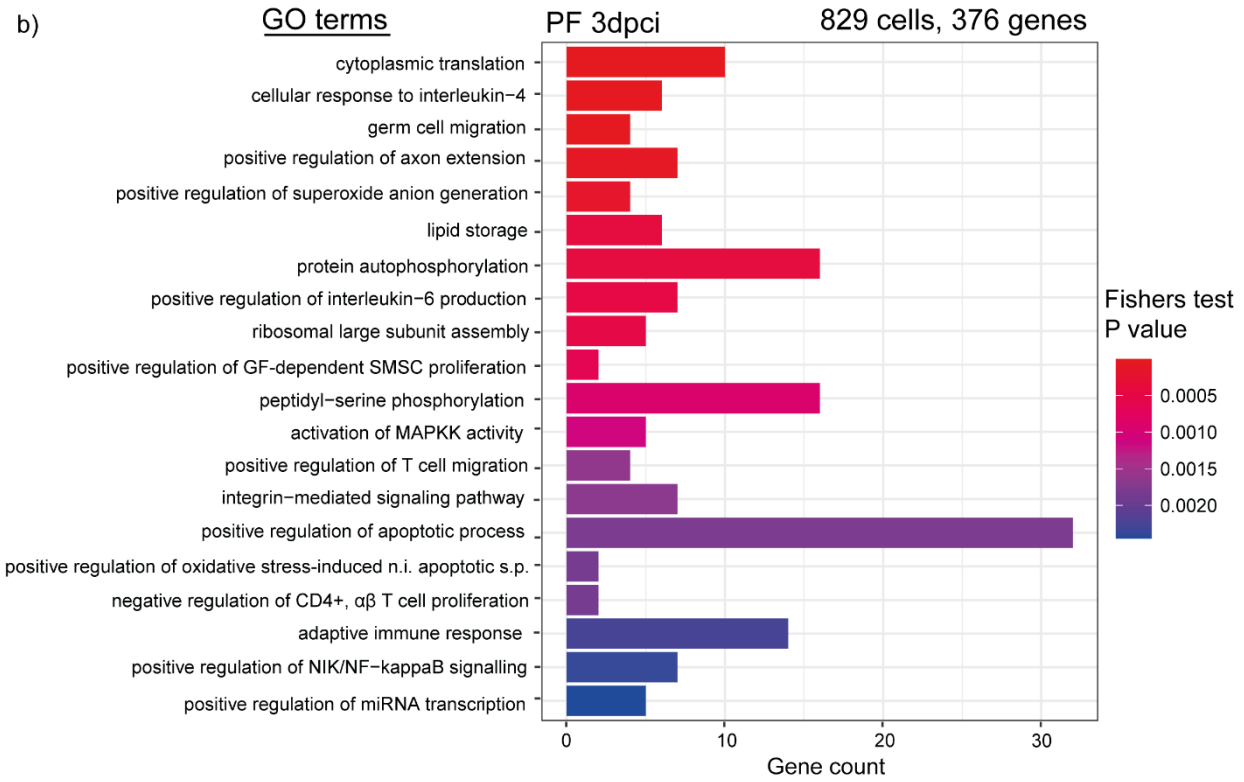
GO terms
PF 3dpci
829 cells, 376 genes
cytoplasmic translation
cellular response to interleukin−4
germ cell migration
positive regulation of axon extension
positive regulation of superoxide anion generation
lipid storage
protein autophosphorylation
positive regulation of interleukin−6 production
ribosomal large subunit assembly
positive regulation of GF-dependent SMSC proliferation
peptidyl−serine phosphorylation
activation of MAPKK activity
positive regulation of T cell migration
integrin−mediated signaling pathway
positive regulation of apoptotic process
positive regulation of oxidative stress-induced n.i. apoptotic s.p.
negative regulation of CD4+, αβ T cell proliferation
adaptive immune response
positive regulation of NIK/NF−kappaB signalling
positive regulation of miRNA transcription
0
10
20
30
Gene count
Fishers test
P value
0.0005
0.0010
0.0015
0.0020

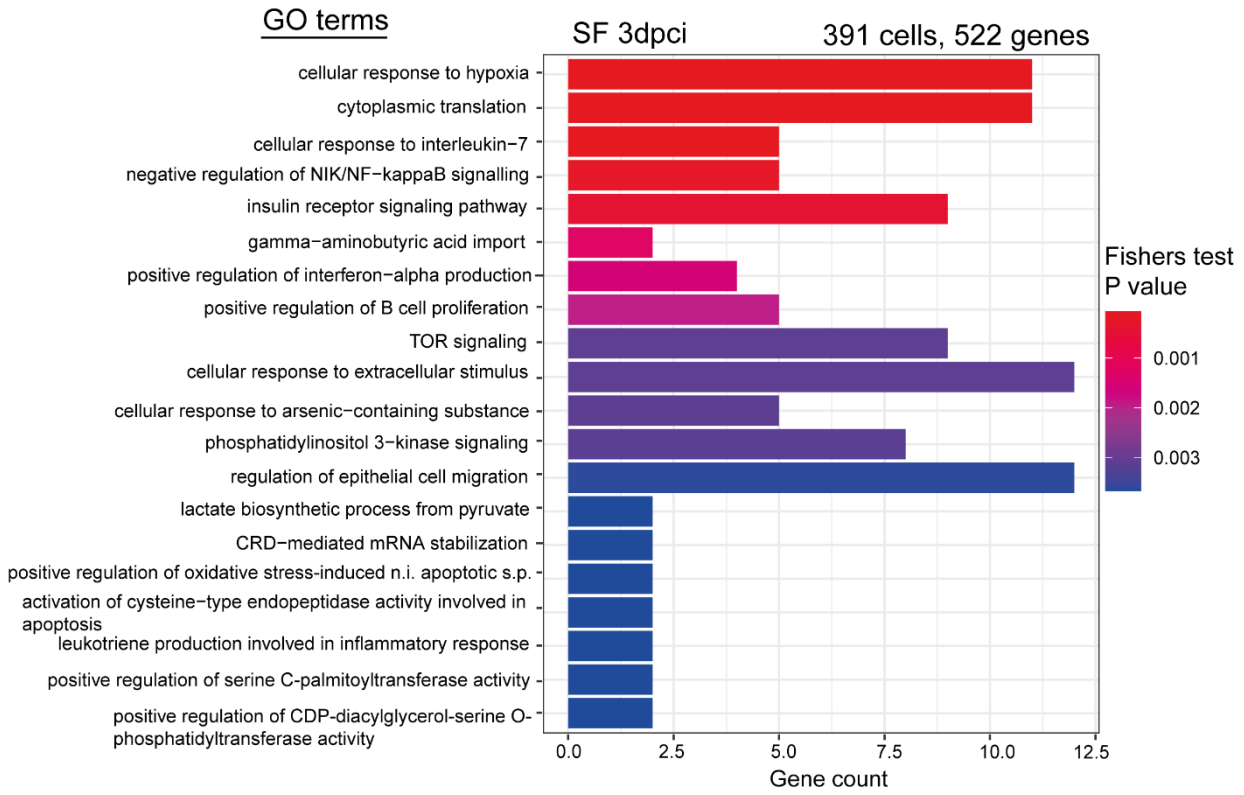
GO terms
SF 3dpci
391 cells, 522 genes
cellular response to hypoxia
cytoplasmic translation
cellular response to interleukin−7
negative regulation of NIK/NF−kappaB signalling
insulin receptor signaling pathway
gamma−aminobutyric acid import
positive regulation of interferon−alpha production
positive regulation of B cell proliferation
TOR signaling
cellular response to extracellular stimulus
cellular response to arsenic−containing substance
phosphatidylinositol 3−kinase signaling
regulation of epithelial cell migration
lactate biosynthetic process from pyruvate
CRD−mediated mRNA stabilization
positive regulation of oxidative stress-induced n.i. apoptotic s.p.
activation of cysteine−type endopeptidase activity involved in apoptosis
leukotriene production involved in inflammatory response
positive regulation of serine C-palmitoyltransferase activity
positive regulation of CDP-diacylglycerol-serine O-phosphatidyltransferase activity
0.0
2.5
5.0
7.5
10.0
12.5
Gene count
Fishers test
P value
0.001
0.002
0.003

c)

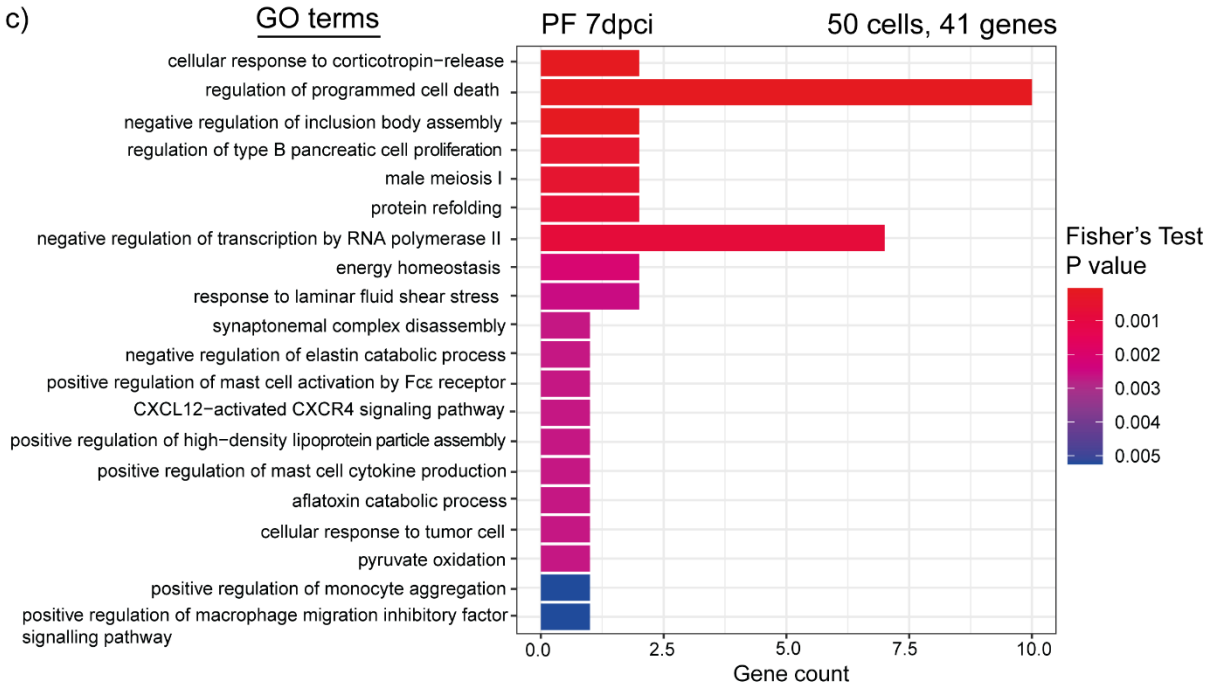
GO terms
PF 7dpci
50 cells, 41 genes
cellular response to corticotropin−release
regulation of programmed cell death
negative regulation of inclusion body assembly
regulation of type B pancreatic cell proliferation
male meiosis I
protein refolding
negative regulation of transcription by RNA polymerase II
energy homeostasis
response to laminar fluid shear stress
synaptonemal complex disassembly
negative regulation of elastin catabolic process
positive regulation of mast cell activation by Fcε receptor
CXCL12−activated CXCR4 signaling pathway
positive regulation of high−density lipoprotein particle assembly
positive regulation of mast cell cytokine production
aflatoxin catabolic process
cellular response to tumor cell
pyruvate oxidation
positive regulation of monocyte aggregation
positive regulation of macrophage migration inhibitory factor signalling pathway
0.0
2.5
5.0
7.5
10.0
Gene count
Fisher's Test P value
0.001
0.002
0.003
0.004
0.005

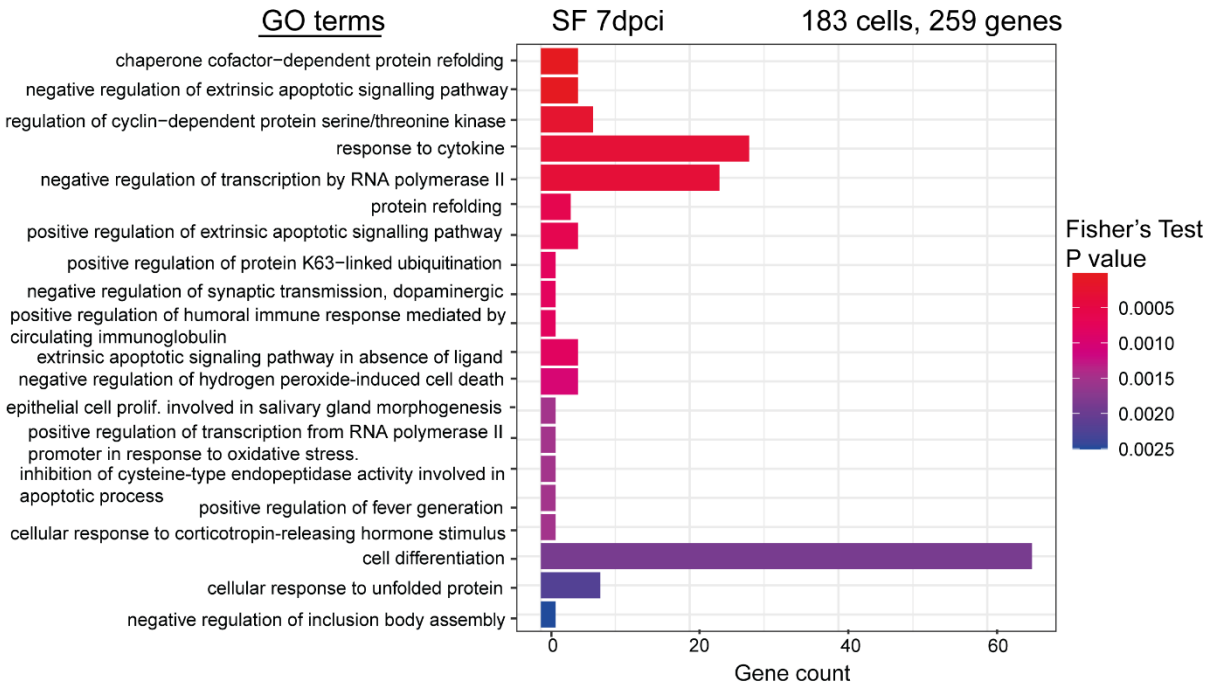
GO terms
SF 7dpci
183 cells, 259 genes
chaperone cofactor−dependent protein refolding
negative regulation of extrinsic apoptotic signalling pathway
regulation of cyclin−dependent protein serine/threonine kinase
response to cytokine
negative regulation of transcription by RNA polymerase II
protein refolding
positive regulation of extrinsic apoptotic signalling pathway
positive regulation of protein K63−linked ubiquitination
negative regulation of synaptic transmission, dopaminergic
positive regulation of humoral immune response mediated by circulating immunoglobulin
extrinsic apoptotic signaling pathway in absence of ligand
negative regulation of hydrogen peroxide-induced cell death
epithelial cell prolif. involved in salivary gland morphogenesis
positive regulation of transcription from RNA polymerase II promoter in response to oxidative stress.
inhibition of cysteine-type endopeptidase activity involved in apoptotic process
positive regulation of fever generation
cellular response to corticotropin-releasing hormone stimulus
cell differentiation
cellular response to unfolded protein
negative regulation of inclusion body assembly
0
20
40
60
Gene count
Fisher's Test P value
0.0005
0.0010
0.0015
0.0020
0.0025

Figure 4. 9: Functional pathway analysis revealed late-stage SF neutrophils are undergoing cellular differentiation

GO term analysis for top cell markers of PF and SF neutrophils at (A) 1dpci, (B) 3dpci, (C) 7dpci and (D) 14dpci.

SF neutrophils are still active at 7- and 14dpci

To probe whether the late-stage SF neutrophil response was still 'on', DGE analysis was performed between uninjured and 7/14dpci neutrophils. If the neutrophil response had been resolved by 7dpci, we would expect any remaining neutrophils in the heart to be transcriptionally indistinct from uninjured neutrophils. Surprisingly, many genes were upregulated in 7- and 14dpci SF neutrophils in comparison to uninjured neutrophils, confirming that late-stage SF neutrophils are still responding to injury. In contrast, only 1 gene reached the cut-offs for differential expression in 7dpci PF neutrophils, whilst no genes were differentially expressed at 14dpci (Fig. 4.10a, see Appendix 4.4 for uninjured vs 1dpci and uninjured vs 3dpci), suggesting that the neutrophils present in late-stage PF hearts are very similar to uninjured PF neutrophils. Therefore, DGE analysis suggested that late-stage SF neutrophils are actively responding to cardiac injury and may be performing distinct neutrophil behaviours that promote regeneration. As it was possible that the substantial influx of neutrophils immediately after injury may have masked any subtle differences in neutrophil numbers that occur in the late stages of cardiac healing, the *mmp9+* cell count data was re-examined to specifically compare 7/14dpci neutrophils to uninjured levels. This revealed that SF neutrophil levels were significantly elevated at 7- and 14dpci in comparison to uninjured hearts whilst PF neutrophil levels were not significantly different from baseline levels (Fig. 4.10b).

Therefore, this data confirms that the SF neutrophil response is still 'on' at 7- and 14dpci as late-stage SF neutrophils were both elevated above baseline levels and were still actively transcribing genes in response to injury.

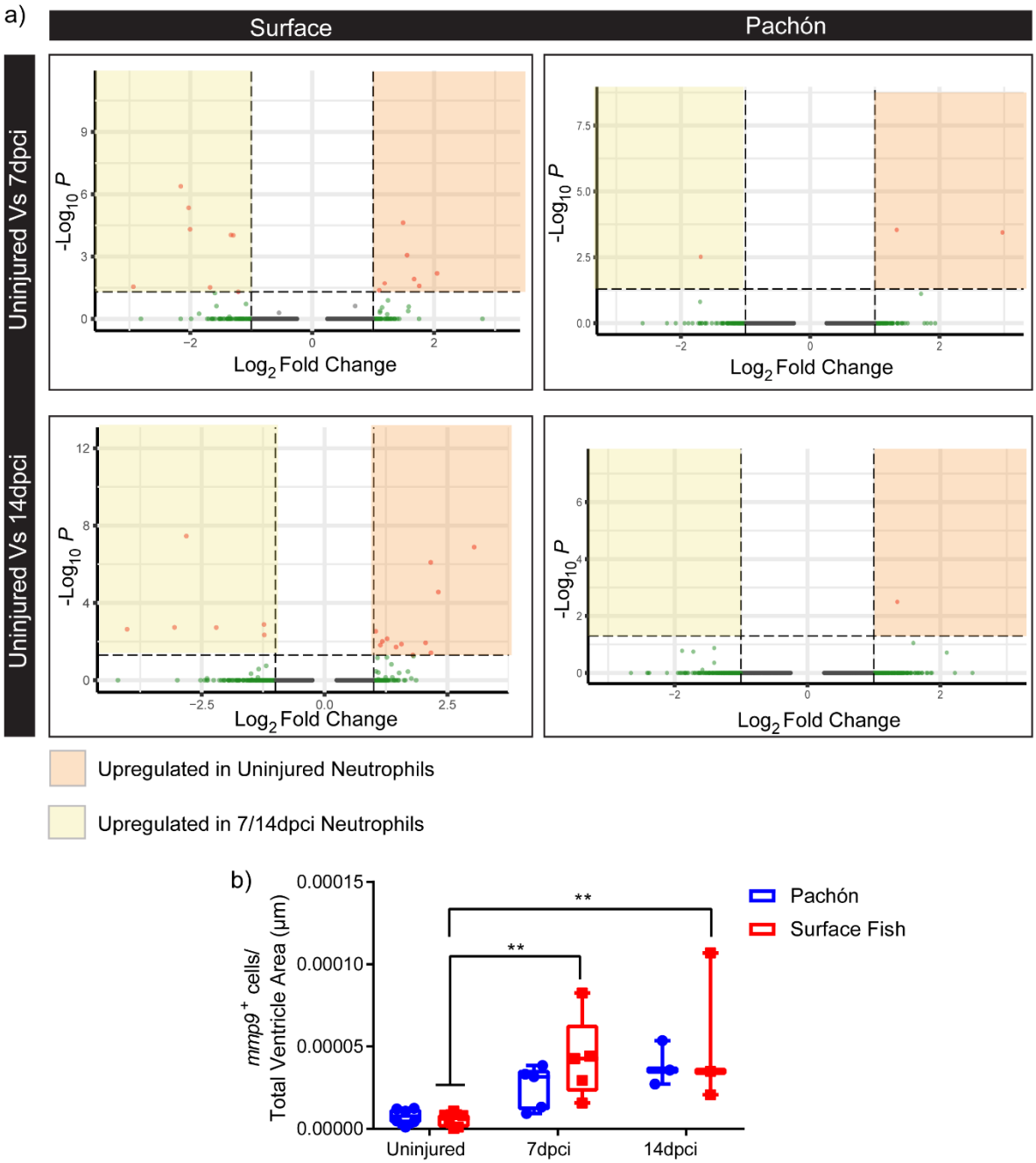

Figure 4. 10: The SF neutrophil response is still active at 7 and 14dpci whereas the PF neutrophil response has been 'turned off' and has returned to the uninjured state

(A) Volcano plots of DGE results, comparing uninjured PF and SF neutrophils to 7- and 14dpci. (B) mmp9+ cells were counted and normalised to total ventricular area for uninjured, 7- and 14dpci neutrophils. SF neutrophils were significantly elevated at 7- and 14dpci compared to uninjured levels whilst late-stage PF neutrophils levels were not significantly elevated from baseline levels (2-way

*ANOVA with Sidak's multiple comparisons test, **, p<0.01, 2-way ANOVA with Sidak's multiple comparisons test, n=3-6).*

Late-stage SF neutrophils represent a transcriptionally unique neutrophil population that is absent from the PF response

Pro-reparative and anti-inflammatory neutrophils have previously been characterised in the heart that show distinct transcriptional and proteomic profiles which only emerge in the later stages of cardiac repair (5-7dpi). Therefore, the transcriptional profile of PF/SF neutrophils was characterised across time to determine whether late-stage SF neutrophils were transcriptionally unique. MAST testing was used to identify the top SF and PF neutrophil markers at each time point (Fig. 4.11a). This showed that SF neutrophils present at 7- and 14dpci have a distinct transcriptional profile that is shared at both late stages of the injury response but is completely absent from the PF and during the early stages of the SF neutrophil response (Fig. 4.11a, Fig. 4.11b shows a simplified version of 4.11a).

To confirm whether the distinct transcriptional profile of late-stage SF neutrophils was driven by the expression of injury-responsive genes, DGE analysis was performed between uninjured and 1-, 3-, 7- and 14dpci neutrophils. Genes that were specifically upregulated in 1-, 3-, 7- and 14dpci neutrophils were then selected and the expression of these genes in PF/SF neutrophils was compared to determine if there was any overlap. Remarkably, although there was a large degree of overlap in injury-responsive genes at 1- and 3dpci, there were no shared genes at 7- and 14dpci (Fig. 4.11c). Furthermore, a comparison of the top neutrophil markers in PF/SF neutrophils at all time points revealed that there were very few overlapping genes between PF/SF neutrophils at 7- and 14dpci (Fig. 4.11d), further supporting the finding that late-stage SF neutrophils are transcriptionally unique.

Finally, as 7/14dpci SF neutrophils shared a unique transcriptional profile, I postulated that late-stage SF neutrophils must be functionally similar. A re-examination of the results of the neutrophil GO term analysis showed that SF 7/14dpci neutrophils share many top GO terms, adding additional support to the finding that late-stage SF neutrophils share a unique transcriptional profile (Fig. 4.11e).

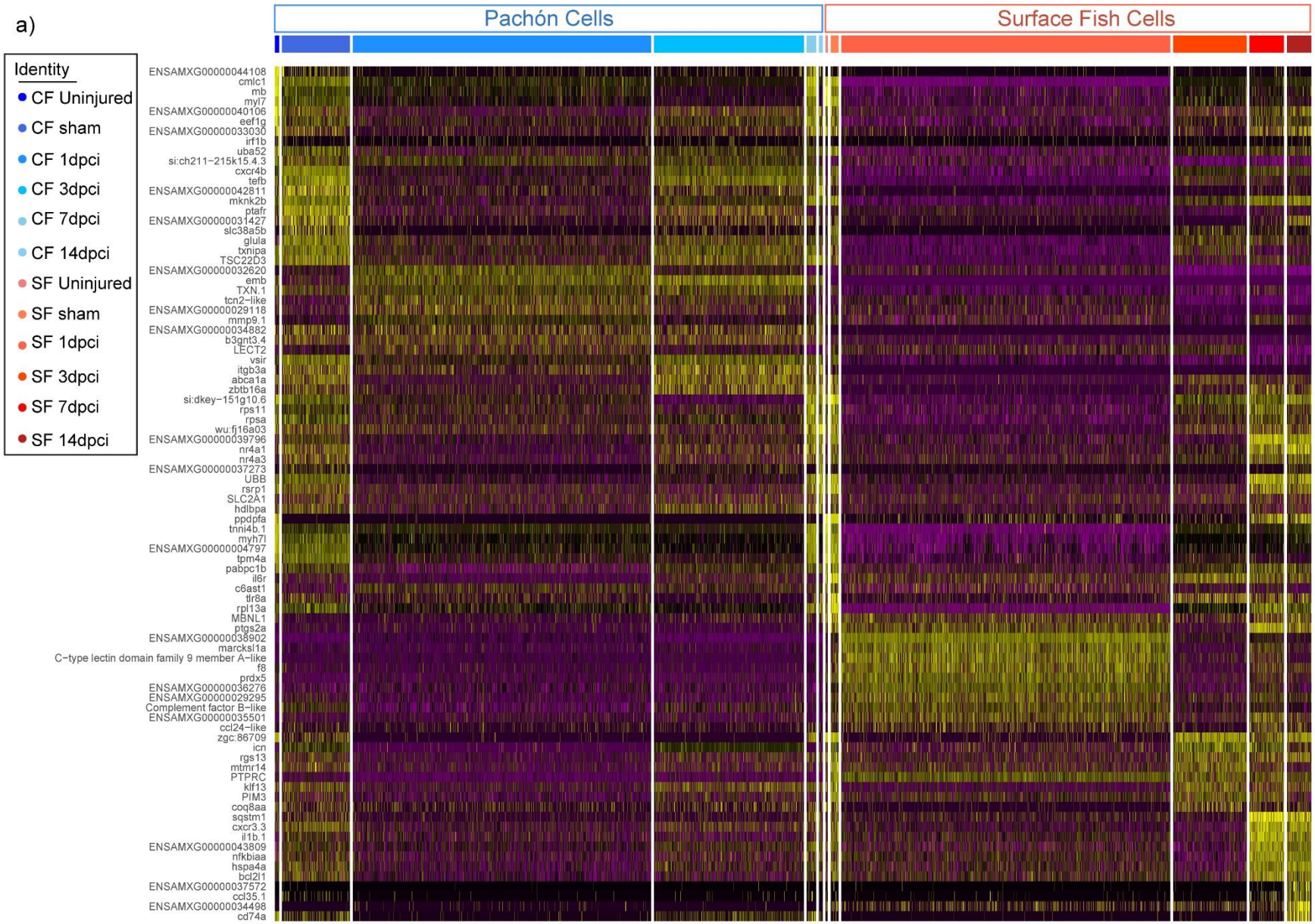
a)
Pachón Cells
Surface Fish Cells
Identity
CF Uninjured
CF sham
CF 1dpci
CF 3dpci
CF 7dpci
CF 14dpci
SF Uninjured
SF sham
SF 1dpci
SF 3dpci
SF 7dpci
SF 14dpci
ENSAMXG00000044108
cmlc1
mb
myl7
ENSAMXG00000040106
eef1g
ENSAMXG00000033030
irf1b
uba52
si:ch211−215k15.4.3
cxcr4b
tefb
ENSAMXG00000042811
mknk2b
ptafr
ENSAMXG00000031427
slc38a5b
glula
txnipa
TSC22D3
ENSAMXG00000032620
emb
TXN.1
tcn2−like
ENSAMXG00000029118
mmp9.1
ENSAMXG00000034882
b3gnt3.4
LECT2
vsir
itgb3a
abca1a
zbtb16a
si:dkey−151g10.6
rps11
rpsa
wu:fj16a03
ENSAMXG00000039796
nr4a1
nr4a3
ENSAMXG00000037273
UBB
rsrp1
SLC2A1
hdlbpa
ppdpfa
tnni4b.1
myh7l
ENSAMXG00000004797
tpm4a
pabpc1b
il6r
c6ast1
tlr8a
rpl13a
MBNL1
ptgs2a
ENSAMXG00000038902
marcksl1a
C−type lectin domain family 9 member A−like
f8
prdx5
ENSAMXG00000036276
ENSAMXG00000029295
Complement factor B−like
ENSAMXG00000035501
ccl24−like
zgc:86709
icn
rgs13
mtmr14
PTPRC
klf13
PIM3
coq8aa
sqstm1
cxcr3.3
il1b.1
ENSAMXG00000043809
nfkbiaa
hspa4a
bcl2l1
ENSAMXG00000037572
ccl35.1
ENSAMXG00000034498
cd74a

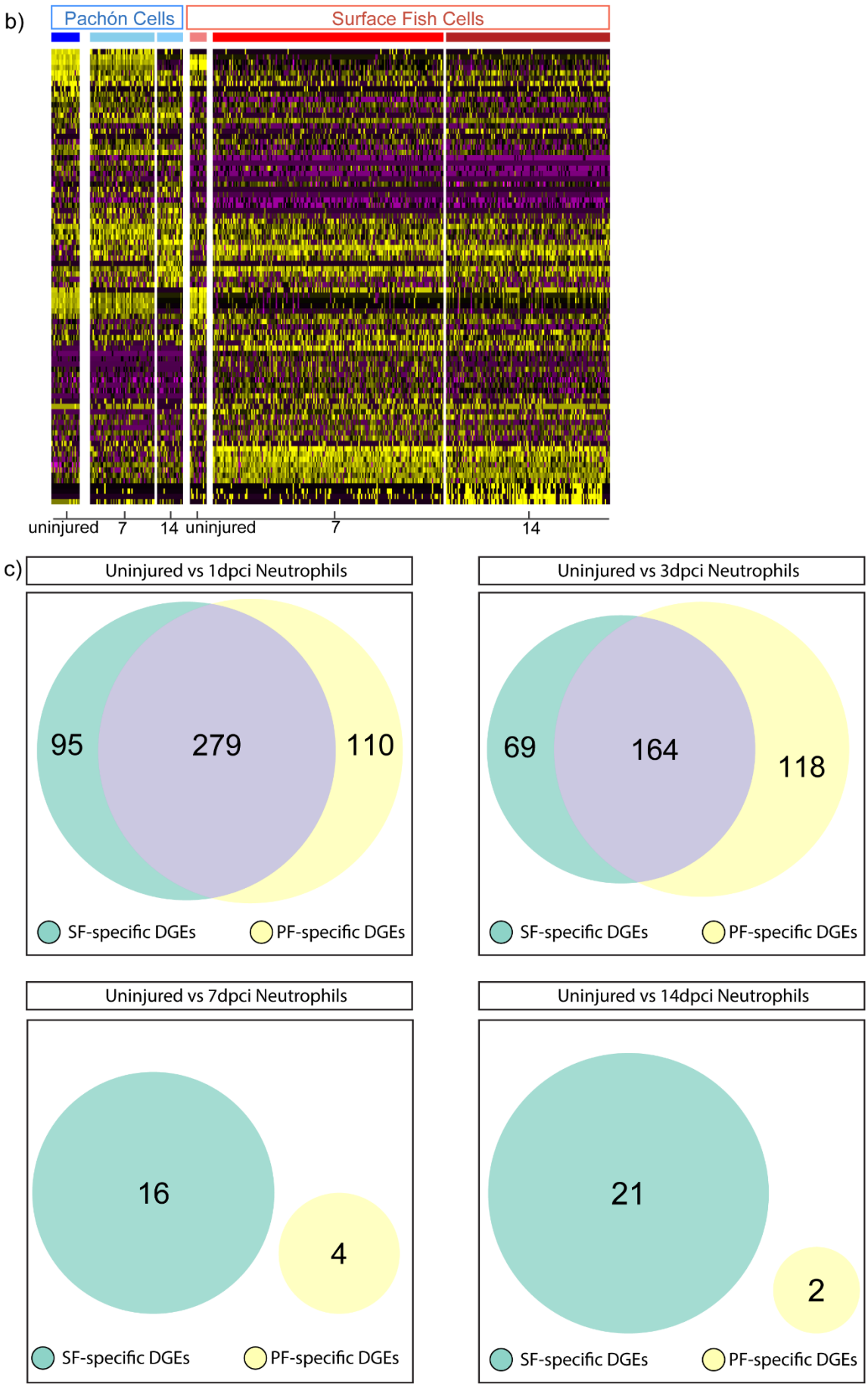
b)
Pachón Cells
Surface Fish Cells
uninjured
7
14
uninjured
7
14
c)
Uninjured vs 1dpci Neutrophils
95
279
110
SF-specific DGEs
PF-specific DGEs
Uninjured vs 3dpci Neutrophils
69
164
118
SF-specific DGEs
PF-specific DGEs
Uninjured vs 7dpci Neutrophils
16
4
SF-specific DGEs
PF-specific DGEs
Uninjured vs 14dpci Neutrophils
21
2
SF-specific DGEs
PF-specific DGEs

d)

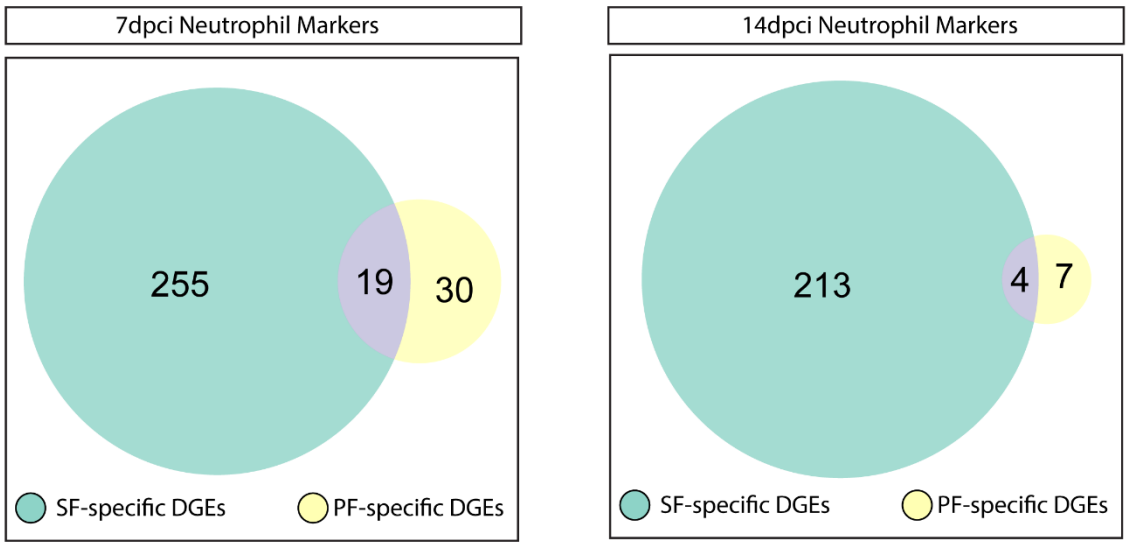
7dpci Neutrophil Markers
255
19
30
SF-specific DGEs
PF-specific DGEs
14dpci Neutrophil Markers
213
4
7
SF-specific DGEs
PF-specific DGEs

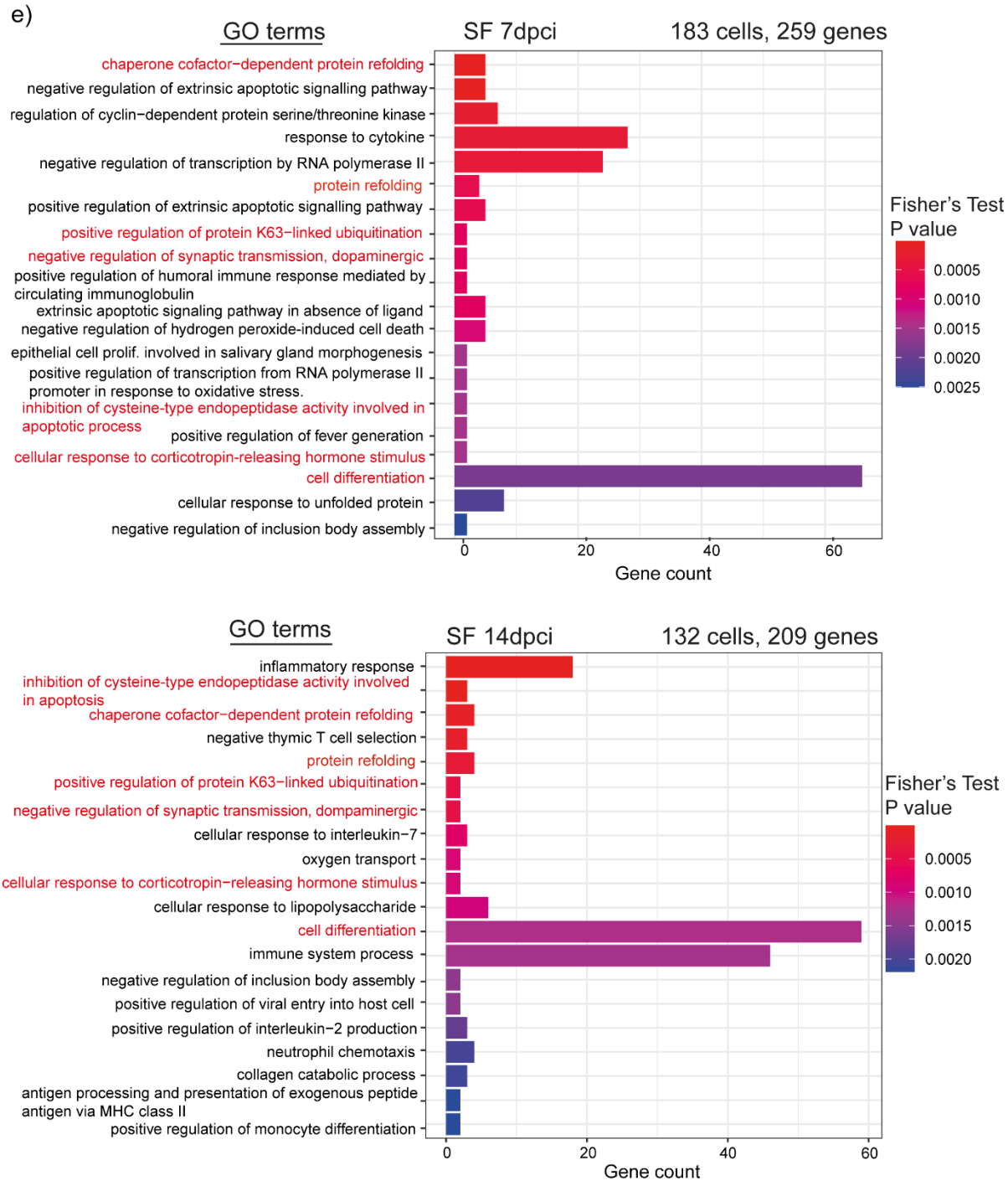

Figure 4. 11: Late-stage SF neutrophils have a unique transcriptional profile that is absent from the PF

(A) Heatmap of the top 5 cell markers of PF and SF neutrophils at each time point. (B) Same heatmap as in (A) but only uninjured, 7- and 14dpci cells have been plotted to allow increased visualisation. (C) Euler plots comparing PF/SF injury response genes at 1-, 3-, 7- and 14dpci. (E) Top GO terms

represented in SF 7- and 14dpci neutrophil markers. Terms in red indicate GO terms shared between late-stage SF neutrophils.

To conclude, data from scRNAseq and cell counts has shown that the PF/SF neutrophil responses are significantly different (Fig. 4.12):

- Immediately after injury, the PF neutrophil response is significantly stronger and is prolonged in comparison to the SF response
- A significantly greater number of neutrophils influx into PF wounds at both 1- and 3dpci, resulting in PF wounds with higher densities of neutrophils than the SF
- The initial SF neutrophil response is brief and is quickly resolved by 3dpci
- The SF neutrophil response significantly diverges from the PF response during the late stages of cardiac healing. SF neutrophil levels remain elevated at 7- and 14dpci in comparison to baseline levels whereas PF neutrophils do not
- The late-stage SF neutrophil response is characterised by a transcriptionally distinct population

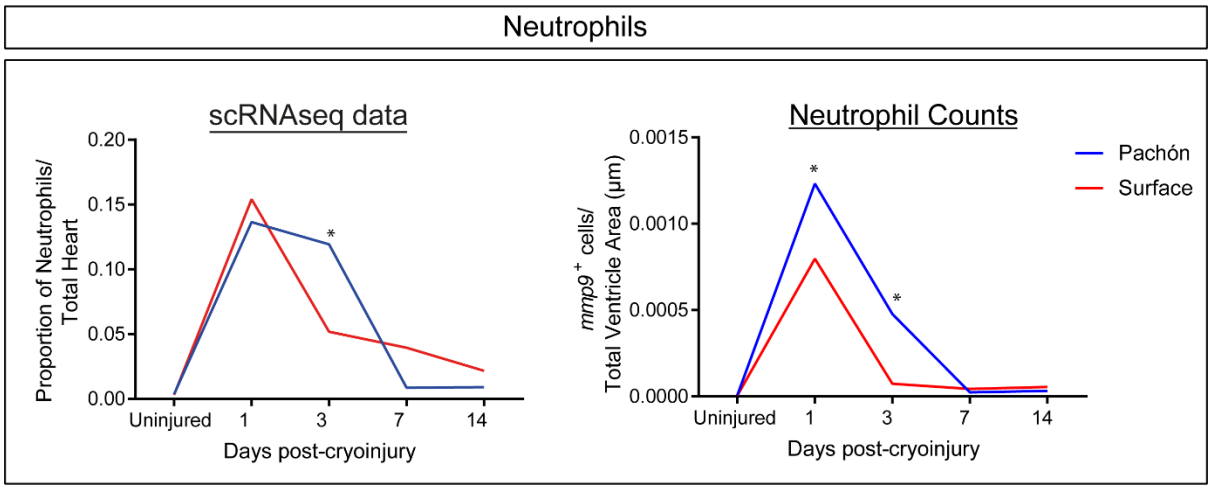

Figure 4. 12: PF/SF neutrophil dynamics post-MI in the scRNAseq and cell count data both independently confirm that PF neutrophils are significantly elevated in comparison to the SF at 3dpci.

4.2.2 PF and SF macrophages show many functional differences

PF and SF show no difference in the number of mpeg1^{+} macrophages at 7dpci

Next, I focused on the macrophages. To characterise the macrophage response to cryoinjury and perform cell counts, *mpeg1* was used as a specific and pan-macrophage marker. *mpeg1* is a well-established macrophage marker in teleosts[265–273] and, during lockdown when the scRNAseq data available was only partially sequenced, *mpeg1* seemed to be a specific and pan-macrophage marker in the AM (Appendix 4.5). Therefore, AM hearts were initially stained with a RNAscope probe for *mpeg1* at 7dpci (Fig. 4.13a) to confirm the previous DPA result that SF macrophage levels are significantly elevated in comparison to the PF at 7dpci. However, *mpeg1*+ cell counts showed no difference in the number of *mpeg1* cells present in PF/SF wounds at 7dpci (Fig. 4.13b).

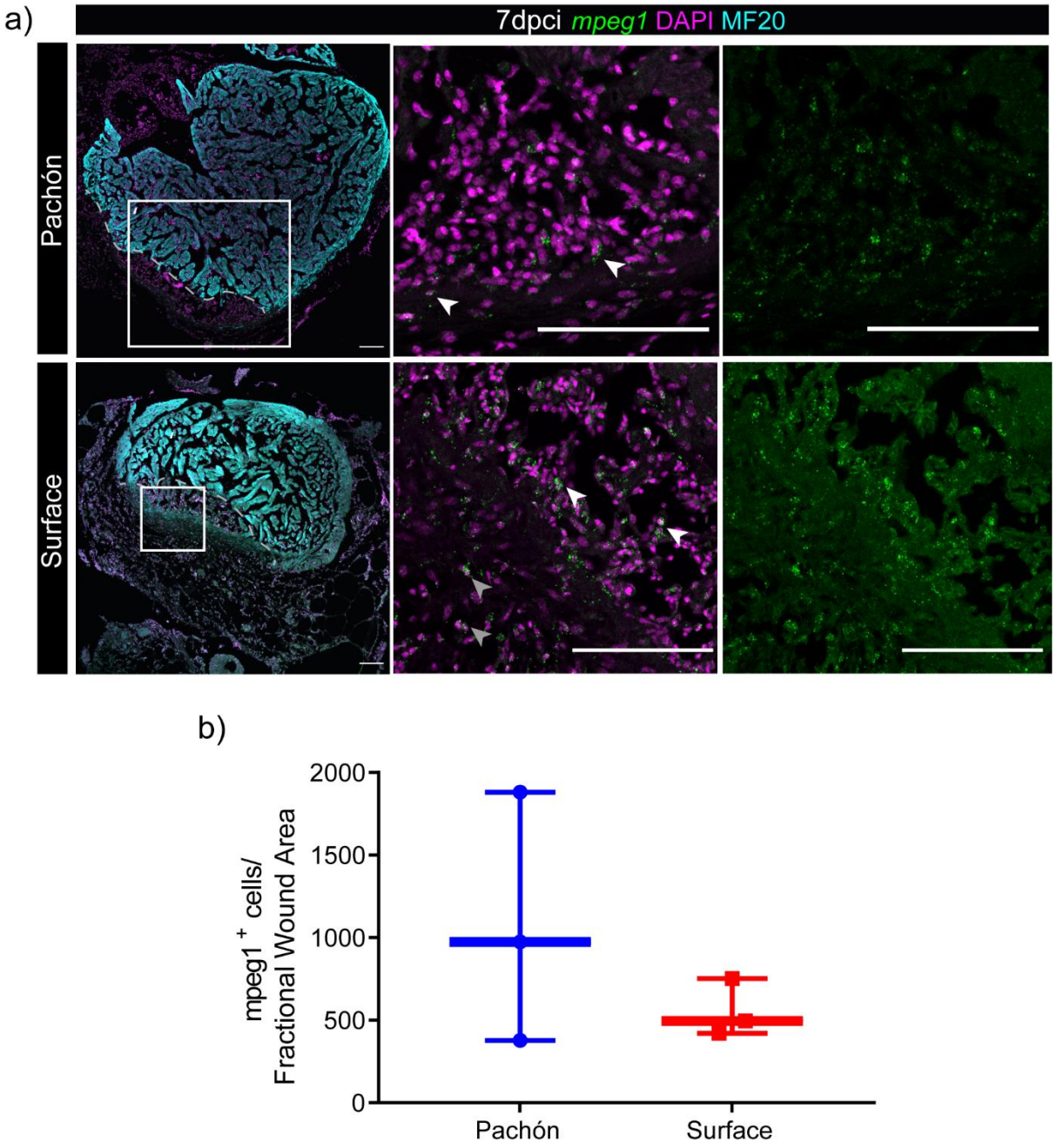

Figure 4. 13: PF/SF show no differences in the number of mpeg1+ cells present in the wound after injury

(A) PF and SF hearts were stained at 7dpci with mpeg1 to label macrophages. Sections were counterstained with MF20 and DAPI. (B) mpeg1+ cells present in the wound were counted and normalised to fractional wound area, showing no difference in the number of PF/SF macrophages (Student's t-test, n=3).

As the *mpeg1* cell count data conflicted with the scRNAseq data, I investigated why SF macrophage numbers were not elevated in SF hearts at 7dpci. One possible explanation was that *mpeg1* was not a suitable pan-macrophage marker in the AM. To confirm that *mpeg1* was a specific and pan-macrophage AM marker, the expression levels of *mpeg1* were re-assessed using the overall scRNAseq dataset that had been sequenced to full depth. Unfortunately, it was apparent that, although *mpeg1* is a specific macrophage marker, it is not expressed in all AM macrophages. Therefore, *mpeg1* cell counts do not represent overall macrophage numbers (Fig. 4.14a) and *mpeg1* staining was not pursued any further to characterise the temporal dynamics of macrophages in response to injury or at baseline. Instead, DGE analysis was used to identify *c1qa*, a member of the complement system, as an accurate pan-macrophage marker for AM that can be used in future studies to characterise the PF and SF macrophage response (Fig. 4.14b).

Therefore, the spatiotemporal dynamics of PF/SF macrophages in response to cardiac tissue damage have not been characterised in this study. However, as macrophages are highly heterogeneous cells with distinct transcriptional profiles regulating different aspects of cardiac repair, the transcriptional profile of PF/SF macrophages was next explored to determine if any pro-scarring and pro-regenerative functional differences could be identified in the scRNAseq dataset.

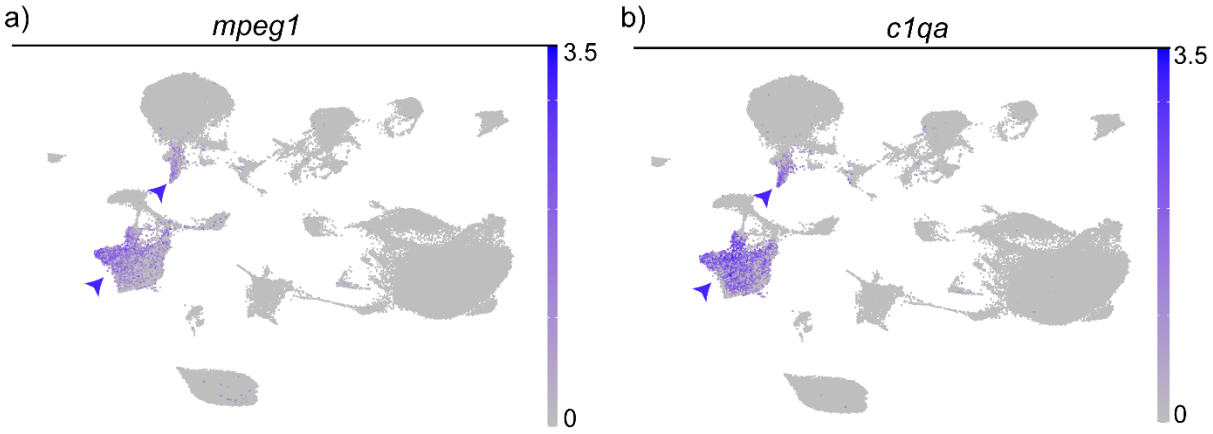

Figure 4. 14: mpeg1 is not a pan-macrophage marker in A. mexicanus

(A) FeaturePlot of mpeg1 expression in overall scRNAseq dataset. mpeg1 is not expressed in all macrophage cells. (B) FeaturePlot of c1qa expression in overall scRNAseq dataset. c1qa is expressed

in all AM macrophage cells and is a better pan-macrophage marker than mpeg1 for future macrophage characterisation studies.

There are no unique PF/SF monocyte/macrophage clusters in the scRNAseq data

To identify transcriptional and functional differences in PF/SF macrophages, monocyte/macrophage clusters were identified from the overall dataset using a combination *of mpeg1, c1qa, c1qb* and *c1qc* expression and subset for re-analysis and clustering. 7 monocyte/macrophage sub clusters were identified as well as 3 doublet clusters which were excluded from downstream analysis (Fig. 4.15a, see Appendix 4.6 for cluster markers). Further classification of these 7 monocyte/macrophage sub clusters into distinct pro-inflammatory φ, anti-inflammatory φ and monocyte subsets was not possible as many of the canonical markers typically used like CD14, CD16, CD206 and CCL5, are not annotated in the AM genome. Therefore, all 7 monocyte/macrophage subclusters were instead compared between PF/SF to identify whether there were any PF/SF-specific macrophage clusters that could be uniquely regulating regeneration or scarring. However, all macrophage clusters were present in both PF and SF (Fig. 4.15b) and at all time points (Fig. 4.15c). A general trend was observed that SF macrophages seem to persist at 7- and 14dpci whereas PF levels start to decrease towards baseline, similar to the neutrophil results.

As no significant differences in PF/SF monocyte/macrophages were initially identified, the next step to identify significant differences in the PF/SF monocyte/macrophage response to injury was to methodically compare the transcriptional profile and functionality of PF/SF monocytes/macrophages at each time point.

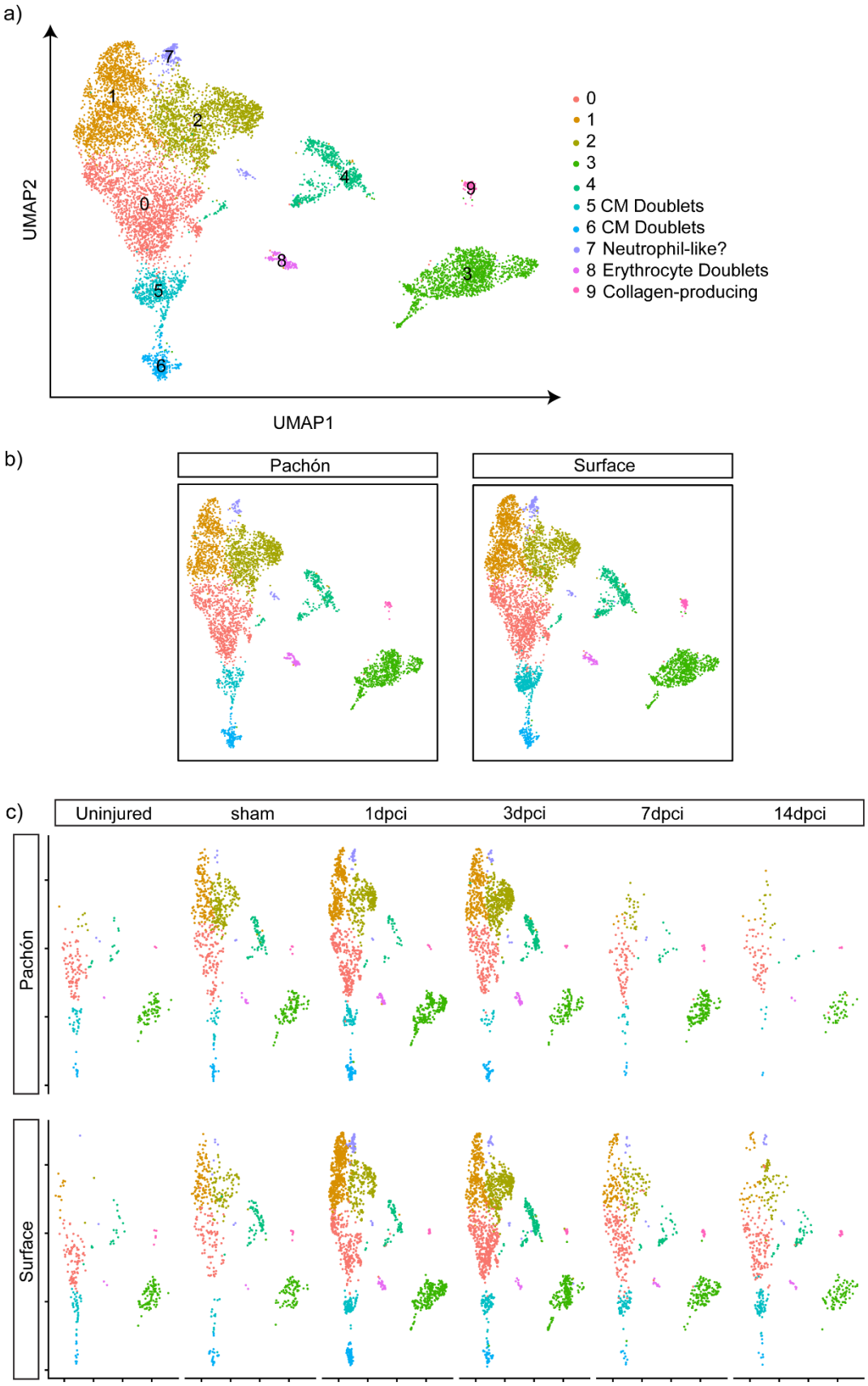

Figure 4. 15*: *Overview of the macrophage scRNAseq dataset

(A) UMAP of the macrophage scRNAseq data. (B) UMAP displaying macrophage scRNAseq data split into PF and SF cells. (C) UMAP displaying macrophage scRNAseq data split into PF/SF cells and split across time.

Uninjured SF and PF macrophages may differ in their ability to present antigens

Uninjured monocytes/macrophages were first compared as tissue-resident macrophages have been shown to be essential for regeneration in both the zebrafish and the neonatal mouse. MAST testing was used to perform DGE analysis, revealing that 13 genes were differentially expressed between uninjured PF/SF macrophages. Visualisation of the DGE results showed that 2 genes were significantly upregulated in SF macrophages: *ENSAMXG00000037572* and *ENSAMXG00000036068* (Fig. 4.16a). In Ensembl, these genes are annotated as major histocompatibility complex II (MHC II) genes. Strikingly, a comparison of the expression of these two MHC II genes in all PF/SF macrophages shows that the expression of MHC II in PF macrophages is drastically decreased in comparison to SF (Fig. 4.16b). In comparison, the top 2 differentially expressed genes in PF are *snora73.2* (a small nucleolar RNA) and *nme2b.1* (nucleoside diphosphate kinase) which play no role in antigen presentation.

The DGE results were then analysed for GO term enrichment to explore the possible functional roles of PF/SF tissue-resident macrophages. This functional analysis showed that only SF macrophage markers were found to be significantly enriched for antigen processing and presentation (Fig. 4.16c), suggesting that tissue-resident PF and SF macrophages display different capacities for antigen presentation.

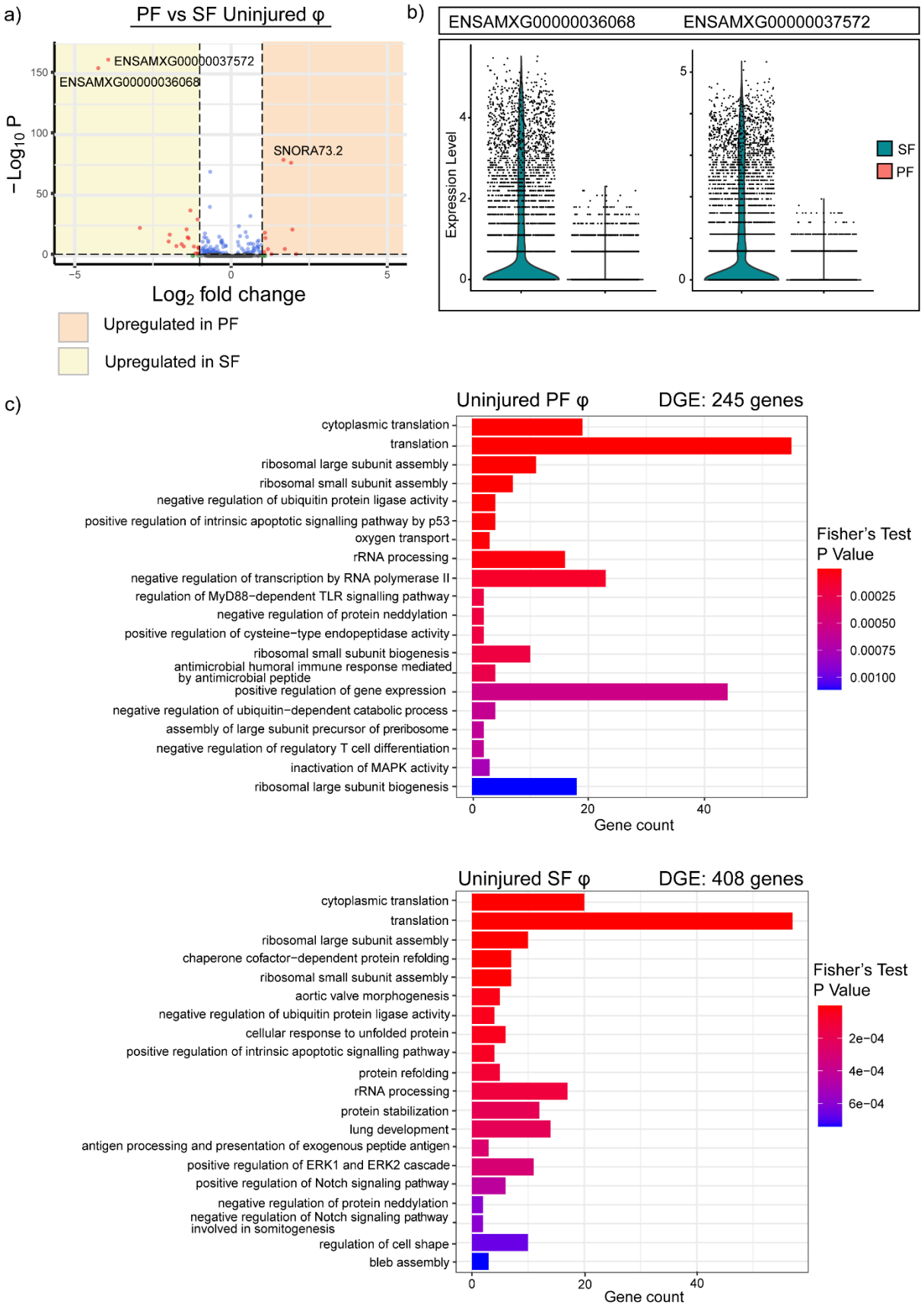

Figure 4. 16: Uninjured PF/SF macrophages differ in their ability to process and present antigens

(A) Volcano plot of the results of DGE analysis between uninjured PF and SF macrophages. (B) Violin plots of MHC II gene expression in all PF and SF macrophages. MHC II expression is severely diminished in all PF macrophages in comparison to SF. (C) GO term analysis of the top PF/SF uninjured markers.

SF/PF macrophages are transcriptionally divergent at all time-points after injury

Functional differences in PF/SF injury-responsive macrophages were the next focus. To compare how similar injury-responsive PF/SF macrophages were, DGE analysis was performed between PF and SF macrophages at each time point after injury. The DGE analysis results showed that many genes were differentially expressed at all time points after injury with 3dpci macrophages showing the greatest number of differentially expressed genes. Additionally, 14dpci SF macrophages were observed to specifically upregulate the two previously identified MHC II genes (Fig. 4.17).

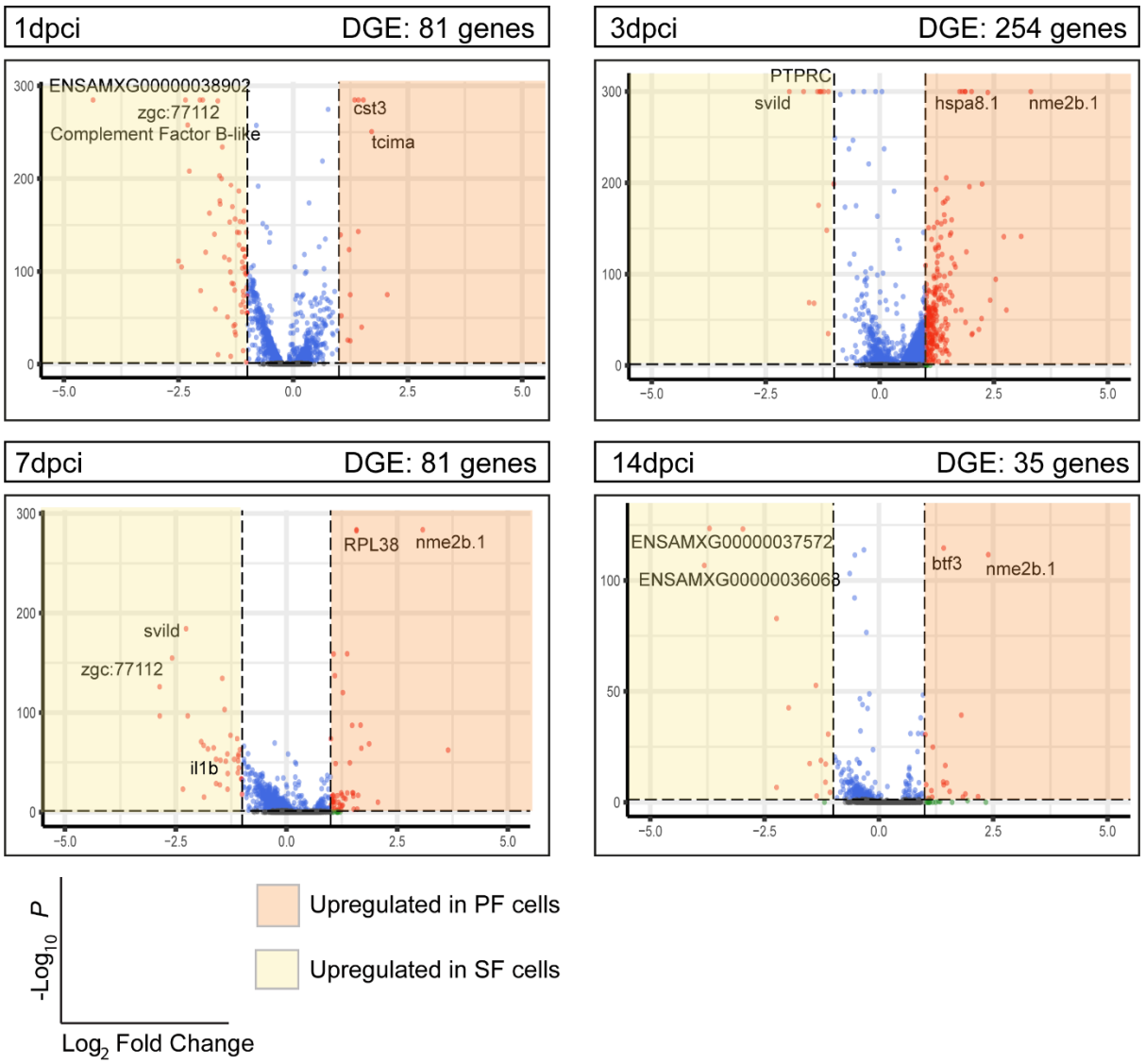

Figure 4. 17: PF/SF macrophages show the greatest transcriptional differenace at 3dpci.

Volcano plots of the DGE analysis at each time point with the number of genes that reached DGE significance threshold annotated

To explore whether the transcriptional differences between PF/SF macrophages resulted in significant functional differences, the results of the DGE analysis were tested for significant enrichment of the Hallmark pathways using GSEA, as had been done for the neutrophils. The GSEA results showed that PF macrophages expressed genes enriched for E2F targets and DNA repair (Fig. 4.18, also see Appendix 4.7). E2F proteins are a family of transcription factors that regulate the

expression of genes involved in DNA replication, the cell cycle and DNA repair, suggesting that PF macrophages may be regulating proliferation and DNA repair via an E2F-mechainsm.

At 7dpci, 9 different Hallmark pathways were enriched in SF macrophages that were not enriched at any other time point, or in the PF (Fig. 4.18). Remarkably these pathways were linked to both the inflammatory (inflammatory response, TNFα/NFκB signalling) and the anti-inflammatory stages of wound healing (oxidative phosphorylation, EMT). This suggests that the 7dpci SF macrophage response may consist of a diverse range of macrophage phenotypes that span the spectrum of inflammation and could be mediating distinct aspects of regeneration.

The results of the DGE analysis and GSEA suggest that PF and SF macrophages show the greatest transcriptional differences at 3dpci and the greatest functional differences at 7dpci.

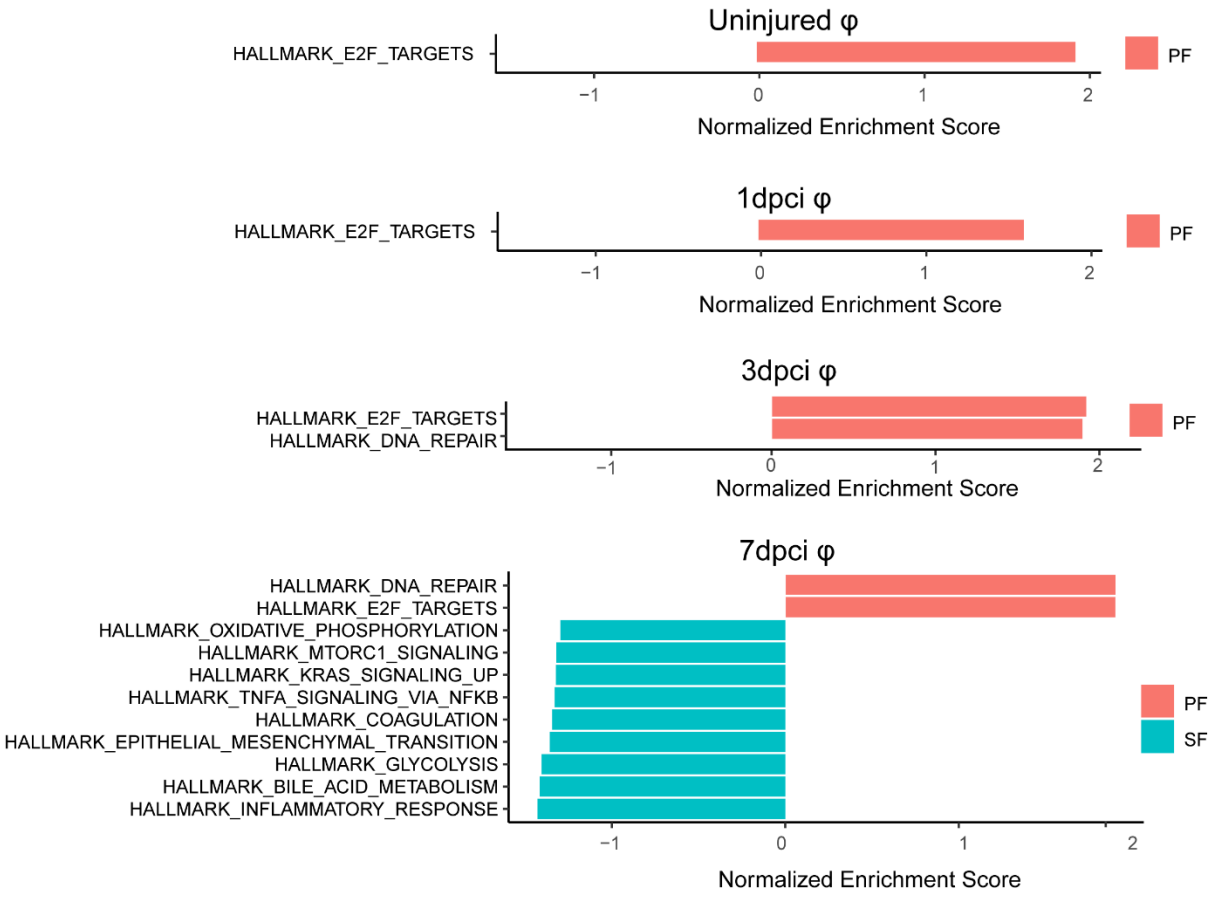

Figure 4. 18: PF and SF macrophages show the greatest functional differences at 7dpci

GSEA results that reached the FDR significance threshold are shown (FDR<0.25).

To further explore the functional roles of PF/SF macrophages at each time point, the top markers of PF/SF macrophages were tested for significant over-representation of GO terms. This showed that at 1dpci, many top GO terms were shared between PF/SF. These shared GO terms were involved in degradation and catabolism, suggesting that at 1dpci, both PF and SF macrophages were acting to clear away dead/dying cells and cellular debris (Fig. 4.19a). In contrast, at 3dpci, fewer GO terms were shared between PF and SF macrophages, although many top GO terms were still involved in catabolism and degradation of proteins. At 3dpci, SF macrophages had many GO terms involved in regulating the actin cytoskeleton, suggesting that 3dpci SF macrophages could be very motile cells (Fig. 4.19b) whereas PF macrophages showed expression of integrin signalling and cell adhesion, suggesting that PF macrophages were less motile and bound strongly to nearby cells. At 7dpci, both PF and SF macrophages shared GO terms involved in the formation of new proteins and blood vessels (Fig. 4.19c), suggesting that PF/SF macrophages were both stimulating angiogenesis and revascularisation of the wounded tissue. At 14dpci, PF/SF macrophages shared many GO terms involved in translation and protein folding (Fig. 4.19d), suggesting that at the late stages of wound healing, both PF and SF macrophages remained transcriptionally and translationally active. Interestingly, at 14dpci, PF and SF macrophages were linked to GO terms that suggest opposing stimulation of T cells with PF macrophages being linked to the negative regulation of T cell differentiation, whereas SF macrophages were linked to the positive regulation of activated T cell proliferation (Fig. 4.19d). This intriguing result suggests that functional differences in PF/SF macrophages could result in different activation of adaptive immune cells as macrophages play a key role in activating T cells via antigen presentation. However, although this warrants further investigation, macrophage/T cell interactions were not pursued further as the scRNAseq data did not identify any differences in PF/SF T cell dynamics after injury.

a)

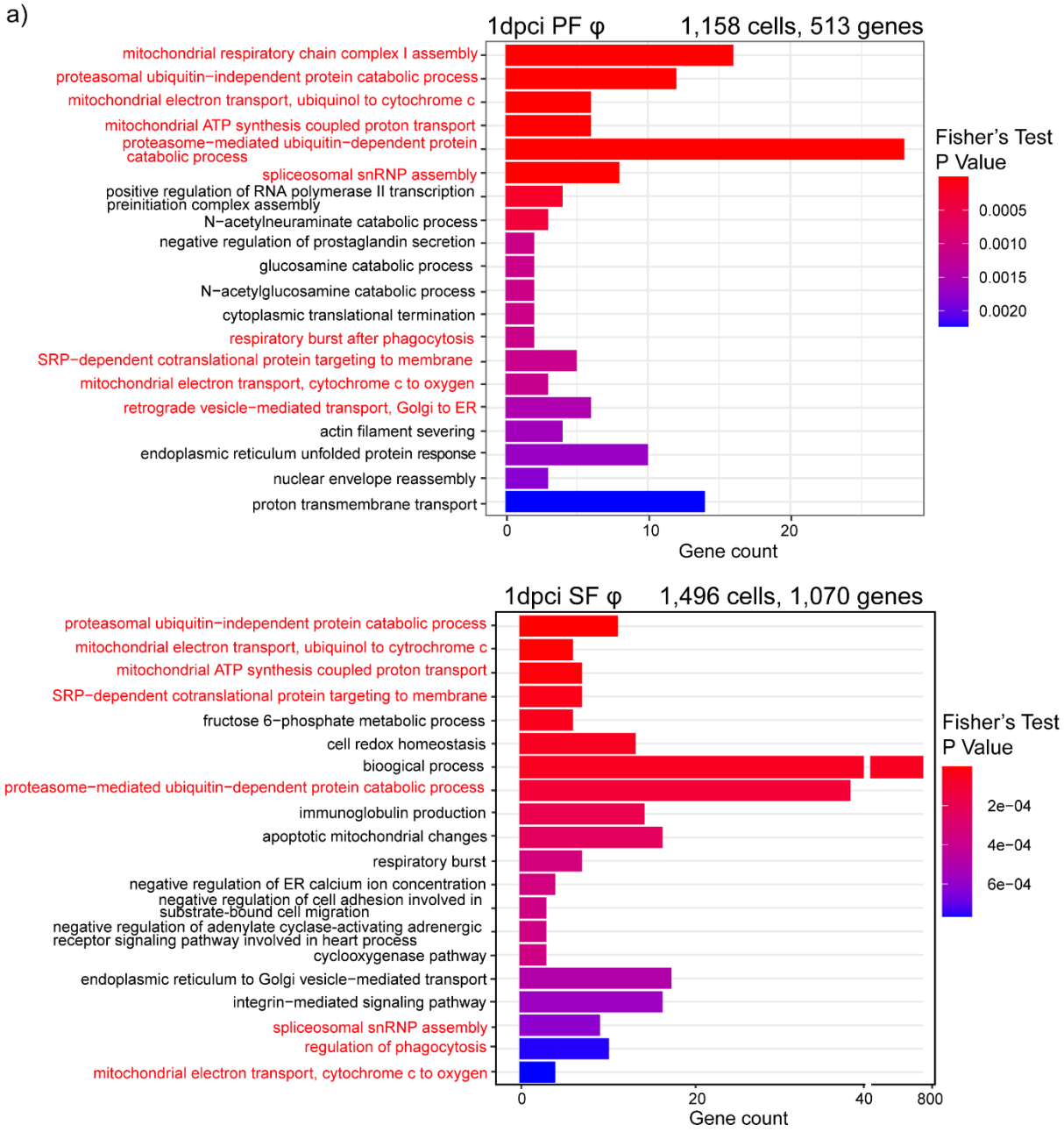
1dpci PF φ
1,158 cells, 513 genes
mitochondrial respiratory chain complex I assembly
proteasomal ubiquitin−independent protein catabolic process
mitochondrial electron transport, ubiquinol to cytochrome c
mitochondrial ATP synthesis coupled proton transport
proteasome−mediated ubiquitin−dependent protein catabolic process
spliceosomal snRNP assembly
positive regulation of RNA polymerase II transcription preinitiation complex assembly
N−acetylneuraminate catabolic process
negative regulation of prostaglandin secretion
glucosamine catabolic process
N−acetylglucosamine catabolic process
cytoplasmic translational termination
respiratory burst after phagocytosis
SRP−dependent cotranslational protein targeting to membrane
mitochondrial electron transport, cytochrome c to oxygen
retrograde vesicle−mediated transport, Golgi to ER
actin filament severing
endoplasmic reticulum unfolded protein response
nuclear envelope reassembly
proton transmembrane transport
0
10
20
Gene count
Fisher's Test P Value
0.0005
0.0010
0.0015
0.0020
1dpci SF φ
1,496 cells, 1,070 genes
proteasomal ubiquitin−independent protein catabolic process
mitochondrial electron transport, ubiquinol to cytrochrome c
mitochondrial ATP synthesis coupled proton transport
SRP−dependent cotranslational protein targeting to membrane
fructose 6−phosphate metabolic process
cell redox homeostasis
bioogical process
proteasome−mediated ubiquitin−dependent protein catabolic process
immunoglobulin production
apoptotic mitochondrial changes
respiratory burst
negative regulation of ER calcium ion concentration
negative regulation of cell adhesion involved in substrate-bound cell migration
negative regulation of adenylate cyclase-activating adrenergic receptor signaling pathway involved in heart process
cyclooxygenase pathway
endoplasmic reticulum to Golgi vesicle−mediated transport
integrin−mediated signaling pathway
spliceosomal snRNP assembly
regulation of phagocytosis
mitochondrial electron transport, cytochrome c to oxygen
0
20
40
800
Gene count
Fisher's Test P Value
2e−04
4e−04
6e−04

b)

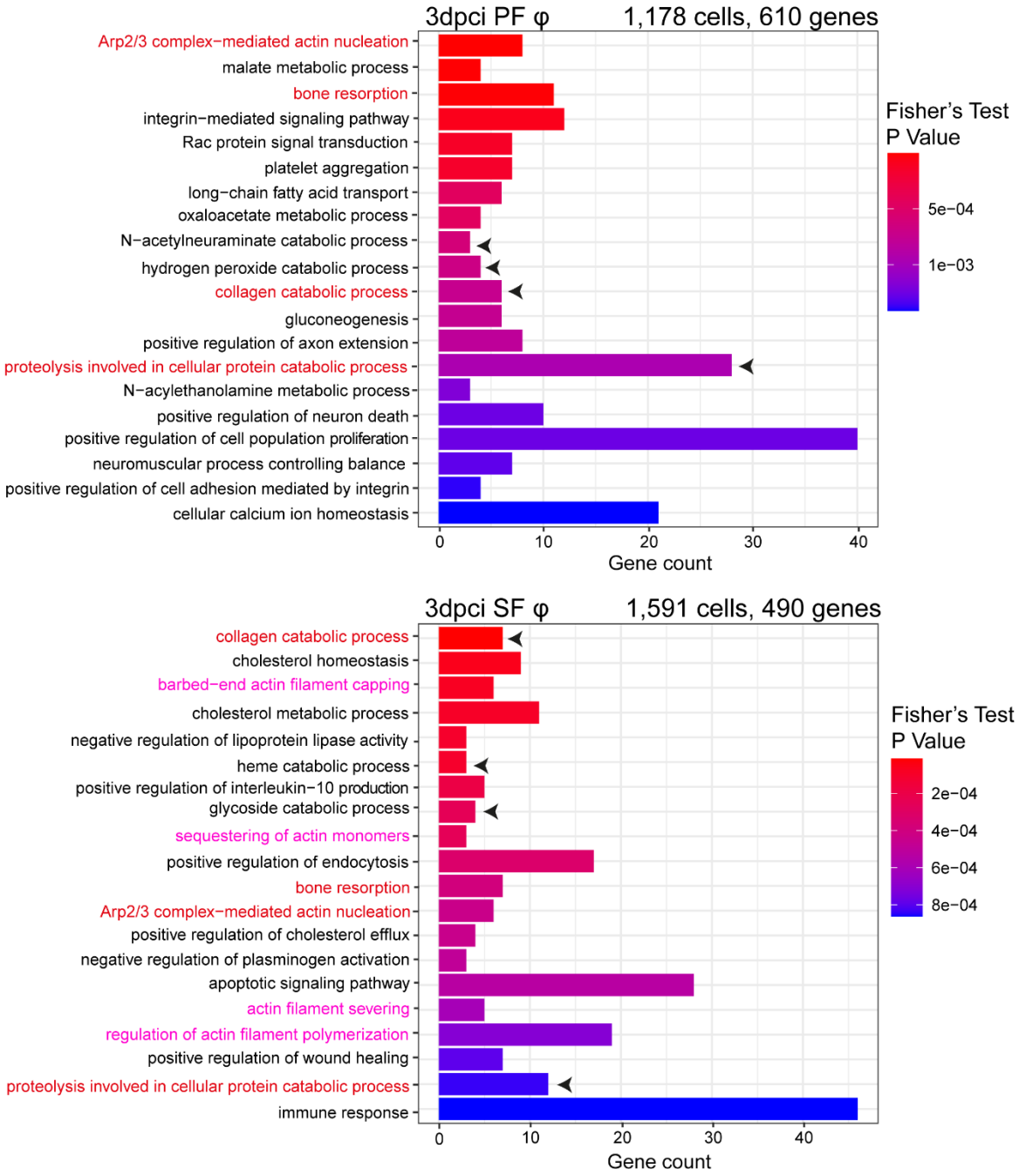
3dpci PF φ
1,178 cells, 610 genes
Arp2/3 complex−mediated actin nucleation
malate metabolic process
bone resorption
integrin−mediated signaling pathway
Rac protein signal transduction
platelet aggregation
long−chain fatty acid transport
oxaloacetate metabolic process
N−acetylneuraminate catabolic process
hydrogen peroxide catabolic process
collagen catabolic process
gluconeogenesis
positive regulation of axon extension
proteolysis involved in cellular protein catabolic process
N−acylethanolamine metabolic process
positive regulation of neuron death
positive regulation of cell population proliferation
neuromuscular process controlling balance
positive regulation of cell adhesion mediated by integrin
cellular calcium ion homeostasis
0
10
20
30
40
Gene count
Fisher's Test
P Value
5e−04
1e−03
3dpci SF φ
1,591 cells, 490 genes
collagen catabolic process
cholesterol homeostasis
barbed−end actin filament capping
cholesterol metabolic process
negative regulation of lipoprotein lipase activity
heme catabolic process
positive regulation of interleukin−10 production
glycoside catabolic process
sequestering of actin monomers
positive regulation of endocytosis
bone resorption
Arp2/3 complex−mediated actin nucleation
positive regulation of cholesterol efflux
negative regulation of plasminogen activation
apoptotic signaling pathway
actin filament severing
regulation of actin filament polymerization
positive regulation of wound healing
proteolysis involved in cellular protein catabolic process
immune response
0
10
20
30
40
Gene count
Fisher's Test
P Value
2e−04
4e−04
6e−04
8e−04

c)

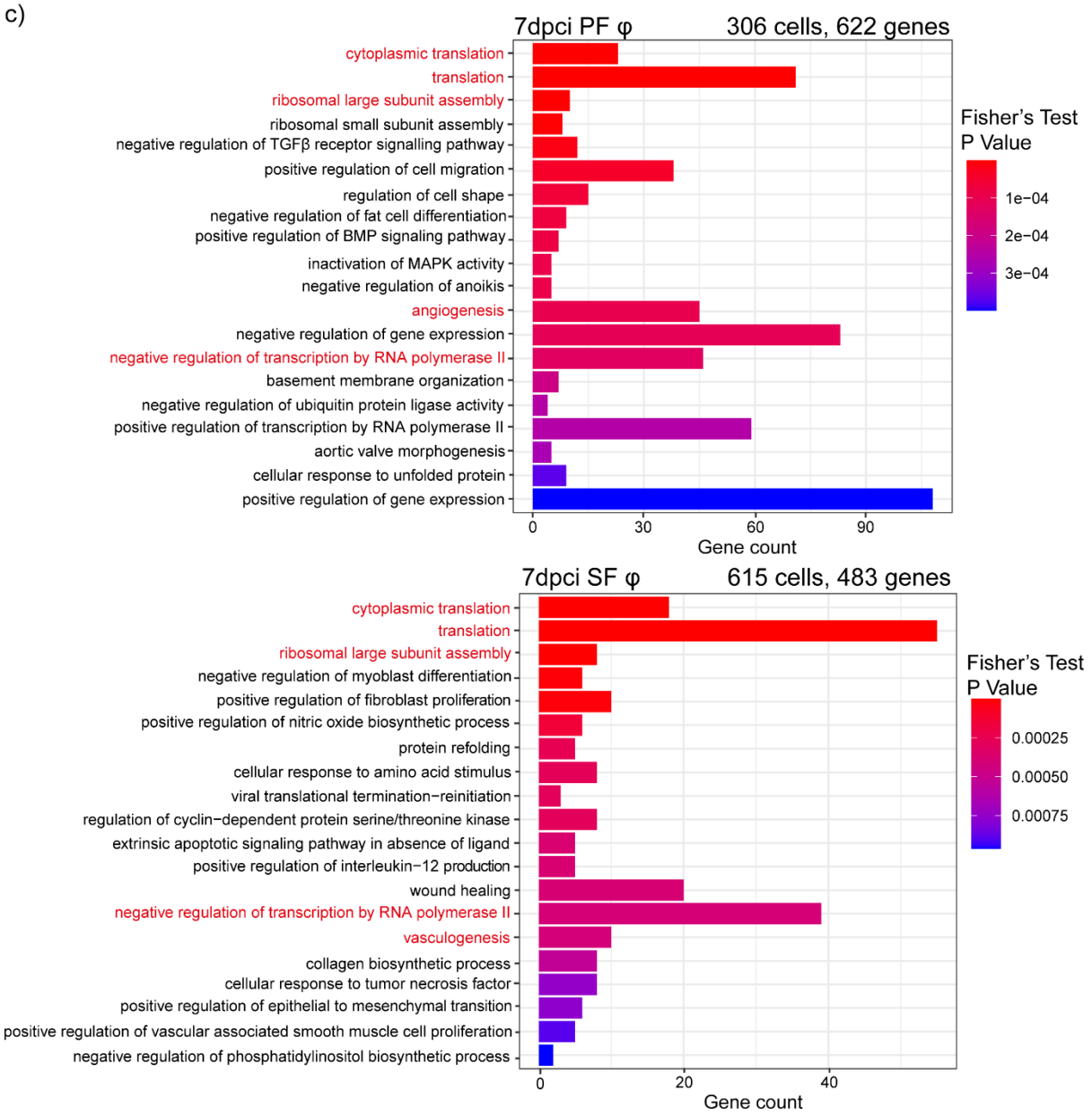
7dpci PF φ
306 cells, 622 genes
cytoplasmic translation
translation
ribosomal large subunit assembly
ribosomal small subunit assembly
negative regulation of TGFβ receptor signalling pathway
positive regulation of cell migration
regulation of cell shape
negative regulation of fat cell differentiation
positive regulation of BMP signaling pathway
inactivation of MAPK activity
negative regulation of anoikis
angiogenesis
negative regulation of gene expression
negative regulation of transcription by RNA polymerase II
basement membrane organization
negative regulation of ubiquitin protein ligase activity
positive regulation of transcription by RNA polymerase II
aortic valve morphogenesis
cellular response to unfolded protein
positive regulation of gene expression
0
30
60
90
Gene count
Fisher's Test
P Value
1e−04
2e−04
3e−04
7dpci SF φ
615 cells, 483 genes
cytoplasmic translation
translation
ribosomal large subunit assembly
negative regulation of myoblast differentiation
positive regulation of fibroblast proliferation
positive regulation of nitric oxide biosynthetic process
protein refolding
cellular response to amino acid stimulus
viral translational termination−reinitiation
regulation of cyclin−dependent protein serine/threonine kinase
extrinsic apoptotic signaling pathway in absence of ligand
positive regulation of interleukin−12 production
wound healing
negative regulation of transcription by RNA polymerase II
vasculogenesis
collagen biosynthetic process
cellular response to tumor necrosis factor
positive regulation of epithelial to mesenchymal transition
positive regulation of vascular associated smooth muscle cell proliferation
negative regulation of phosphatidylinositol biosynthetic process
0
20
40
Gene count
Fisher's Test
P Value
0.00025
0.00050
0.00075

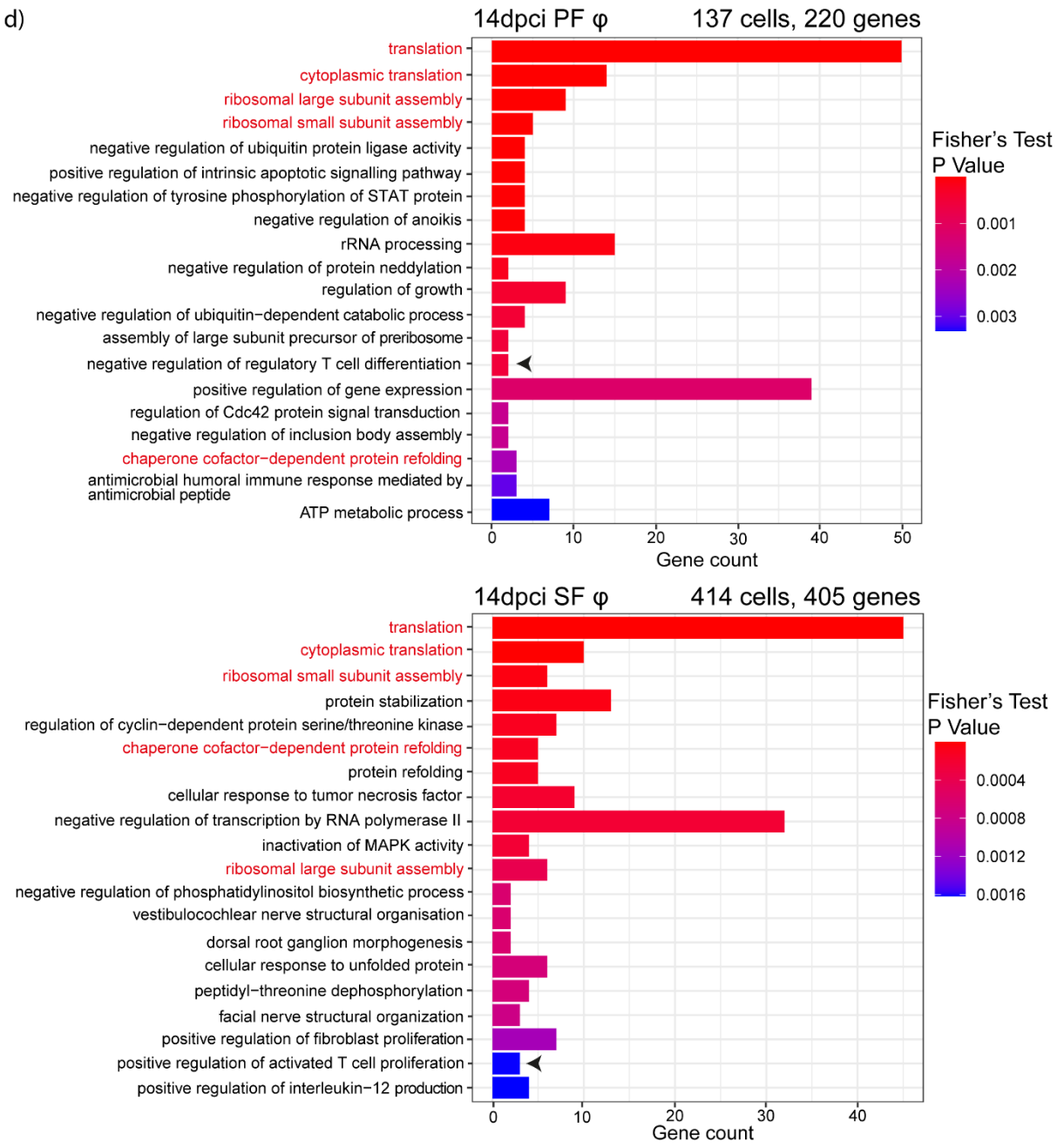

Figure 4. 19: Functional pathway analysis reveals PF/SF macrophages show many functional differences

GO term analysis for top cell markers of PF and SF macrophages at (A) 1dpci, (B) 3dpci, (C) 7dpci and (D) 14dpci. GO terms shared between PF and SF at each time point are highlighted in red. Black arrows highlight the terms specifically referred to in the text. GO terms related to catabolism highlighted in purple in (B).

SF macrophages at 7- and 14dpci share a unique transcriptional profile

During the comparison of top GO terms associated with 7dpci and 14dpci macrophages, late-stage SF macrophages were found to share many GO terms that were absent from PF macrophages (Fig. 4.20a). These GO terms were: response to TNF; positive regulation of fibroblast proliferation; IL-12 production; protein refolding; negative regulation of phosphatidylinositol biosynthesis; and regulation cyclin-dependent serine/threonine kinase. This suggested that late-stage SF macrophages could also share a transcriptional profile similarly to the SF neutrophils. To test this emerging hypothesis, PF/SF macrophage transcriptional signatures were compared at each time point using DGE analysis to identify the top PF and SF macrophage markers and the results were visualised in a heatmap. Strikingly, late-stage SF macrophages were found to display a unique transcriptional profile that was completely absent from PF macrophages and was not found at any other time point within the SF, just as had been observed in the neutrophils (Fig. 4.20b). Additionally, the transcriptional profiles of SF macrophages at 1- and 3dpci were also unique, suggesting that SF macrophages show dynamic gene regulation and are very divergent transcriptionally from PF macrophages.

Finally, to confirm whether 7/14dpci SF macrophages share a unique transcriptional profile, injury-responsive genes were identified and the number of genes shared between PF and SF macrophages was calculated at 7- and 14dpci. This analysis found that a greater proportion of injury-responsive genes were shared between late-stage SF macrophages than late-stage PF macrophages (Fig. 4.20c), further supporting the notion that the transcriptional profile of SF macrophages is shared amongst cells at 7- and 14dpci.

a)

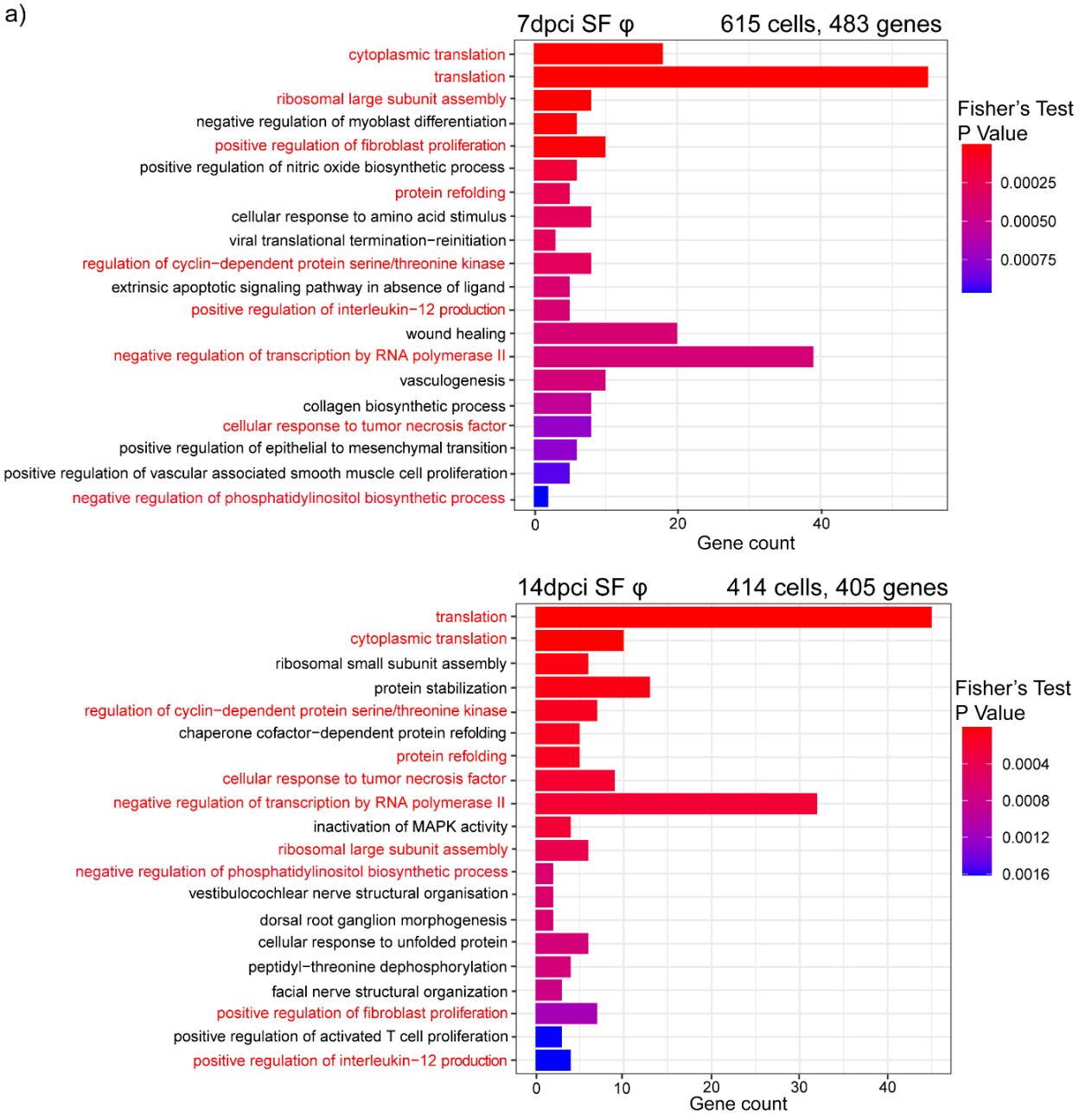
7dpci SF φ
615 cells, 483 genes
cytoplasmic translation
translation
ribosomal large subunit assembly
negative regulation of myoblast differentiation
positive regulation of fibroblast proliferation
positive regulation of nitric oxide biosynthetic process
protein refolding
cellular response to amino acid stimulus
viral translational termination−reinitiation
regulation of cyclin−dependent protein serine/threonine kinase
extrinsic apoptotic signaling pathway in absence of ligand
positive regulation of interleukin−12 production
wound healing
negative regulation of transcription by RNA polymerase II
vasculogenesis
collagen biosynthetic process
cellular response to tumor necrosis factor
positive regulation of epithelial to mesenchymal transition
positive regulation of vascular associated smooth muscle cell proliferation
negative regulation of phosphatidylinositol biosynthetic process
0
20
40
Gene count
Fisher's Test
P Value
0.00025
0.00050
0.00075
14dpci SF φ
414 cells, 405 genes
translation
cytoplasmic translation
ribosomal small subunit assembly
protein stabilization
regulation of cyclin−dependent protein serine/threonine kinase
chaperone cofactor−dependent protein refolding
protein refolding
cellular response to tumor necrosis factor
negative regulation of transcription by RNA polymerase II
inactivation of MAPK activity
ribosomal large subunit assembly
negative regulation of phosphatidylinositol biosynthetic process
vestibulocochlear nerve structural organisation
dorsal root ganglion morphogenesis
cellular response to unfolded protein
peptidyl−threonine dephosphorylation
facial nerve structural organization
positive regulation of fibroblast proliferation
positive regulation of activated T cell proliferation
positive regulation of interleukin−12 production
0
10
20
30
40
Gene count
Fisher's Test
P Value
0.0004
0.0008
0.0012
0.0016

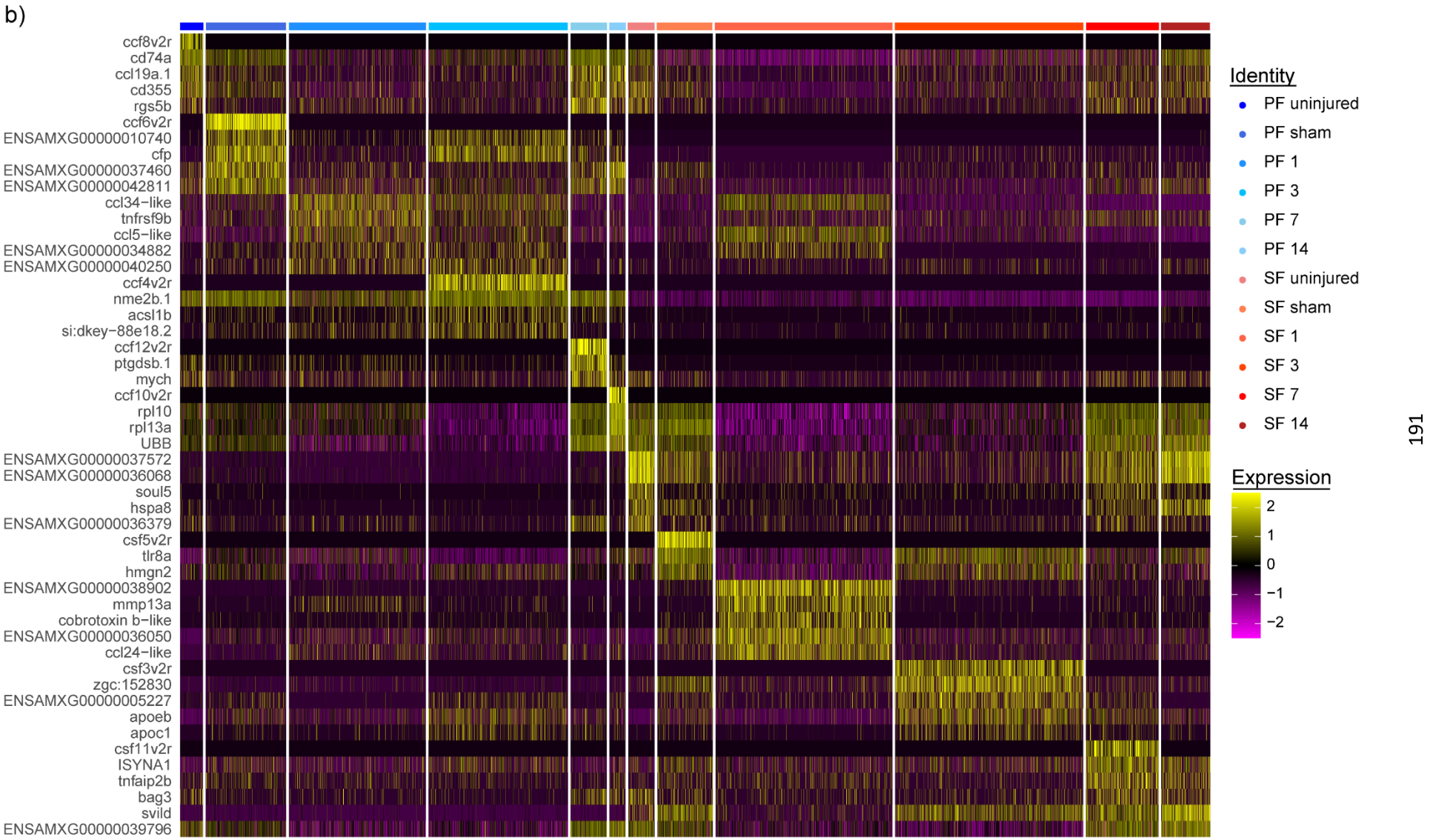
b)
ccf8v2r
cd74a
ccl19a.1
cd355
rgs5b
ccf6v2r
ENSAMXG00000010740
cfp
ENSAMXG00000037460
ENSAMXG00000042811
ccl34-like
tnfrsf9b
ccl5-like
ENSAMXG00000034882
ENSAMXG00000040250
ccf4v2r
nme2b.1
acsl1b
si:dkey-88e18.2
ccf12v2r
ptgdsb.1
mych
ccf10v2r
rpl10
rpl13a
UBB
ENSAMXG00000037572
ENSAMXG00000036068
soul5
hspa8
ENSAMXG00000036379
csf5v2r
tlr8a
hmgn2
ENSAMXG00000038902
mmp13a
cobrotoxin b-like
ENSAMXG00000036050
ccl24-like
csf3v2r
zgc:152830
ENSAMXG00000005227
apoeb
apoc1
csf11v2r
ISYNA1
tnfaip2b
bag3
svild
ENSAMXG00000039796
Identity
PF uninjured
PF sham
PF 1
PF 3
PF 7
PF 14
SF uninjured
SF sham
SF 1
SF 3
SF 7
SF 14
Expression
2
1
0
−1
−2
191

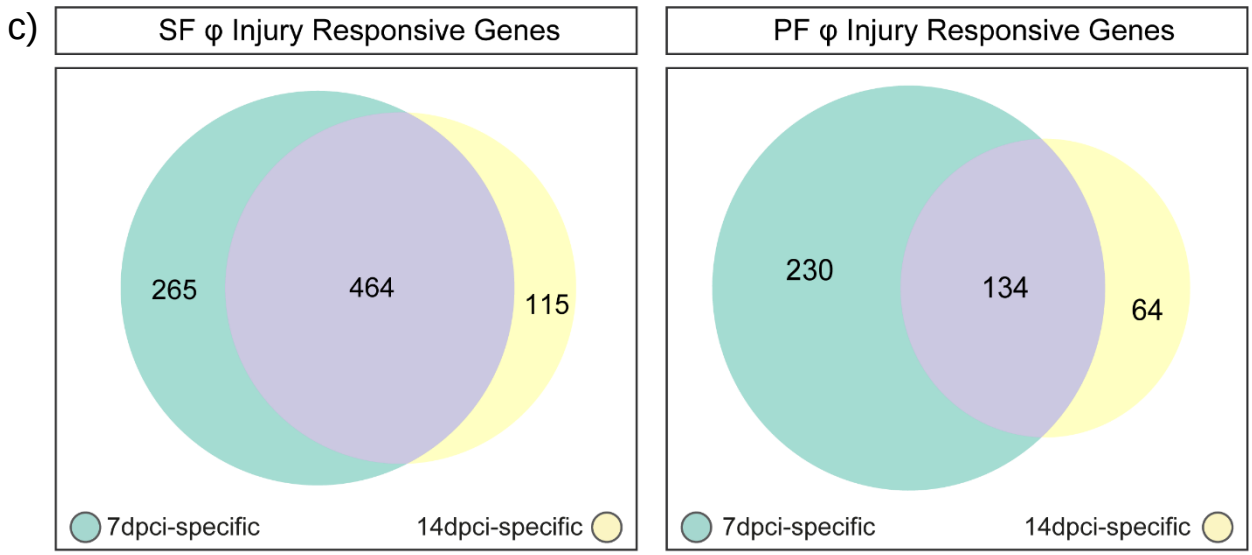

Figure 4. 20: Late-stage SF macrophages share a unique transcriptional response

(A) Comparison of 7- and 14dpci top GO terms reveals that many terms are shared between SF macrophages as highlighted in red. (B) Heatmap of the top markers for PF and SF macrophages at each time point. (C) Euler plots comparing injury responsive genes between 7dpci and 14dpci macrophages for SF and PF.

From the macrophage scRNAseq data it is possible to conclude that SF and PF macrophages are transcriptionally diverse:

- Uninjured PF/SF macrophages may show differences in antigen presentation
- PF/SF macrophages display the most functional differences at 7dpci
- Late-stage SF macrophages display a unique transcriptional profile, similarly to the neutrophils.

5.2.3 The regenerative SF have a unique B cell response to cryoinjury that is almost absent in the scarring PF

B cells significantly influx into the SF heart at 30dpci

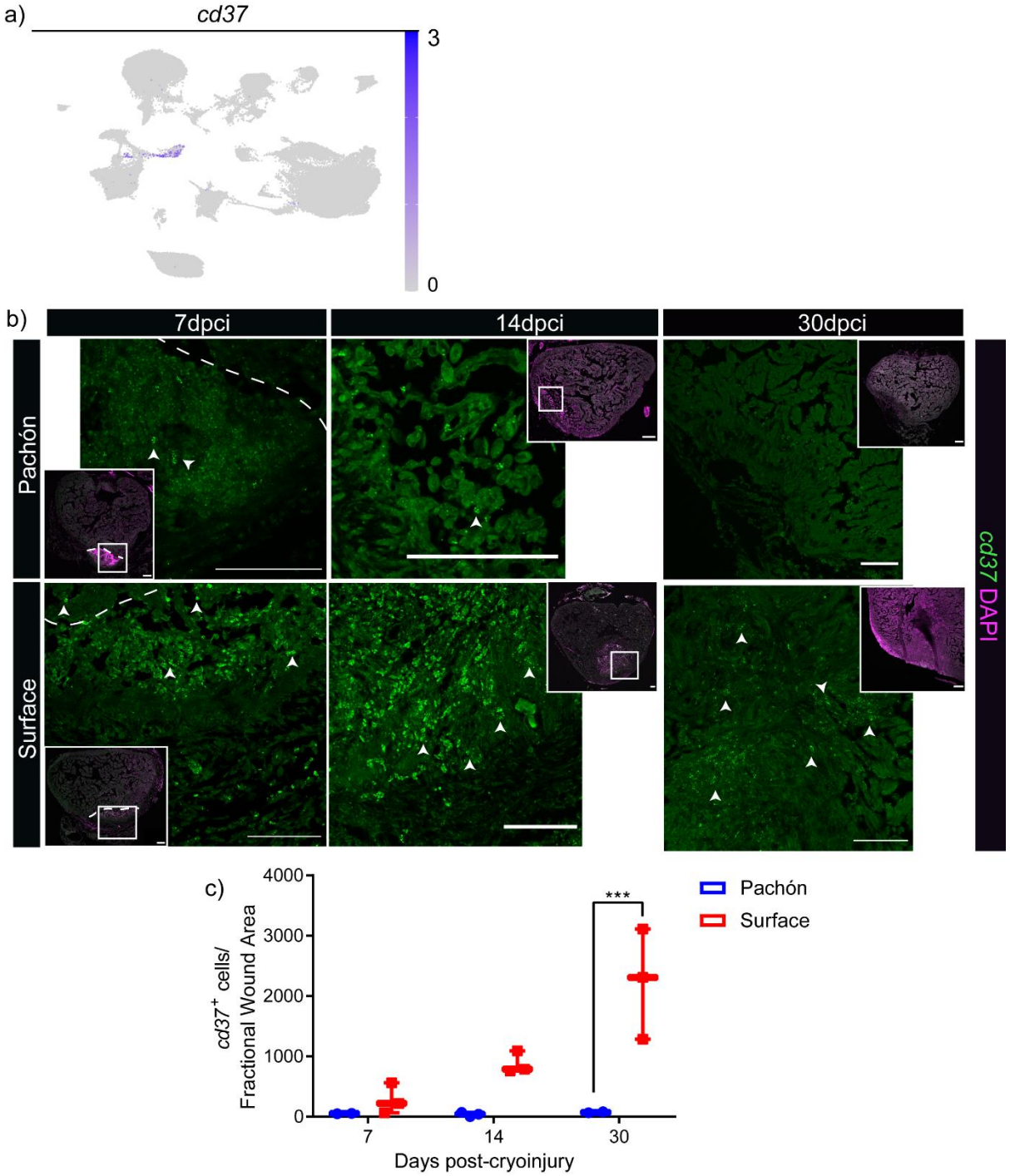

Figure 4. 21: B cells significantly influx into the SF heart at 30dpci whilst their levels remain low in PF

(A) FeaturePlot of cd37 expression in the overall scRNAseq dataset shows that cd37 is a B cell-specific marker. (B) RNAscope staining was used to perform B cell counts. B cells were visualised using a RNAscope probe for cd37 and cells that overlaid with DAPI were counted. (C) cd37+ cells present in the wound were normalised to fractional wound area, revealing that at 30dpci, SF B cell levels are

*significantly elevated (2-way ANOVA with Sidak's multiple comparisons test, *** p<0.001, n=3 at each time point).*

Finally, I focused on the B cells. To characterise the B cell response in PF and SF, the scRNAseq data was first used to identify *cd37* as a B cell-specific marker (Fig. 4.21a). Using a *cd37* RNAscope probe, PF/SF hearts were stained at 7-, 14- and 30dpci (Fig. 4.21b) and the number of B cells present in the wound was counted, normalising to fractional wound area. At 30dpci, SF B cell levels were significantly elevated compared to PF ($p<0.001$) and had increased from B cell levels present at 7- and 14dpci. Therefore, these B cell counts confirmed the previous DPA results and showed that B cells do influx into the SF heart in substantial numbers during the late stages of wound healing (Fig. 4.21c).

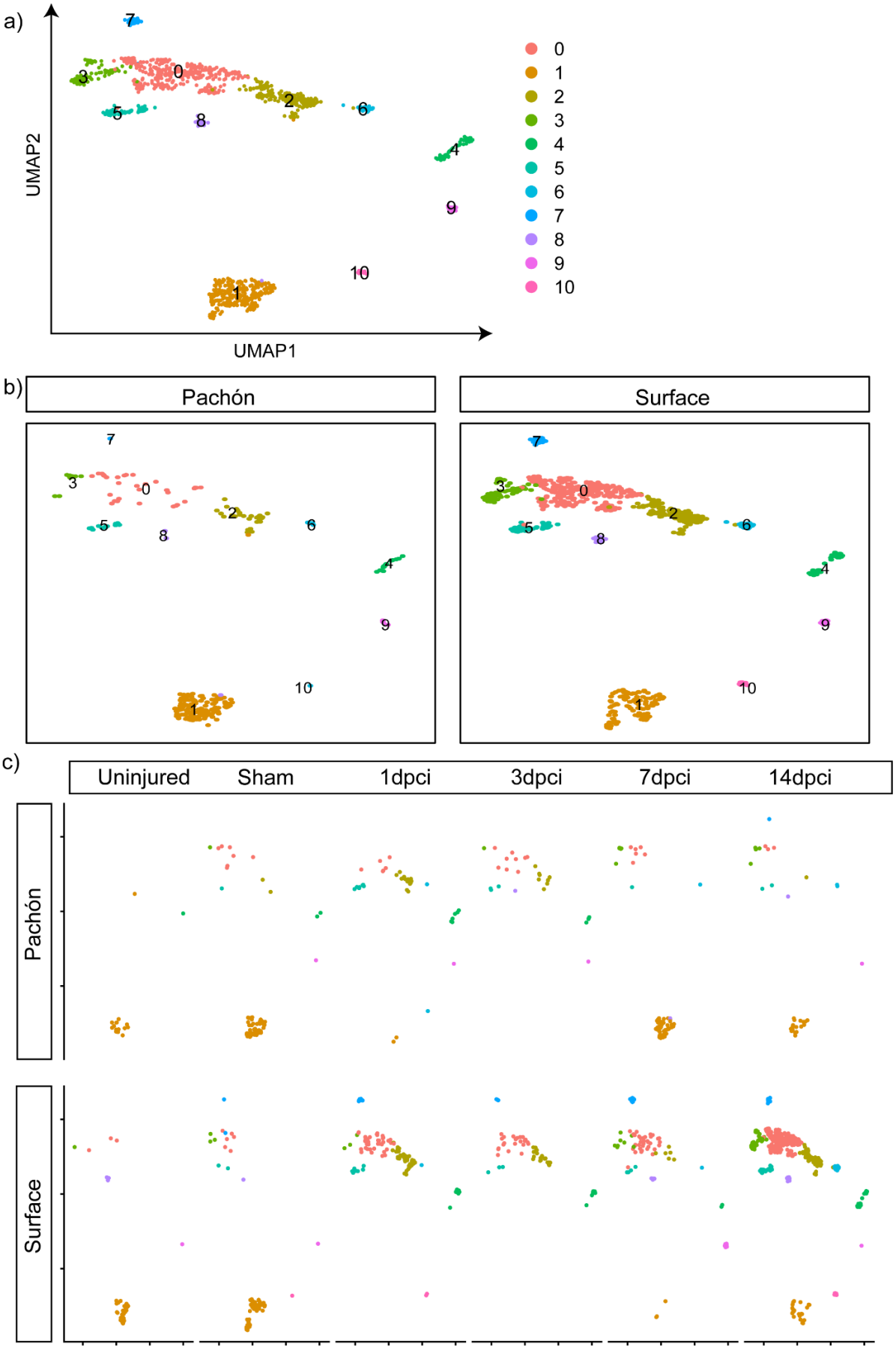
a)
UMAP2
UMAP1
0
1
2
3
4
5
6
7
8
9
10
b)
Pachón
Surface
c)
Uninjured
Sham
1dpci
3dpci
7dpci
14dpci
Pachón
Surface

Figure 4. 22: Overview of the B cell scRNAseq dataset

(A) UMAP of all B cells reveals 11 unique B cell sub-clusters. (B) Comparison of the SF and PF B cell UMAPS reveals that the PF B cell population is dominated by cluster 1 whereas SF has an even distribution of cells throughout all 11 clusters. (C) UMAP of B cell scRNAseq data, split across time and morphotype, shows that the PF and SF B cell responses differ in the temporal dynamics of their sub-clusters.

The significant influx of B cells into the SF heart during the late stages of cardiac healing suggested that B cells may be playing a key role in mediating regeneration in the SF. Therefore, the functionality of PF/SF B cells was next investigated to determine whether PF/SF B cells displayed any significant differences. B cell clusters were identified from the overall scRNAseq dataset based on *cd37* expression and then subset for re-analysis, resulting in the identification of 10 B cell sub-clusters (Fig. 4.22a). To identify differences in PF and SF B cells, the B cell scRNAseq data was first split into PF/SF cells to screen for any unique B cell clusters. Although no unique PF/SF B cell clusters were found, the distribution of PF/SF cells across B cell subclusters was vastly different: most PF B cells were found in cluster 1 whilst SF cells showed an even distribution across all clusters. This finding indicates that SF B cells are more heterogeneous than their PF counterparts (Fig. 4.22b). Next, the B cell scRNAseq data was split across time, showing that most B cell subclusters displayed differential temporal dynamics between the PF and SF (Fig. 4.22c). The SF showed an immediate influx of clusters 0 and 2-9 after injury whereas PF B cell levels were minimal until 7dpci when many B cells from cluster 1 entered the heart.

These significant differences in B cell clusters present in PF/SF hearts after injury suggest that not only do PF/SF B cells show significantly different temporal kinetics, they also show key differences in their cellular behaviours.

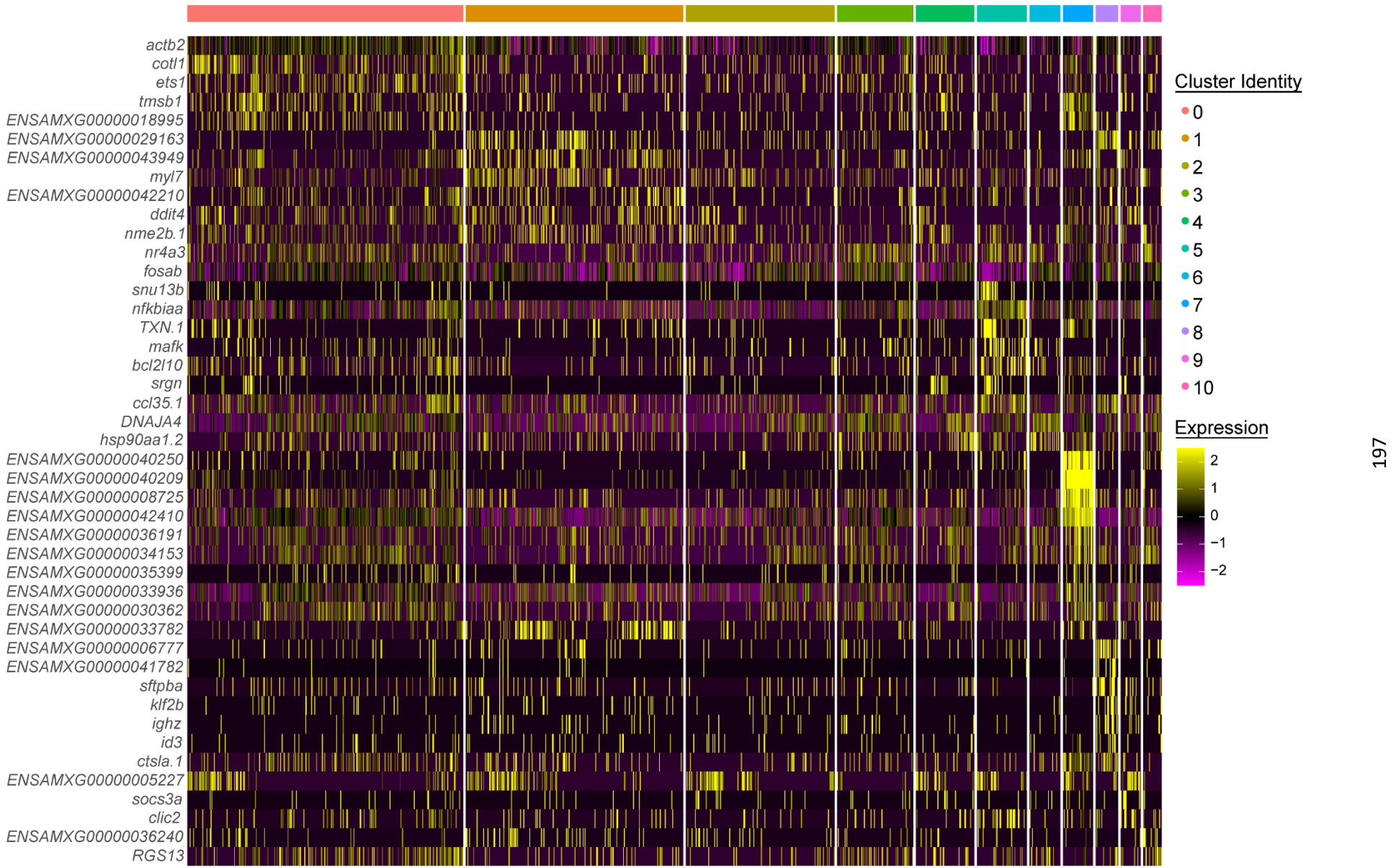
actb2
cotl1
ets1
tmsb1
ENSAMXG00000018995
ENSAMXG00000029163
ENSAMXG00000043949
myl7
ENSAMXG00000042210
ddit4
nme2b.1
nr4a3
fosab
snu13b
nfkbiaa
TXN.1
mafk
bcl2l10
srgn
ccl35.1
DNAJA4
hsp90aa1.2
ENSAMXG00000040250
ENSAMXG00000040209
ENSAMXG00000008725
ENSAMXG00000042410
ENSAMXG00000036191
ENSAMXG00000034153
ENSAMXG00000035399
ENSAMXG00000033936
ENSAMXG00000030362
ENSAMXG00000033782
ENSAMXG00000006777
ENSAMXG00000041782
sftpba
klf2b
ighz
id3
ctsla.1
ENSAMXG00000005227
socs3a
clic2
ENSAMXG00000036240
RGS13
Cluster Identity
0
1
2
3
4
5
6
7
8
9
10
Expression
2
1
0
−1
−2

Figure 4. 23: Heatmap of the top markers for each B cell sub-cluster identified using the ROC test

To explore the cellular behaviours of each B cell subcluster, DGE analysis was performed using the ROC test to identify the top markers for each B cell subcluster (Fig. 4.23). However, due to poor annotation of the AM genome, many of the DGE results were 'novel genes' that were only annotated with an Ensembl ID and no associated protein information, preventing further investigation into the different B cell subclusters. Therefore, differences between all PF and SF B cells were instead focused on, regardless of subcluster identity. The time point after injury was also disregarded in further downstream analysis as the number of cells present at 1-, 3- and 7dpci was insufficient for meaningful DGE analysis at each time point.

Therefore, to compare all PF/SF B cells, the ROC test was used to test differentially expressed genes between the PF and SF. Surprisingly, many of the top PF/SF B cell genes showed completely opposing expression patterns that were population-specific (Fig. 4.24a). This dichotomy of gene expression between PF and SF B cells revealed that PF/SF B cells are very transcriptionally different.

To visualise DGE between PF/SF B cells, the DGE results were plotted using a volcano plot. This showed that 2 genes were significantly upregulated in SF B cells which, remarkably, were the two MHC II genes previously identified in SF macrophages (Fig. 4.24b). Even more remarkably, when MHC II expression was compared in SF and PF B cells, it was found that PF MHC II expression is severely diminished and is almost absent (Fig. 4.24c). This is particularly striking and unexpected as B cells are the classical antigen-presenting cells of the immune system and are the major expressors of MHC II.

As MHC II expression has been consistently observed in the scRNAseq data to be significantly upregulated in SF, MHC II expression was compared at all time points to determine whether MHC II expression was upregulated following injury. Remarkably, this showed that the PF express very low levels of MHC II throughout the response to injury in neutrophils, macrophages and B cells whereas

MHC II is highly expressed in all SF B cells and, particularly, in late-stage SF neutrophils and macrophages (Fig. 4.24d). This suggests that antigen presentation via the MHC II is severely lacking in the PF, resulting in PF B cells which are significantly different from their SF counterparts.

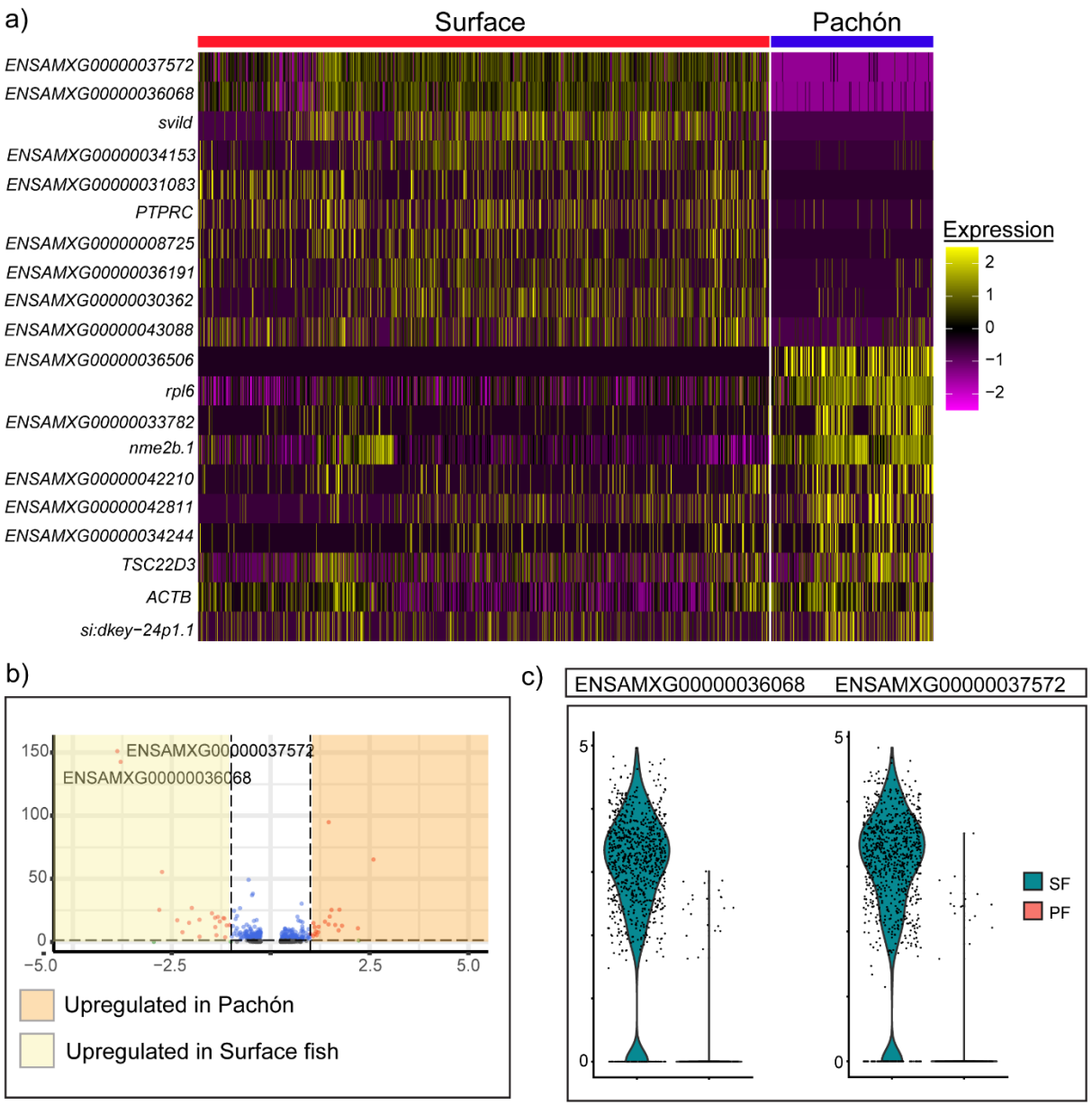

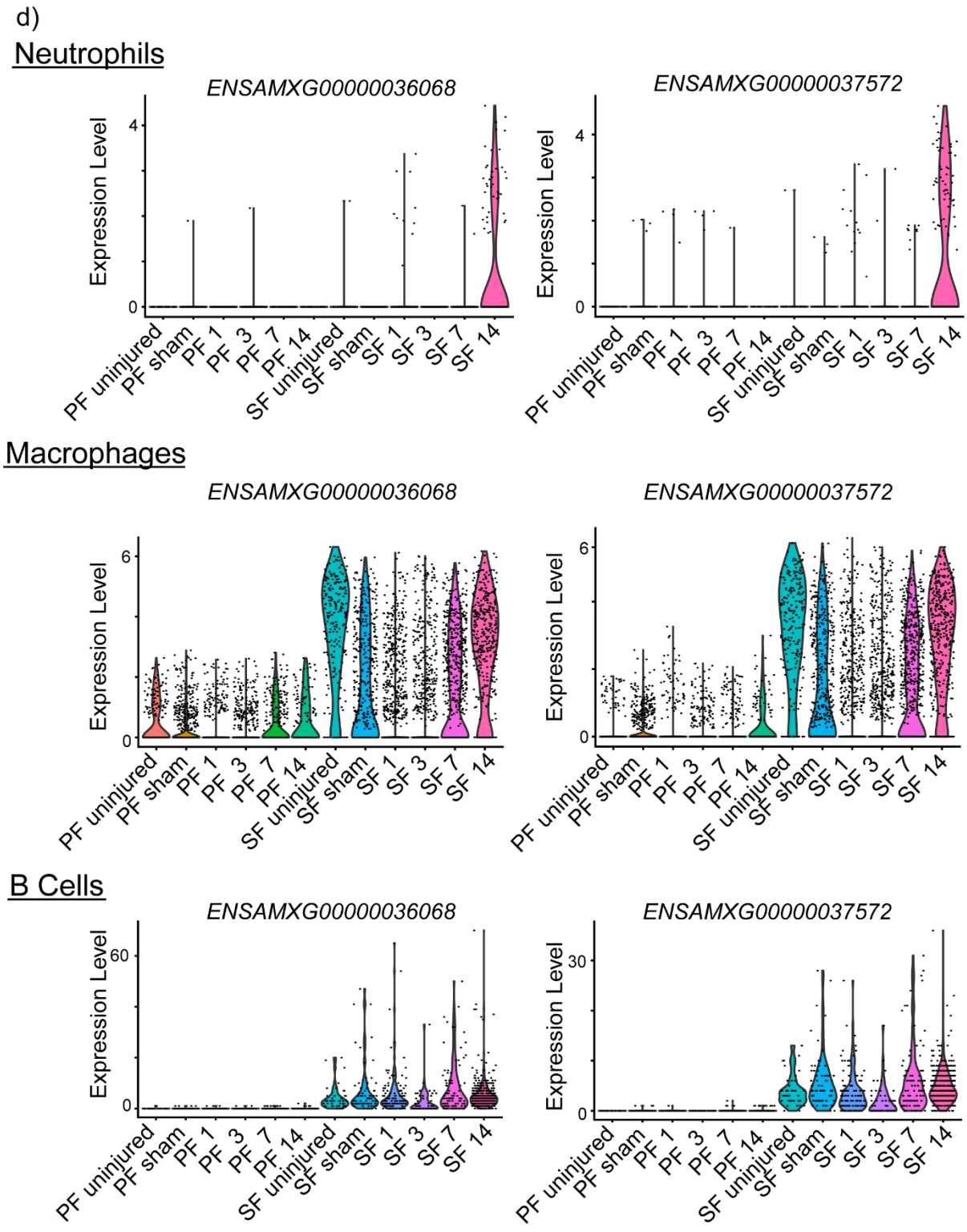

Figure 4. 24: PF and SF B cells are transcriptionally very distinct and show significant differences in their expression of MHC II

(A) Heatmap showing the top PF/SF B cell marker genes are population-specific and all top SF markers are almost absent in the PF. (B) Volcano plot of DGE analysis between PF/SF B cells reveals

that MHC II genes are the most differentially expressed genes (upregulated in SF). (C) Violin plot of MHC II expression in all SF and PF B cells shows that MHC II expression is almost absent in PF. (D) Violin plot of MHC II expression in neutrophils, macrophages and B cells across time shows that PF have severely diminished MHC II expression in all 3 cell types.

To investigate how these striking differences in gene expression may be impacting PF and SF functionality, the DGE results were analysed using GSEA and GO term enrichment. The GSEA results showed that no Hallmark pathways reached the FDR threshold for either PF or SF B cells (see Appendix 4.8). The GO term analysis found that PF B cells seem to be mainly undergoing apoptosis (Fig. 4.25a), suggesting they are not functionally active in the scarring heart. In contrast, many of the top GO terms in SF B cells were found to be involved in protein production and folding (Fig. 4.25b), suggesting that SF B cells are translationally very active. Interestingly, despite the considerable lack of MHC II expression in PF B cells, the GO term 'antigen processing and presentation via MHC II' was specifically enriched in PF B cells, suggesting that PF B cells may be mediating antigen presentation through currently unknown MHC II genes.

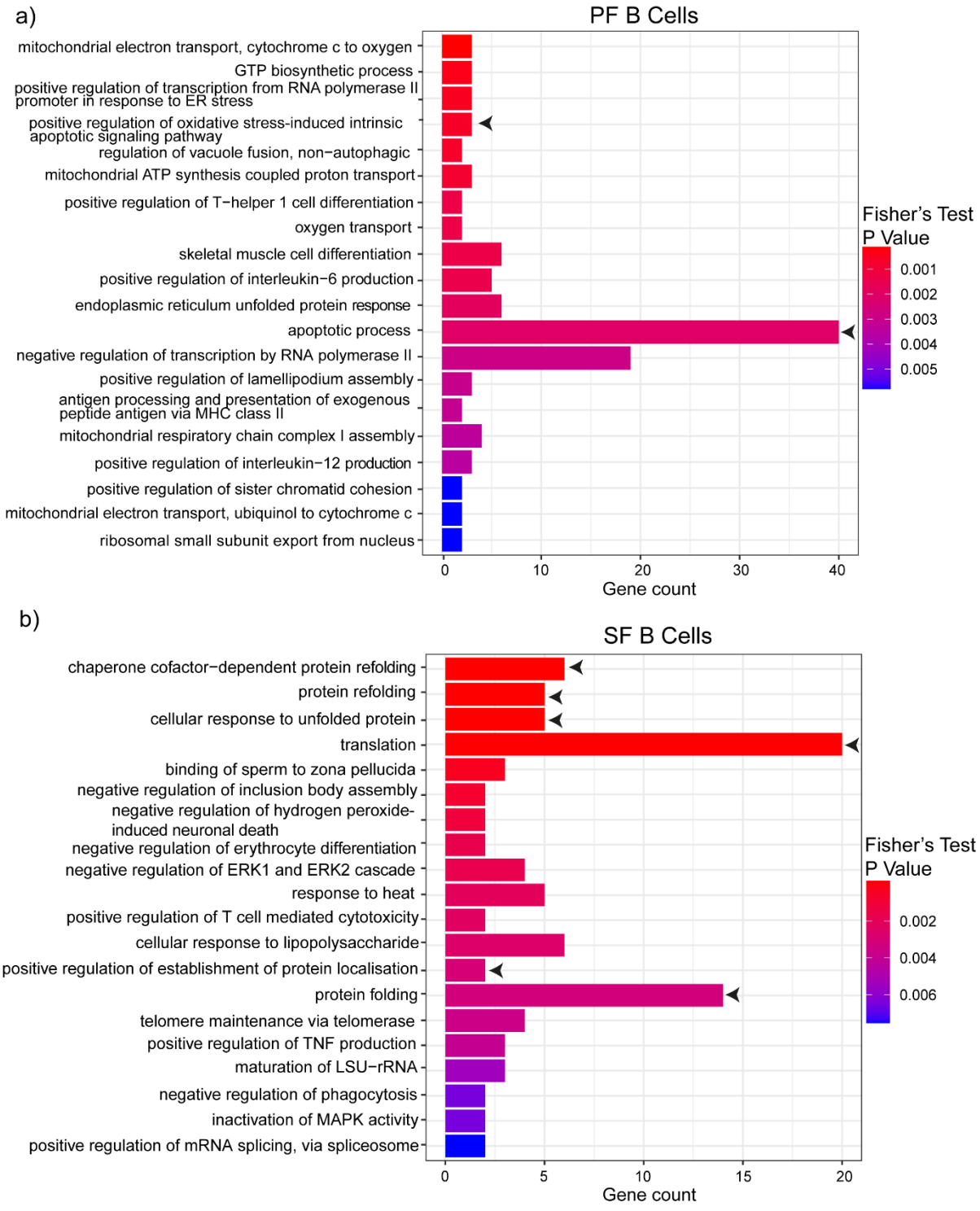

Figure 4. 25: Functional analysis of PF/SF B cells suggests that PF B cells are undergoing apoptosis whereas SF B cells are translationally active

Bar plots of the top GO terms associated with (A) PF and (B) SF B cells. PF B cells are strongly associated with GO terms linked to apoptosis whereas many of the top SF GO terms are linked to the production, localisation and folding of proteins (highlighted by the black arrows).

14dpci SF B cells represent a transcriptionally unique B cell population

As unique transcriptional profiles had been observed in both late-stage SF neutrophils and macrophages, B cells were also investigated to determine whether late-stage SF B cells displayed a similar phenotype. The ROC test was used to identify the top PF/SF B cell markers at each time point and the results were visualised in a heatmap. Once again, the top markers of 14dpci SF B cells were not found in PF and or at any other time point in SF, suggesting that 14dpci SF B cells also display a unique transcriptional signature (Fig. 4.26).

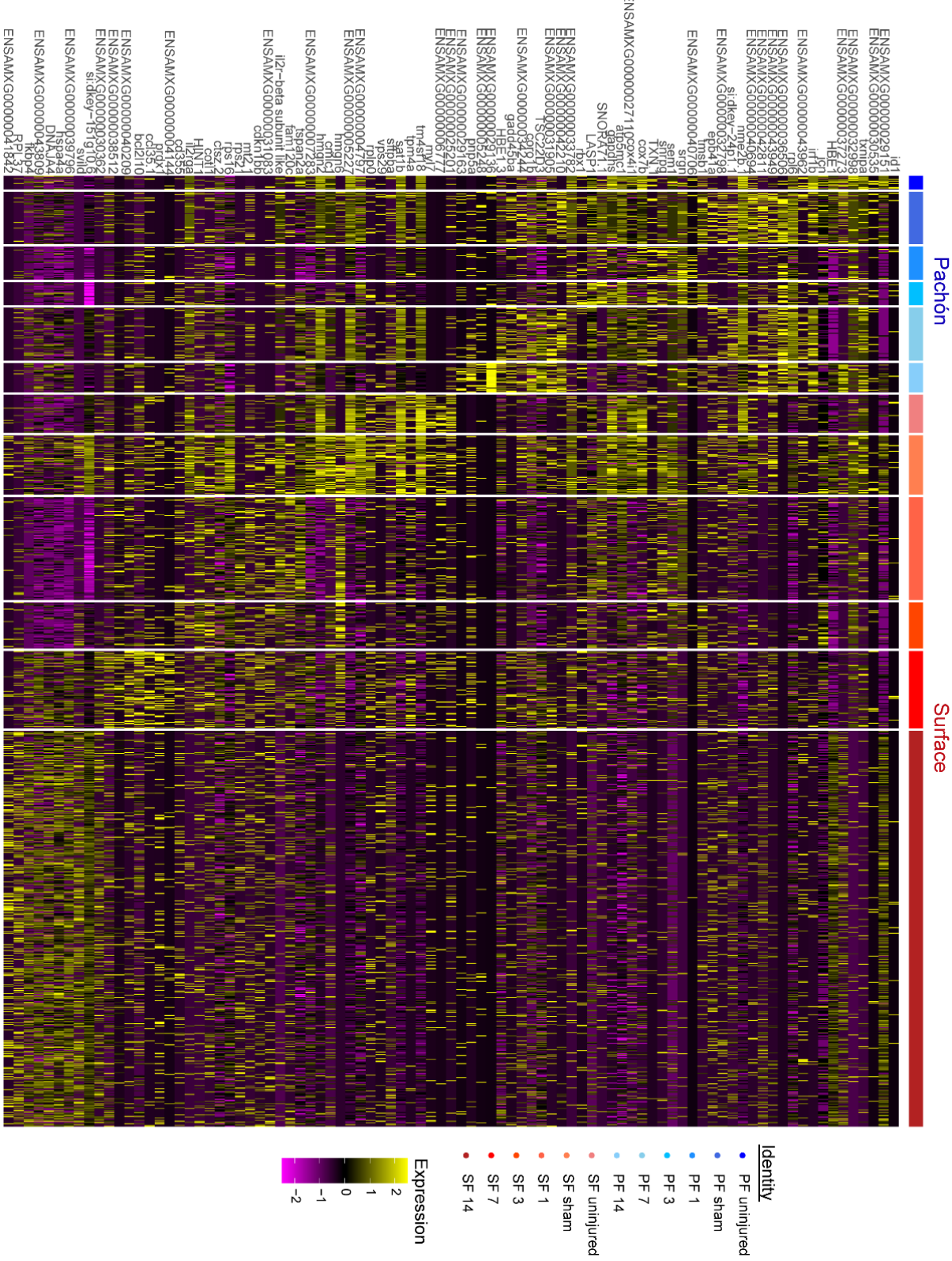

Figure 4. 26: Heatmap of the top cell-markers for SF and PF B cells at each time point suggests that 14dpci SF B cells have a unique transcriptional profile

In conclusion, this initial exploration of B cells in the AM has shown that:

- B cells significantly influx into the SF heart during the late stages of cardiac healing, especially at 30dpci
- PF B cells show significantly decreased levels of MHC II expression
- Late-stage SF B cells show a unique transcriptional profile

4.3 Discussion

Since the immune response was first established as a key regulator of regenerative success, numerous heteogenous leukocyte populations have been identified as essential to regeneration, with many research efforts focused on which aspects of regeneration are mediated by each distinct leukocyte population. However, it is only in recent years that we have begun to understand the importance of leukocyte dynamics in the regulation of regeneration. So far, succesful regeneration has been shown to be critically reliant on timely neutrophil resolution and timely macrophage influx. In contrast, the role of B cells in regulating regeneration and scarring has been almost completely overlooked, despite their presence in both the regenerating zebafish and the scarring adult mouse. In this chapter, scRNAseq data and *in situ* hybridisation have shown, for the first time, that the PF/SF neutrophil and B cell responses are significantly different during the first 30 days following myocardial death. The PF display a significantly stronger initial neutrophil response that could be driving regenerative failure and the formation of a permanent scar. In contrast, the late stages of the SF immune response are characterised by unique neutrophil and B cell responses and transcriptionally distinct leukocytes that could be facilitating regnerative success.

4.3.1 The initial PF neutrophil response could be prohibitive to cardiac regeneration.

The data presented here characteries PF/SF neutrophil dynamics during the first 30 days after cardiac injury. This work has revealed that the PF neutrophil response is prolonged in comparison to the SF. Specifically at 3dpci, PF neutrophils were found to remain elevated whereas SF neutrophils returned to baseline. Neutrophil persistence during wound healing is universally detrimental across the animal kingdom and in a variety of different tissues[274]. Indeed, the prolonged

presence of neutrophils in skin lesions can lead to the complete failure of wound healing and the formation of chronic wounds[275], suggesting that a long neutrophil response will prevent regeneration in the PF. Within the context of the injured heart, the scarring medaka also show a prolonged neutrophil response in comparison to the zebrafish[109]. Manipulations of the neutrophil response in the medaka and zebrafish suggest that neutrophil dynamics can directly regulate regenerative capacity. Accelerating neutrophil clearance in the medaka with poly I:C injections leads to improved regeneration whilst prolonging neutrophil retention in the zebrafish causes regeneration to fail[109,252]. Therefore, the prolonged PF neutrophil response may be inducing regenerative failure and the significant differences in PF/SF neutrophil kinetics catalogued here may be, at least partly, responsible for the differential regenerative capacity of the PF/SF.

The PF neutrophil response was also found to be characterised by the influx of a significantly greater number of neutrophils post-MI than the SF. Excessive neutrophil recruitment is well-established to be detrimental to cardiac repair; clinically, high levels of neutrophils post-MI positively correlate with increased infarct sizes, fibrosis, and HF development[239–241]. Furthermore, excessive neutrophil recruitment is observed in the zebrafish during numerous cases of regenerative failure[107,276]. The damaging effects of neutrophils are attributed to their secretion of ROS and degradative enzymes which cause surrounding cells to die by apoptosis. Findings from GO term analysis indicate that PF neutrophils are actively damaging as they are enriched for superoxide generation at 3dpci. In contrast, at 3dpci SF neutrophil levels have returned to baseline, suggesting that the SF heart is spared any potentially damaging effects of neutrophils by both limiting the extent and duration of neutrophil recruitment. Therefore, although these findings indicate that significant differences in the SF/PF neutrophil responses are regulating AM regenerative capacity, future studies should aim to either restrict the influx of PF neutrophils or accelerate neutrophil clearance in the PF to confirm that the PF neutrophil response is directly leading to permanent scarring.

4.3.2 Regeneration and scarring show a divergent late-stage immune response in the AM

In the adult teleost and mammalian heart, post-MI neutrophil levels return to baseline by 7dpci[144]. In this chapter, however, I present the completely novel finding that neutrophils remain significantly elevated at both 7- and 14dpci in the SF. This data suggests, for the first time, that a prolonged presence of neutrophils is not necessarily prohibitive of regeneration, contradicting the wealth of data that shows that a neutrophil response which fails to resolve quickly is detrimental to wound healing (see above). In contrast to the SF, the scarring PF neutrophil response was transcriptionally inactive by 7dpci and returned to baseline levels, revealing that a late-stage neutrophil response is unique to the regenerative setting. This suggests that late-stage neutrophils may play a pro-regenerative role that is absent from the PF. In recent years, the beneficial roles of neutrophils in wound healing have started to emerge. Indeed, neutrophils have been shown to promote myocardial healiing from 5 days post-MI by resolving inflammation[153,277] and by contributing to the organisation and remodelling of the scar[249]. Therefore, future studies should aim to characterise the functional and transciptional profile of late-stage SF neutrophils to determine whether these cells represent a pro-regenerative population that uniquely drives successful regeneration in the SF.

In addition to identifying novel neutrophil dynamics in the SF, in this chapter I have found that late-stage SF leukocytes display distinct transcriptional profiles that emerge specifically during the late stages of cardiac healing. Strikingly, the distinct transcriptional profiles identified in late-stage SF leukocytes are absent at any other time point after injury and completely from the PF, suggesting that SF leukocytes uniquely launch a transcriptional response to injury that is specific to the late stages of cardiac healing. Furthermore, late-stage SF neutrophils and macrophages were found to display very similar enriched GO terms at 7- and 14dpci, suggesting that the observed transcriptional profiles of late-stage SF leukocytes are responsible for promoting a specific functional response that occurs at both 7- and 14dpci. However, from the analysis presented here, it is not clear as to what functional role late-stage SF neutrophils, macrophages and B cells could be playing.

Therefore, future work should aim to specificlly explore these late-stage immune cells to determine whether they are playing key roles in promoting successful regeneration.

4.3.3 Are B cells essential for regeneration?

In this chapter, I have found that the late-stage AM immune response further diverges significantly due to the substantial SF B cell response which is almost absent in the PF. *cd37*+ cell counts and scRNAseq data have shown that B cells significantly influx into the regenerating heart at 14- and 30dpci whereas PF B cell levels remain minimal during the late stages of cardiac repair. This is an extremely novel finding as it is the first time that B cells have been associated with successful cardiac regeneration. Indeed, so far no reports have investigated the role of B cells in either the zebrafish or the neonatal mouse and, typically, B cells are thought to be detrimental to the injured heart as they have been associated with HF development, increased fibrosis and cell death via the production of auto-reactive antibodies[259,260]. However, recent studies are starting to shed light on the healing properties of B cells. Post-MI, injection of mature B cells can improve cardiac function in the adult mouse by decreasing scar sizes, attenuating fibrosis and decreasing the infiltration of pro-inflammatory monocytes[262], suggesting that late-stage SF B cells could be pro-reparative. Furthermore, evidence from other tissues has revealed that mature B cells are beneficial to wound healing: they accelerate wound healing in the diabetic mouse by stimulating angiogenesis and innervation[278] whilst they can limit ischemic infarct sizes and inflammation after a stroke[279,280] or after mechanical CNS damage[281]. Thus, it is tantilising to hypothesise that high levels of B cells in the regenerating SF heart might be promoting cardiac regeneration during the late stages of wound healing by stimulating blood vessel formation, nerve growth and limiting cardiac tissue damage. Additionally, B cells have also been shown to have immunomodulatory properties and can directly control the leukocyte composition of the heart at baseline by controlling the levels of neutrophils and $CD4^+$ and $CD8^+$ T cells[282]. This further suggests that B cells in the SF might be mediating regenerative success by ensuring that the leukocyte pool in the SF heart is pro-regenerative. Therefore, future studies should aim to explore whether B cells are regulating AM regenerative

capacity, either by selectively depleting B cells in the SF heart or by injecting B cells from the SF into the PF to determne whether regeneration is altered.

The B cell data presented in the chapter is not only novel, but it is also strikingly different from previous bulk RNAseq data from the Mommersteeg lab which suggested that the PF adaptive immune response was significantly upregulated, especially at 7- and 14dpi. However, I have found that the SF adaptive immune response is significantly upregulated at 7- and 14dpci during B cell counts. Although the T cell response to cryoinjury has not yet been validated in the AM, the results of the DPA show T cell levels to be very similar between the PF and SF, suggesting that the adaptive immune response is stronger in the SF after cryoinjury than the PF due to the substantial influx of B cells. Therefore, the results of this chapter not only confirm my initial hypothesis that the AM immune response to necrotic cell death would be substantially different than to resection, but they also suggest that findings from the resection injury model are not necessarily transferable to the cryoinjury model. This is significant and something for cardiac regeneration researchers to be aware of as both cryoinjury and resection are still used extensively throughout the field[283,284]. Furthermore, as the adaptive immune response is differentially upregulated in the AM following resection vs following cryoinjury, this has implications for the other previous bulk RNAseq findings (i.e. that metabolism and scarring are major differences between succesful regeneration vs fibrotic scarring). Therefore, future work should aim to repeat the previous bulk RNAseq experiment using cryoinjury as the cardiac injury model to confirm whether metabolism and scarring remain significantly different in the regenerative and scarring hearts in response to necrotic cell death.

4.3.4 MHC II deficiency in PF

Antigen presentation via MHC II complexes is essential for T cell activation. B cells and macrophages are major antigen-presenting cells (APCs) of the immune system, whilst antigen presentation has also been reported in neutrophils. However, the data presented here has shown that MHC II expression is significanctly diminished in the scarring PF in APCs, suggesting that T cell

activation during PF cardiac healing may be impaired. Lack of T cell activation has alreay been shown to be detrimental to wound healing and MHC II-deficient mice cannot successfully heal skin lesions due to a lack of $CD4^+$ T cell recruitment[285]. Furthermore, MHC II deficiency post-MI has been shown to result in severe disruption of scar formation and adverse ventricular remodelling[286], suggesting that lack of MHC II expression in the PF could be activately detrimental to cardiac regeneration. Interestingly, however, the scRNAseq dataset suggests that T cell dynamics are not significantly different between the PF/SF, suggesting that T cell recruitment is not impaired in the PF (see chapter III). Therefore, this preliminary finding requires further investigation to determine whether MHC II deficiency in PF APCs plays a role in regulating regeneration vs scarring.

4.3.5 Limitations

The scRNAseq analysis presented here has focused on comparing PF/SF leukocytes at each time point, regardless of leukocyte subcluster. Although this analysis enabled the exploration of significant differences in AM leukocytes after injury, it has completely disregarded the heterogenous cluster populations present in the scRNAseq data. Indeed, 9 neutrophil clusters, 7 monocyte/macrophage clusters and 11 B cell clusters were identified in the scRNAseq data which could all be mediating distinct aspects of the regenerative and scarring processes. Distinct macrophage populations have already been identified in the zebrafish heart that mediate differential aspects of cardiac regeneration: *tnfa*+ macrophages mediate scar deposition whilst *tnfa*- macrophages mediate scar resolution[144]. Furthermore, the inflammatory profiles of both neutrophils and macrophages have been shown to change over time with injury: both cell types are pro-inflammatory immediately after injury and then polarise to an anti-inflammatory state during the late stages of cardiac healing. Therefore, it is very likely that both pro- and anti-inflammatory cells will be present at each time point which could be impacting the results of functional pathway analysis as true differences in inflammatory and anti-inflammatory signals between PF/SF cells cannot be distinguished. Indeed, at 7dpci, SF macrophages were observed to be enriched for both inflammatory and anti-inflammatory pathways which is most likely due to the presence of both pro-

and anti-inflammatory cells. Therefore, further analysis of the scRNAseq data should aim to investigate PF/SF differences between distinct neutrophil, macrophage and B cell clusters at each time point.

The functional scRNAseq analysis employed here required all AM genes to be converted to their mouse homologs prior to both GSEA and GO term analysis. This is because GSEA requires the input of either mouse or human genes whilst GO terms are not well annotated in the AM genome but are well annotated in the mouse. Although homology mapping is the best current approach for non-model organism researchers performing functional scRNAseq analysis[30], it does present 2 inherent limitations. Firstly, homology mapping relies on the assumption that the AM: mouse homologs are biologically similar and function in the same way within mouse cells as they do AM cells which may not be the case. Secondly, homology mapping results in the removal and filtration of many AM genes from downstream functional analysis as only AM genes which map to a single mouse homolog are retained during analysis (i.e. AM genes that had no mouse homolog or mapped to multiple genes were removed). Therefore, the GO term and GSEA results presented here could have potentially overlooked key signalling pathways that drive regeneration vs scarring due to the use of AM: mouse homologs. Unfortunately, there is currently no way around this limitation for AM researchers as many scRNAseq functional analysis tools are built for mouse and human datasets. Instead, AM researchers must wait for the GO term annotation of the AM genome to improve and the development of scRNAseq analysis tools that are designed specifically for teleosts to overcome this limitation.

Finally, the results of this chapter are limited by the lack of characterisation of AM monocyte/macrophage spatiotemporal dynamics. Numerous studies have shown that macrophages are critically important to the success of cardiac regeneration[103,109,169]. Therefore, our understanding of the PF/SF immune responses will be incomplete until this key regenerative cell type can be characterised. Future studies should aim to complete the characterisation of the AM

monocyte/macrophage response using *c1qa,* instead of *mpeg1,* which has been identified here as a suitable pan-macrophage AM marker.

4.3.6 Future Directions

This chapter has highlighted that the AM immune response significantly diverges during the late stages of wound healing. Therefore, the next chaper should focus on the late stages of the AM immune response to explore how the divergence in the late-stage AM immune response may be regulating successful regeneration vs permanent scarring. Specifically, the next chapter should aim to explore the unique transcriptional profile identified in late-stage SF neutrophils, macrophages and B cells which could be key in driving regenerative success.

Chapter V

Surface fish neutrophils and macrophages show unique NFκB activation at 7- and 14dpci that is absent from Pachón

5.1 Background

5.1.1 The late stages of cardiac regeneration

During the late stages of cardiac healing (7-14dpi), the regenerating heart enters the reparative phase. Necrotic tissue debris has been cleared and the initial inflammatory insult has been resolved. The resolution of inflammation is a key part of cardiac healing and chronic, aberrant or unresolved inflammation has been well documented to drive the pathology of many cardiovascular diseases such as cardiomyopathy, HF and atherosclerosis[287–291].

To date, the reparative phase of cardiac healing has been relatively unexplored in comparison to the immediate, inflammatory phase of cardiac repair. As such, the cellular and molecular events that mediate the reparative phase are not exactly clear. However, it is during this time that the production of *de novo* cardiac tissue reaches its peak in the regenerating heart. Cardiomyocyte proliferation levels peak at 7dpci in the zebrafish[292] and the AM[29], and at 14dpci in the axolotl[104]. Additionally, collagen scar deposition increases during the late stages of cardiac healing as fibroblasts and myofibroblasts proliferate and produce collagen and ECM proteins[293–295]. From 7dpi onwards, the regenerating heart begins to finely control the rate of tissue replenishment by balancing the levels of cardiomyocyte proliferation, scar deposition and scar degradation so that the collagen scar is gradually replaced by new tissue. However, it is currently unknown what mechanisms are involved to balance tissue production with tissue degradation.

5.1.2 The late stages of the immune response

Although the immune response is thought of as the master regulator of regeneration and scarring, few studies have explored the role of the immune response specifically during the late stages of cardiac healing. As such, the exact role of the immune response in the late stages of cardiac regeneration is still unclear. Recent studies, however, have identified that the late-stage immune response might play a key role in coordinating cardiomyocyte proliferation with scar degradation. For example, Tregs and macrophages (which peak at 7dpi) have both been shown to promote cardiomyocyte proliferation by secreting paracrine mitogens[296], whilst ablation of either cell type will result in decreased levels of myocardial proliferation. Additionally, macrophages have been shown to play major roles in scar remodelling: they deposit collagens, secrete degradative enzymes, facilitate scar removal, and activate scar deposition from fibroblasts and myofibroblasts[136,144,297]. Furthermore, late-stage neutrophils have been found to deposit ECM proteins to the scar and upregulate proteins involved in scar organisation at 7dpi[249].

However, our understanding of the functional roles of late-stage leukocytes in regeneration and scarring is still in its infancy. Indeed, we are only just beginning to understand the complexity of late-stage leukocytes. Recent studies have identified that distinct anti-inflammatory leukocyte populations emerge during the late stages of the immune response that facilitate specific aspects of cardiac repair. In the zebrafish, a population of *tnfa*- macrophages have recently been identified that peak at 7dpci and promote scar removal[144]. In the mouse, fibronectin+ neutrophils have been found to peak between 5-7dpi and seem to contribute to scar remodelling and ECM deposition. These populations suggest that late-stage immune cells may facilitate scar resolution and turnover in the regenerating heart. However, further research is still required if we are to fully understand the role of the late-stage immune response during cardiac regeneration. For instance, the role of many leukocyte populations such as B cells have not yet been explored during the late stages of the immune response. Additionally, there is currently no evidence whether the late stages of the

immune response are essential to regenerative success as no study has yet specifically disrupted the immune response from 7dpi onwards.

5.1.3 Aims

In the previous two chapters, I identified that the AM immune response significantly diverged during the late stages of wound healing. Specifically, I found that SF leukocyte levels remain elevated at 14dpci due to an influx of B cells, and transcriptionally distinct neutrophils and macrophages. In contrast, the PF immune response was resolved during the late stages of wound healing. From this data, I have hypothesised that the unique late-stage SF immune response is essential to SF regenerative success. However, it is still not yet clear whether late-stage SF leukocytes play pro-regenerative roles such as stimulating cardiomyocyte proliferation or facilitating scar removal. Therefore, to delineate how the late-stage SF immune response might be stimulating regeneration, in this chapter, I aimed to:

1) Identify the main genes and signalling pathways that characterise the unique late-stage transcriptional profiles seen in SF neutrophils, macrophages and B cells
2) Determine whether inhibition of SF late-stage leukocytes inhibits regeneration and abrogates successful wound healing

5.2 Results

5.2.1 Late-stage SF neutrophils, macrophages and B cells upregulate *tnfa* and *nfkb2* expression

To achieve the first aim of this chapter and identify genes that were highly expressed in late-stage SF neutrophils, macrophages and B cells, DGE analysis was performed using the scRNAseq data. MAST testing was used to highlight the highest expressed genes at 7- and 14dpci in SF neutrophils (Fig. 5.1a), macrophages (Fig. 5.1b) and B cells (Fig. 5.1c). Comparison of the DGE results showed that many of the top genes expressed in SF late-stage leukocytes were either regulated by Nuclear factor-κB (NFκB - a pleiotropic transcription factor that is involved in cell survival,

inflammation, proliferation and the immune response[298,299]) or were directly involved in the NFκB signalling pathway (as indicated by the black arrows in Fig. 5.1).

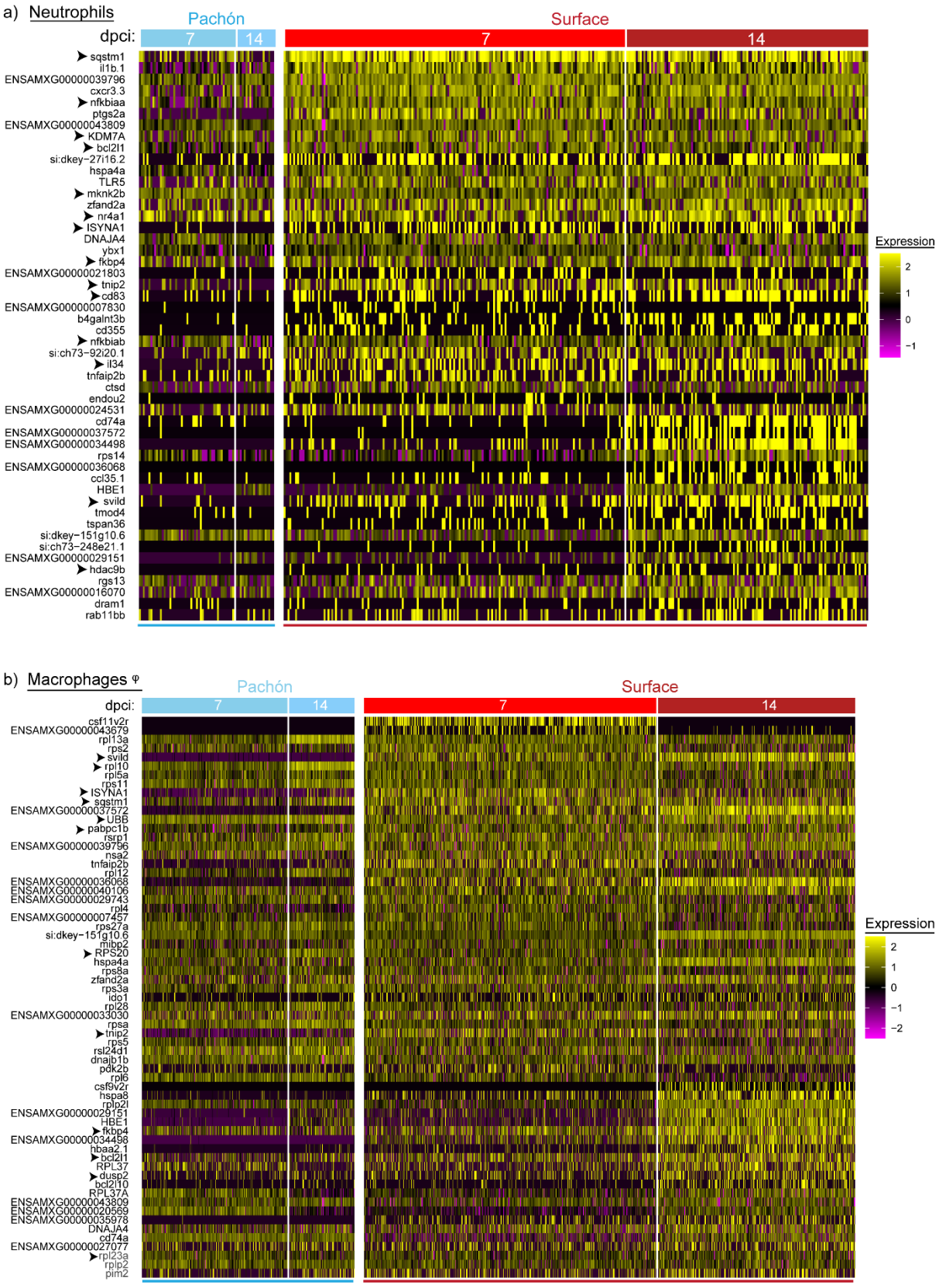

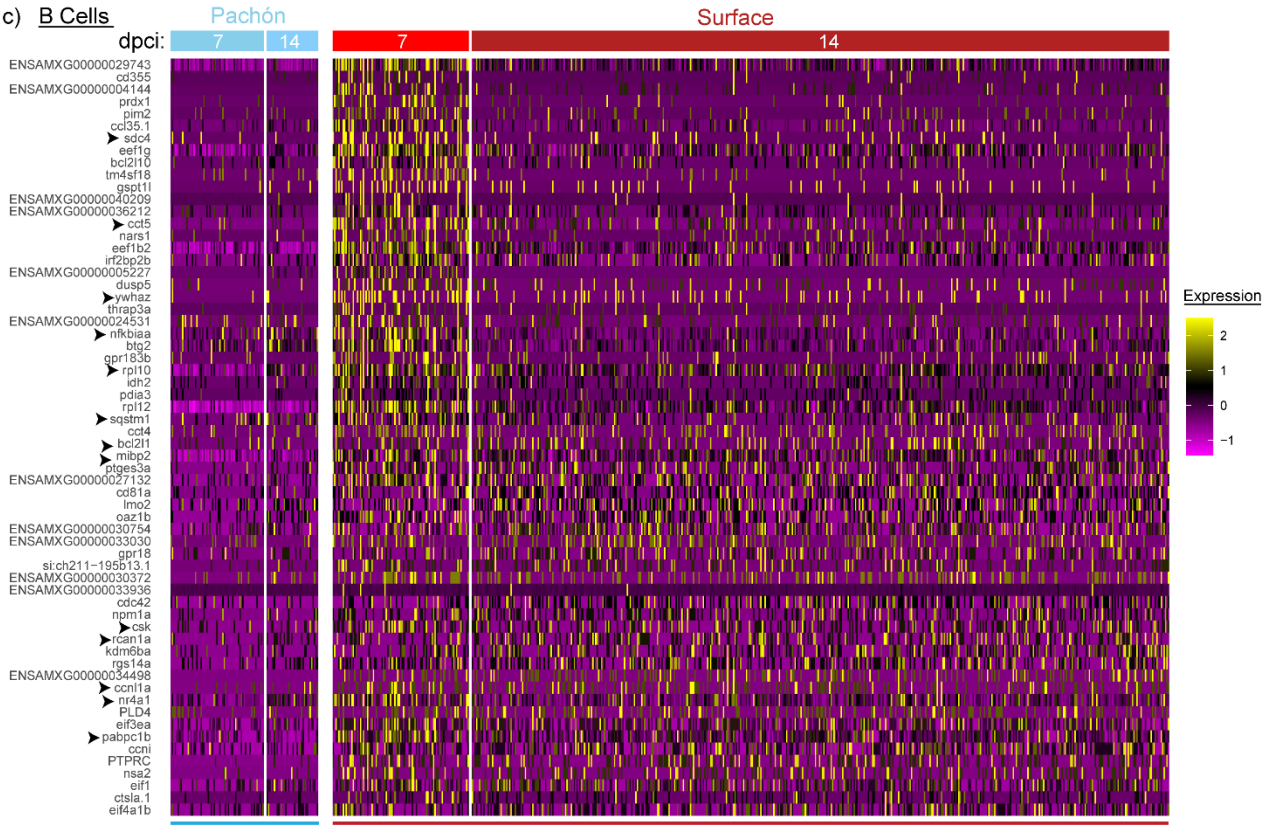

Figure 5. 1: Late-stage SF leukocytes upregulate NFκB signalling

Heatmaps of the top 7dpci and 14dpci markers, as identified by MAST testing, for (A) neutrophils, (B) macrophages and (C) B cells. The black arrows indicate genes identified associated with NFκB signalling using the Harmonizome database[300]

As NFκB is a dynamic transcription factor that can play a multitude of pleiotropic roles during wound healing, the previous GSEA and GO term analysis results were re-examined to explore whether any functional pathways identified in late-stage SF leukocytes could be the result of active NFκB signalling. This revealed that all late-stage SF neutrophils, macrophages and B cells expressed genes that were significantly enriched for TNFα/NFκB signalling (Table 5.1). To confirm this finding, the top markers of PF and SF neutrophils, macrophages and B cells were assessed for enrichment in the PROGENy signalling pathways, another type of functional pathway analysis that has been shown to outperform GO term and GSEA analysis in its application to scRNAseq data[301]. PROGENy analysis

showed that TNFα and NFκB pathways were significantly upregulated in late-stage SF neutrophils, macrophages, and 7dpci SF B cells to a far greater degree than their PF counterparts (Fig. 5.2). Furthermore, late-stage SF neutrophils, macrophages and B cells showed the highest levels of TNFα/NFκB enrichment across all the time points tested.

Typically, TNFα/NFκB signalling is associated with inflammation and the early stages of the immune response; it has not previously been linked to the reparative phase of the immune response. Therefore, this novel result was selected for further exploration.

SF Cells	*7dpci*	*14dpci*
Neutrophils	-	Hallmark TNFα/NFκB signalling
	-	GO term inflammatory response
Macrophages	Hallmark TNFα/NFκB signalling	-
	GO term Cellular Response to TNF	GO term Cellular Response to TNF
B cells	GO term TNF production	

Table 5. 1: Summary of GSEA and GO term analysis results from Chapter IV that identified upregulation of TNFα/NFκB signalling in late-stage SF neutrophils, macrophages and B cells

Neutrophils

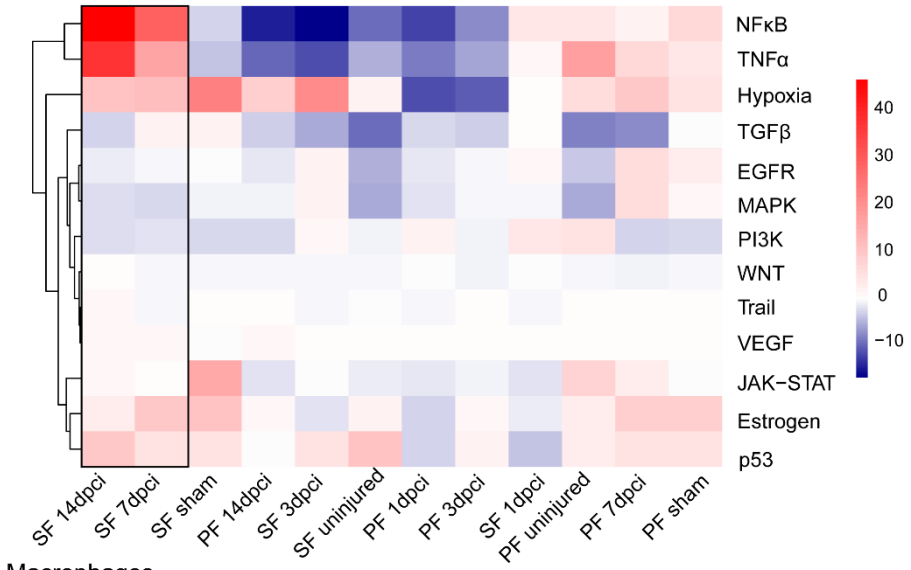

Macrophages

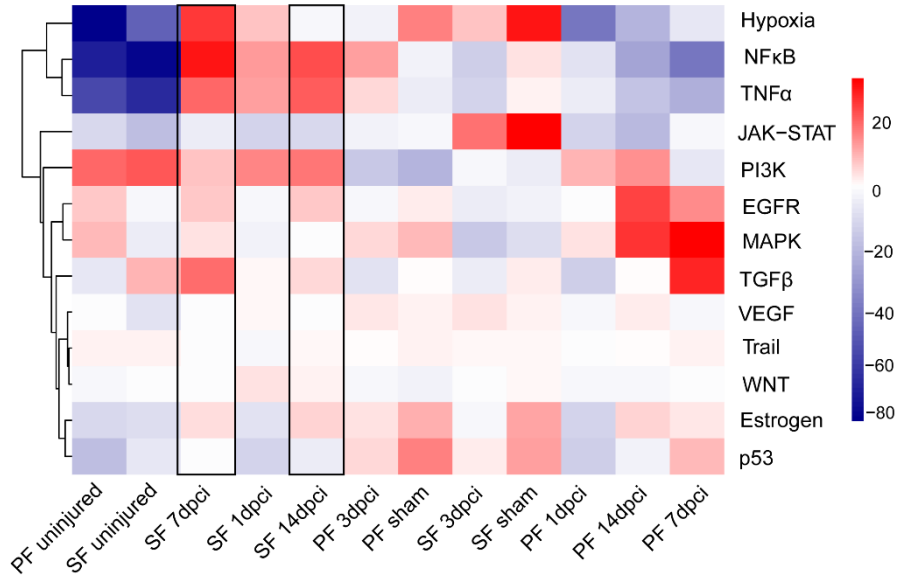

B cells

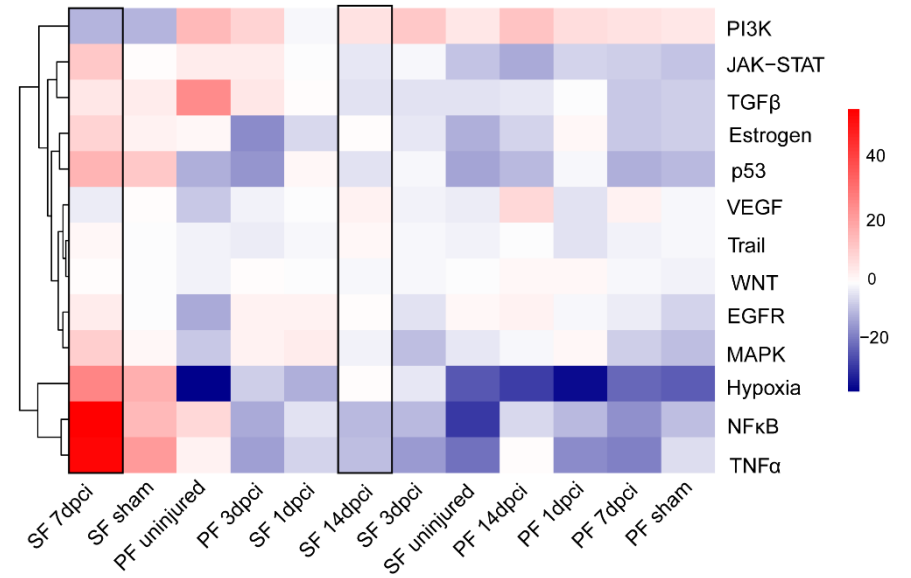

Figure 5. 2: TNFα/NFkB is significantly upregulated in late-stage SF leukocytes compared to PF leukocytes. *Heatmaps display the results of PROGENy pathway analysis. The reported values indicate the activity of each PROGENy pathway tested with positive values (in red) reflecting active pathways whilst negative values (in blue) reflecting inactive pathways.*

To confirm the novel finding that late-stage SF leukocytes upregulate TNFα/NFκB signalling, the expression levels of top TNFα/NFκB genes were evaluated in the scRNAseq dataset. This showed that, for almost all genes, late-stage SF neutrophils and macrophages showed significantly greater expression levels than their PF counterparts (Fig. 5.3). However, SF B cells only showed convincing elevated expression levels for *svild* and *tnip2*.

Therefore, transcriptional profiling of late-stage AM leukocytes using the scRNAseq data showed that SF leukocytes specifically upregulate TNFα/NFκB at 7dpci and 14dpci in response to cardiac injury, whilst this injury response is absent from the PF.

However, TNFα/NFκB expression had never previously been probed in the AM and thus the expression levels of TNFα/NFκB in PF/SF hearts needed to be confirmed *in situ*.

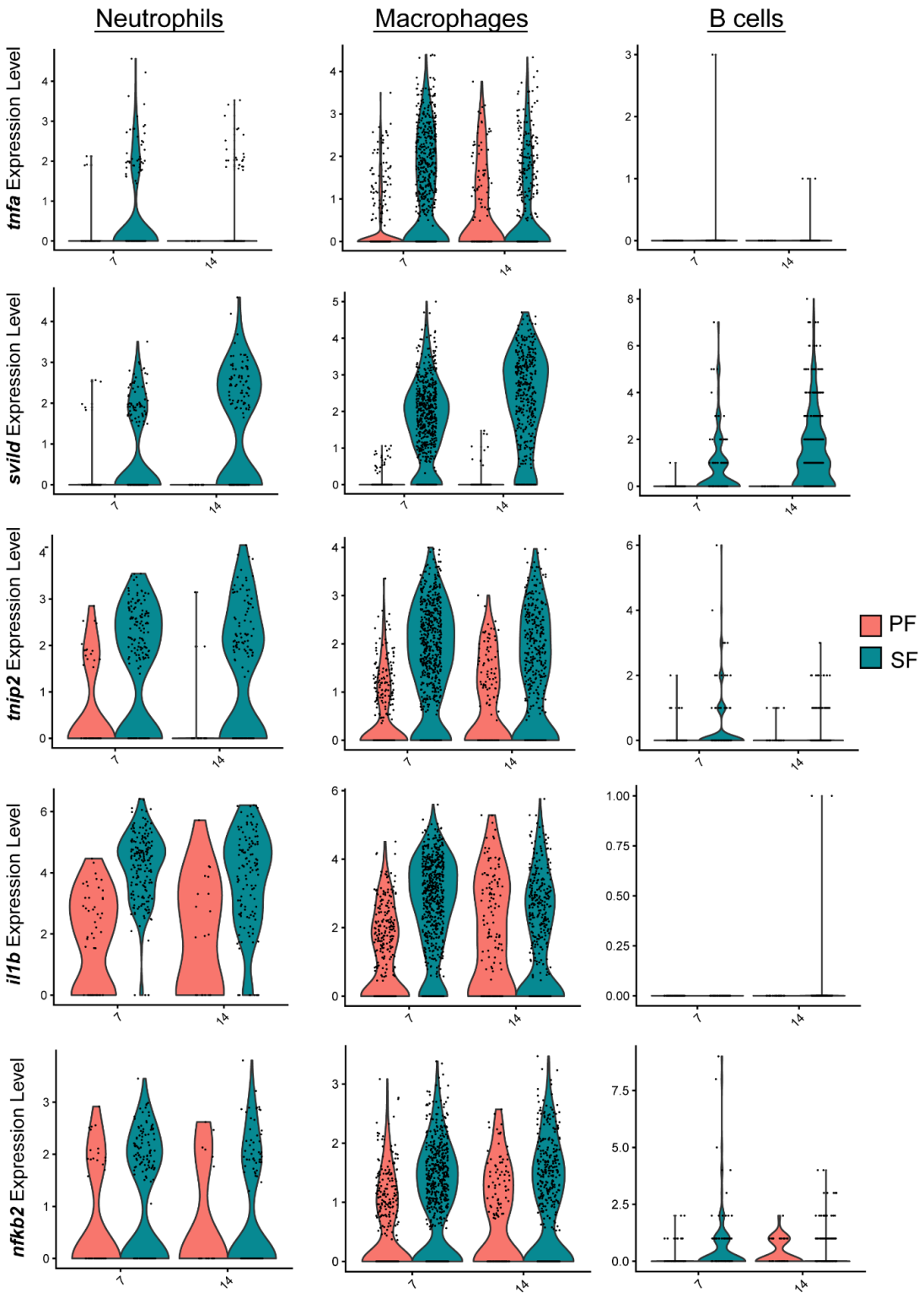

Figure 5. 3: Violin plots of the top identified TNFα/NFκB genes, comparing expression levels between PF and SF neutrophils, macrophages and B cells at 7dpci and 14dpci

To validate SF upregulation of TNFα/NFκB signalling, PF/SF hearts were probed for the expression of *tnfa* and *nfkb2*, two genes which had both shown high levels of expression in late-stage SF leukocytes. 14- and 30dpci hearts were stained using *tnfa* and *nfkb2* RNAscope probes and the number of *tnfa*+ and *nfkb2*+ cells present in the wound was counted (Fig. 5.4a). Cell counts showed that at 14- and 30dpci, *tnfa*+ and *nfkb2*+ cells were elevated in the SF in comparison to the PF, with 30dpci showing the greatest difference for both *tnfa+* cells (Fig. 5.4b) and *nfkb2+* cells (Fig. 5.4c). Although, due to a low sample number at 30dpci, I was unable to confirm whether this observed difference between PF and SF hearts at 30dpci was significant.

Therefore, the scRNAseq and *in situ* hybridisation data suggested that TNFα/NFκB signalling is specifically upregulated in late-stage SF neutrophils, macrophages and 7dpci B cells, resulting in elevated numbers of *tnfa*+ and *nfkb2*+ cells in SF hearts. However, from this data, the functional role of upregulated TNFα/NFκB signalling in late-stage SF leukocytes was unclear.

Due to the absence of TNFα/NFκB signalling in late-stage PF leukocytes, I postulated that TNFα/NFκB signalling could be mediating a pro-regenerative response in the SF. Additionally, as TNFα/NFκB upregulation was conserved amongst SF neutrophils, macrophages and B cells, I postulated that TNFα/NFκB might 'switch on' a pro-regenerative gene program in SF leukocytes in response to injury.

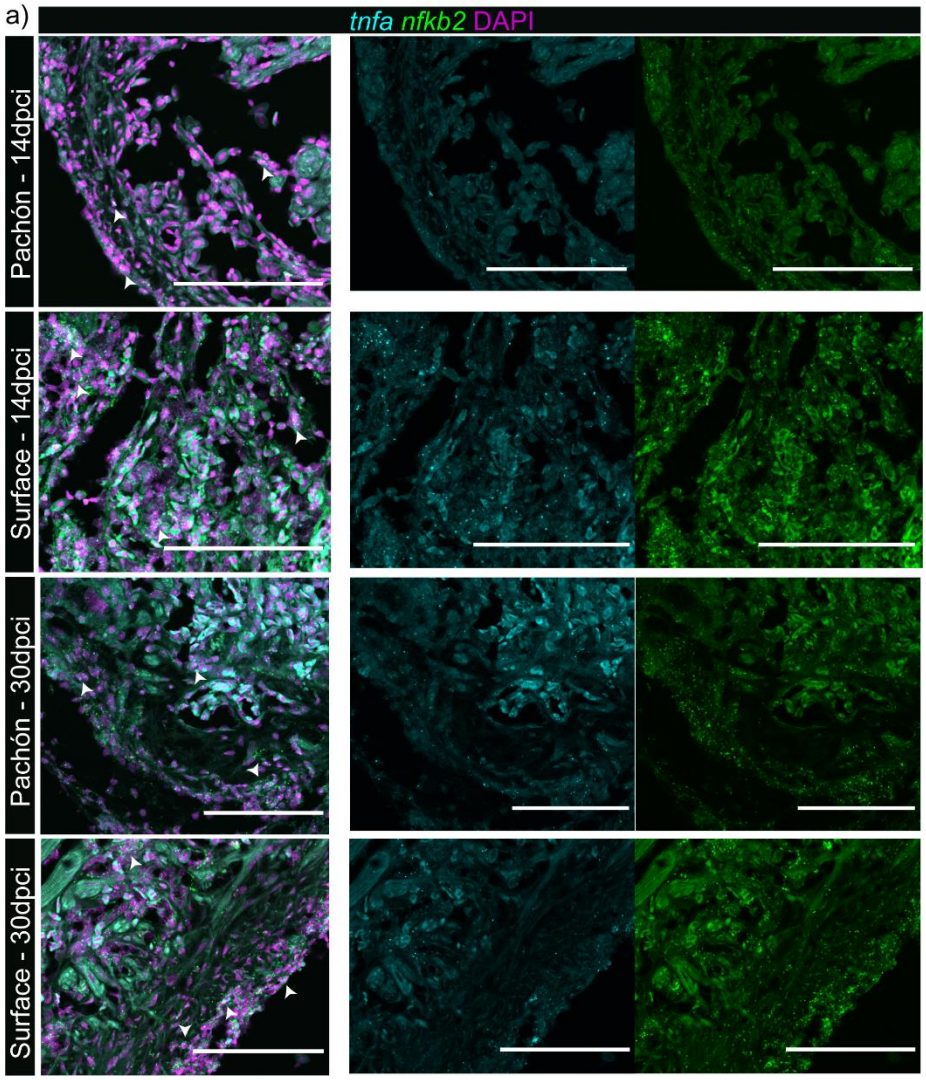
a)
tnfa nfkb2 DAPI
Pachón - 14dpci
Surface - 14dpci
Pachón - 30dpci
Surface - 30dpci

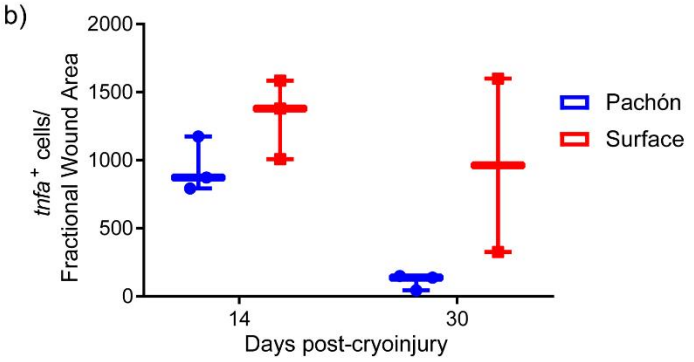
b)
tnfa+ cells/
Fractional Wound Area
2000
1500
1000
500
0
14
30
Days post-cryoinjury
Pachón
Surface

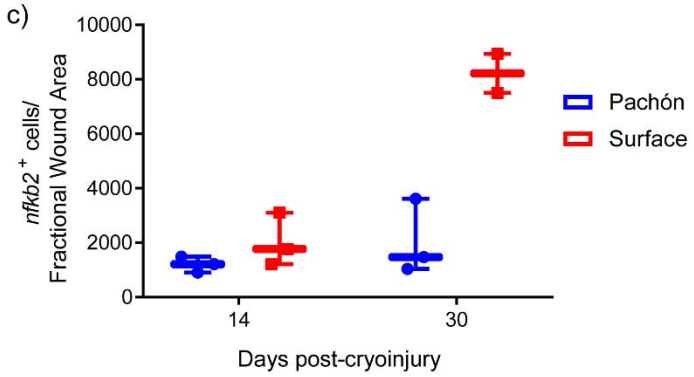
c)
nfkb2+ cells/
Fractional Wound Area
10000
8000
6000
4000
2000
0
14
30
Days post-cryoinjury
Pachón
Surface

Figure 5. 4: Preliminary cell counts show that tnfa+ and nfkb2+ cells are elevated in SF wounds at 14- and 30dpci in comparison to the PF

(A) Representative RNAscope staining tnfa and nfkb2 expression in PF and SF hearts at 14dpci and 30dpci (B). Counts of tnfa+ and nfkb2+ cells were normalised to the fractional wound area. Statistical analysis (Student's t-test) was only performed at 14dpci due to sample number restrictions (n=3 for 14dpci, n=2 for 30dpci).

5.2.2 The distinct transcriptional profile observed in late-stage SF leukocytes is shared between neutrophils and macrophages but not with B cells

To explore whether TNFα/NFκB signalling was upregulating a pro-regenerative gene program in late-stage SF neutrophils, macrophages and B cells, the top markers of each cell type were compared to identify any genes that were commonly upregulated in all 3 leukocyte populations. This found that there was a significant degree of overlapping genes between SF neutrophils and macrophages. In contrast, the top markers of SF B cells did not overlap with SF neutrophils and macrophages, suggesting that a late-stage transcriptional profile is only shared between SF macrophages and neutrophils but not with B cells (Fig. 5.5a,c&d). This finding suggested that, in response to cardiac injury, a gene response program is activated in both SF neutrophils and macrophages. In contrast, only 7- and 14dpci PF macrophages showed any degree of overlapping genes (Fig. 5.5b) which suggested that a universal gene program is not activated in scarring leukocytes in response to cardiac injury.

Therefore, from the scRNAseq data and *in situ* hybridisation analysis, it is possible to conclude that:

1) In the late stages of successful regeneration, the immune response remains active and is significantly stronger than in the scarring setting

2) In the late stages of successful regeneration, TNFα/NFκB signalling is significantly upregulated in response to injury whereas late-stage TNFα/NFκB signalling is completely absent from the scarring response

a)

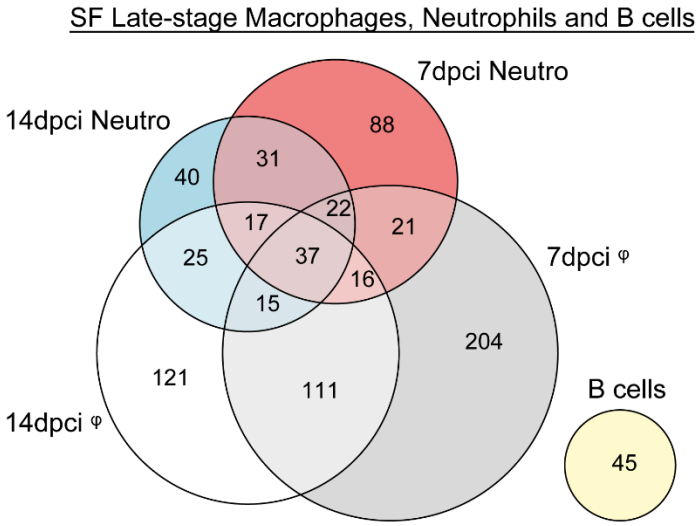
SF Late-stage Macrophages, Neutrophils and B cells
7dpci Neutro
14dpci Neutro
88
31
40
22
17
21
25
37
7dpci φ
16
15
204
121
111
B cells
14dpci φ
45

b)

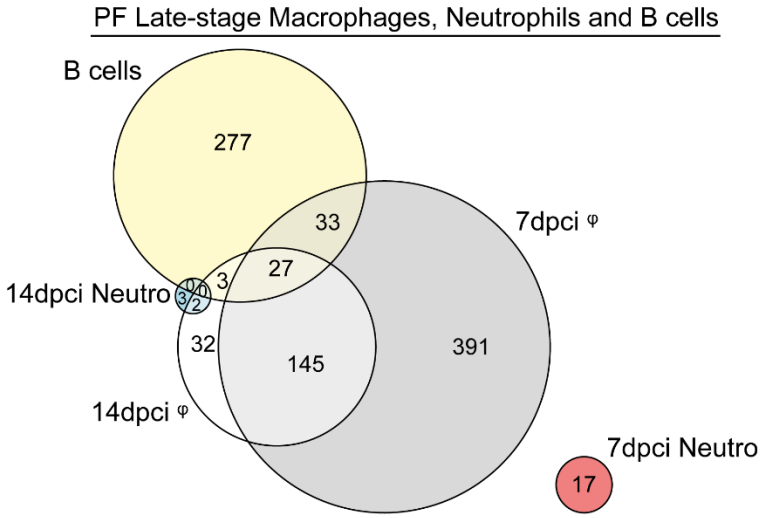
PF Late-stage Macrophages, Neutrophils and B cells
B cells
277
33
7dpci φ
27
3
14dpci Neutro
32
145
391
14dpci φ
7dpci Neutro
17

c)

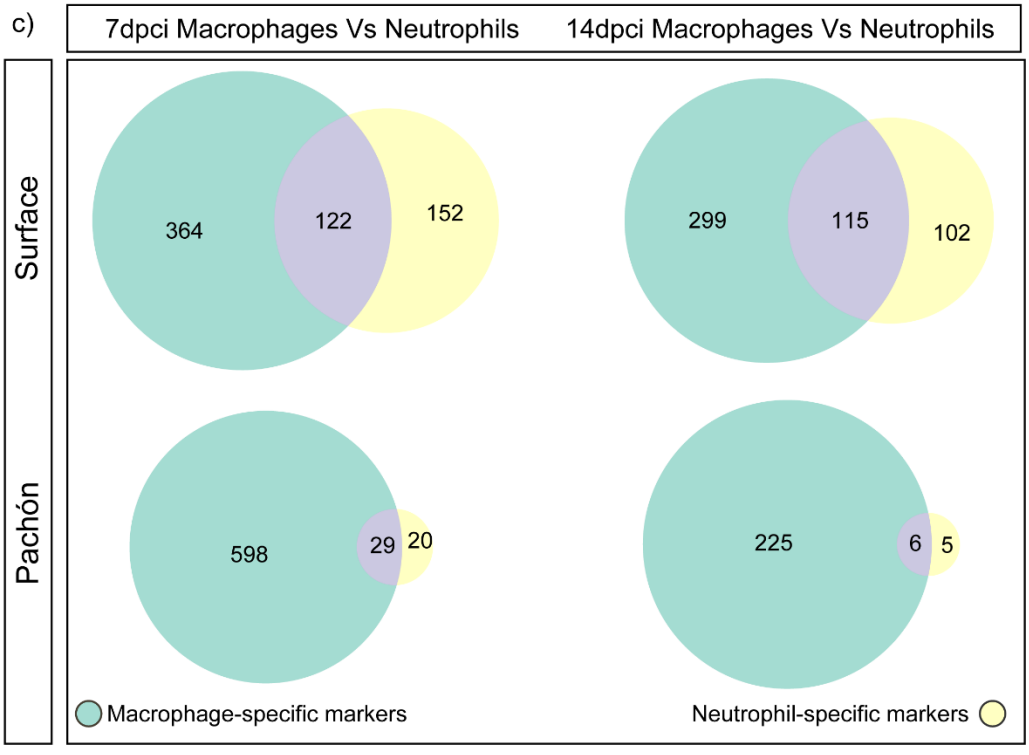
7dpci Macrophages Vs Neutrophils
14dpci Macrophages Vs Neutrophils
Surface
Pachón
364
122
152
299
115
102
598
29
20
225
6
5
Macrophage-specific markers
Neutrophil-specific markers

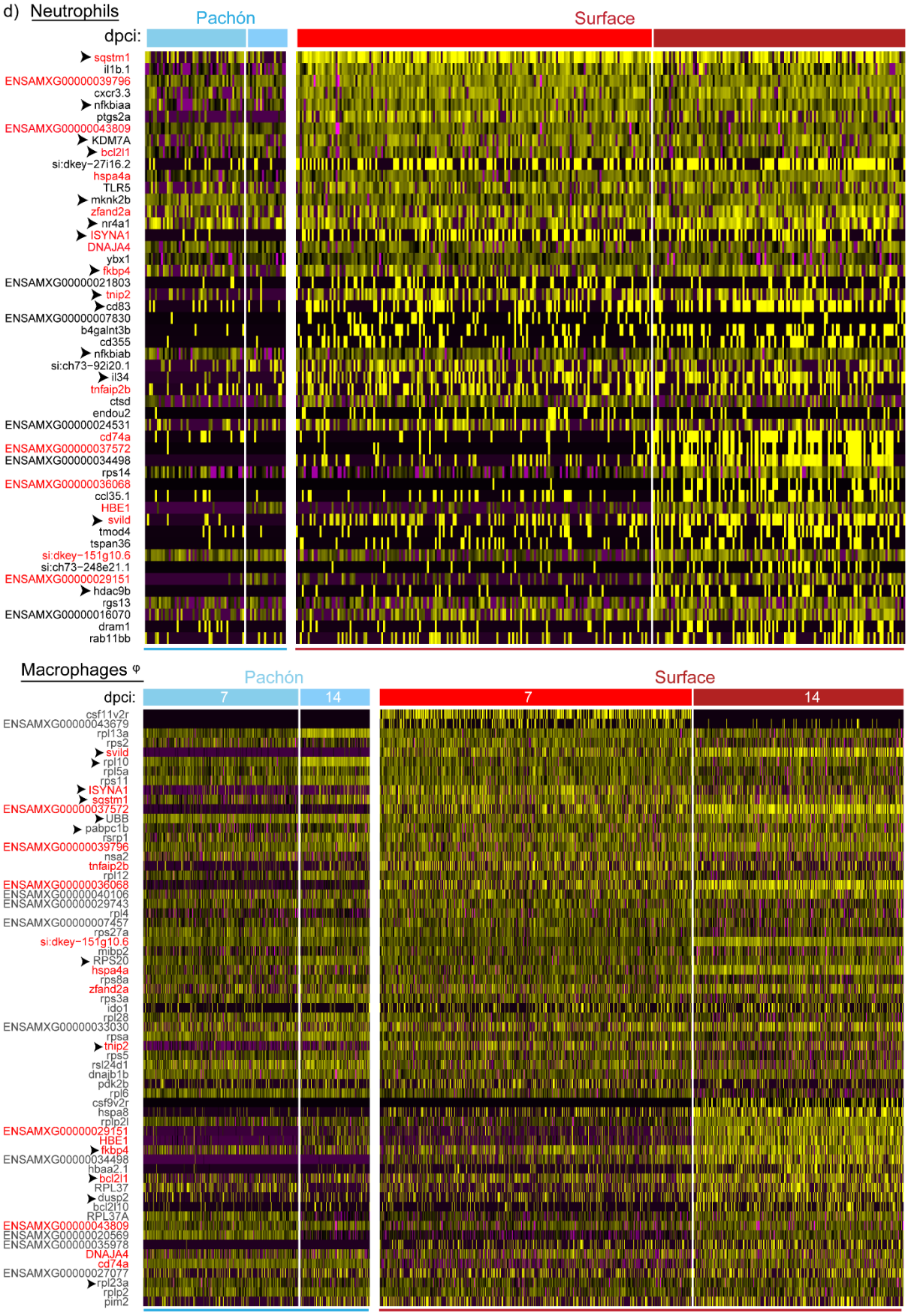
d) Neutrophils
Pachón
Surface
dpci:
sqstm1
il1b.1
ENSAMXG00000039796
cxcr3.3
nfkbiaa
ptgs2a
ENSAMXG00000043809
KDM7A
bcl2l1
si:dkey-27i16.2
hspa4a
TLR5
mknk2b
zfand2a
nr4a1
ISYNA1
DNAJA4
ybx1
fkbp4
ENSAMXG00000021803
tnip2
cd83
ENSAMXG00000007830
b4galnt3b
cd355
nfkbiab
si:ch73-92i20.1
il34
tnfaip2b
ctsd
endou2
ENSAMXG00000024531
cd74a
ENSAMXG00000037572
ENSAMXG00000034498
rps14
ENSAMXG00000036068
ccl35.1
HBE1
svild
tmod4
tspan36
si:dkey-151g10.6
si:ch73-248e21.1
ENSAMXG00000029151
hdac9b
rgs13
ENSAMXG00000016070
dram1
rab11bb
Macrophages φ
Pachón
Surface
dpci:
7
14
7
14
csf1v2r
ENSAMXG00000043679
rpl13a
rps2
svild
rpl10
rpl5a
rps11
ISYNA1
sqstm1
ENSAMXG00000037572
UBB
pabpc1b
rsrp1
ENSAMXG00000039796
nsa2
tnfaip2b
rpl12
ENSAMXG00000036068
ENSAMXG00000040106
ENSAMXG00000029743
rpl4
ENSAMXG00000007457
rps27a
si:dkey-151g10.6
mibp2
RPS20
hspa4a
rps8a
zfand2a
rps3a
ido1
rpl28
ENSAMXG00000033030
rpsa
tnip2
rps5
rsl24d1
dnajb1b
pdk2b
rpl6
csf9v2r
hspa8
rplp2l
ENSAMXG00000029151
HBE1
fkbp4
ENSAMXG00000034498
hbaa2.1
bcl2l1
RPL37
dusp2
bcl2l10
RPL37A
ENSAMXG00000043809
ENSAMXG00000020569
ENSAMXG00000035978
DNAJA4
cd74a
ENSAMXG00000027077
rpl23a
rplp2
pim2

Figure 5. 5: A distinct transcriptional profile is shared between late-stages SF neutrophils and macrophages, but not with B cells

(A) Euler plots analysing the overlap of top markers genes for SF 7dpci neutrophils, 14dpci neutrophils, 7dpci macrophages, 14dpci macrophages and B cells. (B) Euler plots analysing the overlap of top markers genes for PF 7dpci neutrophils, 14dpci neutrophils, 7dpci macrophages, 14dpci macrophages and B cells. (C) Euler plots analysing the overlap of top markers genes for late-stage neutrophils and macrophages show that a transcriptional profile is shared amongst late-stage leukocytes uniquely in the regenerative setting. (D) Heatmap of the top cell markers of late-stage SF neutrophils and macrophages reveals that many top markers are shared between neutrophils and macrophages (highlighted in red).

5.2.3 Is late-stage TNFα/NFκB signalling essential for successful regeneration in the SF?

To test whether late-stage TNFα/NFκB signalling critically regulates regenerative success in the SF, late-stage TNFα/NFκB signalling was inhibited *in vivo* so that it could be determined whether regeneration failed as a result. To interrogate the TNFα/NFκB signalling pathway, five treatment groups were used:

1) CAY10500 (a TNFα inhibitor)
2) DHMEQ (a NFκB inhibitor)
3) Ac-YVAD-cmk (an IL-1β inhibitor)
4) Leaukadherin-1 (a Mac-1 allosteric activator that prevents leukocyte recruitment to the wound by increasing the binding of leukocytes to the endothelium and preventing extravasation)
5) DMSO (vehicle control)

CAY10500 and DHMEQ were used to specifically interrogate the TNFα/NFκB pathway whilst Ac-YVAD-cmk was also used to inhibit inflammasome activation which is a major downstream effector

of inflammatory TNFα/NFκB signalling. Additionally, leukadherin-1 (LA-1) was used to act as a broad proof-of-principle study that would confirm whether the late-stage SF immune response critically regulates SF regenerative capacity (Fig. 5.6).

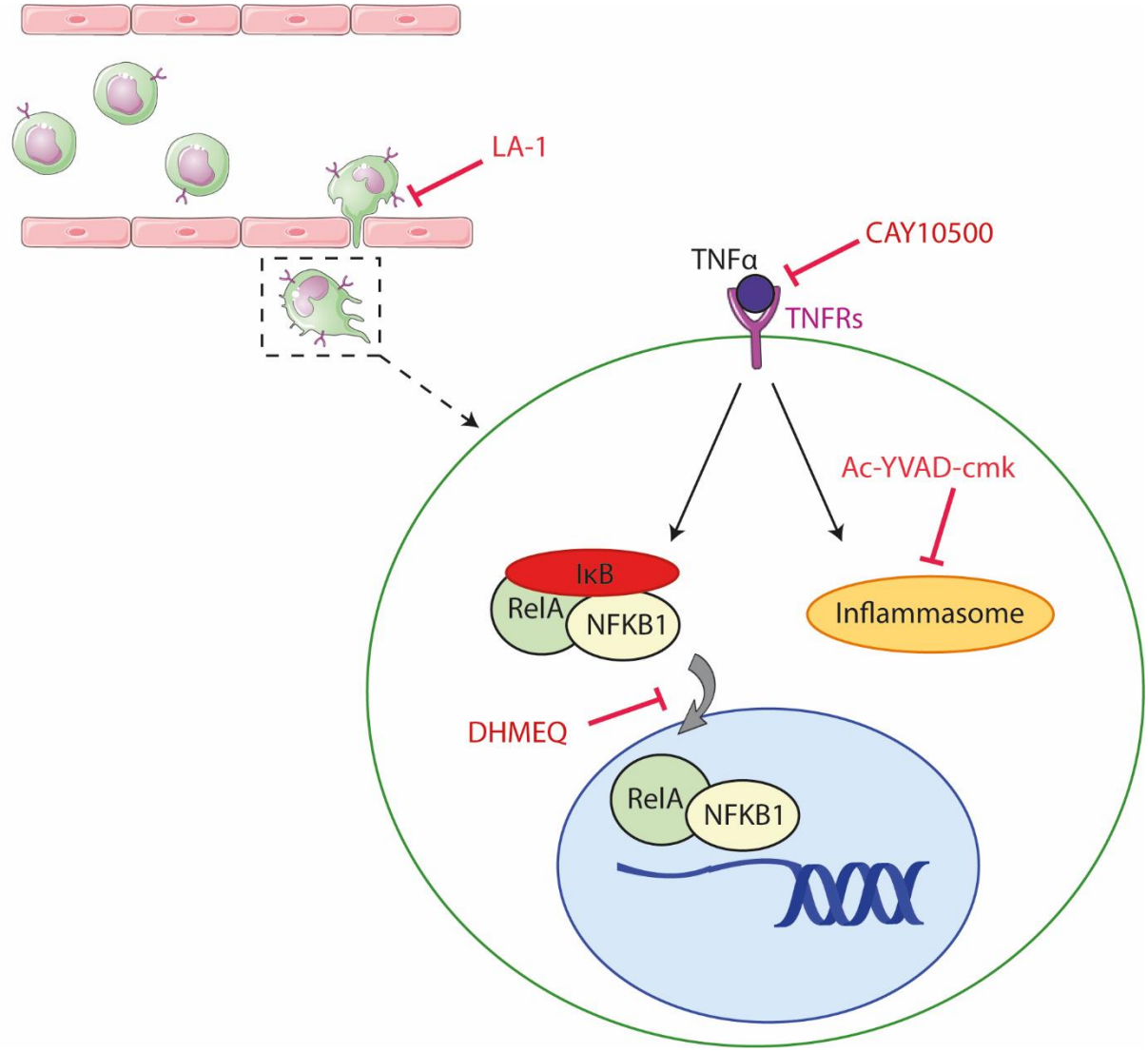

Figure 5. 6: Mechanism of action of LA-1, CAY10500, DHMEQ and Ac-YVAD-cmk

Inhibition of TNFα/NFκB signalling does not alter SF scar sizes

Cryoinjured SF were injected with inhibitor or vehicle control every 24 hours between 7-11dpci and hearts were collected at 21dpci to assess the degree of regeneration (Fig. 5.7a). The area of scar tissue in each heart was visualised using AFOG stain, a histological stain that visualises the collagenous scar in blue and healthy myocardium in orange (Fig. 5.7b). To assess for differences in

regenerative capacity, two independent and blinded measures of regeneration were calculated. Firstly, to compare scar sizes between groups, the ratio of total wound area: total ventricle area was calculated. Secondly, the length of open ventricle (i.e. compact wall disrupted by scar tissue) was measured and compared to the perimeter of the ventricle. The ratio of open wound: ventricle perimeter enabled the rate of regeneration to be compared as wounded tissue is gradually replaced with healthy myocardium from the 'outside in' (i.e. from the compact wall and inwards), making closure of the compact wall one of the first steps in successful regeneration. No difference in scar size or rate of regeneration was found between the DMSO-treated hearts and any of the inhibitor-treated hearts using either regenerative capacity measurement (Fig. 5.c&d). Therefore, these findings suggested that inhibition of the late-stage SF immune response and TNFα/NFκB signalling had no impact on the regenerative capacity of the SF.

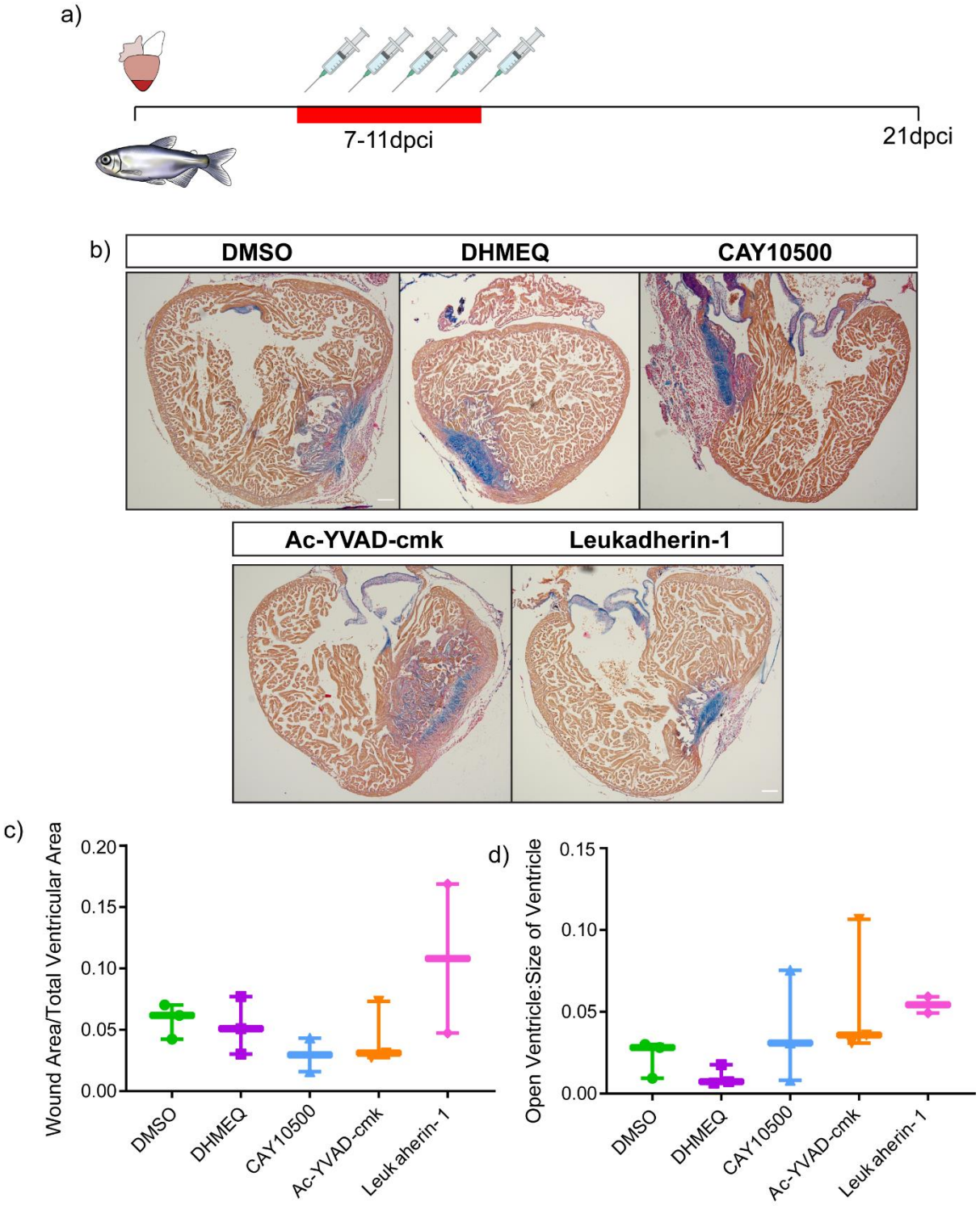

Figure 5. 7: Inhibition of TNFα/NFκB signalling at the late-stages of wound-healing has no impact on the SF regenerative capacity at 21dpci

(A) Overview of experimental design. (B) Representative AFOG images of the inhibitor-treated SF hearts at 21dpci. (C) The ratio of total wound size: total ventricle size was measured, revealing that

inhibitor treatment had no impact on scar size in comparison to DMSO control (1-way ANOVA with Dunnet's multiple comparisons test, n=3). (D) The ratio of open ventricle: ventricle perimeter, revealing that inhibitor treatment had no impact on scar size in comparison to DMSO control (1-way ANOVA with Dunnet's multiple comparisons test, n=3-9).

Inhibition of TNFα/NFκB signalling does not alter SF scar organisation

As discussed in the introduction, leukocytes are known to play a role in scar formation, remodelling and turnover during the reparative phase. Therefore, although inhibitor treatment did not significantly alter scar size, it was plausible that inhibitor treatment could have significantly altered the composition and organisation of the scar without affecting overall scar size.

To investigate whether inhibitor treatment resulted in changes to scar composition, AFOG images were assessed. AFOG stains different components of the scar in different colours: collagen is stained blue, fibrin stains red, whilst blood clots and cellular debris stain brown. Therefore, the area of each scar was measured, and its components were quantified using colour thresholding in ImageJ. SF scars were analysed for the percentage of collagen content (Fig. 5.8a); fibrin content (Fig. 5.7b) and for blood clot/debris content (Fig. 5.8c) and composition comparisons were made between each treatment group. This analysis showed that inhibitor treatment did not significantly alter the ECM composition of the scar at 21dpci. Therefore, scar organisation was next investigated.

To assess whether the organisation and alignment of collagen fibres within the scar was disrupted by inhibitor treatment, the 21dpci hearts were stained with Pico-Sirius red, a histological stain that, when visualised using polarised light microscopy, enables the orientation and properties of collagen fibres to be determined (Fig. 5.8d). Quantification of the Pico-Sirius red images showed that there was no difference in scar organisation between inhibitor treatment groups in terms of collagen fibre straightness (Fig. 5.8e), collagen fibre angle (Fig. 5.8f) and co-alignment of collagen fibres (Fig. 5.8g).

Therefore, analysis of the 21dpci inhibitor-treated hearts with both AFOG and Pico-Sirius red staining suggested that TNFα, NFκB and IL-1β signalling are not required for regenerative success or scar organisation. Additionally, these results suggested that the immune response between 7-11dpci is not essential for regenerative success in the SF.

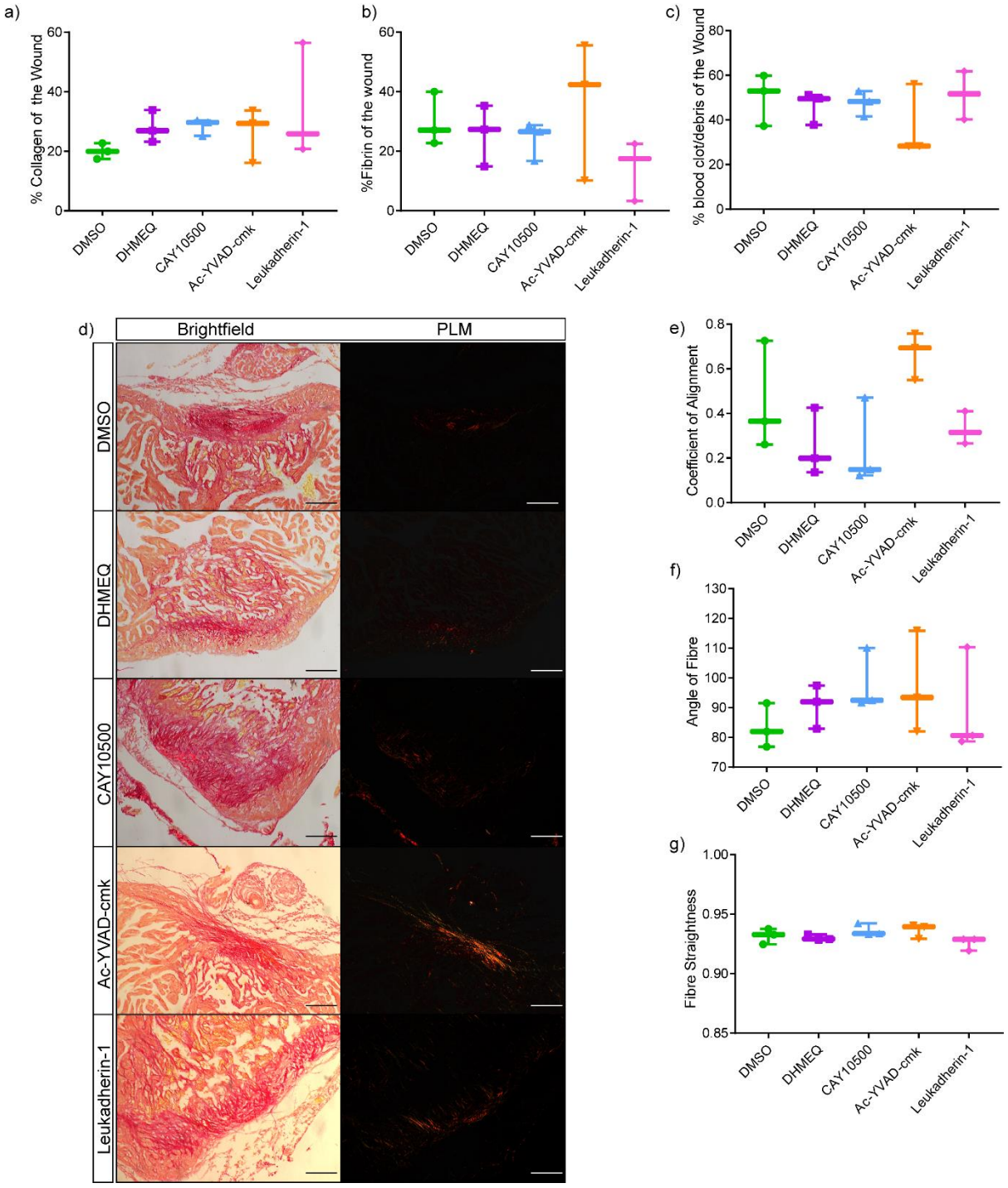

Figure 5. 8: Inhibition of TNFα/NFκB signalling at the late-stages of wound-healing has no impact on scar deposition and organisation

AFOG images from 21dpci inhibitor-treated SF hearts were measured to assess scar composition. (A) The percentage collagen content (blue staining) of scar was measured for each inhibitor treatment group. (B) The percentage fibrin content (red staining) of scar was measured for each inhibitor treatment group. (C) The percentage blood clot/cellular debris (orange/brown staining) was measured for each inhibitor treatment group. (D) Representative images of Pico-Sirius Red staining imaged using the brightfield and polarised light (PLM= polarised light microscopy). Collagen fibres visualised using PLM were assessed using CT-FIRE for their degree of alignment (E); fibre angle (F); and fibre straightness (G). Comparisons between groups were analysed for significance using a 1-way ANOVA with Dunner's multiple comparisons test, n=3.

Although the results of the inhibitor experiment suggested that inflammation and the immune response were not essential to regeneration, none of the inhibitors used in this study had previously been tested in the AM and had only been used in either the zebrafish or mouse. Therefore, one possible explanation for the observed lack of difference in regenerative capacity and scar deposition was that DHMEQ, CAY10500, Ac-YVAD-cmk and LA-1 were not functioning effectively in the AM model. This apparent lack of activity of DHMEQ, CAY10500, Ac-YVAD-cmk and LA-1 could be caused by a multitude of reasons such as incorrect dosage; lack of expression of drug target; or insufficient protein homology between the AM, zebrafish, and mouse conservation for effective binding. Therefore, the next logical step was to validate whether each inhibitor was able to successfully inhibit its target in the AM.

LA-1 had previously been shown to effectively inhibit leukocyte extravasation in the zebrafish at the concentration used in this study. To test for effective inhibition of leukocyte extravasation by LA-1 in the AM, 21dpci SF hearts were stained with lyz, an antibody that will detect

granular-like cells (Fig. 5.9a). Lyz+ cell counts, however, showed no difference in the number of granular-cells present in DMSO-treated hearts and LA-1-treated hearts (Fig. 5.9b), suggesting that LA-1 does not work effectively to prevent leukocyte extravasation in the AM. Additionally, the influx of lyz+ cells was not disrupted by any of the tested inhibitors (Fig. 5.9b), suggesting that none of the inhibitors disrupted leukocyte recruitment.

These results showed that, as LA-1 does not function effectively in the AM, it cannot be concluded whether late-stage SF leukocytes are required for successful regeneration.

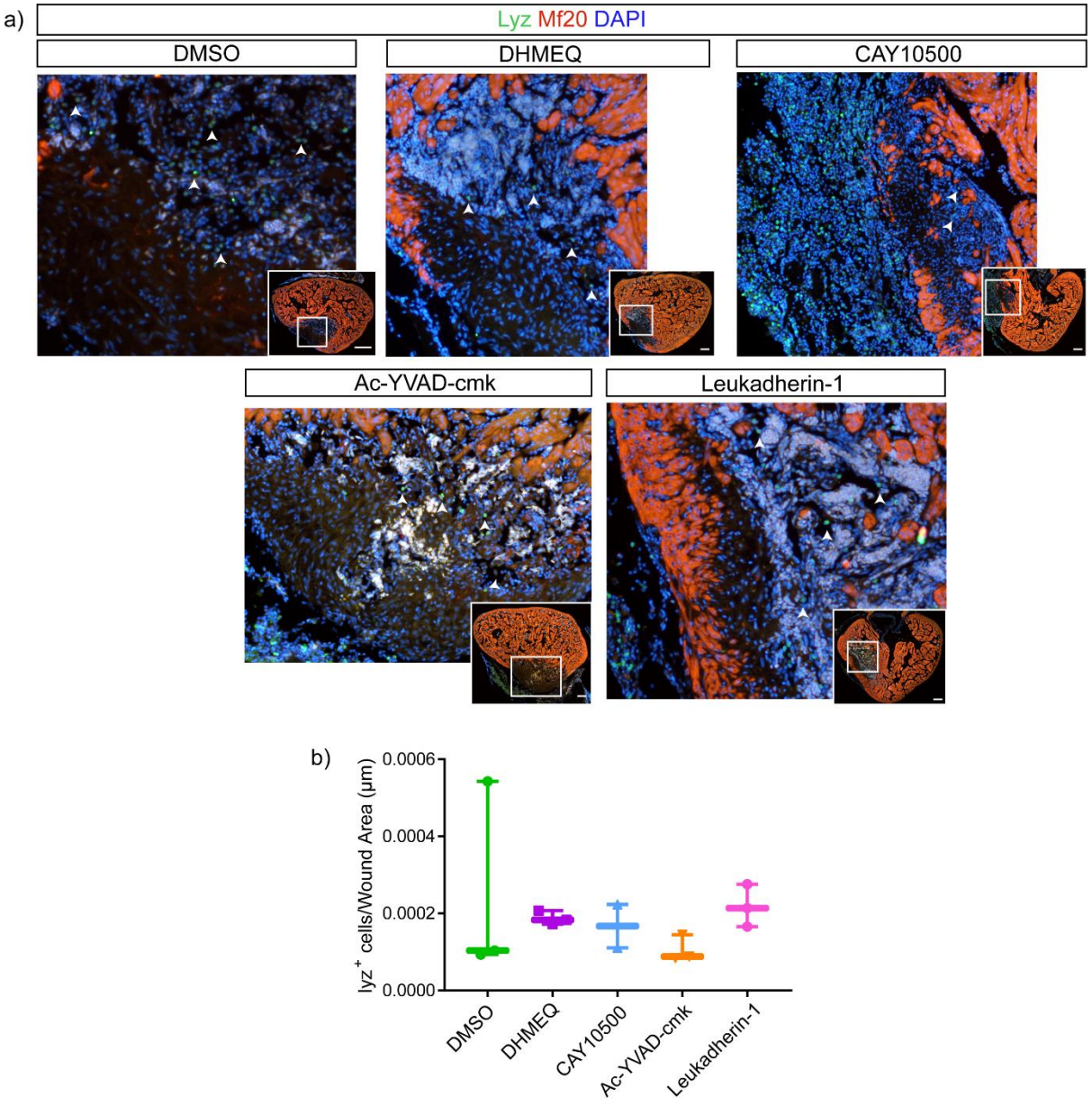

Figure 5. 9: Leukadherin-1 administration by ip injection between 7-11dpci does not effectively inhibit leukocyte extravasation into SF hearts

(A) Representative images of Lyz antibody staining in the inhibitor-treated 21dpci SF hearts. Hearts were counter-stained with MF20 and DAPI. (B) lyz+ cells present in the wound were counted and normalised to wound area. Cell counts were tested for significant differences between DMSO control samples and inhibitor-treated samples (1-way ANOVA with Dunner's multiple comparison's test, n=3).

To interrogate whether CAY10500, DHMEQ and Ac-YVAD-cmk were able to effectively inhibit TNFα/NFκB/IL-1β signalling, an RNAseq approach was adopted so that differences in the TNFα/NFκB/IL-1β signalling pathways could be probed. Specific upregulation of TNFα/NFκB signalling has not been observed previously in the late stages of regeneration in the zebrafish. Therefore, two sets of inhibitor-treated hearts were prepared: 1) hearts that received early-stage inhibition of TNFα/IL-1β/NFκB signalling to act as positive controls; and 2) hearts that received late-stage inhibition of TNFα/ IL-1β/NFκB signalling (Fig. 5.10a). Following RNA isolation and high-throughput sequencing, an initial comparison of the RNAseq data was performed using PCA to compare the sources of overall variance in each treatment group. The PCA plot revealed that all late-stage inhibitor samples clustered together and almost all early-stage inhibitor samples clustered together, whilst DMSO control samples did not cluster separately from the inhibitor samples (Fig. 5.10b). If the inhibitors were functioning effectively, the DMSO and inhibitor-treated samples would be expected to cluster separately on the PCA plot. Therefore, from this lack of variance, I concluded that DHMEQ, CAY10500 and Ac-YVAD-cmk do not work sufficiently in the AM to inhibit their targeted pathways.

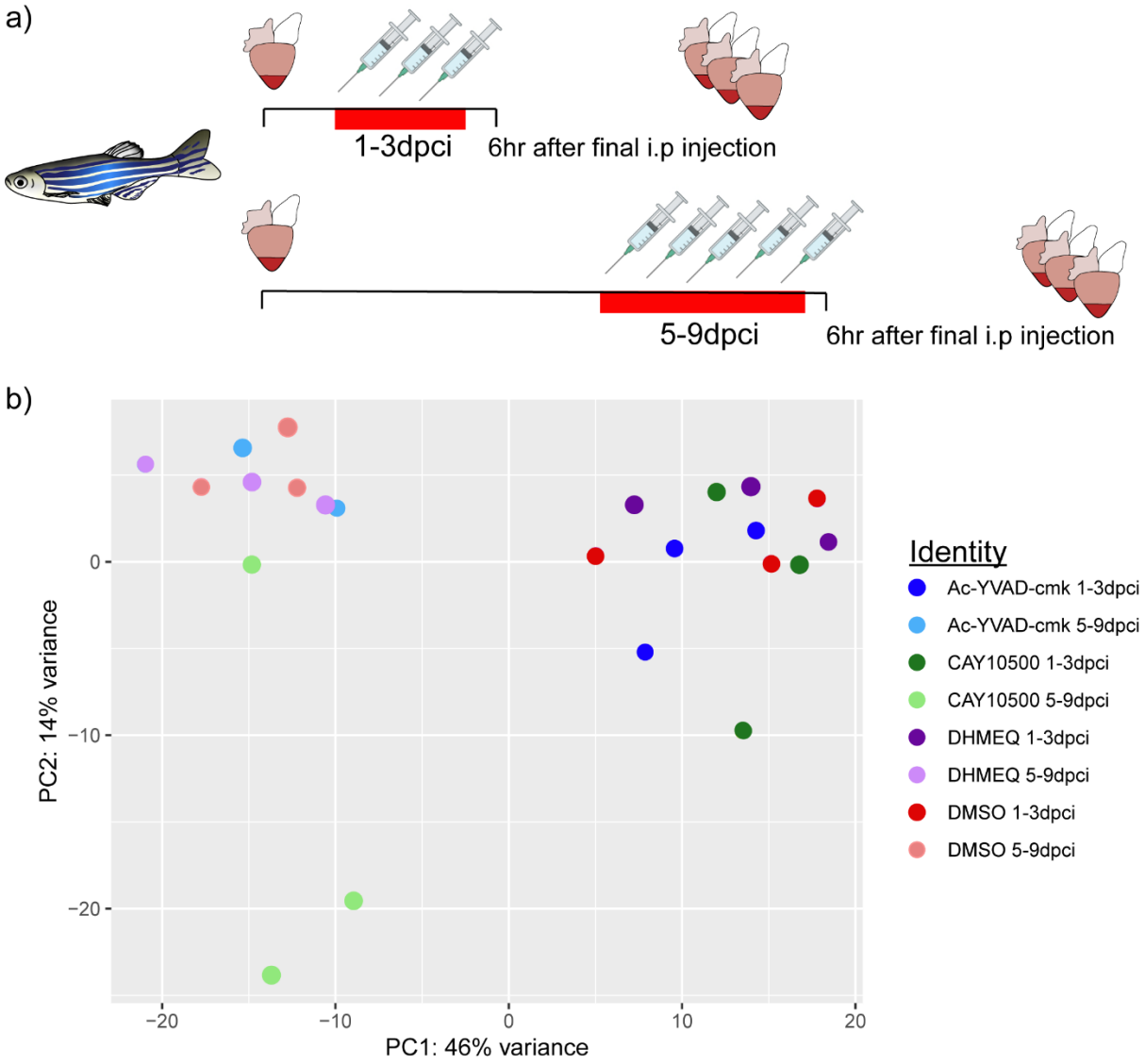

Figure 5. 10: RNAseq data of inhibitor-treated zebrafish shows that Ac-YVAD-cmk, CAY10500 and DHMEQ do not function effectively to inhibit TNFα/NFκB signalling in the heart following ip injection

(A) Overview of the RNAseq experimental design. (B) PCA plot comparing the main sources of variation in the RNAseq dataset reveals that control- and inhibitor-treated hearts are very similar.

5.2.4 Late-stage inflammation is critical for scar formation

Using specific TNFα/NFκB/IL-1β inhibitors to disrupt late-stage inflammation had proved to be ineffective. Therefore, I next sought to use a broad anti-inflammatory agent to inhibit late-stage

TNFα/NFκB signalling in the SF to determine whether late-stage inflammation is essential for regenerative success.

Glucocorticoid agonists are broad anti-inflammatory agents that have been used extensively to suppress inflammation and the immune response[105,302]. Therefore, I designed the following experiment: SF fish were cryoinjured and exposed to Dexamethasone in the water at 100µM every day between 7-14dpci, with Dexamethasone being replenished every 24 hours. Hearts were then collected at 30- and 60dpci to assess whether inhibition of late-stage SF inflammation had inhibited scar resorption and regenerative capacity (Fig. 5.11a). As has been done for the previous inhibitor experiment, collected hearts were stained with AFOG (Fig. 5.11b) and differences in wound size (Fig. 5.11c&d) and open wound: ventricle perimeter (Fig. 5.11e&f) were measured.

At both 30- and 60dpci, no difference in regenerative capacity was observed between Dexamethasone-treated and control samples, although a general trend was observed that Dexamethasone treatment resulted in larger wound sizes at 60dpci (Fig. 5.11d). Therefore, these results suggested that inhibition of late-stage SF inflammation does not result in significantly different wound sizes or rates of wound closure.

However, during analysis, it was observed that Dexamethasone-treated scars seemed to be structurally different from control hearts and were characterised by a thick region of collagen at the edge of the ventricle, suggesting that Dexamethasone treatment might result in structurally different collagen scars.

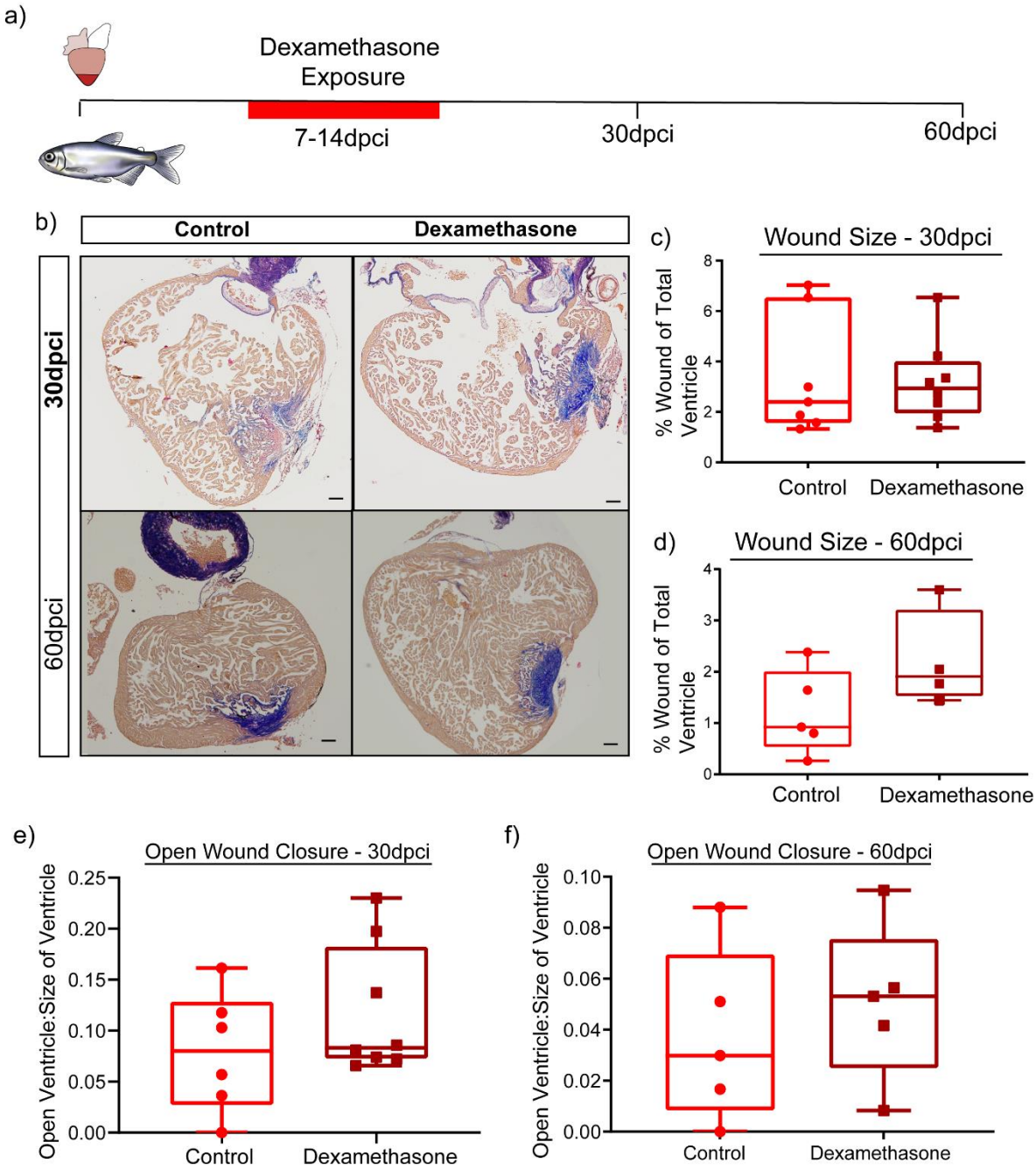

Figure 5. 11: Dexamethasone treatment between 7-14dpci does not inhibit regeneration in the SF

(A) Schematic of experimental design for Dexamethasone exposure. Cryoinjured fish were randomly assigned to one of four groups: 30dpci control, 30dpci Dex, 60dpci control and 60dpci Dex. Between 7-14dpci, control fish were placed in tanks with fresh system water every 24 hours whilst Dexamethasone fish were placed in tanks with Dexamethasone water at 100µM. Hearts were collected at 30dpci and 60dpci. (B) Representative images of AFOG staining. Scale bar represents 100µm. AFOG sections were quantified for wound size at 30dpci (C) and at 60dpci (D); and for open

ventricle: ventricle perimeter at 30dpci (E) and at 60dpci (F). For 30dpci, n=7-8; for 60dpci, n=5. Student's t-test was used to assess statistical significance.

To test whether Dexamethasone treatment had induced the deposition of a significantly different scar from control samples, control and Dexamethasone-treated hearts were first assessed for differences in scar composition. By 30- and 60dpci, the AM scar mainly consists of collagen and so the collagen content of each scar was quantified. Although Dexamethasone-treated scars were not significantly different in percentage collagen content from control samples, a general trend was observed that at both 30- (Fig. 5.12a) and 60dpci (Fig. 5.12b), Dexamethasone-treated samples had consistently greater collagen content. Therefore, these results suggested that inhibition of late-stage SF inflammation might disrupt scar formation and promote the increased deposition of collagen fibres.

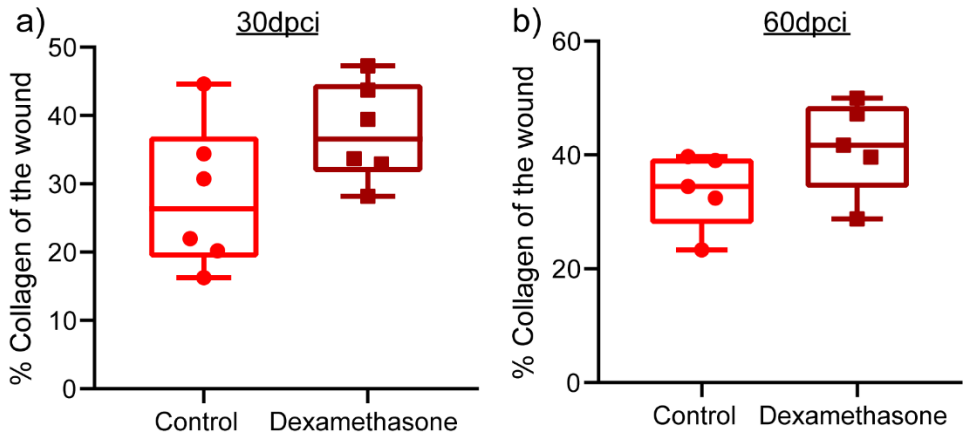

Figure 5. 12: Dexamethasone treatment between 7-14dpci does not significantly alter collagen content of SF scars

The collagen content of SF scars was analysed from AFOG images by measuring the area of blue staining and calculating the percentage of this staining from the overall wound area. Wounds were measured for percentage collagen content at (A) 30dpci and (B) 60dpci. n=6 for 30dpci, n=5 for 60dpci.

Next, the structural organisation of collagen fibres in control and Dexamethasone-treated samples was assessed using Pico-Sirius red staining (Fig. 5.13a&b). No differences were found in collagen fibre angle, straightness or co-alignment at 30dpci (Fig. 5.13c). At 60dpci, although not significant, collagen fibres in Dexamethasone-treated scars were observed to be straighter than controls. Additionally, Dexamethasone-treated scars were found to be significantly disrupted in the organisation of their collagen fibres which were significantly less aligned than controls and closely resembled time-matched PF scars in their alignment (Fig. 5.13d). Therefore, this data suggested that late-stage inflammation is involved in the organisation and orientation of collagen fibres as its inhibition leads to significantly altered scar alignment.

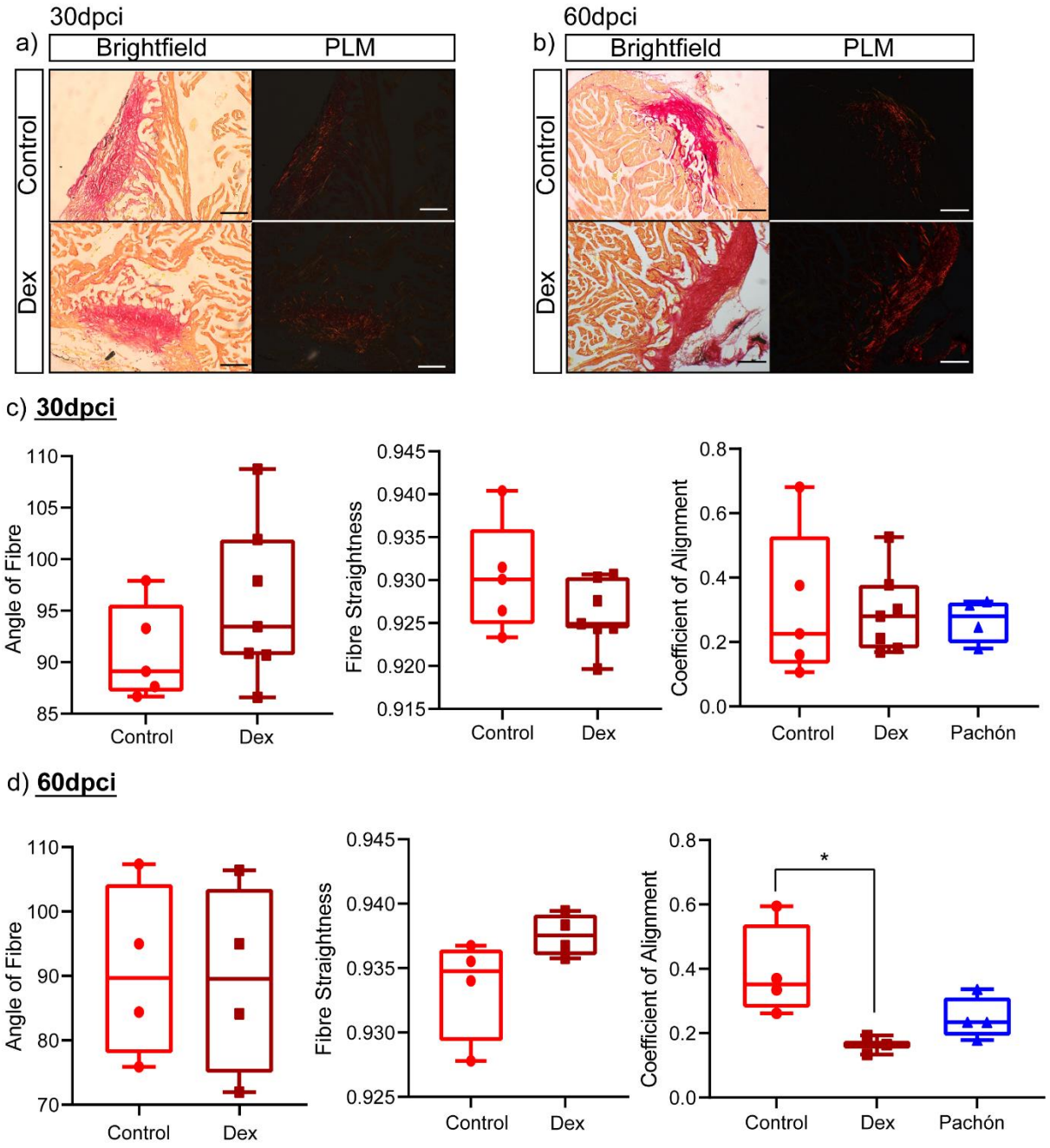

Figure 5. 13: Pico-Sirius red staining of Dexamethasone-treated scars suggests late-stage inflammation is essential for scar organisation

Representative images of Pico-Sirius Red staining captured using brightfield and polarised lighted at (A) 30dpci and (B) 60dpci. Polarised light microscopy images were analysed using CT-FIRE software to extract and quantify the angle, straightness and co-alignment of collagen fibres in (C) 30dpci and (D) 60dpci scars (1-way ANOVA with Dunnet's multiple comparisons test, n=3-7).

5.2.5 Cell-cell signalling is drastically reduced by 14dpci in the PF but not in the SF, especially amongst macrophages, neutrophils and B cells

To probe whether late-stage neutrophils, macrophages and B cells might be regulating scar formation in the SF, I performed ligand-receptor (LR) analysis to explore whether PF and SF leukocytes were interacting with scar forming cells during the late-stages of cardiac healing. To perform LR analysis, AM genes were converted into their mouse homologs and a network of ligand-receptor interactions was built using the STRING database that enabled the weight of cell-cell interactions to be calculated. First, the cell-cell interactions throughout PF/SF hearts at 7- and 14dpci were analysed. This showed that in both the PF and SF, fibroblasts and collagen-producing macrophages form distinct signalling hubs and interact with a variety of cardiac cells, with fibroblasts emerging as a key regulator of cellular cross-talk in both SF and PF hearts (Fig. 5.14a,b,c&d). To pull out the interactions made between neutrophils, macrophages, B cells and all other cardiac cell types, the analysis was filtered for these cells of interest. This found that PF and SF showed similar levels of cellular communication at 7dpci (Fig. 5.14e). However, at 14dpci, I found that collagen-producing macrophages were no longer communicating with other cells in the PF, whereas in the SF, collagen-producing macrophages were still acting as a dominant signalling hub and made many connections with various cardiac cells including scar-forming cells (i.e. fibroblasts and myofibroblasts, Fig. 5.14f). This could suggest that at the late-stages of cardiac healing, scar formation via macrophage-mediated collagen deposition becomes dysregulated in the PF whereas, in the SF, collagen-producing cells are still actively integrating numerous signals from across the heart to regulate scar deposition. Additionally, late-stage PF leukocytes showed a striking decrease in cellular communication both from 7dpci PF leukocytes and from 14dpci SF leukocytes (Fig. 5.14f), suggesting that by 14dpci, PF leukocytes are playing a much smaller role in orchestrating cardiac repair than their SF counterparts.

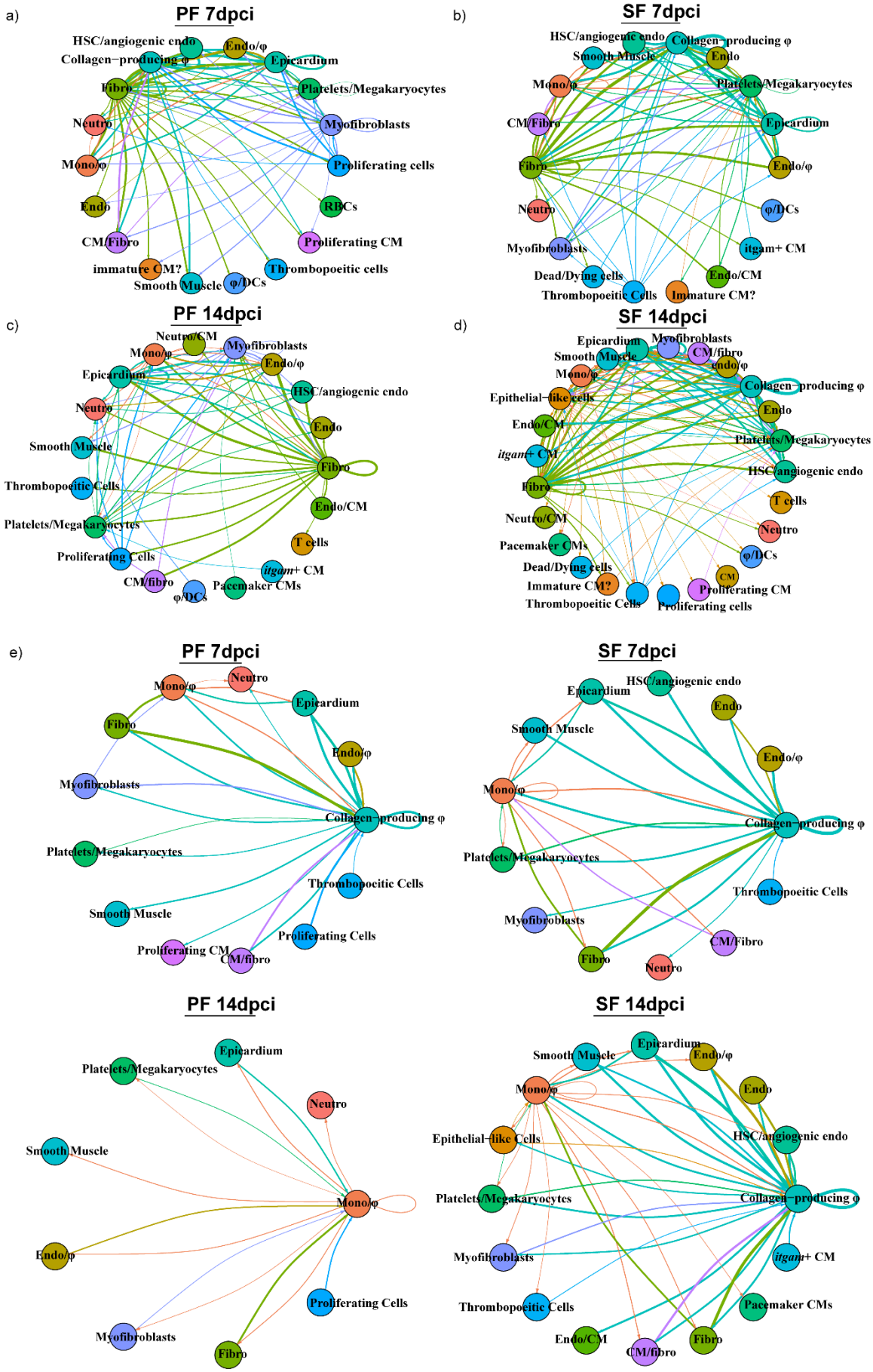
a)
PF 7dpci
HSC/angiogenic endo
Endo/φ
Collagen−producing φ
Epicardium
Fibro
Platelets/Megakaryocytes
Neutro
Myofibroblasts
Mono/φ
Proliferating cells
Endo
RBCs
CM/Fibro
Proliferating CM
immature CM?
Thrombopoeitic cells
Smooth Muscle
φ/DCs
b)
SF 7dpci
HSC/angiogenic endo
Collagen−producing φ
Smooth Muscle
Endo
Mono/φ
Platelets/Megakaryocytes
CM/Fibro
Epicardium
Fibro
Endo/φ
Neutro
φ/DCs
Myofibroblasts
itgam+ CM
Dead/Dying cells
Endo/CM
Thrombopoeitic Cells
Immature CM?
c)
PF 14dpci
Neutro/CM
Myofibroblasts
Mono/φ
Endo/φ
Epicardium
HSC/angiogenic endo
Neutro
Endo
Smooth Muscle
Fibro
Thrombopoeitic Cells
Endo/CM
Platelets/Megakaryocytes
T cells
Proliferating Cells
itgam+ CM
CM/fibro
Pacemaker CMs
φ/DCs
d)
SF 14dpci
Epicardium
Myofibroblasts
Smooth Muscle
CM/fibro
Mono/φ
endo/φ
Epithelial−like cells
Collagen−producing φ
Endo
Endo/CM
Platelets/Megakaryocytes
itgam+ CM
HSC/angiogenic endo
Fibro
T cells
Neutro/CM
Neutro
Pacemaker CMs
φ/DCs
Dead/Dying cells
CM
Immature CM?
Proliferating CM
Thrombopoeitic Cells
Proliferating cells
e)
PF 7dpci
Mono/φ
Neutro
Epicardium
Fibro
Endo/φ
Myofibroblasts
Collagen−producing φ
Platelets/Megakaryocytes
Thrombopoeitic Cells
Smooth Muscle
Proliferating Cells
Proliferating CM
CM/fibro
SF 7dpci
Epicardium
HSC/angiogenic endo
Endo
Smooth Muscle
Endo/φ
Mono/φ
Collagen−producing φ
Platelets/Megakaryocytes
Thrombopoeitic Cells
Myofibroblasts
CM/Fibro
Fibro
Neutro
PF 14dpci
Epicardium
Platelets/Megakaryocytes
Neutro
Smooth Muscle
Mono/φ
Endo/φ
Proliferating Cells
Myofibroblasts
Fibro
SF 14dpci
Epicardium
Smooth Muscle
Endo/φ
Mono/φ
Endo
Epithelial−like Cells
HSC/angiogenic endo
Platelets/Megakaryocytes
Collagen−producing φ
Myofibroblasts
itgam+ CM
Thrombopoeitic Cells
Pacemaker CMs
Endo/CM
CM/fibro
Fibro

Figure 5. 14: Ligand-Receptor analysis reveals that intercellular communication is drastically decreased at 14dpci in late-stage PF leukocytes

Cell-cell communication plots for entire PF hearts at (A) 7dpci and (B) 14dpci; and for entire SF hearts at (C) 7dpci and (D) 14dpci. (E) Filtered cell-cell communication plots for macrophages, neutrophils and B cells reveal that 14dpci PF leukocytes show a drastic reduction in their intercellular signalling.

5.3 Discussion

Since the 5th Century BC, inflammation has been recognised as an essential part of wound healing. However, a central characteristic of inflammation is that it occurs immediately after injury to recruit leukocytes to the wound and then is swiftly resolved. Numerous modern-day diseases have revealed that inflammation that is not limited to immediately after injury (i.e. is chronic or dysregulated) is 'bad' and can drive tissue damage, fibrosis and pathological remodelling. In this chapter, using scRNAseq and *in situ* hybridisation I have shown, for the first time, that inflammatory signalling during the late-stages of wound healing is not necessarily prohibitive of successful repair whilst the inhibition of late-stage inflammation disrupts scar organisation and may lead to the formation of permanent scars.

5.3.1 TNFα/NFκB signalling is uniquely upregulated in late-stage SF immune cells

The TNFα/NFκB signalling pathway is a pro-inflammatory pathway that results in the upregulation of inflammatory cytokines like TNFα, IL-6, IL-18 and IL-1β. Previously, the TNFα/NFκB signalling pathway has been reported to be activated immediately after MI in response to necrotic cell death and PRR activation[299,303]. However, here I have found, using MAST testing and PROGENy analysis, that TNFα/NFκB pathways are upregulated in late-stage SF leukocytes and show the highest levels of activity at 7- and 14dpci. This finding is completely novel as it suggests that late-stage SF leukocytes are inflammatory, and it contradicts the widely held belief that swift resolution of inflammation is essential for regenerative success. Furthermore, the finding that TNFα/NFκB signalling is higher during the late stages of cardiac healing than the early stages is additionally novel

as previous reports of TNFα levels post-MI have found [TNFα] to peak at 1dpci and fall to baseline by 7dpci[304]. Therefore, the identification of late-stage inflammatory neutrophils and macrophages in the SF represents a distinct divergence from the classical understanding of inflammatory neutrophil and macrophage dynamics which are reported to peak between 1-3dpi. The emergence of TNFα/NFκB+ cells uniquely between 7-14dpci suggests that these cells may not be the typical pro-inflammatory neutrophils and macrophages associated with TNFα/NFκB signalling but could be novel populations, adding to the ever-increasing complexity of post-MI neutrophil and macrophage heterogeneity. Therefore, future studies should aim to further characterise these new leukocyte subsets and explore their possible roles within the regenerative setting

In addition to finding TNFα/NFκB to be uniquely upregulated in late-stage SF leukocytes, counts of *tnfa*+ and *nfkb2*+ cells revealed that inflammatory cells remain elevated at 30dpci in the SF, suggesting that successful regeneration is associated with sustained TNFα/NFκB inflammatory signalling between 7-30dpci. This finding is remarkable as previous studies have well-established that sustained and elevated levels of TNFα are detrimental to the injured heart: CHD and HF patients display elevated levels of TNFα months after MI[305,306] whilst decreasing TNFα levels has been documented to improve cardiac function in HF patients[307]. Additionally, chronic NFκB activation has been shown to drive the pathology of a range of inflammatory diseases such as rheumatoid arthritis, inflammatory bowel disease, multiple sclerosis and atherosclerosis[299], whilst NFκB activation post-MI results in increased fibrosis, inflammation, adverse remodelling and cardiomyocyte death[308]. In contrast, the data presented in this chapter suggests that sustained TNFα/NFκB signalling could have potentially pro-regenerative roles. Due to the inactivity of CAY10500 and DHMEQ, I haven't been able to specifically probe the function of late-stage TNFα/NFκB+ leukocytes in regeneration. However, activation of the TNFα/NFκB pathway in neutrophils has already been shown to induce the expression of *mmp9*, a classical matrix remodelling enzyme[309]. Therefore, future research should aim to explore the functional role of sustained TNFα/NFκB signalling in late-stage leukocytes to determine how it links to regenerative success.

5.3.2 Late-stage SF leukocytes may be upregulating a pro-regenerative gene program

In addition to the distinct timing of TNFα/NFκB upregulation in SF leukocytes, I found that many of the injury-responsive genes upregulated during the late-stages of cardiac healing were shared between SF neutrophils and macrophages. This could suggest that SF leukocytes are commonly activating a pro-regenerative gene program (PRP) in response to cardiac injury that is specifically promoting the regenerative response. So far, a PRP of 49 genes has already been identified in the zebrafish and killifish that drives regeneration of the caudal fin and heart but is weakly activated in the non-regenerative mouse[30]. Critically, the authors showed that when PRP activation was inhibited, regeneration failed, suggesting that the regenerative response critically relies on gene programs that are activated in response to cardiac injury. Recently, several groups have identified regenerative-responsive enhancers (RREs) that drive injury-dependent gene expression and may be responsible for the activation of PRPs[143,310–317]. Indeed, activation of the 49-gene PRP was inhibited by mutating its RRE, whilst the orthologous human version of the RRE was unable to drive gene expression and contained numerous nucleotide changes in its sequence. This has led to the hypothesis that mechanisms of regeneration may be conserved across the animal kingdom due to the activation of RREs which, during evolution, have become mutated in regenerative-incompetent models, resulting in silent RREs and failed regeneration. This theory particularly fits with the regenerative competent and incompetent SF/PF populations which have faced drastically different selection pressures as they have adapted to their river- and cave-environments. Therefore, it could be possible that the PF have mutated RREs that prevent their regeneration, explaining why their late-stage leukocytes displayed very few overlapping injury-responsive genes. Furthermore, the unique upregulation of TNFα/NFκB may in fact be responsible for PRP activation as the 49-gene PRP present in the zebrafish and killifish was activated by AP-1, a transcription factor that is downstream of TNFα/NFκB signalling[318–320]. Therefore, future studies should aim to investigate whether the shared expression of injury-responsive genes in SF neutrophils and macrophages is linked to activation of a RRE and could represent a TNFα/NFκB-mediated PRP.

5.3.3 Late-stage inflammation might be essential to scar organisation

Previously, glucocorticoids have been used successfully to inhibit regeneration when administered immediately after injury[105]. Here, however, I have found that inhibiting inflammation during the late stages of SF cardiac healing does not seem to impair SF regeneration. This could suggest that the initial hypothesis that late-stage inflammation is essential for SF regeneration was wrong. However, one possible explanation for why there was no difference in regenerative capacity following Dexamethasone treatment could be that 30dpci and 60dpci timepoints are too early for impaired regenerative capacity in the SF to be distinguished. Indeed, although not significant, Dexamethasone-treated SF hearts at 60dpci had generally larger wounds than controls which displayed a greater percentage of collagen deposition. Thus, it is tempting to speculate that inhibition of late-stage inflammation does result in impaired SF regenerative capacity which is, however, not apparent until later time points when most of the scar has been degraded. Therefore, future experiments should isolate Dexamethasone-treated hearts at 90dpci to fully determine whether SF regenerative capacity is altered by inhibition of inflammation between 7-14dpci.

Additionally, I have shown that Dexamethasone treatment significantly disrupted scar organisation, resulting in the formation of 60dpci scars which are significantly less aligned in their collagen fibres than control samples. Strikingly, comparison of Pico-Sirius red staining from Dexamethasone-treated samples resembled time-matched PF scars in their collagen fibre alignment, suggesting that scars which show misaligned collagen fibres might be more difficult to resorb than coaligned scars and result in regenerative failure. Indeed, the organisation of the collagen scar has already been shown to be key to regenerative capacity as the axolotl fails to regenerate its heart following macrophage ablation due to the formation of a highly-cross linked scar, even though cardiomyocyte proliferation is unaffected[104]. However, failure to regenerate has so far been associated with highly aligned collagen scars in the axolotl and non-regenerative mouse, whereas the partially regenerative spiny mouse (*Acomys*) forms a disorganised collagen scar[321–323] post-MI. As a result, the current consensus within the field is that scars which are co-aligned and have the same

orientation of collagen fibres offer greater tensile strength to the heart but are harder to resorb, resulting in permanent scarring. Therefore, the organisation of the SF/PF and Dexamethasone treated scars are at odds with other regenerative-competent and -incompetent models.

One possible explanation to explain these contradictory results is that teleost, amphibian, and mammalian hearts are significantly different in their size and mechanical properties. Therefore, scar organisation that is beneficial to the mammal/amphibian heart may in fact not be relevant to the teleost heart. For instance, the disorganised *Acomys* scar is associated with increased angiogenesis and the authors suggested that a loosely-compacted scar was beneficial to *Acomys* cardiac healing as it enabled newly forming blood vessels to infiltrate the wound. However, revascularisation of the teleost heart after cryoinjury is rapid and occurs well before collagen scar deposition (within 15 hours after injury)[97], suggesting that loose scar formation would not necessarily be beneficial for the teleost heart. Crucially, scar organisation and collagen fibre alignment have never been quantified in the zebrafish or medaka and so I cannot compare the SF control and Dexamethasone-treated scars to another teleost model of regeneration and scarring. Therefore, although these results seem to be directly opposing the current literature, it is not possible to currently conclude whether having a disorganised and misaligned scar is detrimental to regenerative capacity in the AM. This makes isolating SF hearts at 90dpci after Dexamethasone exposure an essential next step to determine whether inhibition of late-stage inflammation results in permanent scars that cannot be degraded and induces regenerative failure.

5.3.4 Collagen-producing macrophages could be key signalling hubs in the late stages of the regenerative heart

Finally, the results of the ligand-receptor analysis suggest that during the late stages of cardiac healing, collagen-producing macrophages act as major signalling hubs within the regenerative heart and communicate with numerous cardiac cell types. Previously, collagen-producing macrophages have been associated with pathological fibrosis such as atherosclerosis and

pulmonary fibrosis[324,325]. Indeed, the expression of type VI collagen in alveolar macrophages has been associated with fibroblast activation and the extent of lung fibrosis in mice[326]. Therefore, the finding that collagen-producing macrophages seem to play a signalling role within the regenerative heart is intriguing. One possible explanation is that collagen-producing macrophages act to orchestrate the late stages of cardiac regeneration by integrating a wide range of signals across the heart which certainly warrants further investigation. Additionally, collagen-producing macrophages could be secreting a specific type of collagen scaffold that is easy to absorb in the SF or acts as an ECM scaffold that facilitates cardiac repair. For instance, collagen-producing macrophages that directly deposit to the scar have been identified in the zebrafish heart[136]. In this study, the authors found that collagen-producing macrophages specifically deposited collagens at the periphery of the wound, into the pericardial space. They suggested that this specific localisation of macrophage-deposited collagens could facilitate regeneration by forming an ECM scaffold that might promote epicardial regrowth. Indeed, epicardium: collagen-producing macrophages cellular interactions were identified in 7- and 14dpci SF hearts, suggesting that a similar mechanism could occur in the regenerative SF heart. Therefore, future work should aim to explore the spatial localisation of collagen-producing macrophages in the AM after injury, as well as determine whether these cells are essential for integrating cell-cell signals across the regenerating heart.

5.3.5 Limitations

A major limitation of this chapter is that the assessment of SF regenerative capacity relies on consistent cardiac cryoinjuries which cause the same amount of tissue damage in each fish. However, anatomical variation amongst SF can make their hearts more or less accessible to the cryoprobe, resulting in the induction of wounds that are variable in size as some hearts are easier to injure than others. Although standard operating procedures were implemented to keep cryoinjuries as consistent as possible between fish (eg following a standardised protocol for cryoinjury; performing all surgeries blind to treatment group to prevent bias), it is not possible to rule out whether the ability to detect differences in regenerative capacity has been hindered by variable

wound sizes. For example, Dexamethasone wounds that are atypically small and control wounds that are atypically large will have masked the detection of any real differences that inflammation inhibition may have caused in SF regenerative capacity. Indeed, the large variation seen in the regenerative capacity measurements presented here suggest that the control and Dexamethasone-treated fish had variable initial infarct sizes. Therefore, to overcome this limitation in future studies, magnetic resonance imaging (MRI) should be used to quantify regenerative capacity. MRI is non-invasive and can be used to repeatedly measure how cardiac function changes after injury and drug treatment by taking multiple images of the same heart. As each heart is normalised to itself, MRI quantification of regenerative capacity would be resistant to differences in initial wound size and any impact of Dexamethasone treatment would not be confounded by variability in cryoinjury. MRI has already been successfully used to quantity regenerative capacity in the neonatal mouse[327] and the zebrafish[328], suggesting this could well be a feasible option for future AM studies.

This chapter has also been limited by the need to use a broad, anti-inflammatory agent to inhibit late-stage inflammation and leukocyte recruitment. Although glucocorticoids have previously been used extensively to target inflammation, leukocyte recruitment[105,302] and cardiac regeneration[329], they have a wide range of biological effects. These off-target effects could have significant impacts on SF regeneration and could be causative of the observed disruption to collagen fibre alignment. For example, Dexamethasone has been shown to induce gene expression changes in cardiac circadian rhythms and metabolism[330,331], two processes which have been shown to regulate regenerative success[332,333]. Therefore, future work should aim to validate the effects of Dexamethasone exposure in the SF heart to confirm that the significantly altered scar organisation was due to inhibition of the late-stage SF immune response. Furthermore, alternative broad anti-inflammatory agents which act via a different mechanism of action to Dexamethasone, such as Methotrexate, should also be used to inhibit the late-stage SF immune response. If scar organisation is still significantly disrupted following the use of alternate broad anti-inflammatory agents, this

would significantly strengthen the findings of this chapter and help overcome the limitation of having to use a 'dirty' pharmacological agent in the AM that has many off-target effects.

5.3.6 Future Directions

This chapter has highlighted that late-stage SF leukocytes upregulate TNFα/NFκB signalling that may be mediating scar organisation and alignment of collagen fibres within the scar. Critically, I have also identified that late-stage SF neutrophils and macrophages upregulate >100 common genes in the late stages of cardiac healing which could constitute a PRP that mediates regeneration. Therefore, future studies should focus on exploring whether SF macrophage/neutrophil injury-responsive genes are regulated by TNFα/NFκB signalling and determine if these genes could be regulating scar organisation or promoting another aspect of regeneration.

Chapter VI

Discussion & Conclusions

The immune response is essential to cardiac regeneration and critically regulates regenerative capacity, governing the decision to form *de novo* cardiac tissue or a permanent fibrotic scar. However, the exact mechanisms of the immune system that control regeneration vs scarring are still unknown. To advance our understanding of how the immune system regulates regenerative capacity, it is critical that we understand how the regenerative and scarring immune responses differ so that we can pinpoint key immunoregulatory checkpoints at which regeneration can either succeed or fail. By fully understanding how the regenerative and scarring immune responses diverge, it is hoped that promising new therapeutic targets will be identified that can be used to improve endogenous repair in the adult human heart.

The *A. mexicanus* holds great potential for unpicking the key immunoregulatory checkpoints that regulate regenerative success and failure as it enables comparisons between fish-like regeneration and human-like scarring within adult populations of the same species. Prior to this project, the PF and SF immune responses to cardiac tissue damage were completely unknown. Therefore, this work aimed to characterise the regenerative SF and scarring PF immune responses to necrotic cardiac cell death. Specifically, I wished to identify significant differences in the PF/SF immune responses that could be regulating the differential regenerative capacity of the AM.

Main Findings

This work has revealed that the regenerative SF and the scarring PF display significantly different immune responses to cardiac injury, revealing new insights into how the immune system regulates regenerative capacity:

1) Leukocyte counts have shown that the PF immune response dominates immediately after injury (1-3dpci) whereas the SF immune response takes over during the late stages of cardiac healing (14-30dpci) and remains active for at least one month after injury.
2) Neutrophil counts have shown that the PF neutrophil response is significantly stronger than the SF neutrophil response due to the substantial and prolonged recruitment of neutrophils at 1- and 3dpci, resulting in a high-density of neutrophils in PF wounds. In contrast, the SF neutrophil response is brief, with neutrophil levels peaking at 1dpci before returning to baseline levels. These neutrophil counts suggest that elevated PF *ptprc* cells at 3dpci are due to the prolonged PF neutrophil response.
3) B cell counts have shown that B cells significantly influx into the SF heart during the late stages of cardiac healing, reaching peak levels at 30dpci. In contrast, B cells are almost completely absent in the PF heart and show significantly diminished levels of MHC II expression. B cell counts suggest that elevated SF *ptprc* cells at 14dpci are at least partly due to the substantial influx of B cells.
4) The composition of the PF/SF immune responses significantly diverge during the late stages of cardiac healing. The SF immune response is uniquely characterised by B cells and novel neutrophil/macrophage populations at 7- and 14dpci.
5) Single cell transcriptional profiling suggests that TNFα/NFκB signalling is upregulated specifically at 7dpci and 14dpci in SF leukocytes.
6) Inhibition of SF late-stage inflammation between 7-14dpci does not inhibit SF regenerative capacity but does significantly disrupt scar formation, leading to disorganised scars that resemble the PF scar and may be permanent.

In addition to these findings, this project has confirmed that the AM is a great model to study the mechanisms underlying the regenerative and scarring immune responses to necrotic cell death. Indeed, this work has performed an unbiased comparison of the AM immune response to identify that the SF and PF show significant differences during the early neutrophil response and the late

stages of the immune response. These points of divergence represent key immunoregulatory checkpoints that could be critically regulating regenerative success and failure in the AM.

6.1 How has this project enhanced our understanding of how the immune system regulates regeneration

6.1.1 The divergent early PF/SF neutrophil responses may differentially regulate regenerative capacity

During this project, I have characterised the SF and PF neutrophil responses to cardiac cell death, revealing that the neutrophil response is significantly stronger in the scarring setting than in the regenerative setting due to the excessive and prolonged recruitment of neutrophils that influx into the PF wound at high densities. Although this finding is not completely novel as a prolonged presence of neutrophils in the heart has already been shown to result in regenerative failure in the zebrafish and medaka[109,252], it does add further support to the emerging evidence that the duration of the neutrophil response can critically regulate regenerative capacity. Furthermore, this finding strongly suggests that the overarching hypothesis for this thesis was correct (i.e. that differences in the PF/SF immune response drive their differential regenerative capacity). Therefore, this project has confirmed that the immune response may act as a key player in the regulation of SF regenerative success and PF regenerative failure.

In addition to finding that a prolonged neutrophil response seems to be conserved amongst scarring hearts, the characterisation of the SF neutrophil response suggests that a brief neutrophil response might be important in regenerative success. Until now it has been unclear whether a neutrophil response is essential to the regenerating heart as the neonatal mouse heart does not seem to recruit any neutrophils after LAD ligation[103]. However, I have found that SF neutrophil dynamics are identical to the zebrafish, suggesting that a brief neutrophil response immediately after injury could be beneficial to regeneration as it has been conserved across regenerative species. This could potentially redefine how we think of neutrophils that immediately respond to injury.

Currently, they are regarded as wound clearing cells that phagocytose debris and do not promote regeneration. Instead, neutrophils which stimulate repair are thought to only emerge in the later stages of wound healing (from 5dpi) where they mediate inflammation resolution and ECM remodelling[153,249,277]. However, the identical SF and zebrafish neutrophil response suggests that neutrophils which enter the heart straight after cardiac damage might be setting the stage for successful regeneration. This certainly warrants further investigation as the role of 1dpci neutrophils in regulating regenerative capacity has barely been explored. Therefore, this work sheds a new light on debris-clearing neutrophils which could prove to be novel pro-regenerative cells.

Finally, during the characterisation of the PF/SF neutrophil response, the timing of the PF prolonged neutrophil response was found to coincide with a significantly accelerated rate of PF myocardial death. Although currently this finding is only an association and does not substantially link the PF neutrophil response to increased PF myocardial death, it does raise an intriguing, albeit speculative, possibility for future study. This data could suggest that the prolonged PF neutrophil response causes regeneration to fail by rapidly destroying surviving myocardium and stimulating emergency scar deposition. The rapid loss of myocardial tissue from PF wounds by 3dpci will significantly weaken the integrity of the PF ventricular wall which could lead to uncontrolled and permanent scar deposition as the PF heart scrambles to quickly replace the dying cells. In contrast, the absence of neutrophils from the SF heart by 3dpci might enable damaged SF cardiomyocytes to be cleared at a slower rate, resulting in the controlled formation of a replacement scar that is amenable to resorption during the later stages of regeneration. So far, no work has examined whether the rate of tissue death after injury is linked to scar formation. However, comparisons between regenerative and scarring organisms reveal that animals that heal by scarring will undergo very early ECM deposition whereas regenerative animals show a significantly delayed deposition of the scar[334]. For instance, the scarring mouse will deposit collagen by 3dpi in the skin[335] whilst collagen isn't detected until 8dpi in the regenerative spiny mouse[323] and 14dpi in the axolotl[336], suggesting that the timing of scar deposition critically regulates regenerative capacity. Therefore,

this project could point towards a new mechanism by which the immune response might promote regenerative failure. Future studies should investigate whether cytotoxic PF neutrophils are rapidly destroying damaged cardiac tissue and explore whether the PF and SF show significant differences in the timing of their scar formation after cardiac injury.

6.1.2 A fresh perspective on the role of the adaptive immune system in regeneration

To date, the role of the adaptive immune system in successful regeneration has been largely overlooked following the current consensus that the evolution of a complex adaptive immune system is a barrier to regenerative potential. However, the B cell findings in the thesis suggest that the adaptive immune system is not prohibitive to regeneration as substantial numbers of B cells influx into the SF heart at 14- and 30dpci, whereas their numbers remain minimal in the PF. This finding supports recent studies which also suggest that the adaptive immune system is key to regeneration. In the zebrafish, Tregs have been found to secrete organ-specific pro-regenerative paracrine factors that are essential to the regenerative success of the heart, retina and spinal cord[337]. Additionally, comparisons between the zebrafish and medaka have highlighted that, during regeneration, the zebrafish specifically upregulate genes involved in T cell proliferation and B cell receptor signalling[109]. Therefore, the differential regenerative capacity of the AM may in fact be due to significantly different adaptive immune responses.

In support of this new hypothesis, additional observations during this project further suggest that the AM adaptive immune responses are significantly different. Functional analysis of PF/SF macrophages has identified that T cells are differentially regulated by PF/SF macrophages at 14dpci, with SF macrophages positively regulating T cell proliferation whereas PF macrophages negatively regulate Treg differentiation. Furthermore, PF show significantly diminished MHC II expression across all three of their major APCs, suggesting that antigen presentation in PF is impaired in comparison to the SF. This is significant for the adaptive immune response as antigen-presentation via MHC II is essential for activation of CD4+ T cells whilst wound healing is impaired if either MHC II

is deleted or CD4+ T cells cannot be activated[285]. Therefore, these results suggest that the PF may be deficient in their ability to activate the adaptive immune response which could be due to lack of B cell recruitment and/or MHC II-mediated T cell activation. Thus, this project provides a new perspective on the role of the adaptive immune system in the regulation of regenerative success and scarring.

6.1.3 The late-stage SF immune response may be essential for regeneration and scar resolution

Currently, the immune system is not thought to be required during the long-term phases of cardiac regeneration as leukocyte levels in the regenerative zebrafish and neonatal mouse have been reported to largely return to baseline by 14dpi[103,144]. However, during this project I have found that SF leukocyte levels remain elevated at 14- and 30dpci, suggesting that in the SF, the immune response is still active during the late stages of cardiac healing. Teleost cardiac regeneration is a lengthy process, taking approximately 90 days in the SF and 60-180 days in the zebrafish to reach completion. Therefore, it seems plausible that successful regeneration could require the continual recruitment of leukocytes to the site of injury to mediate the long-term regenerative response. Specifically, the timing of elevated SF leukocytes in the late stages of cardiac healing suggests that they could be coordinating scar resorption with the formation of healthy new myocardium.

Although the functional role of late-stage SF leukocytes has not been fully elucidated during this project, some preliminary findings suggest that late-stage SF leukocytes could be regulating scar deposition and resorption. Firstly, I have found that late-stage SF leukocytes upregulate TNFα/NFκB signalling. TNFα/NFκB signalling has already been shown to induce the expression of matrix degrading enzymes in many cell types. Critically, TNFα/NFκB activation in neutrophils and macrophages has been shown to directly induce *mmp1, mmp3* and *mmp9* expression, suggesting that late-stage TNFα/NFκB+ SF leukocytes could be actively helping to resorb the scar by secreting degradative enzymes[309,338]. Additionally, TNFα/NFκB signalling has also been shown to increase

collagenolytic activity, and suppress ECM synthesis by inhibiting the expression of collagens and aggrecan[339,340]. Therefore, TNFα/NFκB+ leukocytes could be uniquely regulating scar resolution from 7dpci onwards in the regenerative setting. This interpretation is further supported by the GO term analysis results which found 14dpci SF neutrophils to be enriched for collagen catabolism, whilst SF macrophages were enriched for collagen biosynthesis, suggesting that SF leukocytes are directly involved in scar turnover.

Secondly, I have found that a substantial population of B cells influx into the SF heart between 14-30dpci. Critically, B cells have already been reported to be involved in scar remodelling following cardiac injury. Indeed, loss of B cells from the injured heart significantly disrupts scar formation and leads to decreased collagen deposition[260]. Furthermore, in response to cardiac injury, B cells have been shown to increase the expression of collagen deposition (*col1a1, col3a1*) and collagen resorption (*mmp9, timp*) genes[260], whilst teleost B cells have been characterised to show high levels of phagocytic activity[341–343]. Therefore, B cells could be contributing to scar degradation during the late stages of cardiac regeneration in the SF by upregulating the expression of degradative enzymes as well as actively facilitating scar break down via phagocytosis.

Thirdly, I have found that Dexamethasone treatment significantly disrupts scar organisation at 60dpci. Dexamethasone is a glucocorticoid receptor agonist that exhibits broad inhibitory effects on both inflammation and leukocyte recruitment[105,302], thus suggesting that disruption to the late-stage SF immune response results in significant changes to scar deposition. Strikingly, significantly unaligned scars were only detected at 60dpci and not at 30dpci, suggesting that a brief disruption to scar organisation between 7-14dpci may induce substantial changes that, over time, result in maladaptive remodelling and permanent scar formation. Although further validation experiments are still required to confirm that scar organisation is regulated by the late-stage SF immune response, the work presented here suggests that disruption to SF scar organisation could result in the formation of permanent scars that are resistant to degradation.

Currently, very little is known about how regenerative models resorb the scar. However, a recent study has proposed that scar resorption in the zebrafish heart relies on a balance between collagen degradation and collagen synthesis, with the levels of collagen synthesis gradually decreasing with time from injury whilst the levels of degradation remain high, leading to scar resorption[344]. Therefore, the constant recruitment of scar-eating leukocytes to the regenerative SF heart at 14- and 30dpci may ensure regenerative success by maintaining the balance of scar degradation>scar deposition. Furthermore, evidence from the zebrafish already implicates that leukocytes play key roles in scar turnover: macrophages directly deposit collagen proteins[136] and are essential for scar formation whilst *tnfa*- macrophages are essential for scar resolution[144]. Thus, this work suggests, for the first time, that continual activation of the immune response may play a key role in mediating regenerative wound healing by facilitating scar remodelling and leukocyte degradation of the scar.

6.2 Will the findings from this project help human MI patients?

Although the immune system of the AM and the human are vastly different, understanding how the PF immune response leads to regenerative failure could identify new therapeutic avenues for preventing HF. It is hoped that modulating components of the human immune system to mimic the regenerative immune response may ameliorate cardiac repair in post-MI patients. So far, this project has identified that accelerating neutrophil clearance in patients could help to reduce infarct sizes and resultant scar formation. Furthermore, my findings have highlighted that B cells represent a promising new target for immunomodulatory therapies for heart attack patients, especially when the recent data is considered that reports that regulatory B cells improve cardiac repair in the scarring mouse heart.

However, considerable research is still required before we determine whether our fish findings will be translatable to humans. The teleost and mammalian immune systems are vastly different in terms of the maturity, complexity and development of leukocytes and not all

mammalian leukocytes (eg eosinophils) have a teleost counterpart. Therefore, pre-clinical findings from the fish that promote cardiac repair will need to be confirmed in the mammalian models before they can be successfully applied to the human heart[262].

6.3 Limitations of this project

This project has been significantly limited by poor AM genome annotation. Indeed, the lack of gene annotation in the AM genome has prevented a full exploration of the scRNAseq dataset as transcriptomic information is unavoidably lost during dataset creation. Furthermore, the incomplete annotation of the AM genome has further prevented the role of identified cells of interest in the regenerative heart from being determined. For instance, currently, it is not possible to probe which cell types may be responding to increased TNFα production from late-stage SF neutrophils and macrophages as neither TNFα receptors are annotated in the AM genome (*tnfr1* and *tnfr2*). This has limited my ability to pin down whether TNFα/NFκB signalling might be regulating scar formation, cardiomyocyte proliferation, leukocyte recruitment or acting on unknown cell types. Therefore, currently, I can only speculate as to the role of TNFα/NFκB leukocytes within the SF heart without considerable further investigation. Furthermore, many key canonical cell type markers are not annotated in the AM genome, such as CD206 and CD14. This has prevented the comparison of AM leukocyte populations to immune cell identities that are well-established within the literature such as regulatory B cells and tissue-resident macrophages, as well as restricted my ability to profile the inflammatory state of PF and SF leukocytes and identify distinct macrophage populations. Unfortunately, until a new AM genome build is available with improved gene annotations, there is very little that can be done to overcome this limitation. It is far beyond the scope of an individual lab to improve gene annotations at a genome-wide level. However, during this project, I have published a novel methodology that AM researchers can use to maximise the transcriptomic information from their scRNAseq data when using the incomplete v1.0.2 and v2.0 AM genome assemblies[174]. Although this is a far cry from the information available when using a well-established genome build like the zebrafish or the mouse, I hope that my integration methodology will help AM researchers to

overcome some of the problems posed by the multiple, incomplete and inconsistent AM genome assemblies.

In addition to a well annotated AM genome, this project would benefit from increased sample sizes. In this project, a minimum threshold of 3 biological samples was set for any statistical analysis whilst parametric testing was employed based on previous data that found PF and SF populations to display normally distributed responses to cardiac injury. However, three samples is still relatively low when sampling from two independent and variable populations. Therefore, increasing the collection of PF/SF samples would minimise the impact of biological variability on the cell count data, increasing the strength of any conclusions made regarding significant differences between PF and SF neutrophil and B cell populations.

6.4 Future Directions

This project has raised many fascinating questions for future study:

1) Does the prolonged PF neutrophil response prohibit regeneration?
2) Is the initial SF neutrophil response at 1dpci essential for successful regeneration?
3) Are cytotoxic neutrophils rapidly destroying the wound and stimulating early scar formation?
4) Are B cells essential to successful regeneration?
5) What is the functional role of TNFα/NFκB leukocytes during the late stages of cardiac healing?
6) What are the spatiotemporal dynamics of PF/SF macrophages in response to cardiac injury?

6.4.1 The PF/SF neutrophil response

To firstly confirm whether SF/PF neutrophil responses are differentially regulating regenerative capacity, it will be essential to modulate the initial PF/SF neutrophil response and assess the impact on regeneration. This could be achieved by a neutrophil depletion study in which SF neutrophils were depleted at 1dpci and PF neutrophils were depleted at 3dpci. However,

currently available neutrophil depletion approaches require the use of monoclonal antibodies which will not be compatible with fish antigens and thus are unlikely to work in the AM. Another approach to deplete neutrophils would be to create a genetic AM line in which neutrophils are time-sensitively depleted (eg using diphtheria toxin A under a neutrophil-specific promoter). However, this approach would take a prohibitively long time (≥ 3 years) as AM juveniles can take up to 1 year to reach sexual maturation. Therefore, the best option to selectively deplete neutrophils in the AM is to use a pharmacological approach. One possible mechanism that could be employed is to stimulate increased neutrophil retention within the head kidney. In the mouse, the CXCL12-CXCR4 axis has been shown to regulate neutrophil retention within the bone marrow and CXCR4 antagonists enhance neutrophil mobilisation from the bone marrow, resulting in increased neutrophil recruitment to wounds[345]. This suggests that CXCL12 injections between 1-3dpci could be a viable way to selectively disrupt PF/SF neutrophil dynamics and prevent their influx into the heart, enabling the impact of 1dpci SF neutrophils and 3dpci PF neutrophils on regenerative capacity to be probed.

Furthermore, such an approach could be used to answer the question of whether cytotoxic PF neutrophils are rapidly destroying the wound and accelerating the death of damaged cardiomyocytes. Indeed, the area of MF20 staining in PF wounds at 3dpci could be measured following disruption to the immediate PF neutrophil response to determine whether a difference in the rate of myocardial death is observed. If this turned out to be the case, a fascinating follow up experiment would be to inject PF neutrophils into the SF heart and determine whether myocardial death was accelerated and if this resulted in early scar deposition and impaired regeneration.

6.4.2 B Cells

To determine whether B cells are essential to the SF regenerative response, an ideal experiment would be to selectively deplete B cells from the SF. However, similarly to neutrophils, most previous B cell depletion approaches have used monoclonal antibodies against B cells which will not work in the AM. Furthermore, currently available pharmacological B cell inhibitors such as

Ibrutinib target the *btk* enzyme which, according to the scRNAseq data, is not well expressed in the AM. Therefore, if AM B cells are to be successfully inhibited in the SF, an alternative approach must be utilised. Although genetic lines take a very long time to make in the AM, recent advances in gene editing technology have shown that complete knock-outs can be created within the F_0 generation by injecting Cas9 proteins with multiple guide RNAs to direct CRISPR-mediated genetic knock out[346]. As only SF gene knock outs would be required to test the function of B cells during successful regeneration, this technology could be used to rapidly create a SF B cell knock-out line. Previous studies have used B cell knock-out mice to explore the role of B cells post-MI, suggesting this could be a viable approach for assessing whether B cells are essential to successful regeneration[259]. Furthermore, the creation of a B cell knock-out SF population would provide additional important insight into the possible roles of B cells with the regenerating heart and reveal whether B cells might be mediating scar resolution.

Additionally, an alternate route to exploring whether B cells are essential to cardiac regeneration would be to isolate B cells from the SF and inject them into the PF heart between 14-30dpci to see whether regenerative success was improved. Indeed, this transplantation approach would provide key insight into the mechanisms of B cells within regeneration by revealing whether SF B cells promoted cardiomyocyte proliferation or scar resolution within the scaring PF heart.

6.4.3 TNFα/NFκB leukocytes

So far, we have discussed how the late-stage SF immune response might uniquely regulate scar formation in the SF. However, TNFα and NFκB are pleiotropic signalling molecules that have been reported to activate a diverse range of downstream signalling pathways. Therefore, late-stage TNFα/NFκB+ SF leukocytes may be facilitating successful regeneration through a variety of mechanisms which require elucidation in future work.

Scar deposition, remodelling, and resolution

From the results of this project, it seems likely that TNFα/NFκB leukocytes are involved in regulating the scar. This has led me to hypothesise that late-stage SF leukocytes are continually recruited to the regenerative heart until cardiac regeneration is complete to mediate scar resorption. To test this hypothesis, two questions need to be answered during future studies.

Firstly, it needs to be determined whether leukocytes remain elevated throughout the late stages of cardiac regeneration in the SF. Thus, the first step would be to perform *ptprc+* cell counts at 60dpci in the SF and PF, to determine whether SF leukocyte levels remain elevated throughout the late stages of cardiac healing and scar resorption.

Secondly, although I have suggested that TNFα/NFκB leukocytes might facilitate scar resolution due to the upregulation of matrix-degrading enzymes, this still needs to be confirmed. Thus, future experiments should seek to explore, using the scRNAseq data, whether ECM remodelling enzymes such as MMPs are expressed in late-stage SF leukocytes. This could identify which matrix-degrading enzymes are downstream of TNFα/NFκB upregulation and reveal whether SF leukocytes are well-primed to play a key role in regulating scar remodelling. Furthermore, if matrix-degrading enzymes can be identified in late-stage SF leukocytes, this could provide targets for pharmacological inhibition so that the role of TNFα/NFκB leukocytes in scar resolution can be determined. A fascinating but potentially technically challenging approach would then be to isolate TNFα/NFκB+ cells from the SF and inject them into the PF between 14-30dpci to see whether scar resolution was improved, and PF regenerative capacity was increased.

Cardiomyocyte Proliferation

In addition to scar resolution, successful regeneration relies on the proliferation of pre-existing cardiomyocytes. Although this project has not explored any links between TNFα/NFκB leukocytes and SF cardiomyocyte proliferation, the literature suggests that the increased production of TNFα from late-stage SF leukocytes could stimulate cardiomyocytes to upregulate glycolysis which

is an essential step in myocardial proliferation[96]. Indeed, glycolysis exerts powerful control over cardiomyocyte proliferation as the induction of glycolysis in non-proliferative cardiomyocytes can cause them to re-enter the cell cycle in the adult mouse[71] and TNFα has already been shown to induce glycolysis in skeletal muscle[347]. Strikingly, unpublished work from the Mommersteeg lab has found that SF cardiomyocytes selectively upregulate glucose uptake and glycolysis following injury but that PF cardiomyocytes fail to activate glycolysis, suggesting that glycolysis is also key to AM cardiomyocyte proliferation. As TNFα/NFκB+ leukocytes are absent from the PF heart at 7- and 14dpci, an exciting possibility is that PF cardiomyocytes fail to metabolically reprogram and activate glycolysis due to a lack of TNFα secretion from late-stage neutrophils and macrophages. Convincingly, the timing of peak TNFα/NFκB leukocytes coincides with the time at which SF cardiomyocytes reach peak proliferation levels, suggesting that TNFα/NFκB+ leukocytes might promote regenerative success by stimulating cardiomyocyte proliferation. Furthermore, differences in metabolism have previously been identified as potential key drivers of the AM differential regenerative capacity. Therefore, future experiments should explore whether TNFα/NFκB+ leukocytes stimulate myocardial proliferation by assessing the number of cells that co-stain for Pcna (a proliferation marker) and Mef2 (a cardiomyocyte nuclei marker) in the Dexamethasone-treated hearts to assess whether inhibition of TNFα/NFκB signalling results in a significant decrease in the number of proliferating cardiomyocytes during the late stages of cardiac healing.

6.4.4 The AM monocyte/macrophage response

As discussed in chapter IV, this project has failed to characterise the spatiotemporal dynamics of the SF and PF monocyte/macrophage responses in the AM. However, if we are to understand the importance of TNFα/NFκB+ leukocytes in mediating SF regenerative success, it will be essential to confirm whether SF macrophages remain elevated during the late stages of cardiac healing. Furthermore, previous studies have shown that macrophages play key roles in regeneration by orchestrating angiogenesis, scar deposition, scar remodelling, scar resolution, cardiomyocyte proliferation, debris removal and inflammation resolution. Therefore, it is critical that we

understand how the spatiotemporal dynamics of the PF/SF monocyte/macrophage responses differ if we are to fully understand how the immune response regulates cardiac regeneration success and failure in the AM. As a result of this project, *c1qa* has been identified as a novel and specific pan-macrophage marker that can be used in future characterisations of the AM spatiotemporal macrophage response.

6.5 Concluding remarks

This project has demonstrated that the SF and PF immune responses of the AM show significant differences in their spatiotemporal leukocyte dynamics, highlighting that the late stages of cardiac healing show the greatest differences in the regenerative and scarring settings. The identification of novel neutrophil, macrophage and B cell populations in late-stage SF hearts suggests a role for the SF immune system in coordinating scar resolution whilst regeneration might fail in the PF due to a lack of leukocyte recruitment. This project has opened a new avenue for future research to explore whether regenerative success is driven in the SF by a continuously active immune response that coordinates myocardial replenishment with scar degradation. Further investigation into the role of late-stage SF leukocytes in regulating regenerative success could expand our understanding of how the immune system can ensure successful tissue replenishment and contribute towards the new therapeutic treatments for post-MI patients.

Appendix
Publications

First-Author

Cells (2022)

Discordant Genome Assemblies Drastically Alter the Interpretation of Single-Cell RNA Sequencing Data Which Can Be Mitigated by a Novel Integration Method

Helen G. Potts; Madeleine E. Lemieux; Edward S. Rice; Wesley Warren; Robin P. Choudhury; Mathilda T. M. Mommersteeg

Journal of Cardiovascular Development and Disease (2021)

Unlocking the secrets of the regenerating fish heart: Comparing regenerative models to shed light on successful regeneration

Helen G. Potts*; William T. Stockdale*; Mathilda T. M. Mommersteeg

Co-Author

Journal of the American Heart Association (2022)

Tissue-Specific Roles for the Slit–Robo Pathway During Heart, Caval Vein, and Diaphragm Development

Juanjuan Zhao; Susann Bruche; **Helen G. Potts**; Benjamin Davies; Mathilda T. M. Mommersteeg

Development (2020)

Runx1 promotes scar deposition and inhibits myocardial proliferation and survival during zebrafish heart regeneration

Jana Koth*; Xiaonan Wang*; Abigail C. Killen*; William T. Stockdale; **Helen G. Potts;** Andrew Jefferson; Florian Bonkhofer; Paul R. Riley; Roger K. Patient; Berthold Göttgens; Mathilda T. M. Mommersteeg

Figures

3.1 Integrating v.1.0.2 and v2.0 datasets into an integrated dataset enables more accurate identification of doublets.

Over 1,290 cells changed cell-type annotation in the integrated dataset from the original v1.0.2 and v2.0 datasets. When we investigated the transcriptional profile of the cells that changed annotation, it was apparent that many of these cells were in fact doublets as they expressed markers from multiple cardiac cell types.

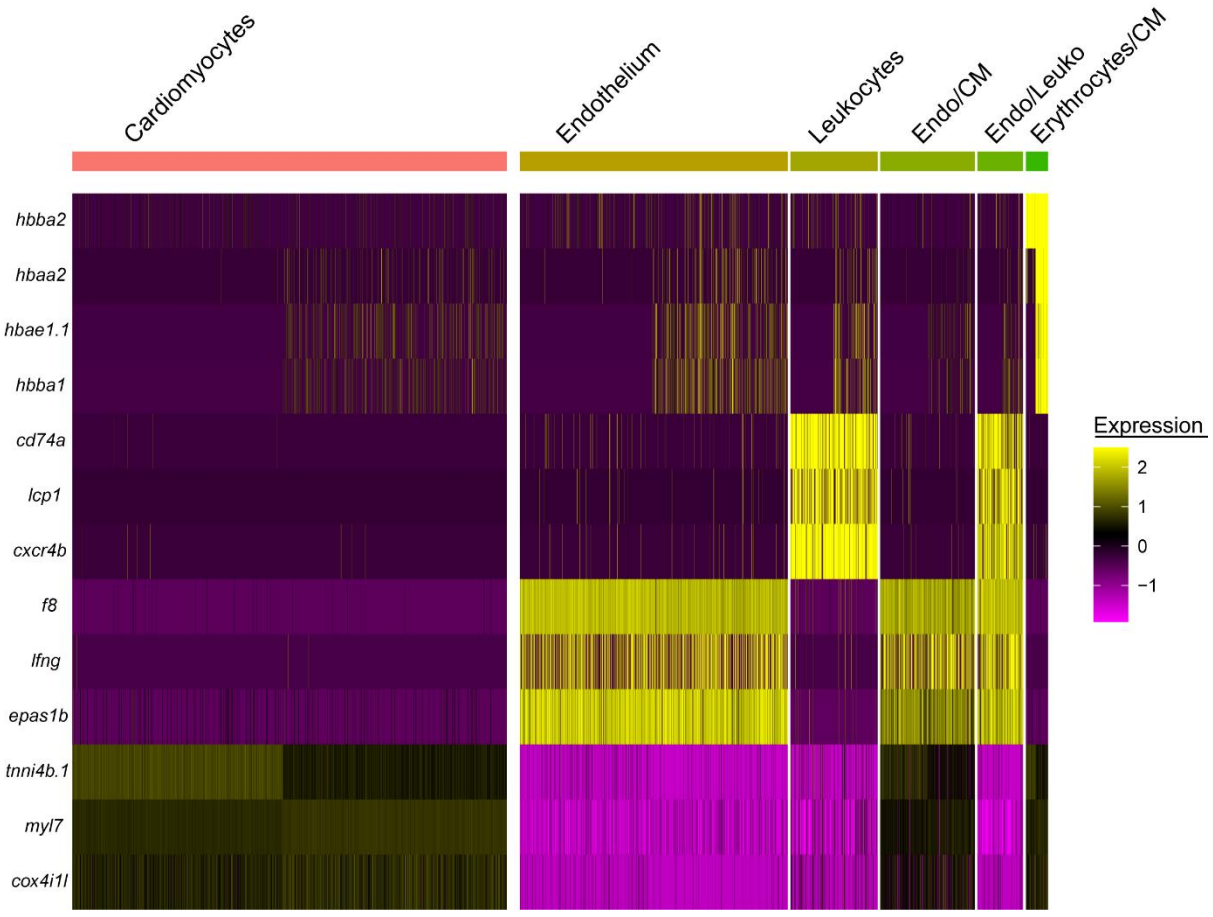

Appendix 3. 1: Heatmap of the transcriptional profile of identified doublet clusters shows that cells from each doublet cluster expressed top genes from multiple cardiac cell types

3.2 Integration of the 12 scRNAseq samples to produce the overall scRNAseq dataset of 85,516 cells

Reciprocal PCA and SCT integration with Harmony were tested to determine which methodology was able to minimise batch-effects and integrate all 12 samples together most effectively. We found that when we assessed reciprocal PCA analysis integration by grouping cells according to their PF/SF, dpci and sample origin, we did not observe thorough mixing of cardiomyocytes and neutrophils, suggesting incomplete integration (Fig. 4.1a). However, we found that SCT integration with Harmony offered better mixing of cells within clusters, especially when cells were grouped by dpci and sample origin (Fig. 4.1b). Therefore, we elected to use SCT integration with Harmony as our methodology to integrate our large scRNAseq dataset. Literature suggests that optimal integration of large scRNAseq datasets from multiple samples requires some changes to the default SCT Integration pipeline: a larger number of features should be used for integration (default is 2000 features) and the dataset should be scaled and centred following SCT Integration and before Harmony (default is to centre and scale during SCTransform). Therefore, we tested whether incorporating these amendments during integration improved our final dataset. We found that using 5000 features produced a similar dataset to using 2000 features (Fig. 4.1c) whilst centring and scaling after SCTransform of each sample resulted in better separation of the endothelial and leukocyte clusters from each other. Therefore, for our overall scRNAseq dataset we used SCT Integration with 5000 features and only scaled and centred the data prior to Harmony (Fig. 4.1d).

a)

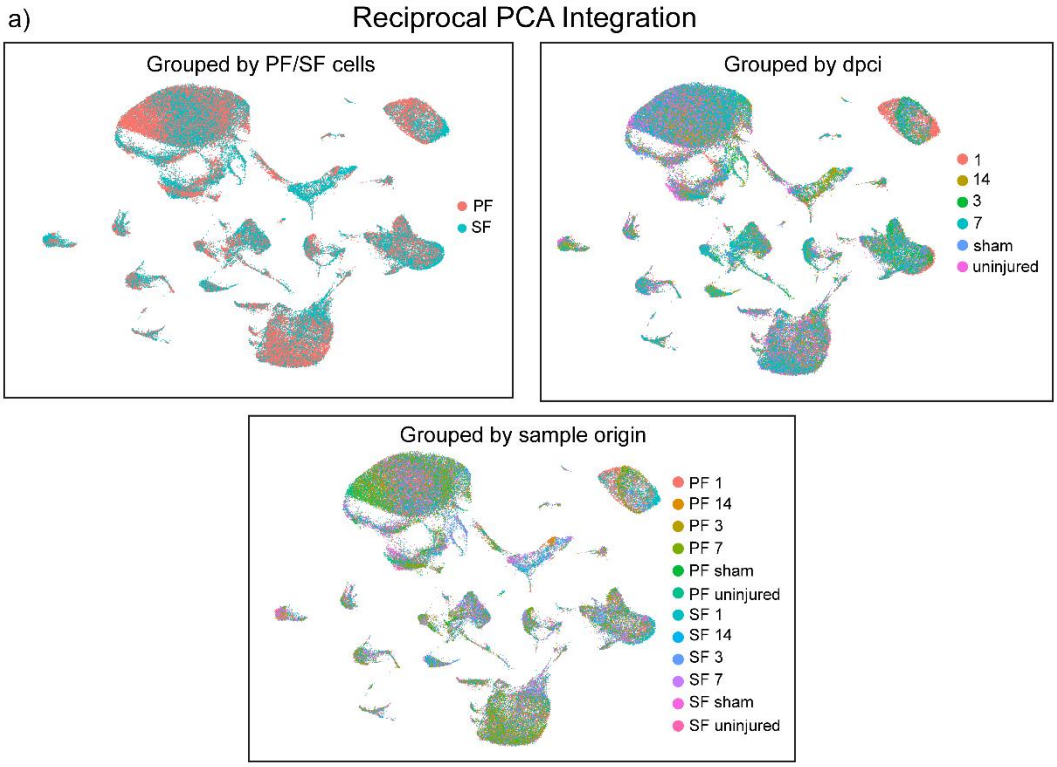

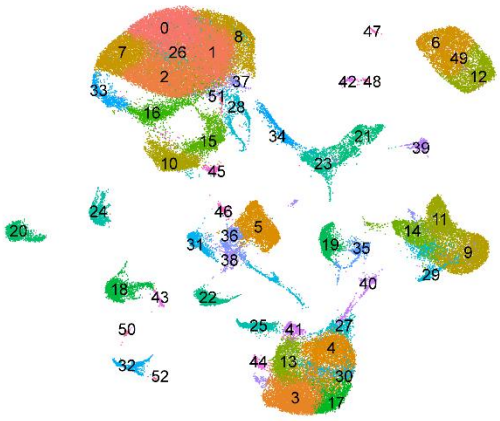

0- Cardiomyocytes
1- "
2- "
3- Endothelium
4- "
5- Fibroblasts
6- Neutrophils
7- Cardiomyocytes
8- "
9- Monocytes/Macrophages
10- Cardiomyocytes
11- Macrophages
12- Neutrophils
13- Endothelium
14- Macrophages
15- Cardiomyocytes
16- "
17- Endothelium
18-
19- T cells
20- Immature Cardiomyocytes
21- RBCs
22- B cells
23- RBCs
24- Itgam+ Cardiomyocytes
25- CM/endo
26- Cardiomyocytes
27- Macrophage/endo
28- Cardiomyocytes
29- Macrophages
30- Endothelium
31- Epicardium
32- Endocardium
33- Cardiomyocytes
34- CM/RBCs
35- Macrophages
36- Fibroblasts
37- CM/Macrophages
38- Fibroblasts
39- Platelets/megakaryocytes
40- Macrophages/endo
41- Endothelium
42- T cells
43- Myofibroblasts
44- Endo/RBCs
45- Cardiomyocytes
46- CM/Fibroblasts
47- Macrophages
48- T cells
49- Neutrophils
50- ?
51- Cardiomyocytes
52- ?

b)

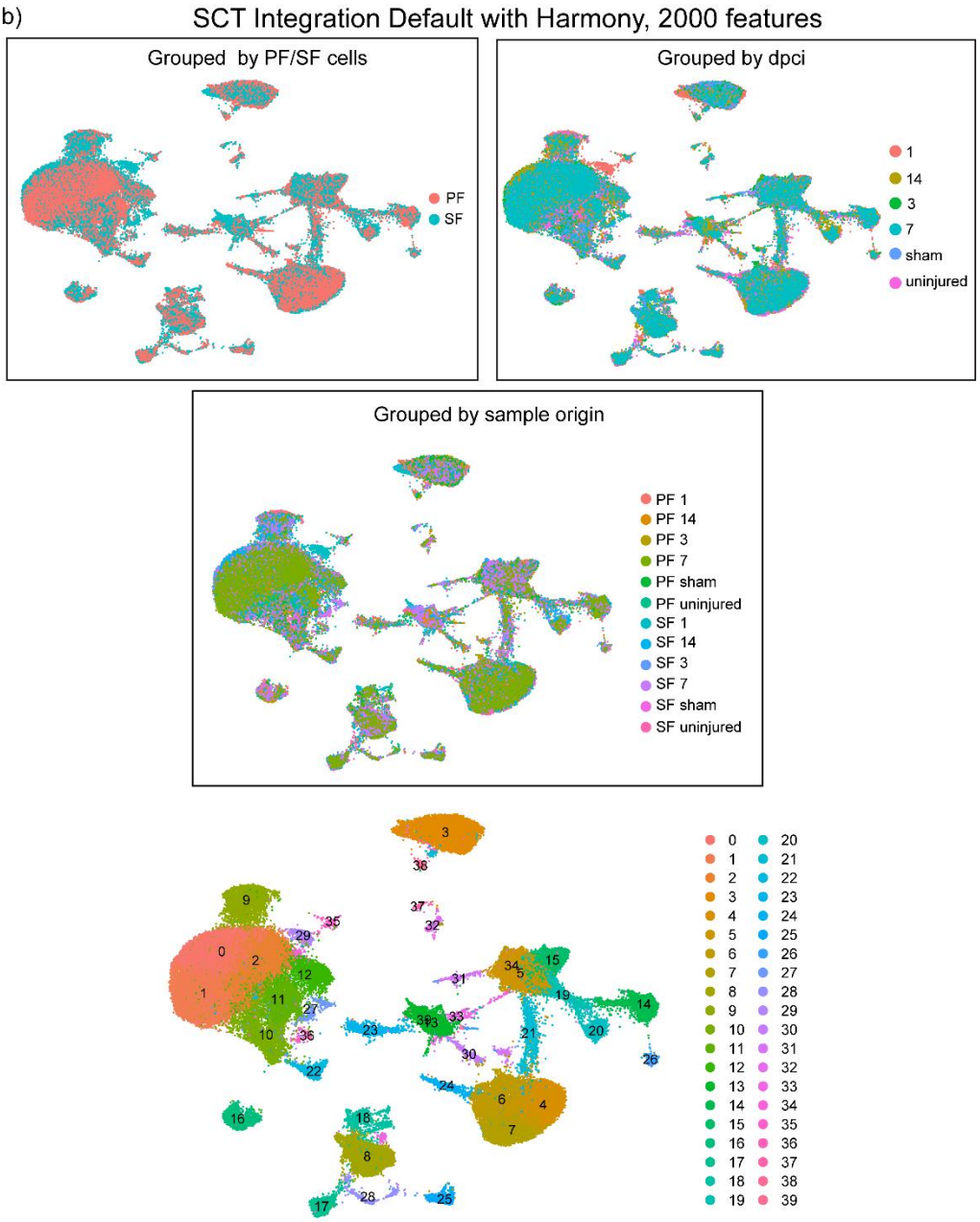
SCT Integration Default with Harmony, 2000 features
Grouped by PF/SF cells
PF
SF
Grouped by dpci
1
14
3
7
sham
uninjured
Grouped by sample origin
PF 1
PF 14
PF 3
PF 7
PF sham
PF uninjured
SF 1
SF 14
SF 3
SF 7
SF sham
SF uninjured
0 1 2 3 4 5 6 7 8 9 10 11 12 13 14 15 16 17 18 19
20 21 22 23 24 25 26 27 28 29 30 31 32 33 34 35 36 37 38 39

c)

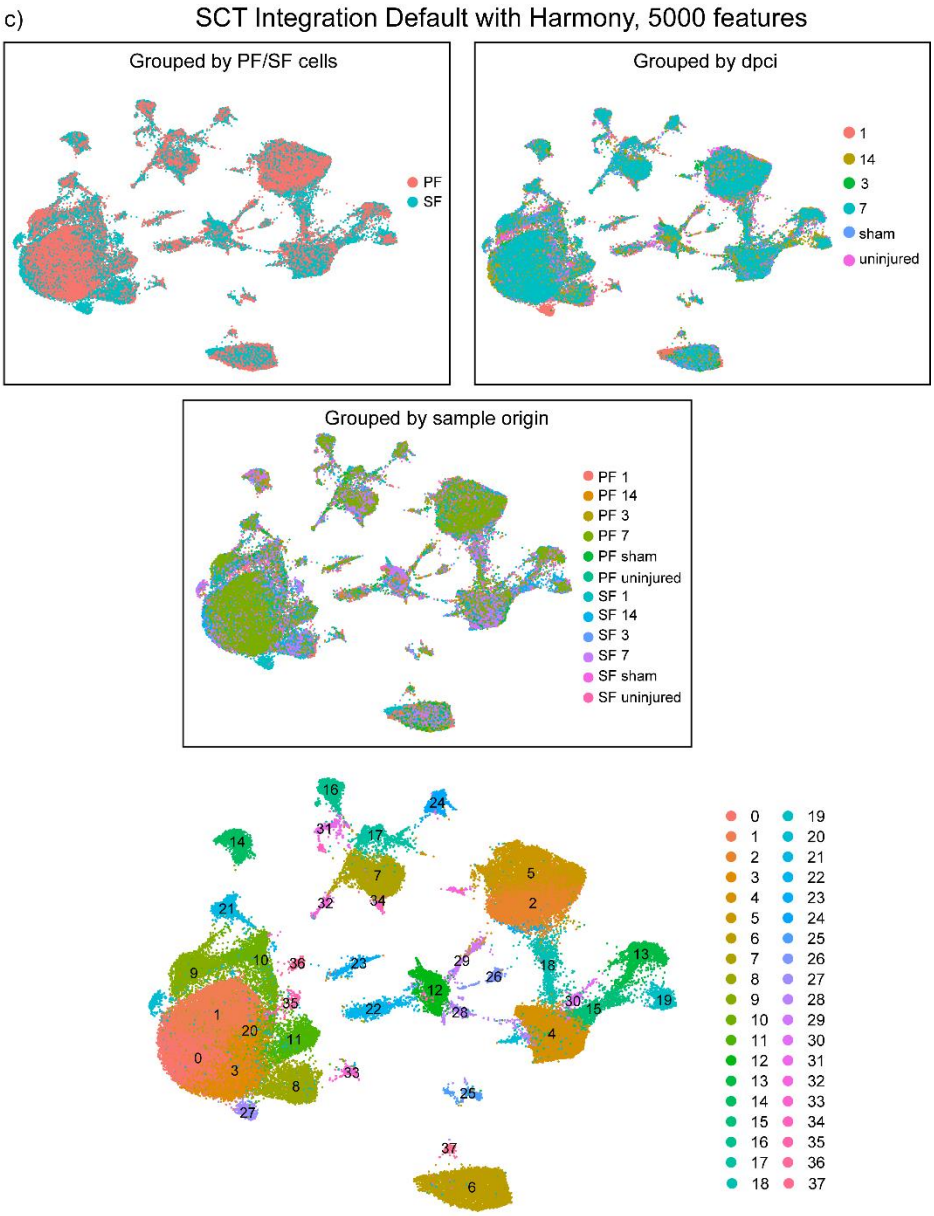
SCT Integration Default with Harmony, 5000 features
Grouped by PF/SF cells
PF
SF
Grouped by dpci
1
14
3
7
sham
uninjured
Grouped by sample origin
PF 1
PF 14
PF 3
PF 7
PF sham
PF uninjured
SF 1
SF 14
SF 3
SF 7
SF sham
SF uninjured
0 19
1 20
2 21
3 22
4 23
5 24
6 25
7 26
8 27
9 28
10 29
11 30
12 31
13 32
14 33
15 34
16 35
17 36
18 37

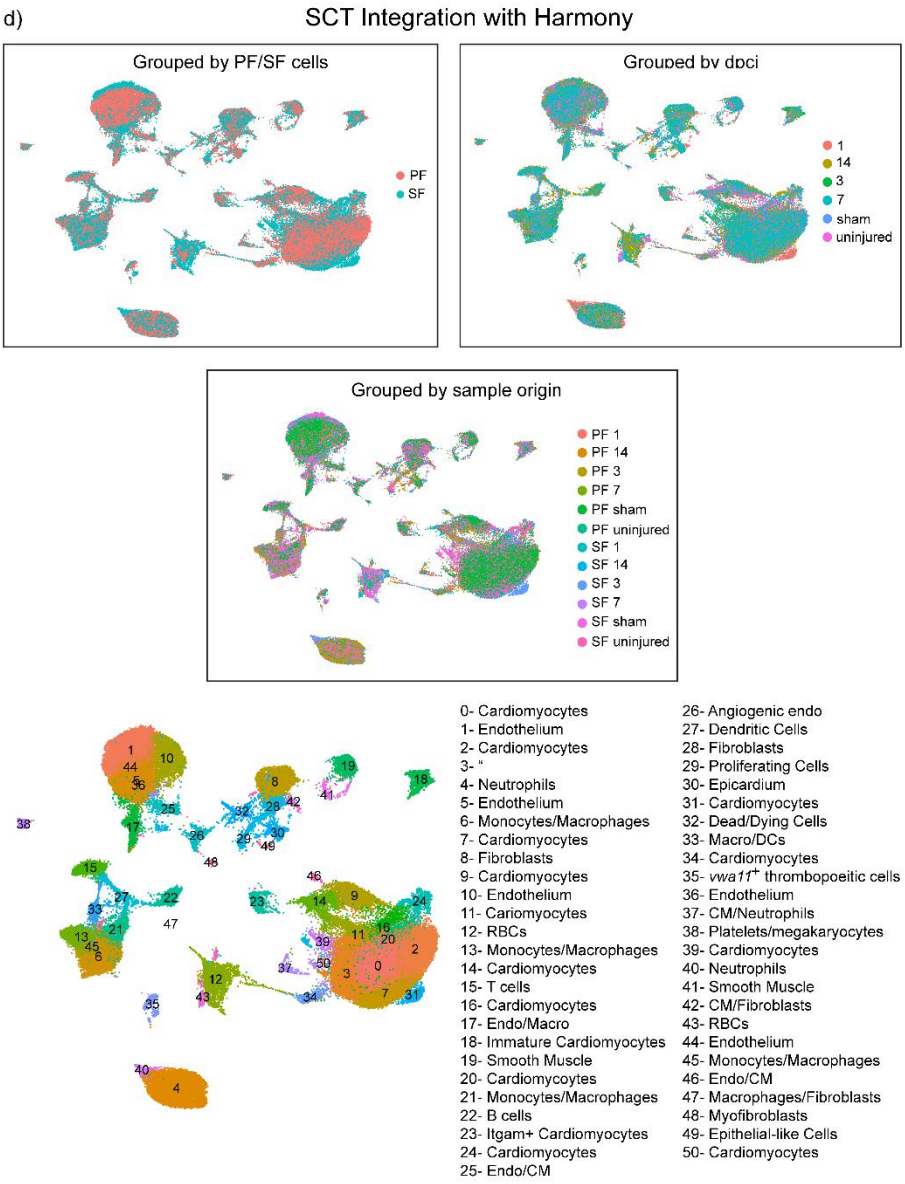

Appendix 3. 2: SCT integration with Harmony and post-integration scaling was used as the integration methodology to produce the overall scRNAseq dataset

(A) UMAPs showing that reciprocal PCA integration produced a resultant dataset of 53 clusters that were not efficiently integrated across PF/SF cells, time point and sample origin (B) UMAPs showing that default SCT integration based on 2000 features with Harmony produced a resultant dataset of 40 clusters (C) UMAPs showing that default SCT integration based on 5000 features with Harmony produced a resultant dataset of 40 clusters (D) SCT Integration based on 5000 features with post-integration scaling and Harmony was chosen as the integration methodology for the overall scRNAseq dataset.

3.3 Characterisation of the *A. mexicanus* non-immune cell types present in the heart at baseline and following injury

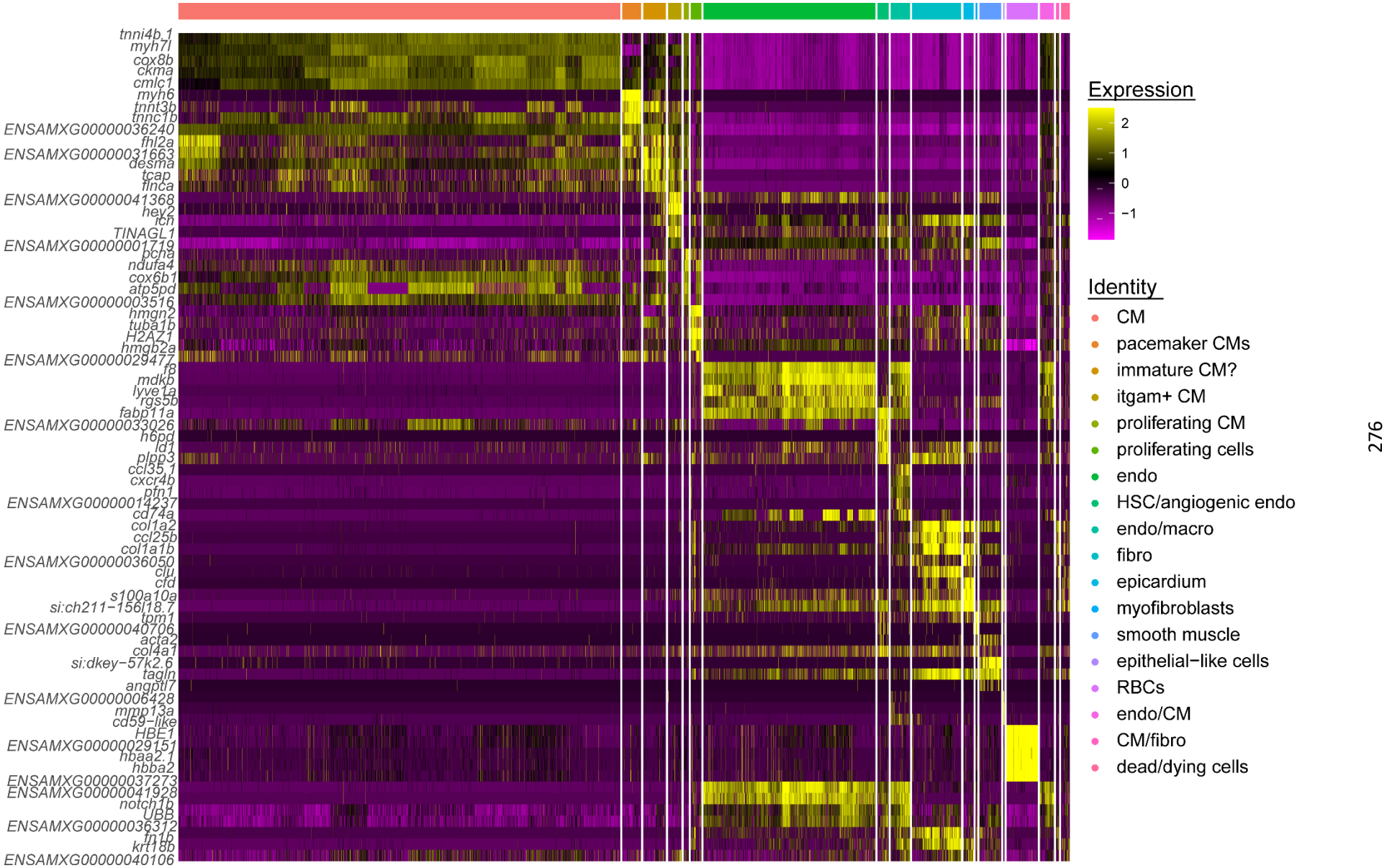
tnni4b.1
myh7l
cox8b
ckma
cmlc1
myh6
tnnt3b
tnnc1b
ENSAMXG00000036240
fhl2a
ENSAMXG00000031663
desma
tcap
flnca
ENSAMXG00000041368
hey2
ich
TINAGL1
ENSAMXG00000001719
pcna
ndufa4
cox6b1
atp5pd
ENSAMXG00000003516
hmgn2
tuba1b
H2AZ1
hmgb2a
ENSAMXG00000029477
fn1
mdkb
lyve1a
rgs5b
fabp11a
ENSAMXG00000033026
h6pd
id1
plpp3
ccl35.1
cxcr4b
ptn1
ENSAMXG00000014237
cd74a
col1a2
ccl25b
col1a1b
ENSAMXG00000036050
clu
cfd
s100a10a
si:ch211−156l18.7
tpm1
ENSAMXG00000040706
acta2
col4a1
si:dkey−57k2.6
tagln
angptl7
ENSAMXG00000006428
mmp13a
cd59−like
HBE1
ENSAMXG00000029151
hbaa2.1
hbba2
ENSAMXG00000037273
ENSAMXG00000041928
notch1b
UBB
ENSAMXG00000036312
fn1b
krt18b
ENSAMXG00000040106
Expression
2
1
0
−1
Identity
CM
pacemaker CMs
immature CM?
itgam+ CM
proliferating CM
proliferating cells
endo
HSC/angiogenic endo
endo/macro
fibro
epicardium
myofibroblasts
smooth muscle
epithelial−like cells
RBCs
endo/CM
CM/fibro
dead/dying cells
276

Appendix 3. 3: Heatmap displaying top 5 cell type markers for the major non-immune cardiac cell types in the AM heart

3.4 *ptprc* is not expressed in dead/dying PF myocardium at 3dpci

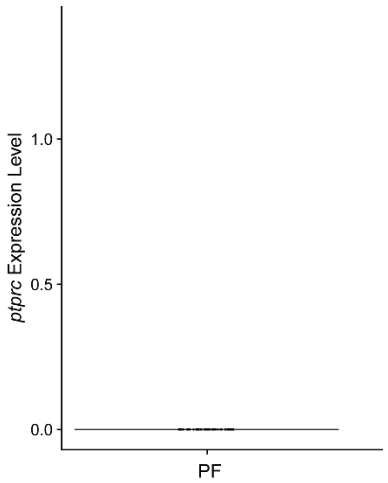

Appendix 3. 4: Violin Plot of ptprc expression levels in PF dead/dying myocardial cells at 3dpci, confirming that ptprc is not expressed

3.5 Identification of leukocyte cell-type markers in the *A. mexicanus*

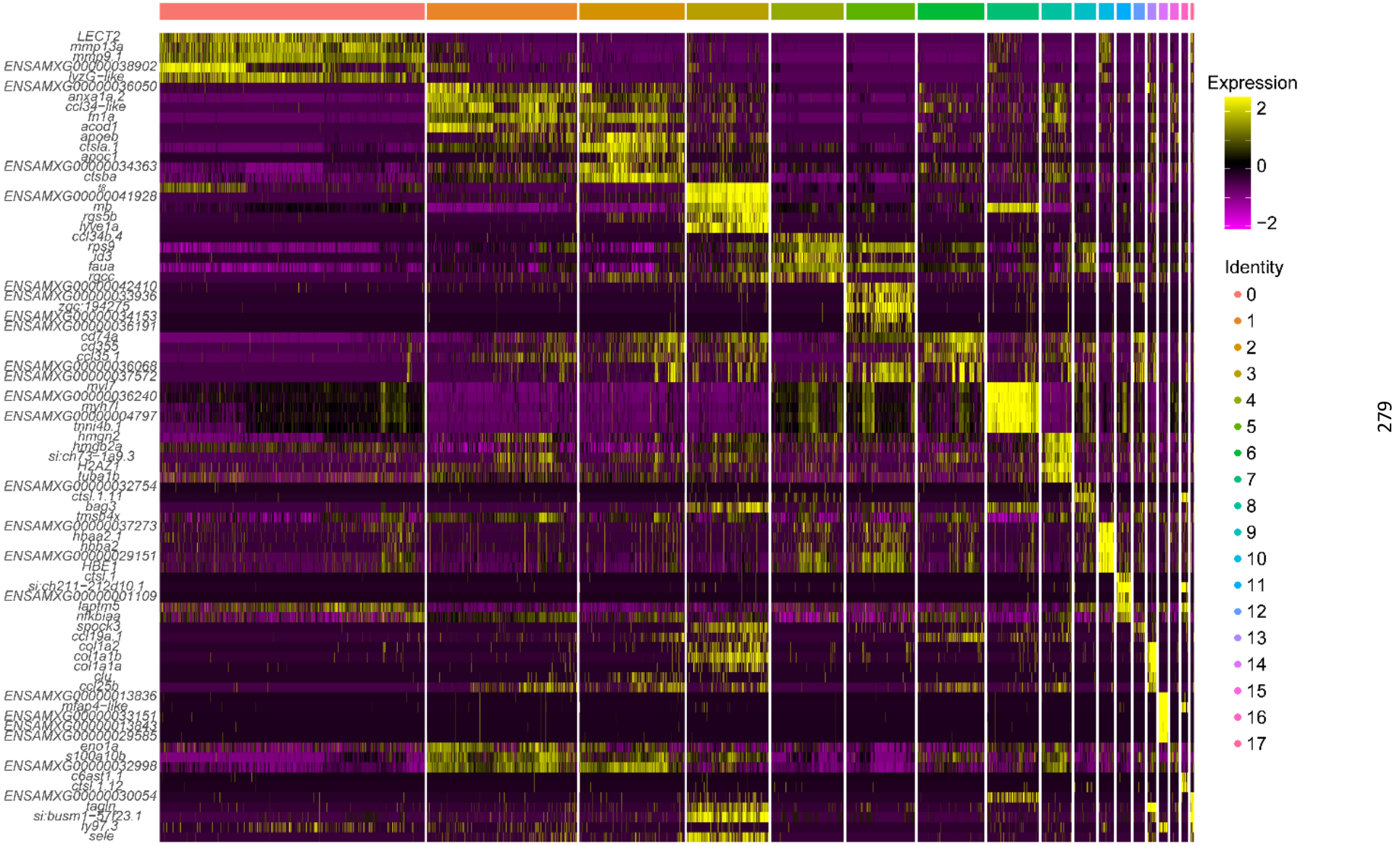
LECT2
mmp13a
mmp9.1
ENSAMXG00000038902
lyzG-like
ENSAMXG00000036050
anxa1a.2
ccl34-like
fn1a
acod1
apoeb
ctsla.1
apoc1
ENSAMXG00000034363
ctsba
ENSAMXG00000041928
mb
rgs5b
lyve1a
ccl34b.4
rps9
fd3
faua
rgcc
ENSAMXG00000042410
ENSAMXG00000033936
zgc:194275
ENSAMXG00000034153
ENSAMXG00000036191
cd74a
cd359
ccl35.1
ENSAMXG00000036068
ENSAMXG00000037572
myl1
ENSAMXG00000036240
myh7l
ENSAMXG00000004797
tnni4b.1
hmgn2
hmgb2a
si:ch73-1a9.3
H2AZ1
tuba1b
ENSAMXG00000032754
ctsl.1.11
bag3
tmsb4x
ENSAMXG00000037273
hbaa2.1
hbba2
ENSAMXG00000029151
HBE1
ctsl.1
si:ch211-212d10.1
ENSAMXG00000001109
laptm5
nfkbiaa
spock3
ccl19a.1
col1a2
col1a1b
col1a1a
glu
ccl25b
ENSAMXG00000013836
mfap4-like
ENSAMXG00000033151
ENSAMXG00000013843
ENSAMXG00000029585
eno1a
s100a10b
ENSAMXG00000032998
c6ast1.1
ctsl.1.12
ENSAMXG00000030054
tagln
si:busm1-57f23.1
ly97.3
sele
Expression
2
0
−2
Identity
0
1
2
3
4
5
6
7
8
9
10
11
12
13
14
15
16
17
279

Appendix 3. 5: Heatmap of the top5 leukocyte cluster markers identified using the ROC test

3.5 Characterisation of *A. mexicanus* leukocytes

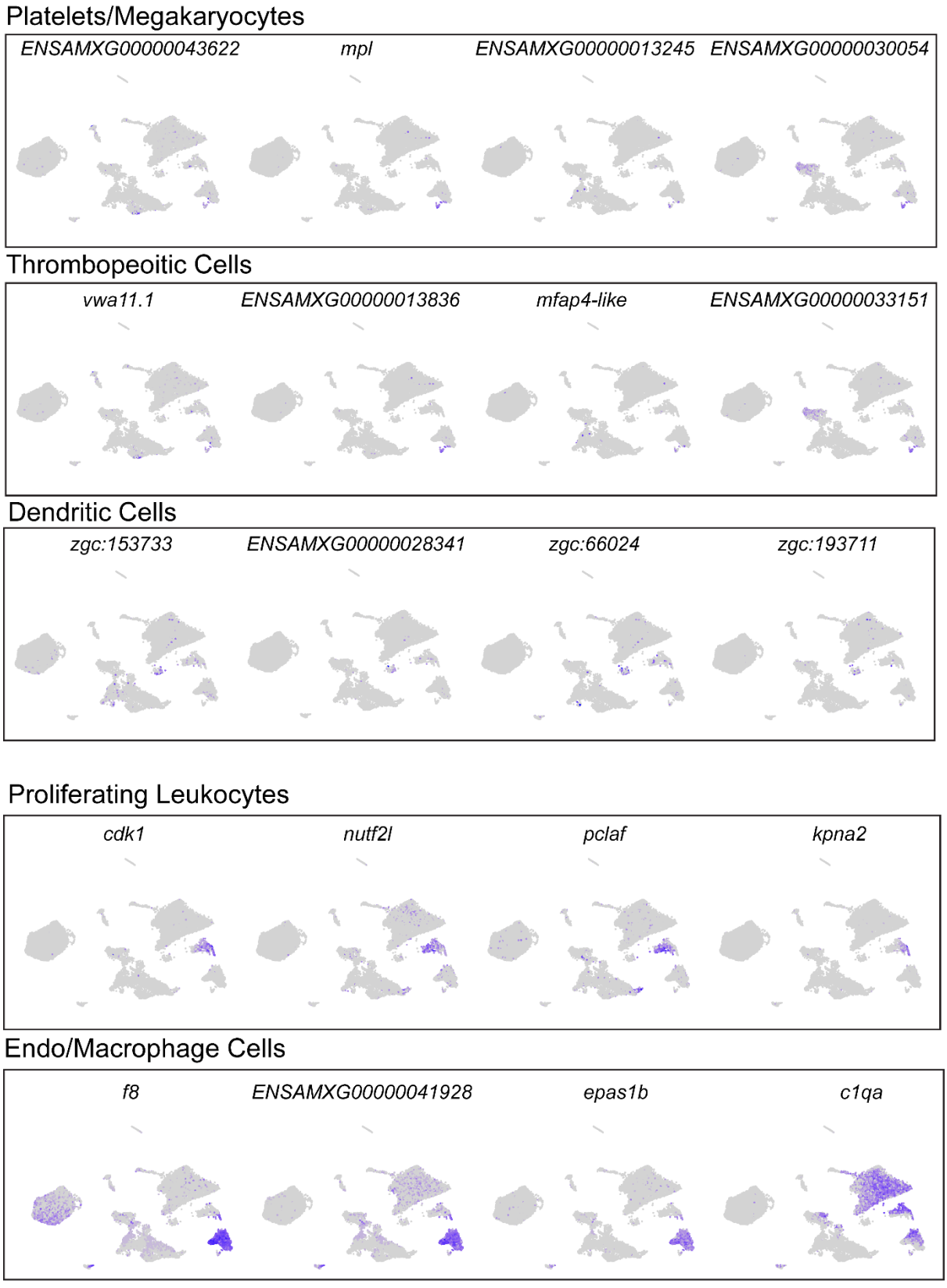

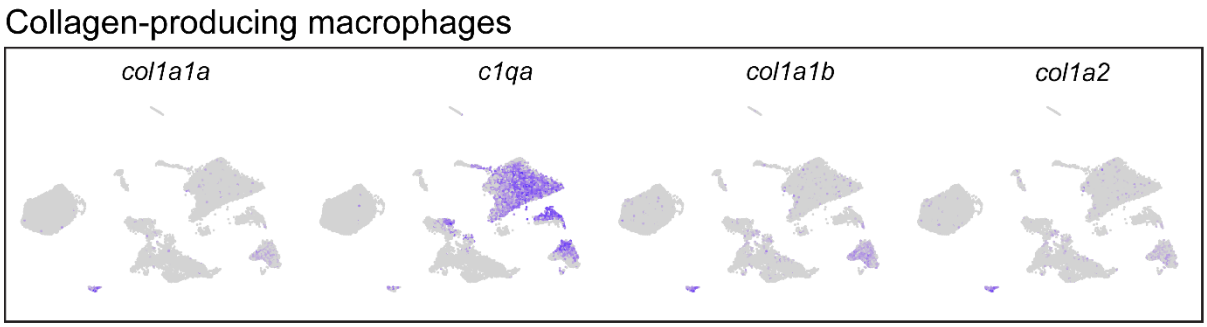

Appendix 3. 6: FeaturePlots of the top markers for leukocyte sub-populations

3.6 DPA analysis of *A. mexicanus* non-immune cells following cryoinjury

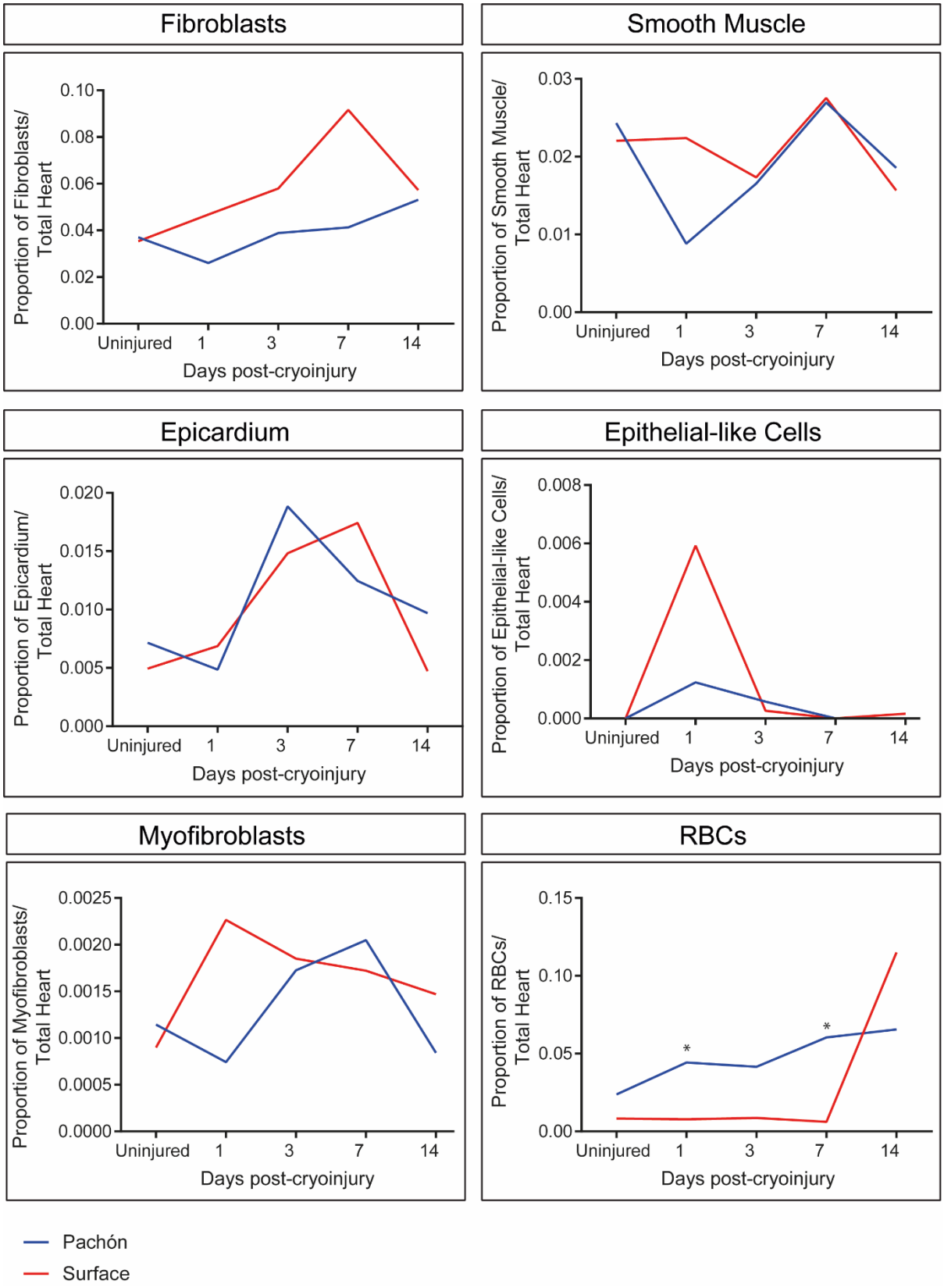
Fibroblasts
Proportion of Fibroblasts/ Total Heart
0.10
0.08
0.06
0.04
0.02
0.00
Uninjured 1 3 7 14
Days post-cryoinjury
Smooth Muscle
Proportion of Smooth Muscle/ Total Heart
0.03
0.02
0.01
0.00
Uninjured 1 3 7 14
Days post-cryoinjury
Epicardium
Proportion of Epicardium/ Total Heart
0.020
0.015
0.010
0.005
0.000
Uninjured 1 3 7 14
Days post-cryoinjury
Epithelial-like Cells
Proportion of Epithelial-like Cells/ Total Heart
0.008
0.006
0.004
0.002
0.000
Uninjured 1 3 7 14
Days post-cryoinjury
Myofibroblasts
Proportion of Myofibroblasts/ Total Heart
0.0025
0.0020
0.0015
0.0010
0.0005
0.0000
Uninjured 1 3 7 14
Days post-cryoinjury
RBCs
Proportion of RBCs/ Total Heart
0.15
0.10
0.05
0.00
*
*
Uninjured 1 3 7 14
Days post-cryoinjury
Pachón
Surface

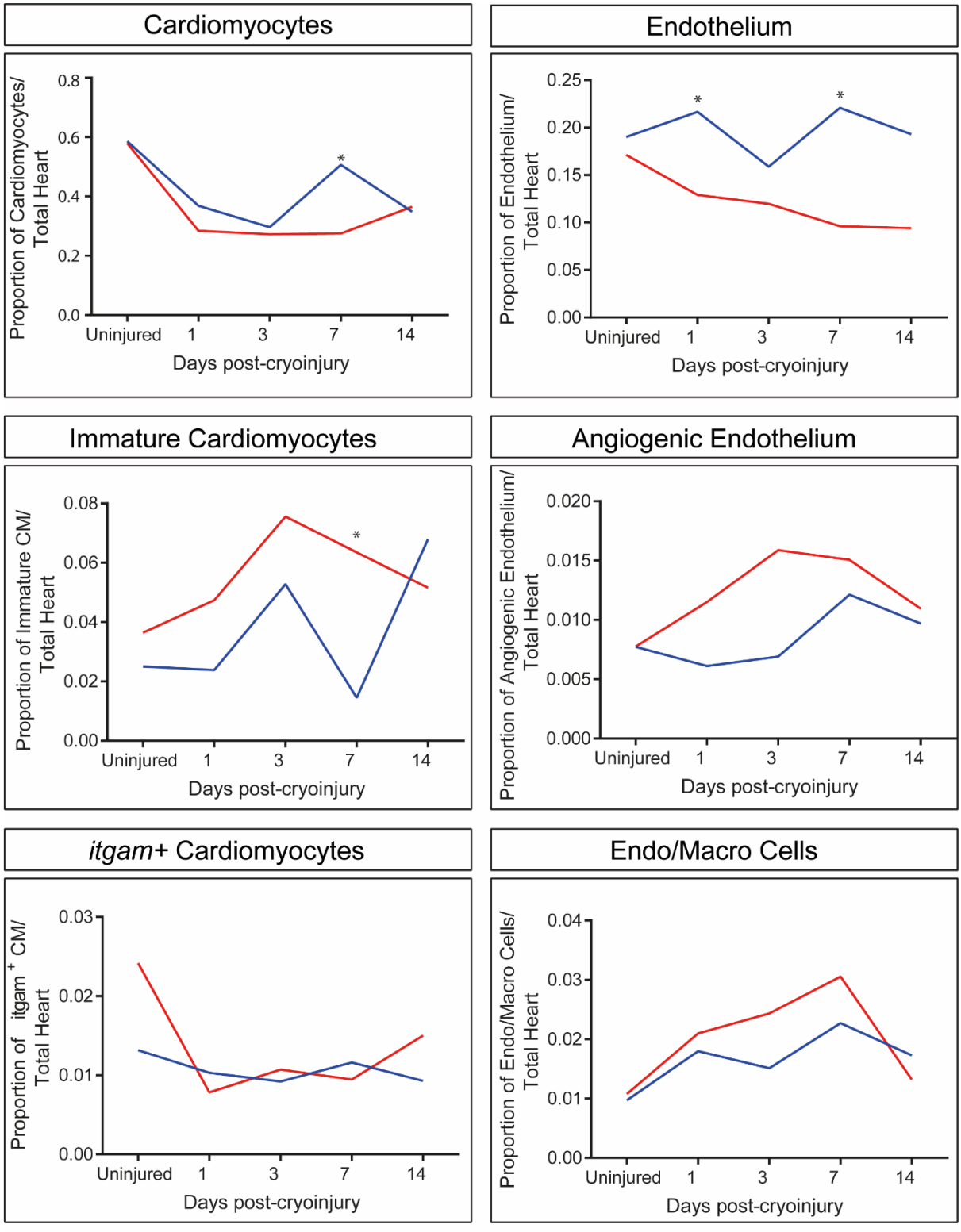
Cardiomyocytes
Proportion of Cardiomyocytes/ Total Heart
0.8
0.6
0.4
0.2
0.0
*
Uninjured 1 3 7 14
Days post-cryoinjury
Endothelium
Proportion of Endothelium/ Total Heart
0.25
0.20
0.15
0.10
0.05
0.00
* *
Uninjured 1 3 7 14
Days post-cryoinjury
Immature Cardiomyocytes
Proportion of Immature CM/ Total Heart
0.08
0.06
0.04
0.02
0.00
*
Uninjured 1 3 7 14
Days post-cryoinjury
Angiogenic Endothelium
Proportion of Angiogenic Endothelium/ Total Heart
0.020
0.015
0.010
0.005
0.000
Uninjured 1 3 7 14
Days post-cryoinjury
itgam+ Cardiomyocytes
Proportion of itgam+ CM/ Total Heart
0.03
0.02
0.01
0.00
Uninjured 1 3 7 14
Days post-cryoinjury
Endo/Macro Cells
Proportion of Endo/Macro Cells/ Total Heart
0.04
0.03
0.02
0.01
0.00
Uninjured 1 3 7 14
Days post-cryoinjury

Appendix 3. 7: DPA analysis reveals that cardiomyocytes, endothelial cells and erythrocytes show significant differences in their proportions following cryoinjury between PF and SF (*, p<0.05)

4.1 Identification of neutrophils from overall dataset

Neutrophils were identified from the overall scRNAseq dataset using a combination of canonical markers expression (eg. *mmp9*, *mmp13a* and *lect2*), and the unbiased screening of top markers in each cluster using the Wilcox test.

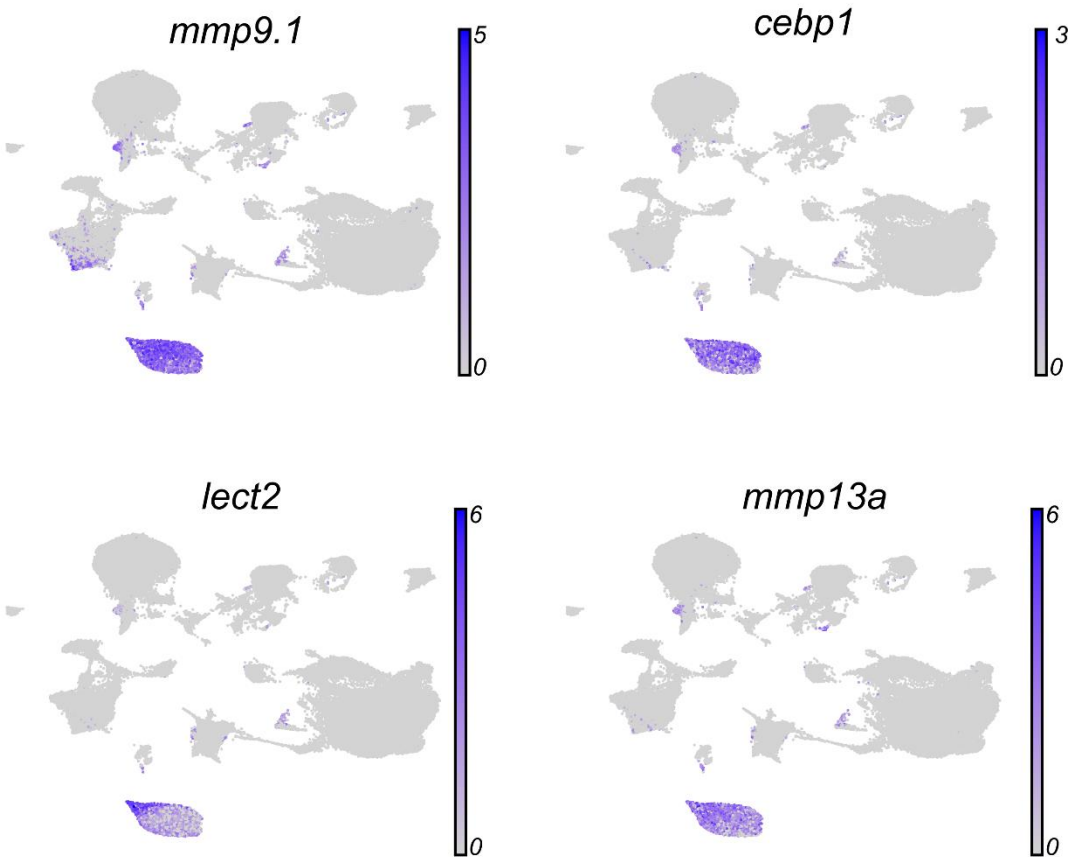

Appendix 4. 1: FeaturePlots showing gene expression of top neutrophil-specific markers in cluster 4 and 40 in the overall scRNAseq dataset

4.2 Neutrophil sub-cluster top markers

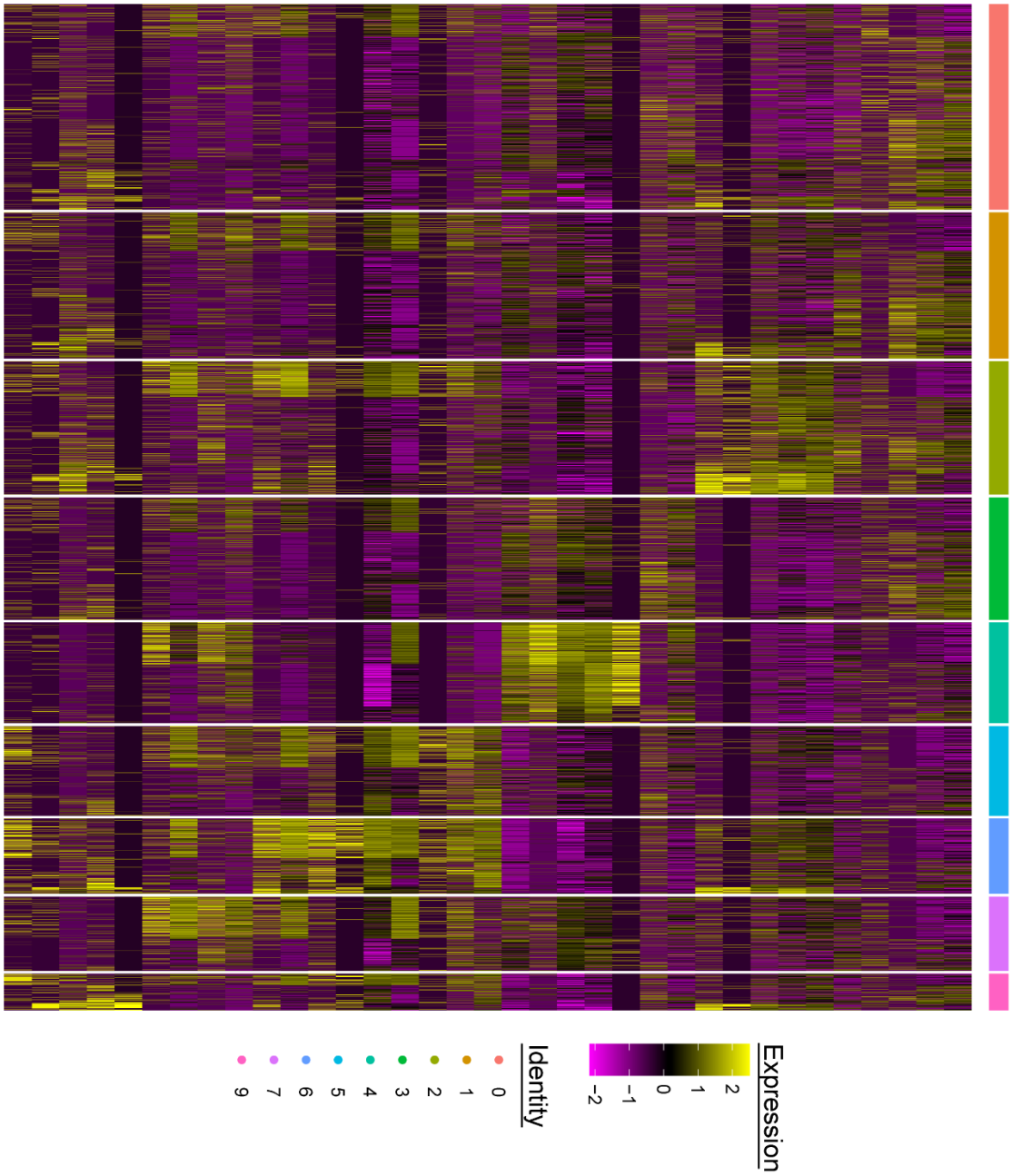

Appendix 4. 2: Heatmap of the top 5 cluster markers for each neutrophil subcluster identified using the ROC test

Doublet clusters 8, 10, 1 and 12 excluded from heatmap

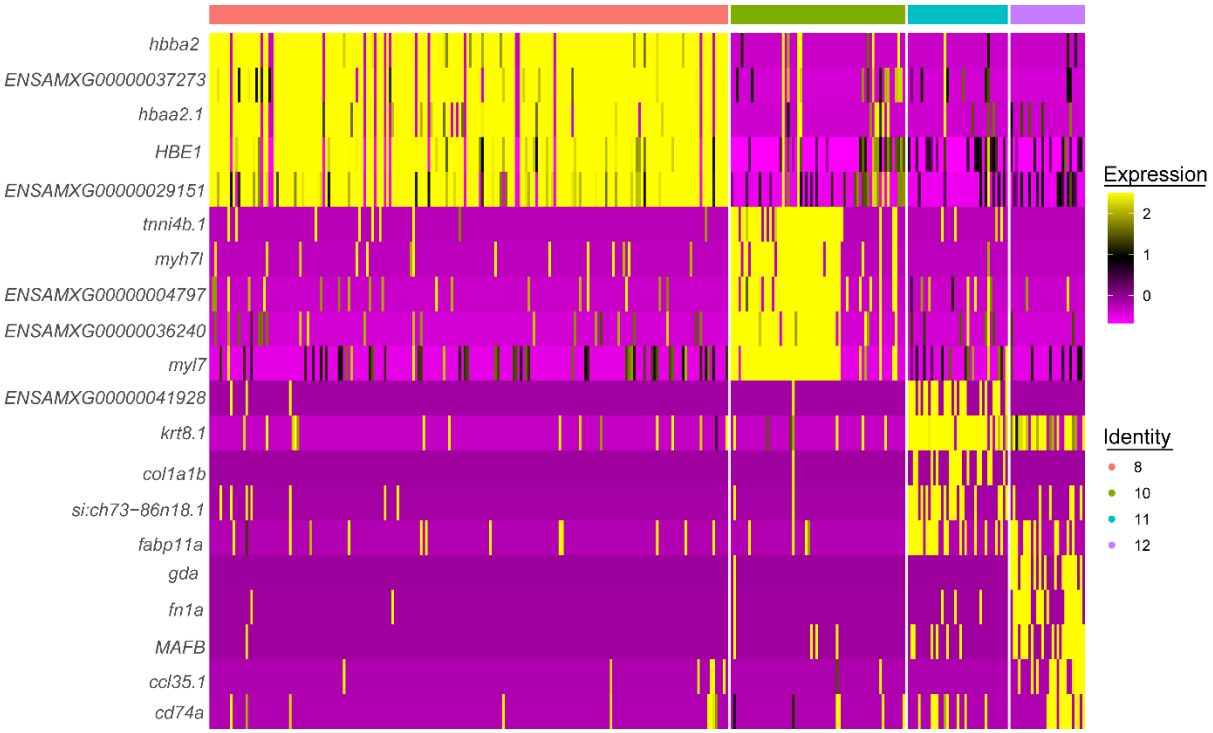

Appendix 4. 3: Heatmap of the top 5 cluster markers for each doublet cluster identified in the neutrophil scRNAseq dataset.

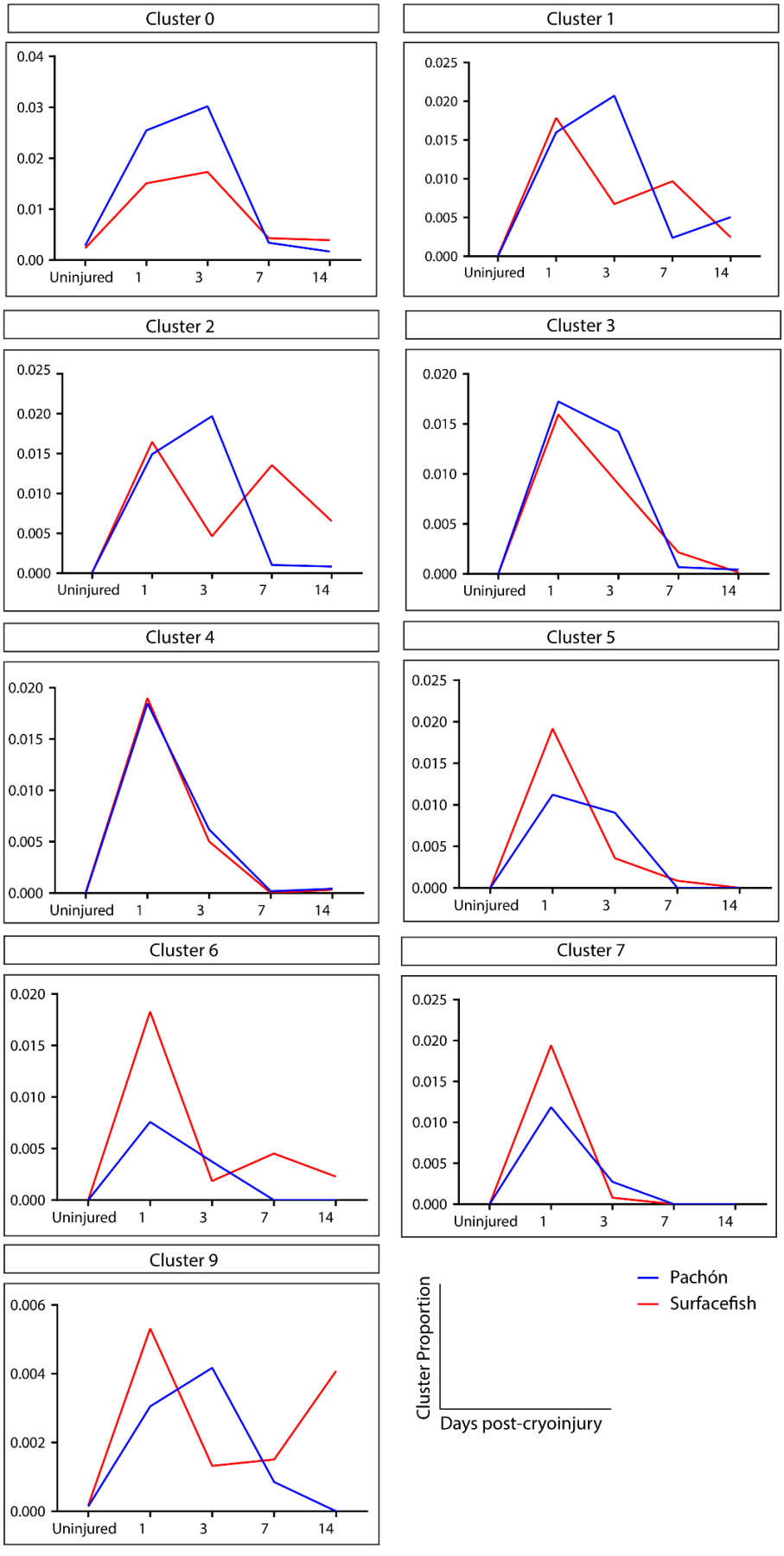
Cluster 0
Cluster 1
Cluster 2
Cluster 3
Cluster 4
Cluster 5
Cluster 6
Cluster 7
Cluster 9
Uninjured
1
3
7
14
Pachón
Surfacefish
Cluster Proportion
Days post-cryoinjury

Appendix 4. 4: Plots representing the temporal dynamics and proportions of each neutrophil sub-cluster over time for PF and SF

4.3 GSEA results for PF/SF neutrophils

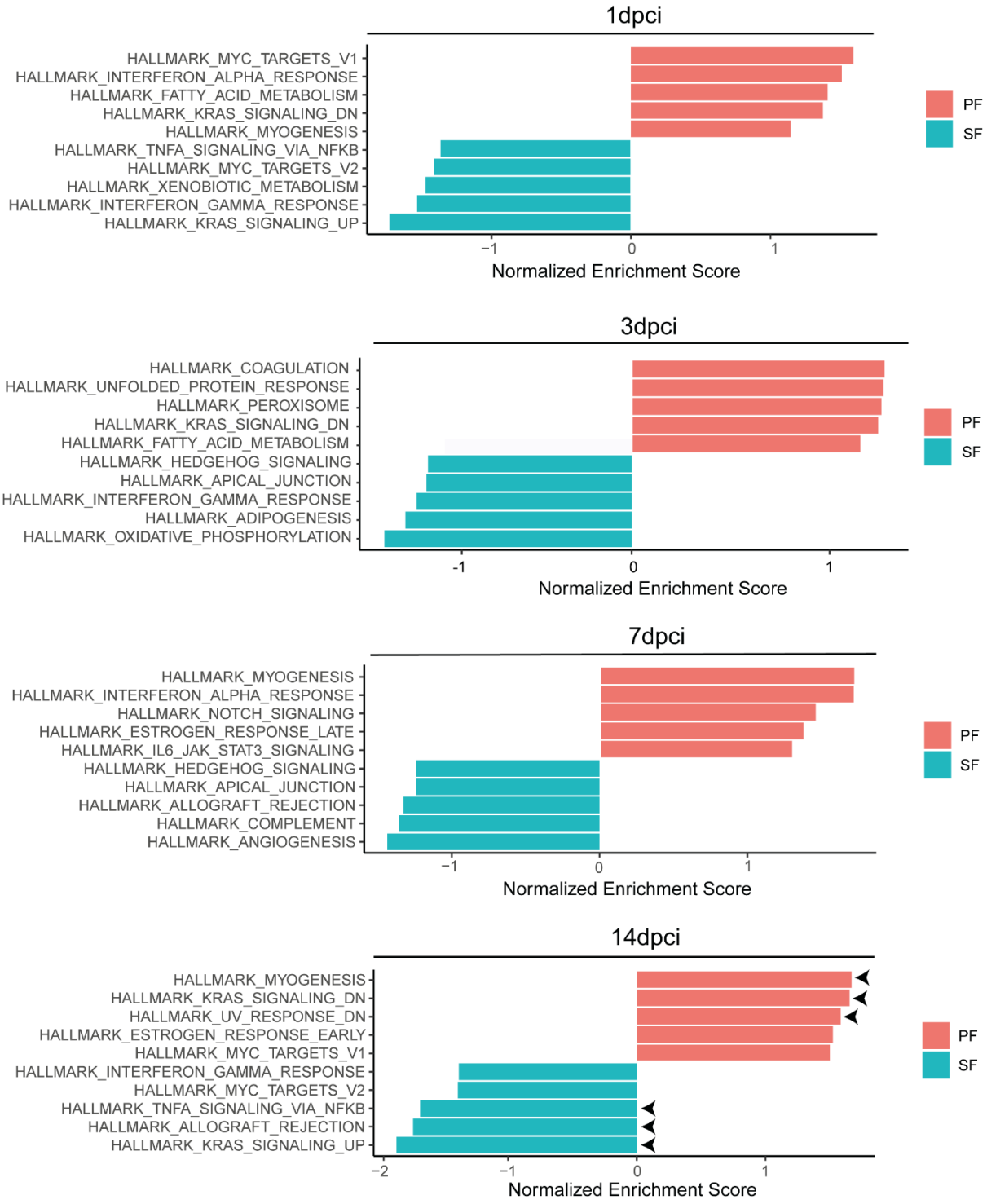

Appendix 4. 5: Plots representing the top 5 results of GSEA for PF/SF neutrophils at 1-, 3-, 7- and 14dpci. *Black arrows indicate Hallmark pathways that reached the threshold for significance (FDR<0.25)*

4.4 DGE analysis between uninjured neutrophils at 1dpci and 3pdci neutrophils

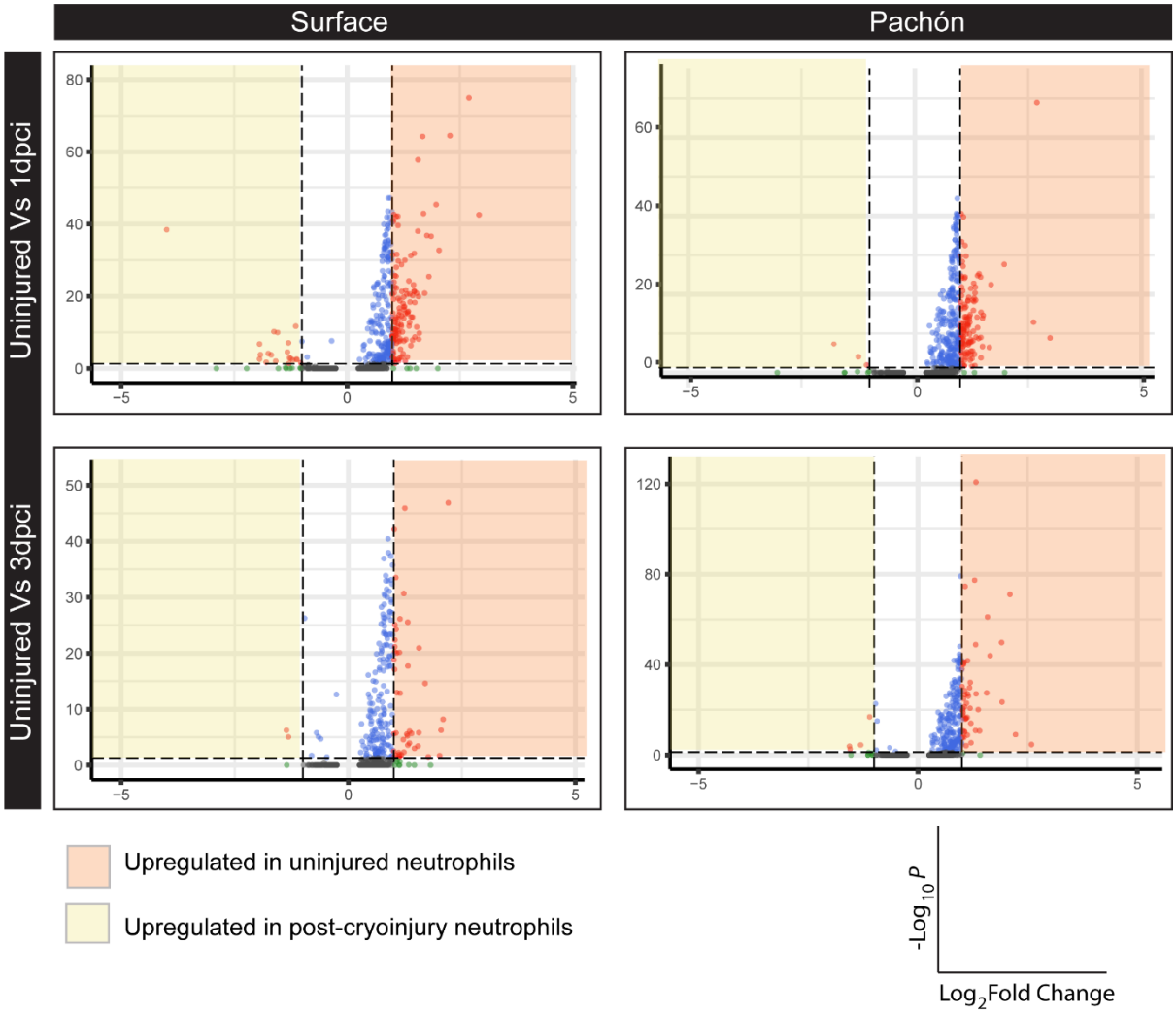

Appendix 4. 6: Volcano Plots showing the results of DGE analysis between uninjured Vs 1- and 3-dpci neutrophils for SF and PF

4.5 *mpeg1* expression in partially sequenced scRNAseq dataset

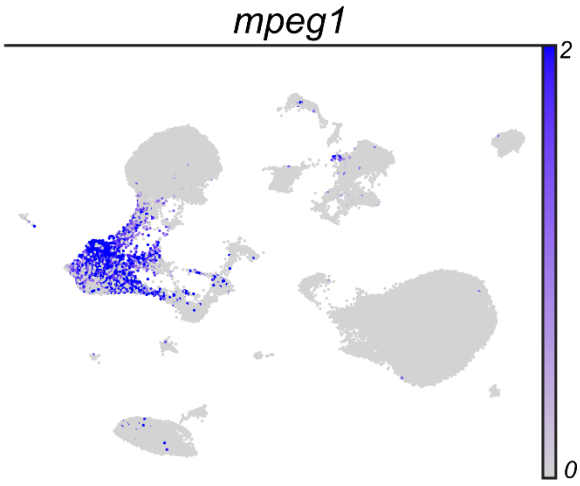

Appendix 4. 7: Expression levels of mpeg1 in the partially sequenced scRNAseq dataset (4 sequencing runs) suggested that mpeg1 was a macrophage-specific marker that was expressed in all macrophages

4.6 Top markers for macrophage sub-clusters

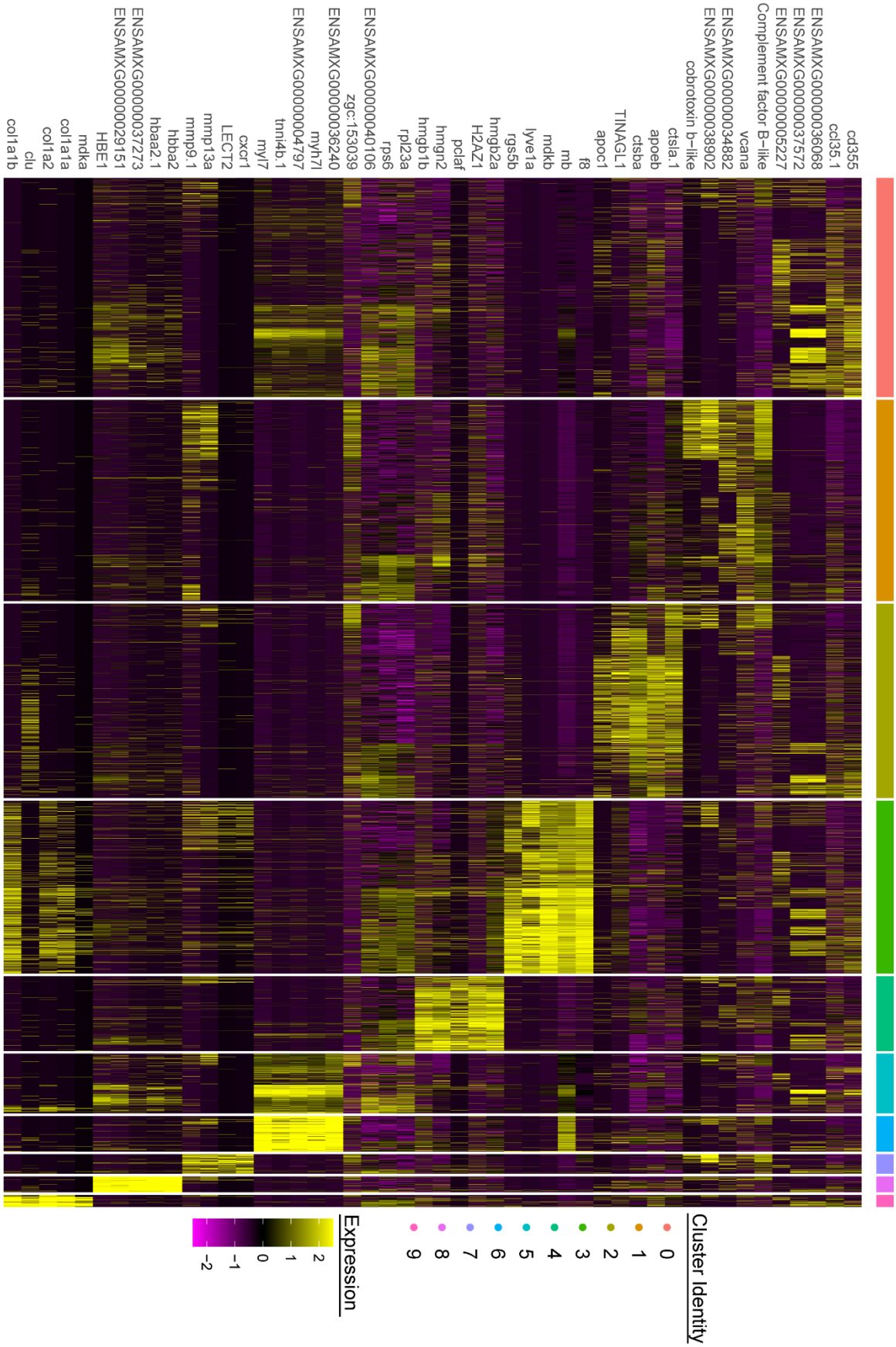

Appendix 4. 8: Heatmap of the top 5 cluster markers for each macrophage subcluster identified using the ROC test

4.7 GSEA results for PF/SF macrophages

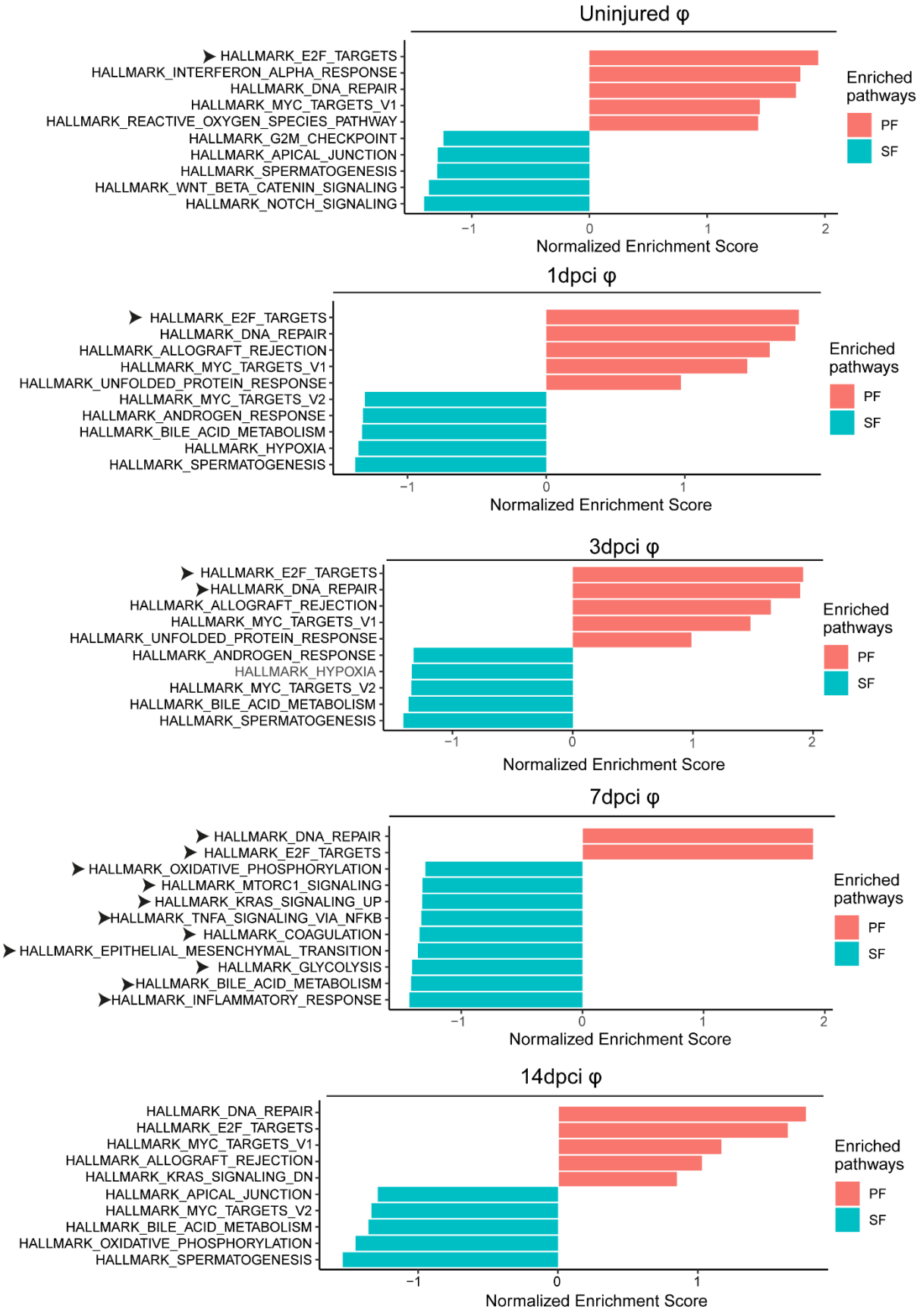

Appendix 4. 9: Plots representing the top 5 results of GSEA for PF/SF macrophages at uninjured, 1-, 3-, 7- and 14dpci. *Black arrows indicate Hallmark pathways that reached the threshold for significance (FDR<0.25)*

4.8 Results of B cell GSEA

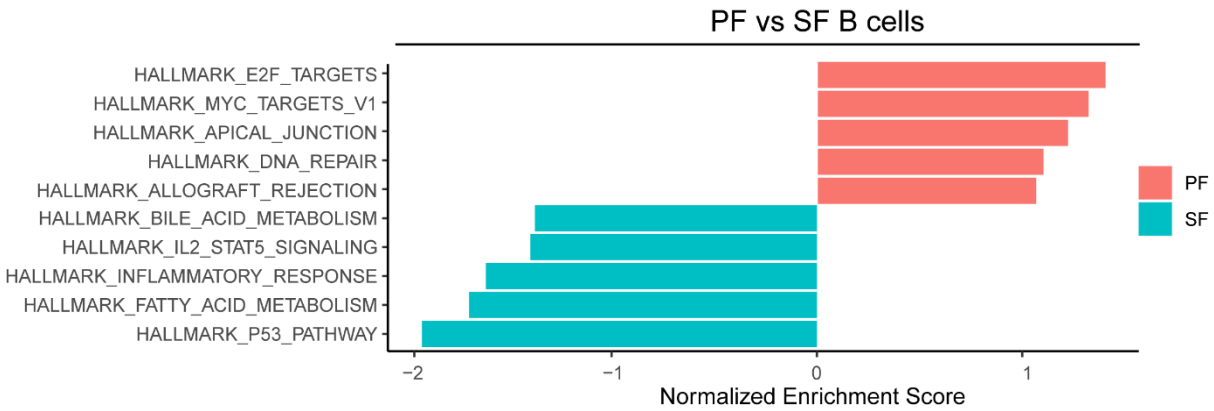

Appendix 4. 10: Plot representing the top 5 results of GSEA for PF/SF B cells. No pathways reached the FDR significance threshold

Bibliography

1. Khan, M. A. *et al.* Global Epidemiology of Ischemic Heart Disease: Results from the Global Burden of Disease Study. *Cureus* **12**, (2020).

2. The Lancet Gastroenterology & Hepatology. Obesity: another ongoing pandemic. *Lancet Gastroenterol. Hepatol.* **6**, 411 (2021).

3. Singer, M. E., Dorrance, K. A., Oxenreiter, M. M., Yan, K. R. & Close, K. L. The type 2 diabetes 'modern preventable pandemic' and replicable lessons from the COVID-19 crisis. *Prev. Med. Reports* **25**, 101636 (2022).

4. St. John Sutton, M. G. & Sharpe, N. Left Ventricular Remodeling After Myocardial Infarction. *Circulation* **101**, 2981–2988 (2000).

5. Virani, S. S. *et al.* Heart Disease and Stroke Statistics—2021 Update. *Circulation* E254–E743 (2021). doi:10.1161/CIR.0000000000000950

6. Libby, P. *et al.* Atherosclerosis. *Nat. Rev. Dis. Prim. 2019 51* **5**, 1–18 (2019).

7. Gerbin, K. A. & Murry, C. E. The winding road to regenerating the human heart. *Cardiovascular Pathology* **24**, 133–140 (2015).

8. Prabhu, S. D. & Frangogiannis, N. G. The Biological Basis for Cardiac Repair After Myocardial Infarction: From Inflammation to Fibrosis. *Circ. Res.* **119**, 91 (2016).

9. Cahill, T. J., Choudhury, R. P. & Riley, P. R. Heart regeneration and repair after myocardial infarction: Translational opportunities for novel therapeutics. *Nature Reviews Drug Discovery* **16**, 699–717 (2017).

10. Ertl, G., Gaudron, P., Eilles, C., Schorb, W. & Kochsiek, K. Compensatory mechanisms for cardiac dysfunction in myocardial infarction. *Basic Res. Cardiol.* **86 Suppl 3**, 159–165 (1991).

11. Travers, J. G., Kamal, F. A., Robbins, J., Yutzey, K. E. & Blaxall, B. C. Cardiac Fibrosis: The

Fibroblast Awakens. *Circ. Res.* **118**, 1021–40 (2016).

12. Braunwald, E. The war against heart failure: the Lancet lecture. *Lancet* **385**, 812–824 (2015).

13. British Heart Foundation (BHF). BHF Statistics - UK [Factsheet]. (2022).

14. Chen, C.-H., Sereti, K.-I., Wu, B. M. & Ardehali, R. Translational aspects of cardiac cell therapy. *J. Cell. Mol. Med.* **19**, 1757–72 (2015).

15. Lin, Z. & Pu, W. T. Strategies for Cardiac Regeneration and Repair. *Sci. Transl. Med.* **6**, (2014).

16. Chong, J. J. H. *et al.* Human embryonic-stem-cell-derived cardiomyocytes regenerate non-human primate hearts. *Nature* **510**, 273–277 (2014).

17. Liu, Y. W. *et al.* Human embryonic stem cell-derived cardiomyocytes restore function in infarcted hearts of non-human primates. *Nat. Biotechnol.* **36**, 597–605 (2018).

18. Isomi, M. *et al.* Overexpression of Gata4, Mef2c, and Tbx5 Generates Induced Cardiomyocytes Via Direct Reprogramming and Rare Fusion in the Heart. *Circulation* **143**, 2123–2125 (2021).

19. Qian, L. *et al.* In vivo reprogramming of murine cardiac fibroblasts into induced cardiomyocytes. *Nature* **485**, 593–598 (2012).

20. Mei, X. & Cheng, K. Recent Development in Therapeutic Cardiac Patches. *Front. Cardiovasc. Med.* **7**, 294 (2020).

21. Sadahiro, T. & Ieda, M. In vivo reprogramming as a new approach to cardiac regenerative therapy. *Semin. Cell Dev. Biol.* **122**, 21–27 (2022).

22. Poss, K. D., Wilson, L. G. & Keating, M. T. Heart Regeneration in Zebrafish. *Science (80-.).* **298**, 2188–2190 (2002).

23. Porrello, E. R. *et al.* Transient Regenerative Potential of the Neonatal Mouse Heart. *Science*

(80-.). **331**, 1078–1080 (2011).

24. Haubner, B. J. *et al.* Functional Recovery of a Human Neonatal Heart after Severe Myocardial Infarction. *Circ. Res.* **118**, 216–221 (2016).

25. Fratz, S. *et al.* Long-term myocardial scarring after operation for anomalous left coronary artery from the pulmonary artery. *Ann. Thorac. Surg.* **92**, 1761–1765 (2011).

26. Tsang, V. *et al.* Late donor cardiectomy after paediatric heterotopic cardiac transplantation. *Lancet* **374**, 387–392 (2009).

27. Lafontant, P. J. *et al.* The Giant Danio (D. Aequipinnatus) as A Model of Cardiac Remodeling and Regeneration. *Anat. Rec.* **295**, 234–248 (2012).

28. Grivas, J. *et al.* Cardiac repair and regenerative potential in the goldfish (Carassius auratus) heart. in *Comparative Biochemistry and Physiology Part - C: Toxicology and Pharmacologyy* **163**, 14–23 (Elsevier Inc., 2014).

29. Stockdale, W. T. *et al.* Heart Regeneration in the Mexican Cavefish. *Cell Rep.* **25**, 1997–2007 (2018).

30. Wang, W. *et al.* Changes in regeneration-responsive enhancers shape regenerative capacities in vertebrates. *Science (80-.).* **369**, (2020).

31. Bettencourt-Dias, M., Mittnacht, S. & Brockes, J. P. Heterogeneous proliferative potential in regenerative adult newt cardiomyocytes. *J. Cell Sci.* **116**, 4001–4009 (2003).

32. Laube, F., Heister, M., Scholz, C., Borchardt, T. & Braun, T. Re-programming of newt cardiomyocytes is induced by tissue regeneration. *J. Cell Sci.* **119**, 4719–4729 (2006).

33. Witman, N., Murtuza, B., Davis, B., Arner, A. & Morrison, J. I. Recapitulation of developmental cardiogenesis governs the morphological and functional regeneration of adult newt hearts following injury. *Dev. Biol.* **354**, 67–76 (2011).

34. Uemasu, H. *et al.* Cryo-injury procedure-induced cardiac regeneration shows unique gene expression profiles in the newt Pleurodeles waltl. *Dev. Dyn.* (2021). doi:10.1002/DVDY.450

35. Potts, H. G., Stockdale, W. T. & Mommersteeg, M. T. M. Unlocking the Secrets of the Regenerating Fish Heart: Comparing Regenerative Models to Shed Light on Successful Regeneration. *J. Cardiovasc. Dev. Dis.* **8**, 4 (2021).

36. Wang, J. *et al.* The regenerative capacity of zebrafish reverses cardiac failure caused by genetic cardiomyocyte depletion. *Development* **138**, 3421–30 (2011).

37. Lavine, K. J. *et al.* Distinct macrophage lineages contribute to disparate patterns of cardiac recovery and remodeling in the neonatal and adult heart. *Proc. Natl. Acad. Sci. U. S. A.* **111**, 16029–16034 (2014).

38. Curado, S. *et al.* Conditional targeted cell ablation in zebrafish: a new tool for regeneration studies. *Dev. Dyn.* **236**, 1025–1035 (2007).

39. Chablais, F., Veit, J., Rainer, G. & Jaźwińska, A. The zebrafish heart regenerates after cryoinjury-induced myocardial infarction. *BMC Dev. Biol.* **11**, 21 (2011).

40. González-Rosa, J. M. & Mercader, N. Cryoinjury as a myocardial infarction model for the study of cardiac regeneration in the zebrafish. *Nat. Protoc.* **7**, 782–788 (2012).

41. Polizzotti, B. D., Ganapathy, B., Haubner, B. J., Penninger, J. M. & Kühn, B. A cryoinjury model in neonatal mice for cardiac translational and regeneration research. *Nat. Protoc.* **11**, 542–552 (2016).

42. Dittrich, A. & Lauridsen, H. Cryo-injury Induced Heart Regeneration in the Axolotl and Echocardiography and Unbiased Quantitative Histology to Evaluate Regenerative Progression. *J. Vis. Exp.* **2021**, (2021).

43. Dyck, P. K. Van *et al.* Cauterization as a Simple Method for Regeneration Studies in the

Zebrafish Heart. *J. Cardiovasc. Dev. Dis.* **7**, 41 (2020).

44. Flink, I. L. Cell cycle reentry of ventricular and atrial cardiomyocytes and cells within the epicardium following amputation of the ventricular apex in the axolotl, Amblystoma mexicanum: confocal microscopic immunofluorescent image analysis of bromodeoxyuridine-labeled nuclei. *Anat. Embryol. (Berl).* **205**, 235–244 (2002).

45. Blom, J. N., Lu, X., Arnold, P. & Feng, Q. Myocardial Infarction in Neonatal Mice, A Model of Cardiac Regeneration. *J. Vis. Exp.* (2016). doi:10.3791/54100

46. Jopling, C. *et al.* Zebrafish heart regeneration occurs by cardiomyocyte dedifferentiation and proliferation. *Nature* **464**, 606–609 (2010).

47. Kikuchi, K. *et al.* Primary contribution to zebrafish heart regeneration by gata4+ cardiomyocytes. *Nature* **464**, 601–605 (2010).

48. Porrello, E. R. *et al.* Regulation of neonatal and adult mammalian heart regeneration by the miR-15 family. *Proc. Natl. Acad. Sci. U. S. A.* **110**, 187–192 (2013).

49. Senyo, S. E. *et al.* Mammalian heart renewal by pre-existing cardiomyocytes. *Nature* **493**, 433–436 (2013).

50. Kirillova, A., Han, L., Liu, H. & Kühn, B. Polyploid cardiomyocytes: Implications for heart regeneration. *Dev.* **148**, (2021).

51. Bergmann, O. *et al.* Evidence for cardiomyocyte renewal in humans. *Science (80-.).* **324**, 98–102 (2009).

52. Fu, W. bin, Wang, W. E. & Zeng, C. yu. Wnt signaling pathways in myocardial infarction and the therapeutic effects of Wnt pathway inhibitors. *Acta Pharmacol. Sin.* **40**, 9–12 (2019).

53. Peng, X. *et al.* Induction of Wnt signaling antagonists and p21-activated kinase enhances cardiomyocyte proliferation during zebrafish heart regeneration. *J. Mol. Cell Biol.* **13**, 41–58

(2021).

54. Peng, X. *et al.* Wnt2bb Induces Cardiomyocyte Proliferation in Zebrafish Hearts via the jnk1/c-jun/creb1 Pathway. *Front. Cell Dev. Biol.* **8**, 323 (2020).

55. Oerlemans, M. I. F. J. *et al.* Active Wnt signaling in response to cardiac injury. *Basic Res. Cardiol.* **105**, 631–641 (2010).

56. MacGrogan, D., Münch, J. & de la Pompa, J. L. Notch and interacting signalling pathways in cardiac development, disease, and regeneration. *Nat. Rev. Cardiol. 2018 1511* **15**, 685–704 (2018).

57. Zhao, L. *et al.* Notch signaling regulates cardiomyocyte proliferation during zebrafish heart regeneration. *Proc. Natl. Acad. Sci. U. S. A.* **111**, 1403–1408 (2014).

58. Zhang, R. *et al.* In vivo cardiac reprogramming contributes to zebrafish heart regeneration. *Nature* **498**, 497–501 (2013).

59. Münch, J., Grivas, D., González-Rajal, Á., Torregrosa-Carrión, R. & de la Pompa, J. L. Notch signalling restricts inflammation and serpine1 expression in the dynamic endocardium of the regenerating zebrafish heart. *Development* **144**, 1425–1440 (2017).

60. Zhao, L., Ben-Yair, R., Burns, C. E. & Burns, C. G. Endocardial Notch Signaling Promotes Cardiomyocyte Proliferation in the Regenerating Zebrafish Heart through Wnt Pathway Antagonism. *Cell Rep.* **26**, 546-554.e5 (2019).

61. Gude, N. A. *et al.* Activation of Notch-Mediated Protective Signaling in the Myocardium. *Circ. Res.* **102**, 1025 (2008).

62. Kratsios, P. *et al.* Distinct roles for cell-autonomous Notch signaling in cardiomyocytes of the embryonic and adult heart. *Circ. Res.* **106**, 559–572 (2010).

63. He, Y. *et al.* Blockade of RBP-J-Mediated Notch Signaling Pathway Exacerbates Cardiac

Remodeling after Infarction by Increasing Apoptosis in Mice. *Biomed Res. Int.* **2018**, (2018).

64. Mia, M. M. & Singh, M. K. The Hippo Signaling Pathway in Cardiac Development and Diseases. *Front. Cell Dev. Biol.* **7**, 211 (2019).

65. Heallen, T. *et al.* Hippo signaling impedes adult heart regeneration. *Development* **140**, 4683–4690 (2013).

66. Xin, M. *et al.* Hippo pathway effector Yap promotes cardiac regeneration. *Proc. Natl. Acad. Sci. U. S. A.* **110**, 13839–13844 (2013).

67. Flinn, M. A., Jeffery, B. E., O'Meara, C. C. & Link, B. A. Yap is required for scar formation but not myocyte proliferation during heart regeneration in zebrafish. *Cardiovasc. Res.* **115**, 570–577 (2019).

68. Riley, S. E., Feng, Y. & Hansen, C. G. Hippo-Yap/Taz signalling in zebrafish regeneration. *npj Regen. Med. 2022 71* **7**, 1–16 (2022).

69. Gemberling, M., Karra, R., Dickson, A. L. & Poss, K. D. Nrg1 is an injury-induced cardiomyocyte mitogen for the endogenous heart regeneration program in zebrafish. *Elife* (2015). doi:10.7554/ELIFE.05871

70. D'uva, G. *et al.* ERBB2 triggers mammalian heart regeneration by promoting cardiomyocyte dedifferentiation and proliferation. *Nat. Cell Biol.* **17**, 627 (2015).

71. Honkoop, H. *et al.* Single-cell analysis uncovers that metabolic reprogramming by ErbB2 signaling is essential for cardiomyocyte proliferation in the regenerating heart. *Elife* **8**, 50163 (2019).

72. Cao, J. & Poss, K. D. The epicardium as a hub for heart regeneration. *Nat. Rev. Cardiol.* **15**, 631–647 (2018).

73. Hui, S. P. *et al.* Zebrafish Regulatory T Cells Mediate Organ-Specific Regenerative Programs.

Dev. Cell **43**, 659-672.e5 (2017).

74. Huang, Y. *et al.* Igf Signaling is Required for Cardiomyocyte Proliferation during Zebrafish Heart Development and Regeneration. *PLoS One* **8**, e67266 (2013).

75. Chablais, F. & Jaźwińska, A. The regenerative capacity of the zebrafish heart is dependent on TGFβ signaling. *Development* **139**, 1921–1930 (2012).

76. Wang, J., Cao, J., Dickson, A. L. & Poss, K. D. Epicardial regeneration is guided by cardiac outflow tract and Hedgehog signalling. *Nat. 2015 5227555* **522**, 226–230 (2015).

77. McAlpine, H. M. & Cobbe, S. M. Neuroendocrine changes in acute myocardial infarction. *Am. J. Med.* **84**, 61–66 (1988).

78. Sigurdsson, A., Held, P. & Swedberg, K. Short- and long-term neurohormonal activation following acute myocardial infarction. *Am. Heart J.* **126**, 1068–1075 (1993).

79. Karlsberg, R. P., Cryer, P. E. & Roberts, R. Serial plasma catecholamine response early in the course of clinical acute myocardial infarction: relationship to infarct extent and mortality. *Am. Heart J.* **102**, 24–29 (1981).

80. Graham, L. N., Smith, P. A., Stoker, J. B., Mackintosh, A. F. & Mary, D. A. S. G. Time course of sympathetic neural hyperactivity after uncomplicated acute myocardial infarction. *Circulation* **106**, 793–797 (2002).

81. Lombardi, F. *et al.* Heart rate variability in the early hours of an acute myocardial infarction. *Am. J. Cardiol.* **77**, 1037–1044 (1996).

82. Mahmoud, A. I. *et al.* Nerves Regulate Cardiomyocyte Proliferation and Heart Regeneration. *Dev. Cell* **34**, 387–399 (2015).

83. Chute, M., Aujla, P., Jana, S. & Kassiri, Z. The Non-Fibrillar Side of Fibrosis: Contribution of the Basement Membrane, Proteoglycans, and Glycoproteins to Myocardial Fibrosis. *J. Cardiovasc.*

Dev. Dis. 2019, Vol. 6, Page 35 **6**, 35 (2019).

84. Silva, A. C., Pereira, C., Fonseca, A. C. R. G., Pinto-do-Ó, P. & Nascimento, D. S. Bearing My Heart: The Role of Extracellular Matrix on Cardiac Development, Homeostasis, and Injury Response. *Front. Cell Dev. Biol.* **8**, 1705 (2021).

85. Yahalom-Ronen, Y., Rajchman, D., Sarig, R., Geiger, B. & Tzahor, E. Reduced matrix rigidity promotes neonatal cardiomyocyte dedifferentiation, proliferation and clonal expansion. *Elife* **4**, (2015).

86. Chen, W. C. W. *et al.* Decellularized zebrafish cardiac extracellular matrix induces mammalian heart regeneration. *Sci. Adv.* **2**, (2016).

87. Bassat, E. *et al.* The extracellular matrix protein agrin promotes heart regeneration in mice. *Nature* **547**, 179–184 (2017).

88. Kühn, B. *et al.* Periostin induces proliferation of differentiated cardiomyocytes and promotes cardiac repair. *Nat. Med.* **13**, (2007).

89. Ieda, M. *et al.* Cardiac Fibroblasts Regulate Myocardial Proliferation through β1 Integrin Signaling. *Dev. Cell* **16**, 233–244 (2009).

90. Chen, Z. *et al.* Ablation of periostin inhibits post-infarction myocardial regeneration in neonatal mice mediated by the phosphatidylinositol 3 kinase/glycogen synthase kinase 3β/cyclin D1 signalling pathway. *Cardiovasc. Res.* **113**, 620–632 (2017).

91. Wang, Z. *et al.* Decellularized neonatal cardiac extracellular matrix prevents widespread ventricular remodeling in adult mammals after myocardial infarction. *Acta Biomater.* **87**, 140–151 (2019).

92. Sakaguchi, A. & Kimura, W. Metabolic regulation of cardiac regeneration: roles of hypoxia, energy homeostasis, and mitochondrial dynamics. *Curr. Opin. Genet. Dev.* **70**, 54–60 (2021).

93. Puente, B. N. *et al.* The oxygen-rich postnatal environment induces cardiomyocyte cell-cycle arrest through DNA damage response. *Cell* **157**, 565–579 (2014).

94. Jopling, C. *et al.* Hypoxia Induces Myocardial Regeneration in Zebrafish. *Circulation* **126**, 3017–3027 (2012).

95. Nakada, Y. *et al.* Hypoxia induces heart regeneration in adult mice. *Nat. 2017 5417636* **541**, 222–227 (2016).

96. Fukuda, R. *et al.* Stimulation of glycolysis promotes cardiomyocyte proliferation after injury in adult zebrafish. *EMBO Rep.* **21**, e49752 (2020).

97. Marín-Juez, R. *et al.* Fast revascularization of the injured area is essential to support zebrafish heart regeneration. *Proc. Natl. Acad. Sci. U. S. A.* **113**, 11237–11242 (2016).

98. Marín-Juez, R. *et al.* Coronary Revascularization During Heart Regeneration Is Regulated by Epicardial and Endocardial Cues and Forms a Scaffold for Cardiomyocyte Repopulation. *Dev. Cell* **51**, 503-515.e4 (2019).

99. Lepilina, A. *et al.* A Dynamic Epicardial Injury Response Supports Progenitor Cell Activity during Zebrafish Heart Regeneration. *Cell* **127**, 607–619 (2006).

100. Itou, J. *et al.* Migration of cardiomyocytes is essential for heart regeneration in zebrafish. *Development* **139**, 4133–4142 (2012).

101. Grivas, D., González-Rajal, Á. & de la Pompa, J. L. Midkine-a Regulates the Formation of a Fibrotic Scar During Zebrafish Heart Regeneration. *Front. Cell Dev. Biol.* **9**, 1084 (2021).

102. Wang, J., Karra, R., Dickson, A. L. & Poss, K. D. Fibronectin is deposited by injury-activated epicardial cells and is necessary for zebrafish heart regeneration. *Dev. Biol.* **382**, 427–435 (2013).

103. Aurora, A. B. *et al.* Macrophages are required for neonatal heart regeneration. *J. Clin. Invest.*

124, 1382–92 (2014).

104. Godwin, J. W., Debuque, R., Salimova, E. & Rosenthal, N. A. Heart regeneration in the salamander relies on macrophage-mediated control of fibroblast activation and the extracellular landscape. *npj Regen. Med.* **2**, 22 (2017).

105. Huang, W.-C. *et al.* Treatment of Glucocorticoids Inhibited Early Immune Responses and Impaired Cardiac Repair in Adult Zebrafish. *PLoS One* **8**, 66613 (2013).

106. Han, C. *et al.* Acute inflammation stimulates a regenerative response in the neonatal mouse heart. **25**, 1137–1151 (2015).

107. Xu, S. *et al.* Excessive inflammation impairs heart regeneration in zebrafish breakdance mutant after cryoinjury. *Fish Shellfish Immunol.* **89**, 117–126 (2019).

108. De Preux Charles, A. S., Bise, T., Baier, F., Marro, J. & Jaźwińska, A. Distinct effects of inflammation on preconditioning and regeneration of the adult zebrafish heart. *Open Biol.* **6**, (2016).

109. Lai, S. L. *et al.* Reciprocal analyses in zebrafish and medaka reveal that harnessing the immune response promotes cardiac regeneration. *Elife* **6**, (2017).

110. Gaspar, H. B., Gilmour, K. C. & Jones, A. M. Severe combined immunodeficiency—molecular pathogenesis and diagnosis. *Arch. Dis. Child.* **84**, 169–173 (2001).

111. Buchmann, K. Evolution of innate immunity: Clues from invertebrates via fish to mammals. *Front. Immunol.* **5**, 459 (2014).

112. Flajnik, M. F. & Kasahara, M. Origin and evolution of the adaptive immune system: genetic events and selective pressures. *Nat. Rev. Genet.* **11**, 47–59 (2009).

113. Livák, F. & Petrie, H. T. Somatic generation of antigen-receptor diversity: a reprise. *Trends Immunol.* **22**, 608–612 (2001).

114. Janeway CA Jr, Travers, P. & M, W. Immunological Memory. in *Immunobiology: The Immune System in Health and Disease* (2001).

115. Sattler, S. & Rosenthal, N. The neonate versus adult mammalian immune system in cardiac repair and regeneration. *Biochim. Biophys. Acta - Mol. Cell Res.* **1863**, 1813–1821 (2016).

116. Basha, S., Surendran, N. & Pichichero, M. Immune Responses in Neonates. *Expert Rev. Clin. Immunol.* **10**, 1171 (2014).

117. Godwin, J. W., Pinto, A. R. & Rosenthal, N. A. Chasing the recipe for a pro-regenerative immune system. *Semin. Cell Dev. Biol.* **61**, 71–79 (2017).

118. Abnave, P. & Ghigo, E. Role of the immune system in regeneration and its dynamic interplay with adult stem cells. *Semin. Cell Dev. Biol.* **87**, 160–168 (2019).

119. Julier, Z., Park, A. J., Briquez, P. S. & Martino, M. M. *Promoting tissue regeneration by modulating the immune system*. **53**, 13–28 (2017).

120. Lai, S. L., Marín-Juez, R. & Stainier, D. Y. R. Immune responses in cardiac repair and regeneration: a comparative point of view. *Cellular and Molecular Life Sciences* **76**, 1365–1380 (2019).

121. Kany, S., Vollrath, J. T. & Relja, B. Cytokines in Inflammatory Disease. *Int. J. Mol. Sci.* **20**, (2019).

122. Dittrich, A. & Lauridsen, H. Myocardial infarction and the immune response - Scarring or regeneration? A comparative look at mammals and popular regenerating animal models. *J. Immunol. Regen. Med.* **4**, 100016 (2019).

123. Relja, B. & Land, W. G. Damage-associated molecular patterns in trauma. *Eur. J. Trauma Emerg. Surg.* **46**, 751–775 (2020).

124. Toldo, S., Mauro, A. G., Cutter, Z. & Abbate, A. Inflammasome, pyroptosis, and cytokines in

myocardial ischemia-reperfusion injury. *Am. J. Physiol. - Hear. Circ. Physiol.* **315**, H1553–H1568 (2018).

125. Vandendriessche, S., Cambier, S., Proost, P. & Marques, P. E. Complement Receptors and Their Role in Leukocyte Recruitment and Phagocytosis. *Front. Cell Dev. Biol.* **9**, 144 (2021).

126. Freeley, S., Kemper, C. & Le Friec, G. The 'Ins and Outs' of complement-driven immune responses. *Immunol. Rev.* **274**, 16 (2016).

127. Marchini, T., Mitre, L. S. & Wolf, D. Inflammatory Cell Recruitment in Cardiovascular Disease. *Front. Cell Dev. Biol.* **9**, (2021).

128. Puhl, S.-L. & Steffens, S. Neutrophils in Post-myocardial Infarction Inflammation: Damage vs. Resolution? *Front. Cardiovasc. Med.* **6**, 25 (2019).

129. Mentkowski, K. I., Euscher, L. M., Patel, A., Alevriadou, B. R. & Lang, J. K. Inflammation: From Cellular Mechanisms to Immune Cell Education Monocyte recruitment and fate specification after myocardial infarction. *Am. J. Physiol. - Cell Physiol.* **319**, C797–C806 (2020).

130. Hofmann, U. & Frantz, S. Role of Lymphocytes in Myocardial Injury, Healing, and Remodeling After Myocardial Infarction. *Circ. Res.* **116**, 354–367 (2015).

131. Corliss, B. A., Azimi, M. S., Munson, J., Peirce, S. M. & Murfee, W. L. Macrophages: An Inflammatory Link between Angiogenesis and Lymphangiogenesis. *Microcirculation* **23**, 95–121 (2016).

132. Barker, T. H. & Engler, A. J. The provisional matrix: setting the stage for tissue repair outcomes. *Matrix Biol.* **60**–**61**, 1–4 (2017).

133. Motley, M. P. *et al.* A CCR2 macrophage endocytic pathway mediates extravascular fibrin clearance in vivo. *Blood* **127**, 1085–1096 (2016).

134. Hanna, A. & Frangogiannis, N. G. The Role of the TGF-β Superfamily in Myocardial Infarction.

Front. Cardiovasc. Med. **6**, (2019).

135. O'Rourke, S., Dunne, S. A. & Monaghan, A. G. The Role of Macrophages in the Infarcted Myocardium: Orchestrators of ECM Remodeling. *Orch. ECM Remodel. Front. Cardiovasc. Med* **6**, 101 (2019).

136. Simões, F. C. *et al.* Macrophages directly contribute collagen to scar formation during zebrafish heart regeneration and mouse heart repair. *Nat. Commun.* **11**, 1–17 (2020).

137. Psarras, S., Beis, D., Nikouli, S., Tsikitis, M. & Capetanaki, Y. Three in a Box: Understanding Cardiomyocyte, Fibroblast, and Innate Immune Cell Interactions to Orchestrate Cardiac Repair Processes. *Front. Cardiovasc. Med.* **6**, 32 (2019).

138. Natarajan, N. *et al.* Complement receptor C5AR1 plays an evolutionarily conserved role in successful cardiac regeneration. *Circulation* **137**, 2152–2165 (2018).

139. Hui, S. P. *et al.* Zebrafish Regulatory T Cells Mediate Organ-Specific Regenerative Programs. *Dev. Cell* **43**, 659-672.e5 (2017).

140. Li, J. *et al.* Regulatory T-cells regulate neonatal heart regeneration by potentiating cardiomyocyte proliferation in a paracrine manner. *Theranostics* **9**, 4324–4341 (2019).

141. Wang, Z. *et al.* Cell-Type-Specific Gene Regulatory Networks Underlying Murine Neonatal Heart Regeneration at Single-Cell Resolution. *Cell Rep.* **33**, 108472 (2020).

142. Li, Y. *et al.* Gp130 Controls Cardiomyocyte Proliferation and Heart Regeneration. *Circulation* 967–982 (2020). doi:10.1161/CIRCULATIONAHA.119.044484

143. Wang, Z. *et al.* Mechanistic basis of neonatal heart regeneration revealed by transcriptome and histone modification profiling. *Proc. Natl. Acad. Sci. U. S. A.* **116**, 18455–18465 (2019).

144. Bevan, L. *et al.* Specific macrophage populations promote both cardiac scar deposition and subsequent resolution in adult zebrafish. *Cardiovasc. Res.* **116**, 1357–1371 (2020).

145. Italiani, P. & Boraschi, D. From monocytes to M1/M2 macrophages: Phenotypical vs. functional differentiation. *Front. Immunol.* **5**, 514 (2014).

146. Sager, H. B., Kessler, T. & Schunkert, H. Monocytes and macrophages in cardiac injury and repair. *J. Thorac. Dis.* **9**, S30 (2017).

147. Kim, Y., Nurakhayev, S., Nurkesh, A., Zharkinbekov, Z. & Saparov, A. Macrophage Polarization in Cardiac Tissue Repair Following Myocardial Infarction. *Int. J. Mol. Sci.* **22**, 1–15 (2021).

148. Bozkurt, B. *et al.* Pathophysiologically Relevant Concentrations of Tumor Necrosis Factor-α Promote Progressive Left Ventricular Dysfunction and Remodeling in Rats. *Circulation* **97**, 1382–1391 (1998).

149. Riehle, C. & Bauersachs, J. Key inflammatory mechanisms underlying heart failure. *Herz* **44**, 96 (2019).

150. Westman, P. C. *et al.* Inflammation as a Driver of Adverse Left Ventricular Remodeling After Acute Myocardial Infarction. *J. Am. Coll. Cardiol.* **67**, 2050–2060 (2016).

151. Reina-Couto, M. *et al.* Inflammation in Human Heart Failure: Major Mediators and Therapeutic Targets. *Front. Physiol.* **12**, 1753 (2021).

152. Tøllefsen, I. M. *et al.* High levels of interleukin-6 are associated with final infarct size and adverse clinical events in patients with STEMI. *Open Hear.* **8**, e001869 (2021).

153. Horckmans, M. *et al.* Neutrophils orchestrate post-myocardial infarction healing by polarizing macrophages towards a reparative phenotype. *Eur. Heart J.* **38**, 187–197 (2017).

154. Huynh, M.-L. N., Fadok, V. A. & Henson, P. M. Phosphatidylserine-dependent ingestion of apoptotic cells promotes TGF-β1 secretion and the resolution of inflammation. **109**, 41–50 (2002).

155. Zhang, Y., Kim, H. J., Yamamoto, S., Kang, X. & Ma, X. Regulation of Interleukin-10 Gene

Expression in Macrophages Engulfing Apoptotic Cells. *https://home.liebertpub.com/jir* **30**, 113–121 (2010).

156. Abe, H. *et al.* Macrophage hypoxia signaling regulates cardiac fibrosis via Oncostatin M. *Nat. Commun. 2019 101* **10**, 1–10 (2019).

157. Kino, T., Khan, M. & Mohsin, S. The Regulatory Role of T Cell Responses in Cardiac Remodeling Following Myocardial Infarction. *Int. J. Mol. Sci.* **21**, 1–13 (2020).

158. Gross, J. B., Meyer, B. & Perkins, M. The rise of Astyanax cavefish. *Dev. Dyn.* **244**, 1031–1038 (2015).

159. Gross, J. B. The complex origin of Astyanax cavefish. *BMC Evol. Biol.* **12**, 105 (2012).

160. Herman, A. *et al.* The role of gene flow in rapid and repeated evolution of cave-related traits in Mexican tetra, Astyanax mexicanus. *Mol. Ecol.* **27**, 4397–4416 (2018).

161. Fumey, J. *et al.* Evidence for late Pleistocene origin of Astyanax mexicanus cavefish. *BMC Evol. Biol.* **18**, 43 (2018).

162. Wilkens, H. The role of selection in the evolution of blindness. *Biol J Lin Soc* **130**, 421–432 (2020).

163. Jeffery, W. R. Regressive Evolution in *Astyanax* Cavefish. *Annu. Rev. Genet.* **43**, 25–47 (2009).

164. Riddle, M. R. *et al.* Insulin resistance in cavefish as an adaptation to a nutrient-limited environment. *Nature* **555**, 647–651 (2018).

165. Kearsey, M. J. The principles of QTL analysis (a minimal mathematics approach). *J. Exp. Bot.* **49**, 1619–1623 (1998).

166. Peuß, R. *et al.* Adaptation to low parasite abundance affects immune investment and immunopathological responses of cavefish. *Nat. Ecol. Evol.* (2020). doi:10.1038/s41559-020-1234-2

167. Simkin, J., Gawriluk, T. R., Gensel, J. C. & Seifert, A. W. Macrophages are necessary for epimorphic regeneration in African spiny mice. *Elife* **6**, (2017).

168. Leach, L. L., Hanovice, N. J., George, S. M., Gabriel, A. E. & Gross, J. M. The immune response is a critical regulator of zebrafish retinal pigment epithelium regeneration. *Proc. Natl. Acad. Sci. U. S. A.* **118**, (2021).

169. Godwin, J. W., Pinto, A. R. & Rosenthal, N. A. Macrophages are required for adult salamander limb regeneration. *Proc. Natl. Acad. Sci. U. S. A.* **110**, 9415–9420 (2013).

170. Maiguel, D. *et al.* Small molecule-mediated activation of the integrin CD11b/CD18 reduces inflammatory disease. *Sci. Signal.* **4**, ra57 (2011).

171. Smith, A. M., Dykeman, C. A., King, B. L. & Yin, V. P. Modulation of TNFα Activity by the microRNA Let-7 Coordinates Zebrafish Heart Regeneration. *iScience* **15**, 1–15 (2019).

172. Watanabe, M. *et al.* Dual targeting of transformed and untransformed HTLV-1-infected T cells by DHMEQ, a potent and selective inhibitor of NF-kappaB, as a strategy for chemoprevention and therapy of adult T-cell leukemia. *Blood* **106**, 2462–2471 (2005).

173. Tyrkalska, S. D. *et al.* Neutrophils mediate Salmonella Typhimurium clearance through the GBP4 inflammasome-dependent production of prostaglandins. *Nat. Commun.* **7**, (2016).

174. Potts, H. G. *et al.* Discordant Genome Assemblies Drastically Alter the Interpretation of Single-Cell RNA Sequencing Data Which Can Be Mitigated by a Novel Integration Method. *Cells 2022, Vol. 11, Page 608* **11**, 608 (2022).

175. Sander, V., Su, G., Jopling, C., Morera, C. & Carlos Izpisua Belmonte, J. Isolation and in vitro culture of primary cardiomyocytes from adult zebrafish hearts. (2013). doi:10.1038/nprot.2013.041

176. Hafemeister, C. & Satija, R. Normalization and variance stabilization of single-cell RNA-seq

data using regularized negative binomial regression. *Genome Biol.* **20**, 296 (2019).

177. Zappia, L. & Oshlack, A. Clustering trees: a visualization for evaluating clusterings at multiple resolutions. **7**, 1–9 (2018).

178. Korsunsky, I. *et al.* Fast, sensitive and accurate integration of single-cell data with Harmony. doi:10.1038/s41592-019-0619-0

179. Finak, G. *et al.* MAST: a flexible statistical framework for assessing transcriptional changes and characterizing heterogeneity in single-cell RNA sequencing data. (2015). doi:10.1186/s13059-015-0844-5

180. Korotkevich, G. *et al.* Fast gene set enrichment analysis. *bioRxiv* 060012 (2021). doi:10.1101/060012

181. Schubert, M. *et al.* Perturbation-response genes reveal signaling footprints in cancer gene expression. *Nat. Commun.* **9**, 1–11 (2018).

182. Farbehi, N. *et al.* Single-cell expression profiling reveals dynamic flux of cardiac stromal, vascular and immune cells in health and injury. *Elife* **8**, (2019).

183. Ramilowski, J. A. *et al.* A draft network of ligand–receptor-mediated multicellular signalling in human. *Nat. Commun. 2015 61* **6**, 1–12 (2015).

184. Szklarczyk, D. *et al.* The STRING database in 2017: quality-controlled protein-protein association networks, made broadly accessible. *Nucleic Acids Res.* **45**, D362–D368 (2017).

185. Bredfeldt, J. S. *et al.* Computational segmentation of collagen fibers from second-harmonic generation images of breast cancer. *J. Biomed. Opt.* **19**, 016007 (2014).

186. Tang, F. *et al.* mRNA-Seq whole-transcriptome analysis of a single cell. *Nat. Methods* **6**, 377–382 (2009).

187. Wu, A. R., Wang, J., Streets, A. M. & Huang, Y. Single-Cell Transcriptional Analysis.

https://doi.org/10.1146/annurev-anchem-061516-045228 **10**, 439–462 (2017).

188. Haque, A., Engel, J., Teichmann, S. A. & Lönnberg, T. A practical guide to single-cell RNA-sequencing for biomedical research and clinical applications. *Genome Medicine* **9**, 1–12 (2017).

189. Shao, Y. *et al.* Genome and single-cell RNA-sequencing of the earthworm Eisenia andrei identifies cellular mechanisms underlying regeneration. *Nat. Commun.* **11**, 1–15 (2020).

190. Londono, R. *et al.* Single cell sequencing analysis of lizard phagocytic cell populations and their role in tail regeneration. *J. Immunol. Regen. Med.* **8**, 100029 (2020).

191. Tosches, M. A. *et al.* Evolution of pallium, hippocampus, and cortical cell types revealed by single-cell transcriptomics in reptiles. *Science (80-.).* **360**, 881–888 (2018).

192. Picelli, S. *et al.* Smart-seq2 for sensitive full-length transcriptome profiling in single cells. *Nat. Methods 2013 1011* **10**, 1096–1098 (2013).

193. Klein, A. M. *et al.* Droplet Barcoding for Single-Cell Transcriptomics Applied to Embryonic Stem Cells. *Cell* **161**, 1187–1201 (2015).

194. Pollen, A. A. *et al.* Low-coverage single-cell mRNA sequencing reveals cellular heterogeneity and activated signaling pathways in developing cerebral cortex. *Nat. Biotechnol. 2014 3210* **32**, 1053–1058 (2014).

195. Macosko, E. Z. *et al.* Highly Parallel Genome-wide Expression Profiling of Individual Cells Using Nanoliter Droplets. *Cell* **161**, 1202–1214 (2015).

196. Zhang, X. *et al.* Comparative Analysis of Droplet-Based Ultra-High-Throughput Single-Cell RNA-Seq Systems. *Mol. Cell* **73**, 130-142.e5 (2019).

197. Zheng, G. X. Y. *et al.* Massively parallel digital transcriptional profiling of single cells. *Nat. Commun. 2017 81* **8**, 1–12 (2017).

198. See, P., Lum, J., Chen, J. & Ginhoux, F. A single-cell sequencing guide for immunologists. *Front. Immunol.* **9**, 2425 (2018).

199. Tang, J. L. Y. *et al.* The developmental origin of heart size and shape differences in Astyanax mexicanus populations. *Dev. Biol.* **441**, 272 (2018).

200. Schnabel, K., Wu, C.-C., Kurth, T. & Weidinger, G. Regeneration of Cryoinjury Induced Necrotic Heart Lesions in Zebrafish Is Associated with Epicardial Activation and Cardiomyocyte Proliferation. *PLoS One* **6**, e18503 (2011).

201. Chablais, F., Veit, J., Rainer, G. & Jawiska, A. The zebrafish heart regenerates after cryoinjury-induced myocardial infarction. *BMC Dev. Biol.* **11**, 21 (2011).

202. González-Rosa, J. M., Martín, V., Peralta, M., Torres, M. & Mercader, N. Extensive scar formation and regression during heart regeneration after cryoinjury in zebrafish. *Development* **138**, 1663–1674 (2011).

203. Kannan, S. *et al.* Large particle fluorescence-activated cell sorting enables high-quality single-cell RNA sequencing and functional analysis of adult cardiomyocytes. **125**, 567–569 (2019).

204. Litviňuková, M. *et al.* Cells of the adult human heart. *Nat. 2020 5887838* **588**, 466–472 (2020).

205. Skelly, D. A. *et al.* Single-Cell Transcriptional Profiling Reveals Cellular Diversity and Intercommunication in the Mouse Heart. *Cell Rep.* **22**, 600–610 (2018).

206. DeLaughter, D. M. *et al.* Single-Cell Resolution of Temporal Gene Expression during Heart Development. *Dev. Cell* **39**, 480–490 (2016).

207. Forte, E. *et al.* Dynamic Interstitial Cell Response during Myocardial Infarction Predicts Resilience to Rupture in Genetically Diverse Mice. *Cell Rep.* **30**, 3149-3163.e6 (2020).

208. Koth, J. *et al.* Runx1 promotes scar deposition and inhibits myocardial proliferation and

survival during zebrafish heart regeneration. *Dev.* **147**, (2020).

209. Rolland, L. *et al.* The regenerative response of cardiac interstitial cells. *bioRxiv* 2021.10.25.465720 (2021). doi:10.1101/2021.10.25.465720

210. McGaugh, S. E. *et al.* The cavefish genome reveals candidate genes for eye loss. *Nat. Commun.* **5**, 5307 (2014).

211. Warren, W. C. *et al.* A chromosome-level genome of Astyanax mexicanus surface fish for comparing population-specific genetic differences contributing to trait evolution. *Nat. Commun. 2021 121* **12**, 1–12 (2021).

212. Imarazene, B. *et al.* A supernumerary 'B-sex' chromosome drives male sex determination in the Pachón cavefish, Astyanax mexicanus. *Curr. Biol.* **31**, 4800-4809.e9 (2021).

213. Shafer, M. E. R., Sawh, A. N. & Schier, A. F. Gene family evolution underlies cell-type diversification in the hypothalamus of teleosts. *Nat. Ecol. Evol. 2021* 1–14 (2021). doi:10.1038/s41559-021-01580-3

214. Krishnan, J. *et al.* Comparative transcriptome analysis of wild and lab populations of Astyanax mexicanus uncovers differential effects of environment and morphotype on gene expression. **334**, (2020).

215. Cao, J. *et al.* Single epicardial cell transcriptome sequencing identifies caveolin 1 as an essential factor in zebrafish heart regeneration. *Dev.* **143**, 232–243 (2016).

216. Patra, C. *et al.* The zebrafish ventricle: A hub of cardiac endothelial cells for in vitro cell behavior studies. *Sci. Rep.* **7**, 1–11 (2017).

217. F, G. Fibroblasts, myofibroblasts, and wound contraction. *J. Cell Biol.* **124**, 401–404 (1994).

218. W, S., TA, S. & G, G. The myofibroblast: a quarter century after its discovery. *Am. J. Surg. Pathol.* **22**, 141–147 (1998).

219. Gabbiani, G., Ryan, G. B. & Majno, G. Presence of modified fibroblasts in granulation tissue and their possible role in wound contraction. *Exp. 1971 275* **27**, 549–550 (1971).

220. Sogah, V. M. *et al.* Distinct Troponin C Isoform Requirements in Cardiac and Skeletal Muscle. *Dev. Dyn.* **239**, 3115 (2010).

221. Nakano, A., Harada, T., Morikawa, S. & Kato, Y. Expression of leukocyte common antigen (CD45) on various human leukemia/lymphoma cell lines. *Acta Pathol. Jpn.* **40**, 107–115 (1990).

222. Han, P. *et al.* Hydrogen peroxide primes heart regeneration with a derepression mechanism. *Cell Res. 2014 249* **24**, 1091–1107 (2014).

223. López-Muñoz, A. *et al.* An Adult Zebrafish Model Reveals that Mucormycosis Induces Apoptosis of Infected Macrophages. *Sci. Reports 2018 81* **8**, 1–12 (2018).

224. Yang, Q., Yan, C. & Gong, Z. Activation of liver stromal cells is associated with male-biased liver tumor initiation in xmrk and Myc transgenic zebrafish. *Sci. Reports 2017 71* **7**, 1–9 (2017).

225. Beckers, A. *et al.* Injury-induced Autophagy Delays Axonal Regeneration after Optic Nerve Damage in Adult Zebrafish. *Neuroscience* **470**, 52–69 (2021).

226. Muraro, M. J. *et al.* A Single-Cell Transcriptome Atlas of the Human Pancreas. *Cell Syst.* **3**, 385 (2016).

227. Bakken, T. E. *et al.* Single-nucleus and single-cell transcriptomes compared in matched cortical cell types. *PLoS One* **13**, e0209648 (2018).

228. Lelek, S. *et al.* Morphine alleviates pain after heart cryoinjury in zebrafish without impeding regeneration. *bioRxiv* (2020). doi:10.1101/2020.10.01.322560

229. Smith, J. J. *et al.* A chromosome-scale assembly of the axolotl genome. *Genome Res.* **29**, 317–

324 (2019).

230. Quijada, P., Trembley, M. A. & Small, E. M. The Role of the Epicardium during Heart Development and Repair. *Circulation Research* **126**, 377–394 (2020).

231. Ferrari, J. P. *et al.* Correlation between leukocyte count and infarct size in ST segment elevation myocardial infarction. *Arch. Med. Sci. Atheroscler. Dis.* **1**, e44 (2016).

232. Furman, M. I. *et al.* Effect of Elevated Leukocyte Count on In-Hospital Mortality Following Acute Myocardial Infarction. *Am. J. Cardiol.* **78**, 945–948 (1996).

233. Li, J. *et al.* Specific ablation of CD4 + T-cells promotes heart regeneration in juvenile mice. *Issue 18 Theranostics* **10**, 8018–8035 (2020).

234. Yan, X. *et al.* Temporal dynamics of cardiac immune cell accumulation following acute myocardial infarction. *J. Mol. Cell. Cardiol.* **62**, 24–35 (2013).

235. Bansal, S. S. *et al.* Activated T lymphocytes are essential drivers of pathological remodeling in ischemic heart failure. *Circ. Hear. Fail.* **10**, (2017).

236. Sager, H. B. *et al.* Proliferation and Recruitment Contribute to Myocardial Macrophage Expansion in Chronic Heart Failure. *Circ. Res.* **119**, 853–864 (2016).

237. Tania Nevers Ane M. Salvador Anna Grodecki-Pena Andrew Knapp Francisco Velázquez Mark Aronovitz Navin K. Kapur Richard H. Karas, R. M. B. and P. A. Left Ventricular T-Cell Recruitment Contributes to the Pathogenesis of Heart Failure. *Circ. Hear. Fail.* **8**, 776–787 (2015).

238. Ismahil, M. A. *et al.* Remodeling of the mononuclear phagocyte network underlies chronic inflammation and disease progression in heart failure critical importance of the cardiosplenic axis. *Circ. Res.* **114**, 266–282 (2014).

239. Arruda-Olson, A. M., Reeder, G. S., Bell, M. R., Weston, S. A. & Roger, V. L. Neutrophilia

predicts death and heart failure after myocardial infarction: A community-based study. *Circ. Cardiovasc. Qual. Outcomes* **2**, 656–662 (2009).

240. Dogan, I., Karaman, K., Sonmez, B., Celik, S. & Turker, O. Relationship between serum neutrophil count and infarct size in patients with acute myocardial infarction. *Nucl. Med. Commun.* **30**, 797–801 (2009).

241. Kyne, L. *et al.* Neutrophilia and congestive heart failure after acute myocardial infarction. *Am. Heart J.* **139**, 94–100 (2000).

242. Ma, Y., Yabluchanskiy, A. & Lindsey, M. L. Neutrophil roles in left ventricular remodeling following myocardial infarction. *Fibrogenes. Tissue Repair* **6**, 1–10 (2013).

243. Von Harsdorf, R., Li, P. F. & Dietz, R. Signaling Pathways in Reactive Oxygen Species–Induced Cardiomyocyte Apoptosis. *Circulation* **99**, 2934–2941 (1999).

244. Romson, J. L. *et al.* Reduction of the extent of ischemic myocardial injury by neutrophil depletion in the dog. *Circulation* **67**, 1016–1023 (1983).

245. Jolly, S. R. *et al.* Reduction of myocardial infarct size by neutrophil depletion: Effect of duration of occlusion. *Am. Heart J.* **112**, 682–690 (1986).

246. Horckmans, M. *et al.* Neutrophils orchestrate post-myocardial infarction healing by polarizing macrophages towards a reparative phenotype. *Eur. Heart J.* **38**, ehw002 (2016).

247. Bao, L. *et al.* Engineered neutrophil apoptotic bodies ameliorate myocardial infarction by promoting macrophage efferocytosis and inflammation resolution. *Bioact. Mater.* **9**, 183–197 (2022).

248. Glinton, K. E. *et al.* Macrophage-produced VEGFC is induced by efferocytosis to ameliorate cardiac injury and inflammation. *J. Clin. Invest.* (2022). doi:10.1172/JCI140685

249. Daseke, M. J. *et al.* Neutrophil proteome shifts over the myocardial infarction time

continuum. *Basic Res. Cardiol.* **114**, 1–13 (2019).

250. Calcagno, D. M. *et al.* Siglecf(Hi) marks late-stage neutrophils of the infarcted heart: A single-cell transcriptomic analysis of neutrophil diversification. *J. Am. Heart Assoc.* **10**, 1–39 (2021).

251. Vafadarnejad, E. *et al.* Dynamics of cardiac neutrophil diversity in murine myocardial infarction. *Circ. Res.* E232–E249 (2020). doi:10.1161/CIRCRESAHA.120.317200

252. Xu, S. *et al.* Prolonged neutrophil retention in the wound impairs zebrafish heart regeneration after cryoinjury. *Fish Shellfish Immunol.* **94**, 447–454 (2019).

253. Panizzi, P. *et al.* Impaired Infarct Healing in Atherosclerotic Mice With Ly-6ChiMonocytosis. *J. Am. Coll. Cardiol.* (2010). doi:10.1016/J.JACC.2009.08.089

254. Nahrendorf, M. *et al.* The healing myocardium sequentially mobilizes two monocyte subsets with divergent and complementary functions. *J. Exp. Med.* **204**, 3037–3047 (2007).

255. Ryan, R., Moyse, B. R. & Richardson, R. J. Zebrafish cardiac regeneration—looking beyond cardiomyocytes to a complex microenvironment. *Histochemistry and Cell Biology* **154**, 533–548 (2020).

256. Petrie, T. A., Strand, N. S., Tsung-Yang, C., Rabinowitz, J. S. & Moon, R. T. Macrophages modulate adult zebrafish tail fin regeneration. *Dev.* **141**, 2581–2591 (2014).

257. Kyaw, T. *et al.* Alarmin-activated B cells accelerate murine atherosclerosis after myocardial infarction via plasma cell-immunoglobulin-dependent mechanisms. *Eur. Heart J.* **42**, 938–947 (2021).

258. García-Rivas, G. *et al.* The role of B cells in heart failure and implications for future immunomodulatory treatment strategies. *ESC Hear. Fail.* **7**, 1387 (2020).

259. Zouggari, Y. *et al.* B lymphocytes trigger monocyte mobilization and impair heart function after acute myocardial infarction. *Nat. Med.* **19**, 1273–1280 (2013).

260. Mo, F. *et al.* Are activated B cells involved in the process of myocardial fibrosis after acute myocardial infarction? An in vivo experiment. *BMC Cardiovasc. Disord.* **21**, 1–14 (2021).

261. Goodchild, T. T. *et al.* Bone Marrow-Derived B Cells Preserve Ventricular Function After Acute Myocardial Infarction. *JACC Cardiovasc. Interv.* **2**, 1005–1016 (2009).

262. Jiao, J. *et al.* Regulatory B cells improve ventricular remodeling after myocardial infarction by modulating monocyte migration. *Basic Res. Cardiol.* **116**, 1–18 (2021).

263. Wu, L. *et al.* IL-10–producing B cells are enriched in murine pericardial adipose tissues and ameliorate the outcome of acute myocardial infarction. *Proc. Natl. Acad. Sci. U. S. A.* **116**, 21673–21684 (2019).

264. Moyse, B. R. & Richardson, R. J. A population of injury-responsive lymphoid cells expresses mpeg1.1 in the adult zebrafish heart. *ImmunoHorizons* **4**, 464–474 (2020).

265. Spilsbury, K. *et al.* Isolation of a Novel Macrophage-Specific Gene by Differential cDNA Analysis. *Blood* **85**, 1620–1629 (1995).

266. Travnickova, J. *et al.* Primitive macrophages control HSPC mobilization and definitive haematopoiesis. *Nat. Commun. 2015 61* **6**, 1–9 (2015).

267. Peri, F. & Nüsslein-Volhard, C. Live Imaging of Neuronal Degradation by Microglia Reveals a Role for v0-ATPase a1 in Phagosomal Fusion In Vivo. *Cell* **133**, 916–927 (2008).

268. Gerri, C. *et al.* Hif-1α regulates macrophage-endothelial interactions during blood vessel development in zebrafish. *Nat. Commun. 2017 81* **8**, 1–14 (2017).

269. Tobin, D. M. *et al.* The lta4h Locus Modulates Susceptibility to Mycobacterial Infection in Zebrafish and Humans. *Cell* **140**, 717–730 (2010).

270. Madigan, C. A. *et al.* A Macrophage Response to Mycobacterium leprae Phenolic Glycolipid Initiates Nerve Damage in Leprosy. *Cell* **170**, 973-985.e10 (2017).

271. Roh-Johnson, M. *et al.* Macrophage-Dependent Cytoplasmic Transfer during Melanoma Invasion In Vivo. *Dev. Cell* **43**, 549-562.e6 (2017).

272. van den Berg, M. C. W. *et al.* Proteolytic and Opportunistic Breaching of the Basement Membrane Zone by Immune Cells during Tumor Initiation. *Cell Rep.* **27**, 2837-2846.e4 (2019).

273. Chia, K., Mazzolini, J., Mione, M. & Sieger, D. Tumor initiating cells induce cxcr4- mediated infiltration of pro-tumoral macrophages into the brain. *Elife* **7**, (2018).

274. Peiseler, M. & Kubes, P. More friend than foe: the emerging role of neutrophils in tissue repair. *J. Clin. Invest.* **129**, 2629–2639 (2019).

275. Wilgus, T. A., Roy, S. & McDaniel, J. C. Neutrophils and Wound Repair: Positive Actions and Negative Reactions. *Adv. Wound Care* **2**, 379 (2013).

276. Bise, T., Sallin, P., Pfefferli, C. & Jaźwińska, A. Multiple cryoinjuries modulate the efficiency of zebrafish heart regeneration. **10**, 1–15 (2020).

277. Ma, Y. *et al.* Temporal neutrophil polarization following myocardial infarction. *Cardiovasc. Res.* **110**, 51 (2016).

278. Sîrbulescu, R. F. *et al.* Mature B cells accelerate wound healing after acute and chronic diabetic skin lesions. **25**, 774–791 (2017).

279. Bodhankar, S., Chen, Y., Vandenbark, A. A., Murphy, S. J. & Offner, H. IL-10-producing B-cells limit CNS inflammation and infarct volume in experimental stroke. *Metab. Brain Dis.* **28**, 375–386 (2013).

280. Bodhankar, S., Chen, Y., Vandenbark, A. A., Murphy, S. J. & Offner, H. Treatment of experimental stroke with IL-10-producing B-cells reduces infarct size and peripheral and CNS inflammation in wild-type B-cell-sufficient mice. *Metab. Brain Dis.* **29**, 59–73 (2014).

281. Sîrbulescu, R. F. *et al.* Intraparenchymal Application of Mature B Lymphocytes Improves

Structural and Functional Outcome after Contusion Traumatic Brain Injury. *J. Neurotrauma* **36**, 2579–2589 (2019).

282. Adamo, L. *et al.* Myocardial B cells are a subset of circulating lymphocytes with delayed transit through the heart. *JCI Insight* **5**, (2020).

283. Sheng, D. Z., Zheng, D. & Kikuchi, K. Cardiac Resection Injury in Zebrafish. *Methods Mol. Biol.* **2158**, 63–69 (2021).

284. Ellman, D. G. *et al.* Apex resection in zebrafish (Danio rerio) as a model of heart regeneration: A video-assisted guide. *Int. J. Mol. Sci.* **22**, (2021).

285. Schäffer, M., Bongartz, M., Hoffmann, W. & Viebahn, R. MHC-class-II-deficiency impairs wound healing. *J. Surg. Res.* **138**, 100–105 (2007).

286. Hofmann, U. *et al.* Activation of CD4 + T lymphocytes improves wound healing and survival after experimental myocardial infarction in mice. *Circulation* **125**, 1652–1663 (2012).

287. Hamid, T. *et al.* Cardiomyocyte NF-κB p65 promotes adverse remodelling, apoptosis, and endoplasmic reticulum stress in heart failure. *Cardiovasc. Res.* **89**, 129–138 (2011).

288. Young, D., Popovic, Z. B., Jones, W. K. & Gupta, S. Blockade of NF-kappaB using IkappaB alpha dominant-negative mice ameliorates cardiac hypertrophy in myotrophin-overexpressed transgenic mice. *J. Mol. Biol.* **381**, 559–568 (2008).

289. Liu, Q., Chen, Y., Auger-Messier, M. & Molkentin, J. D. Interaction between NFκB and NFAT coordinates cardiac hypertrophy and pathological remodeling. *Circ. Res.* **110**, 1077–1086 (2012).

290. Zhou, B. *et al.* Functional polymorphism of the NFKB1 gene promoter is related to the risk of dilated cardiomyopathy. *BMC Med. Genet.* **10**, 1–5 (2009).

291. Pamukcu, B., Lip, G. Y. H. & Shantsila, E. The nuclear factor--kappa B pathway in

atherosclerosis: a potential therapeutic target for atherothrombotic vascular disease. *Thromb. Res.* **128**, 117–123 (2011).

292. Bednarek, D. *et al.* Telomerase Is Essential for Zebrafish Heart Regeneration. *Cell Rep.* **12**, 1691–1703 (2015).

293. Ma, Y., Iyer, R. P., Jung, M., Czubryt, M. P. & Lindsey, M. L. Cardiac Fibroblast Activation Post-Myocardial Infarction: Current Knowledge Gaps. *Trends Pharmacol. Sci.* **38**, 448–458 (2017).

294. Daseke, M. J., Tenkorang, M. A. A., Chalise, U., Konfrst, S. R. & Lindsey, M. L. Cardiac Fibroblast Activation during Myocardial Infarction Wound Healing. *Matrix Biol.* **91**–**92**, 109 (2020).

295. Richardson, W. J., Clarke, S. A., Alexander Quinn, T. & Holmes, J. W. Physiological Implications of Myocardial Scar Structure. *Compr. Physiol.* **5**, 1877 (2015).

296. Zacchigna, S. *et al.* Paracrine effect of regulatory T cells promotes cardiomyocyte proliferation during pregnancy and after myocardial infarction. *Nat. Commun. 2018 91* **9**, 1–12 (2018).

297. Molenaar, B. *et al.* Single-cell transcriptomics following ischemic injury identifies a role for B2M in cardiac repair. *Commun. Biol. 2021 41* **4**, 1–15 (2021).

298. Muxel, S. M., Laranjeira-Silva, M. F., Carvalho-Sousa, C. E., Floeter-Winter, L. M. & Markus, R. P. The RelA/cRel nuclear factor-κB (NF-κB) dimer, crucial for inflammation resolution, mediates the transcription of the key enzyme in melatonin synthesis in RAW 264.7 macrophages. *J. Pineal Res.* **60**, 394–404 (2016).

299. Liu, T., Zhang, L., Joo, D. & Sun, S.-C. NF-κB signaling in inflammation. *Signal Transduct. Target. Ther. 2017 21* **2**, 1–9 (2017).

300. Rouillard, A. D. *et al.* The harmonizome: a collection of processed datasets gathered to serve and mine knowledge about genes and proteins. *Database* **2016**, (2016).

301. Holland, C. H. *et al.* Robustness and applicability of transcription factor and pathway analysis tools on single-cell RNA-seq data. *Genome Biol.* **21**, 1–19 (2020).

302. Coutinho, A. E. & Chapman, K. E. The anti-inflammatory and immunosuppressive effects of glucocorticoids, recent developments and mechanistic insights. *Mol. Cell. Endocrinol.* **335**, 2 (2011).

303. Fiordelisi, A., Iaccarino, G., Morisco, C., Coscioni, E. & Sorriento, D. NFkappaB is a Key Player in the Crosstalk between Inflammation and Cardiovascular Diseases. *Mol. Sci.* **20**, (2019).

304. Zhang, Y. *et al.* Tumor Necrosis Factor-α and Lymphotoxin-α Mediate Myocardial Ischemic Injury via TNF Receptor 1, but Are Cardioprotective When Activating TNF Receptor 2. *PLoS One* **8**, e60227 (2013).

305. Xing, J., Liu, Y. & Chen, T. Correlations of chemokine CXCL16 and TNF-α with coronary atherosclerotic heart disease. *Exp. Ther. Med.* **15**, 773–776 (2018).

306. Li, X. *et al.* Interplay of TNF-α, soluble TNF receptors and oxidative stress in coronary chronic total occlusion of the oldest patients with coronary heart disease. *Cytokine* **125**, (2020).

307. Shao, T. *et al.* Effects of milrinone on serum IL-6, TNF-α, Cys-C and cardiac functions of patients with chronic heart failure. *Exp. Ther. Med.* **16**, 4162–4166 (2018).

308. Zhang, X. Q. *et al.* Cardiomyocyte-specific p65 NF-κB deletion protects the injured heart by preservation of calcium handling. *Am. J. Physiol. - Hear. Circ. Physiol.* **305**, H1089 (2013).

309. Ong, C. W. M. *et al.* Complex regulation of neutrophil-derived MMP-9 secretion in central nervous system tuberculosis. *J. Neuroinflammation* **14**, (2017).

310. Kang, J. *et al.* Modulation of tissue repair by regeneration enhancer elements. *Nature* **532**, 201–206 (2016).

311. Begeman, I. J. *et al.* Decoding an Organ Regeneration Switch by Dissecting Cardiac

Regeneration Enhancers. *Deve* 74–78 (2020). doi:https://doi.org/10.1242/dev.194019

312. Goldman, J. A. *et al.* Resolving Heart Regeneration by Replacement Histone Profiling. *Dev. Cell* **40**, 392-404.e5 (2017).

313. Harris, R. E., Setiawan, L., Saul, J. & Hariharan, I. K. Localized epigenetic silencing of a damage-activated WNT enhancer limits regeneration in mature Drosophila imaginal discs. *Elife* **5**, (2016).

314. Suzuki, N., Hirano, K., Ogino, H. & Ochi, H. Arid3a regulates nephric tubule regeneration via evolutionarily conserved regeneration signal-response enhancers. *Elife* **8**, (2019).

315. Thompson, J. D. *et al.* Identification and requirements of enhancers that direct gene expression during zebrafish fin regeneration. *Dev.* **147**, (2020).

316. Vizcaya-Molina, E. *et al.* Damage-responsive elements in Drosophila regeneration. *Genome Res.* **28**, 1852–1866 (2018).

317. Soukup, A. A. *et al.* Single-nucleotide human disease mutation inactivates a blood-regenerative GATA2 enhancer. *J. Clin. Invest.* **129**, 1180–1192 (2019).

318. Fujioka, S. *et al.* NF-κB and AP-1 Connection: Mechanism of NF-κB-Dependent Regulation of AP-1 Activity. *Mol. Cell. Biol.* **24**, 7806 (2004).

319. Redhu, N. S., Saleh, A., Halayko, A. J., Ali, A. S. & Gounni, A. S. Essential role of NF-κB and AP-1 transcription factors in TNF-α-induced TSLP expression in human airway smooth muscle cells. *Am. J. Physiol. Lung Cell. Mol. Physiol.* **300**, (2011).

320. Qiao, Y. *et al.* AP-1 Is a Key Regulator of Proinflammatory Cytokine TNFα-mediated Triple-negative Breast Cancer Progression. *J. Biol. Chem.* **291**, 5068–5079 (2016).

321. Peng, H. *et al.* Adult spiny mice (Acomys) exhibit endogenous cardiac recovery in response to myocardial infarction. *npj Regen. Med. 2021 61* **6**, 1–15 (2021).

322. Koopmans, T. *et al.* Ischemic tolerance and cardiac repair in the spiny mouse (Acomys). *npj Regen. Med. 2021 61* **6**, 1–16 (2021).

323. Seifert, A. W. *et al.* Skin shedding and tissue regeneration in African spiny mice (Acomys). *Nature* **489**, 561 (2012).

324. Weitkamp, B. *et al.* Human macrophages synthesize type VIII collagen in vitro and in the atherosclerotic plaque. *FASEB J.* **13**, 1445–1457 (1999).

325. Ucero, Á. C., Bakiri, L. & Wagner, E. Collagen VI-producing macrophages mediate lung fibrosis. *Eur. Respir. J.* **54**, PA3862 (2019).

326. Ucero, A. *et al.* Collagen-producing macrophages can mediate lung fibrosis throughFra-2/AP-1 expression. *Eur. Respir. J.* **52**, LSC-1216 (2018).

327. Gunadasa-Rohling, M. *et al.* Magnetic Resonance Imaging of the Regenerating Neonatal Mouse Heart. *Circulation* **138**, 2439–2441 (2018).

328. Koth, J. *et al.* High-Resolution Magnetic Resonance Imaging of the Regenerating Adult Zebrafish Heart. *Sci. Reports 2017 71* **7**, 1–12 (2017).

329. Huang, W. C. *et al.* Treatment of Glucocorticoids Inhibited Early Immune Responses and Impaired Cardiac Repair in Adult Zebrafish. *PLoS One* **8**, e66613 (2013).

330. Balsalobre, A. *et al.* Resetting of circadian time in peripheral tissues by glucocorticoid signaling. *Science* **289**, 2344–2347 (2000).

331. Malkawi, A. K. *et al.* Metabolomics based profiling of Dexamethasone side effects in rats. *Front. Pharmacol.* **9**, 46 (2018).

332. Bae, J., Paltzer, W. G. & Mahmoud, A. I. The Role of Metabolism in Heart Failure and Regeneration. *Front. Cardiovasc. Med.* **0**, 763 (2021).

333. Ruby, C. L., Major, R. J. & Hinrichsen, R. D. Regulation of tissue regeneration by the circadian

clock. *Eur. J. Neurosci.* **53**, 3576–3597 (2021).

334. Erickson, J. R. & Echeverri, K. Learning from regeneration research organisms: The circuitous road to scar free wound healing. *Dev. Biol.* **433**, 144–154 (2018).

335. Chmielowiec, J. *et al.* c-Met is essential for wound healing in the skin. *J. Cell Biol.* **177**, 151–162 (2007).

336. Erickson, J. R. *et al.* A novel role for SALL4 during scar-free wound healing in axolotl. *npj Regen. Med. 2016 11* **1**, 1–11 (2016).

337. Hui, S. P. *et al.* Zebrafish Regulatory T Cells Mediate Organ-Specific Regenerative Programs. *Dev. Cell* **43**, 659-672.e5 (2017).

338. Chase, A. J., Bond, M., Crook, M. F. & Newby, A. C. Role of nuclear factor-κB activation in metalloproteinase-1, -3, and -9 secretion by human macrophages in vitro and rabbit foam cells produced in vivo. *Arterioscler. Thromb. Vasc. Biol.* **22**, 765–771 (2002).

339. Park, J. *et al.* Blocking TNFα attenuates progressive cartilage matrix degradation in inflammatory arthritis. *Exp. Ther. Med.* **22**, 1–11 (2021).

340. Kang, S. *et al.* Inflammation and Extracellular Matrix Degradation Mediated by Activated Transcription Factors Nuclear Factor-κB and Activator Protein-1 in Inflammatory Acne Lesions in Vivo. *Am. J. Pathol.* **166**, 1691 (2005).

341. Li, J. *et al.* B lymphocytes from early vertebrates have potent phagocytic and microbicidal abilities. *Nat. Immunol.* **7**, 1116–1124 (2006).

342. Wu, L. *et al.* Recent Advances on Phagocytic B Cells in Teleost Fish. *Front. Immunol.* **11**, 824 (2020).

343. Zhu, L. yun *et al.* Evolutionary implication of B-1 lineage cells from innate to adaptive immunity. *Mol. Immunol.* **69**, 123–130 (2016).

344. Gamba, L., Amin-Javaheri, A., Kim, J., Warburton, D. & Lien, C. L. Collagenolytic Activity Is Associated with Scar Resolution in Zebrafish Hearts after Cryoinjury. *J. Cardiovasc. Dev. Dis.* **4**, 2 (2017).

345. Eash, K. J., Greenbaum, A. M., Gopalan, P. K. & Link, D. C. CXCR2 and CXCR4 antagonistically regulate neutrophil trafficking from murine bone marrow. *J. Clin. Invest.* **120**, 2423–2431 (2010).

346. Zuo, E. *et al.* One-step generation of complete gene knockout mice and monkeys by CRISPR/Cas9-mediated gene editing with multiple sgRNAs. *Cell Res. 2017 277* **27**, 933–945 (2017).

347. Remels, A. H. V., Gosker, H. R., Verhees, K. J. P., Langen, R. C. J. & Schols, A. M. W. J. TNF-α-Induced NF-κB Activation Stimulates Skeletal Muscle Glycolytic Metabolism Through Activation of HIF-1α. *Endocrinology* **156**, 1770–1781 (2015).